



## Lectures in Radiation physics & Detectors

(Code No: ف 423)

Prof. Dr. Shaban Harb  
2023-2024

## Discovery of Radioactivity

In November 1895 Wilhelm Conrad Röntgen discovered X-rays. In a meeting of the French Academy of Science, the following January in Paris, Henri Becquerel heard Poincaré report the recent discovery. The X-rays discovered by Röntgen were the result of fluorescence produced by cathode rays in a cathode ray tube. Becquerel wondered if luminescence was a precondition for the observation of X-rays – he had already studied phosphorescence of uranium compounds.



**Fig. 1.1.** Henri Becquerel and family in their library. © R. Oldenbourg Verlag



**Fig. 1.2.** Pierre and Marie Curie, about 1898. © R. Oldenbourg Verlag

In one of his early attempts, Becquerel exposed uranium-containing minerals to sunlight to cause the material to glow (phosphorescence). The sample was placed on top of a photographic plate wrapped in black paper. Following development of the plate he could observe if radiation had penetrated the paper. This was indeed the case. By placing various objects (coins etc.) between the mineral and the photographic plate, he could reproduce the shapes of the objects.

From his detailed records, it is known that Becquerel decided to develop plates that had been in his drawer together with the uranium mineral. These had not been exposed to sunlight. Remarkably, the plates had been “fogged” by the uranium without activation by sunlight. The uranium was emitting rays by itself. Becquerel had discovered radioactivity.

Shortly after this event, Pierre and Marie Curie showed that thorium also acted like uranium. In an effort to try to isolate the source of the rays, they discovered the elements polonium and radium. Rutherford started working with these newly discovered uranium rays believing that they were similar to the X-rays discovered by Röntgen. In 1899, he discovered that these “rays” could be bent by a magnetic field and that there were two types of rays: alpha and beta. Today we know that the

alpha particle is a nucleus of helium and the beta particle is an electron. In later experiments, Rutherford would use these alpha particles to probe the structure of atoms.

### Structure of the Atom: Kelvin-Thomson “Plum Pudding” Atom

The discovery of radioactivity, and the discovery of the electron [2], were the starting points for theories of atomic structure. One of the problems associated with the discovery of the electron as a fundamental constituent of matter, was how to explain the electrical neutrality of the atom.

A first step in this direction was taken by Lord Kelvin (Sir William Thomson) and J. J. Thomson who proposed almost simultaneously one of the first models of the structure of the atom. In order to enforce electrical neutrality, Kelvin proposed a configuration, in 1902, in which the negative charges of the electrons and the positive charges cancelled out. He considered the atom to consist of a sphere in which the mass and charge are distributed uniformly with electrons embedded like plums in a pudding. In this model, electromagnetic radiation would be emitted if external forces caused the electrons in the atom to vibrate. In 1903–1904, J. J. Thomson proposed a modification of this in which the electrons moved at high speed in concentric circles in a sphere of continuous positive charge.

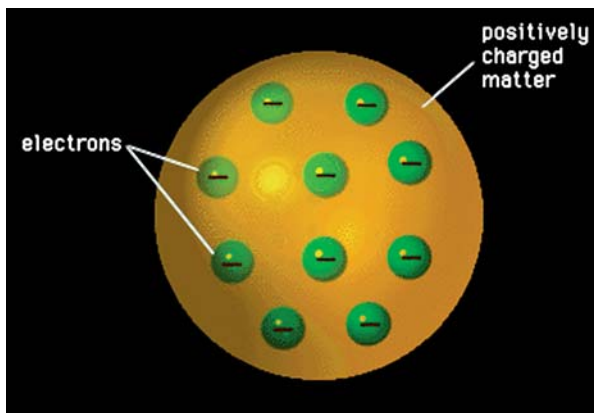


**Fig. 1.3.** Kelvin-Thomson “plum pudding” model of the atom [3]

### Rutherford’s Planetary Model of the Atom

In 1911 [4], Rutherford postulated that, in contrast to the “plum pudding” model, the positive charge of the atom was concentrated in a central “nucleus” much smaller than the atom which contained most of the atom’s mass, with the negative electrons orbiting around the nucleus similar to the way planets move around the sun. Each atom with its specific number of electrons, must contain an equal and opposite number of positive charges to ensure electrical neutrality. Since the electron is the fundamental unit of negative charge, Rutherford postulated that the unit of positive charge in the nucleus is the “proton”.

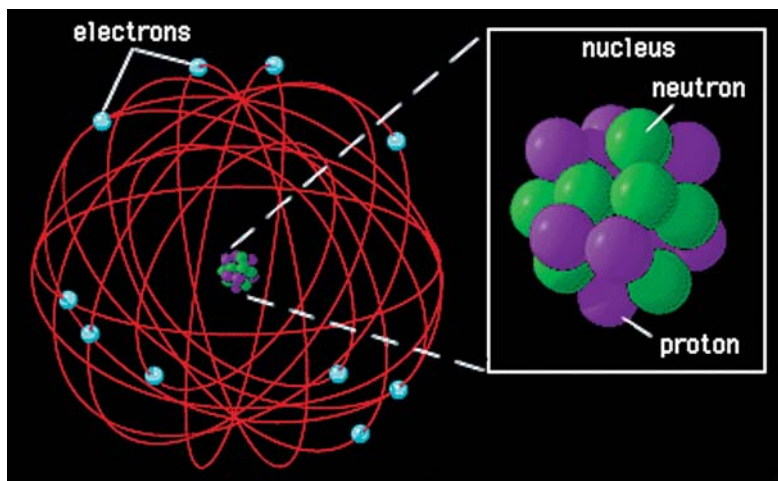


**Fig. 1.4.** Rutherford's nuclear atom [5]



**Fig. 1.5.** Ernest Rutherford (1871–1937).

© The Nobel Foundation

These ideas were put to test by two of Rutherford's students Geiger and Marsden in 1913 [6]. In a classic experiment, they bombarded thin gold foils with alpha particles emitted from radioactive polonium. If Rutherford's ideas on the structure of the atom were correct, then most of the alpha particles would pass through the thin foils with no interaction while a few would be scattered strongly due to close contact between the projectile and the nucleus.

The experiments confirmed Rutherford's ideas by showing that a collection of atoms consisted of positively charged nuclei with diameter of  $5 \times 10^{-15}$  m and that these nuclei were separated by distances of approximately  $10^{-10}$  m. It was also found that the number of unit charges in the nucleus was approximately equal to the atomic number of the atom and to about one half of the atomic weight.

Although these ideas were revolutionary at the time, there were two unsatisfactory aspects of Rutherford's proposed atomic structure. The first concerned how electrons are held in place outside the nucleus and the second how the protons can be held together in view of the strong repulsive forces of the positively charged particles. The idea of a small solar system with the electrons orbiting the positively charged nucleus seemed attractive but this was unacceptable to classical theory. According to this theory, such orbiting electrons experience a radial acceleration and should emit radiation. In doing so they would lose their kinetic energy and spiral into the nucleus.

Another limitation of the model was the fact that it could not account for the emission spectra of atoms. Emission spectra were first identified by Kirchhoff and

Bunsen who showed that spectral lines constitute a fingerprint which could be used to identify atoms.

These difficulties were to be resolved by Niels Bohr [7] who introduced a series of revolutionary ideas which were to change twentieth century science.

## Bohr-Sommerfeld Model of the Atom

### Bohr Atom

Rutherford's ideas were indeed irreconcilable with the classical theory of electromagnetism. Around this time new ideas were emerging on the structure of the atom. In 1913 Bohr [7] developed a model based on the new "quantum" theory proposed by Planck for radiation. In his investigations into the distribution of light from heated bodies and how this changes with temperature (blackbody radiation), Planck showed in 1900 that bodies emit radiation only in discrete amounts which are some multiple of  $h\nu$ , the quantum of energy, where  $\nu$  is the frequency of the radiation and  $h$  is a constant known as Planck's constant. This discovery was to set the scene for the foundations of quantum theory some twenty years later. These ideas were further substantiated with the discovery of the photoelectric effect by Einstein in 1905. In his investigations of how electrons are emitted from metal plates under the action of ultraviolet light, Einstein showed that the energy of the emitted electrons depends only on the frequency of the incident light and not on its intensity – in contrast to classical theory. He showed further that the light must be composed of discrete "photons" each with energy  $h\nu$ .

In a series of three papers published in 1913, Bohr invoked the ideas of Planck and Einstein into a new model of the atom. He proposed that atoms are in stationary states and that any emission of energy is associated with a transition of one state to the other. On this basis, emitted radiation must satisfy the condition  $h\nu = E_1 - E_2$ . With this idea, Bohr resolved the difficulty of classical theories in which orbiting electrons must emit radiation continuously.

Bohr's postulates can be summarised as follows:

1. Electrons orbit around the nucleus in discrete energy states without emitting radiation.
2. The allowed states for the electron are those for which the orbital angular momentum  $L$  is an integral multiple of  $h/2\pi$  i.e.  $L = n \cdot h/2\pi$  where  $n$  is the quantum number for discrete energy states.
3. When an electron jumps from a higher energy  $E_2$  state to a lower energy state  $E_1$  radiation of frequency  $\nu$  is emitted, where  $h\nu = E_2 - E_1$ .

A spectacular success of Bohr's model over that of Rutherford lay in the fact that it could explain the sharp line atomic spectra which results from, for example, the electrical excitation of gases. As early as 1885 Balmer had shown that the series of frequencies characteristic of spectral lines for the visible spectrum of hydrogen were governed by the relation

$$\nu = R \left( \frac{1}{i^2} - \frac{1}{j^2} \right),$$

where  $R$  is known as the Rydberg constant. The first series is given by setting  $i = 1$ , and  $j = 1, 2, 3, \dots$ . The second series corresponds to  $i = 2$ , and  $j = 3, 4, 5$ , etc.

With Bohr's postulates, it can be shown that from conservation of energy and angular momentum the electron energy is given by

$$E_n = -\frac{1}{n^2} \cdot \frac{(2\pi)^2 k^2 q^4 m}{2h^2} = -\frac{1}{n^2} \times 13.58 \text{ eV},$$

where  $q$  and  $m$  are the electron charge and mass respectively, and  $k = 2\pi/\lambda$  with  $\lambda$  the wavelength. For  $n = 1$ ,  $E_1 = -13.58 \text{ eV}$  in agreement with the ionisation energy of the hydrogen atom. Higher lying energy states are then given by [8]

$$E_n = -\frac{E_1}{4}, -\frac{E_1}{9}, -\frac{E_1}{16}, \dots \text{ etc.}$$

with  $E_1 = -13.58 \text{ eV}$ . The energy levels are shown in Fig. 1.6. From the energy levels, the frequencies of the emissions (and absorptions) can be calculated. Bohr showed that for  $n = 3$ , he could reproduce the Balmer series of frequencies. For other values of  $n$  (1, 2, 4 etc.) Bohr predicted other series of frequencies not known at the time. Following Bohr's prediction, these series were also found providing a spectacular success for the theory.

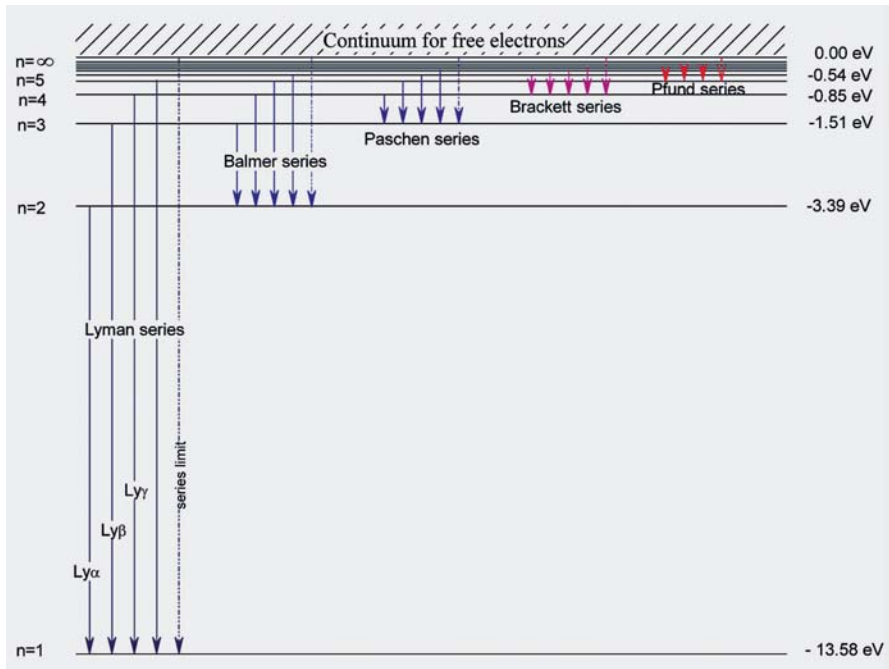


Fig. 1.6. Energy states of electrons in the hydrogen atom [8]

### Sommerfeld's Extension of the Bohr Theory

In 1916, Sommerfeld extended Bohr's circular orbits, with the main or principal quantum number  $n$ , to elliptical orbits with an "azimuthal" quantum number  $l$ . Shortly later the magnetic quantum number was introduced to account for the effects of magnetic fields. These three quantum numbers  $n, l, m$ , can be regarded as giving the size, shape, and spatial orientation of the orbits.

**Table 1.2.** Characterisation of orbits in Bohr-Sommerfeld model

$l$	0	1	2	3
<b>Orbital</b>	$s$	$p$	$d$	$f$

These elliptical orbits, including the circular orbit, for one quantum number  $n$  have the same length of the major axes and with this the same energy levels, but different lengths of the minor axes. Different proportions between the major axes and minor axes (i.e. the eccentricity of the elliptical orbit) show different azimuthal quantum numbers  $l$ . The number of different quantum numbers  $l$  depends on the main quantum number through the relation  $l_{\max} = n - 1$ . The different  $l$  numbers characterise the different orbitals as shown in Table 1.2. This model is shown schematically in Fig. 1.7.

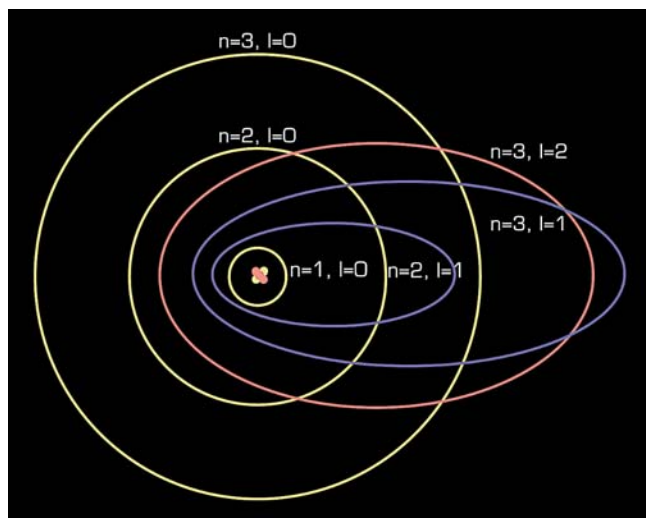


**Fig. 1.7.**  
Bohr-Sommerfeld  
model of the atom [5]

In general, the number of orbitals with the same azimuthal quantum number  $l$  is given through the expression  $2l + 1$ . Each of these orbits is characterised by the orbital magnetic moment  $m_l$ , where  $m_l$  has the values  $l, l - 1, l - 2, \dots, -l + 1, -l$ . The results are summarised in Table 1.3.

**Table 1.3.** Number and orbital angular momentum of orbits for a given quantum number  $l$ 

$l$	0	1	2	3
<b>Number of orbitals</b>	1	3	5	7
$m_l$	0	1, 0, -1	2, 1, 0, -1, -2	3, 2, 1, 0, -1, -2, -3

**Fig. 1.8.** Image of Niels Bohr (1885–1962) on a Danish stamp

To explain the very fine structure of atomic lines, it was necessary to postulate that an orbital electron can spin in one of two directions about its own axis in the same way that the earth spins about its axis as it orbits the sun. The associated spin magnetic momentum  $m_s$  can take one of two values,  $+\frac{1}{2}$  and  $-\frac{1}{2}$ , with the condition, that the two electrons in one orbital have different spins.

The total magnetic moment, the quantum number  $m$ , is the sum of the orbital magnetic moment  $m_l$  and spin magnetic moment  $m_s$ . The magnetic moment may be positive or negative depending on the direction of the orbital motion. When the atoms of a substance are placed in a magnetic field, the electrons will arrange themselves in definite directions with respect to the applied field.

With the Bohr-Sommerfeld atomic model, all elements of the periodic table can be categorised with these four quantum numbers  $n$ ,  $l$ ,  $m_l$  and  $m_s$ .

## The Neutron

The second difficulty of Rutherford's model of the atom was to explain how the protons can be held together in view of the strong repulsive forces of the positively charged particles. Hydrogen, the simplest atom, consists of a single proton in the nucleus. If heavier nuclei contained multiple protons, then the mass number and the atomic numbers should be the same. This was not the case. The mass numbers were found to be approximately twice the atomic number for light nuclei. Similarly, the Coulombic repulsion of these multiple proton nuclei would be enormous – what can hold the nuclei together?

These difficulties were resolved by the discovery of the neutron by Chadwick in 1932. Its presence in the nucleus explains the difference between the atomic and mass numbers. More importantly, the neutron is responsible for the cohesive force that holds the nucleus together. This *nuclear force* is attractive and extremely short range – about  $2-3 \times 10^{-15}$  m.





**Fig. 1.9.** James Chadwick (1891–1974). © 1999 Awards of Outstanding International Importance to Statesmen and Heroines

Because of the very short range of the nuclear force, neutrons can only interact with their nearest neighbour nucleons, in contrast to the longer-range repulsive electrical forces of the protons. For this reason, in a stable nucleus, the number of neutrons must increase more rapidly than the number of protons. The discovery of the neutron also explained the existence of isotopes discovered in 1913 by Soddy for radioactive elements.

In addition to the proton, neutron, and electron, there are considerably more than 100 other fundamental particles which have been discovered or hypothesized. The majority of these fall into one of two classes, leptons (consisting of electrons, muons, and neutrinos) or hadrons (e.g. protons and neutrons). According to the Standard Model (see Glossary), these elementary particles can be grouped in a similar manner to chemical elements in the periodic table. From

these groupings, it has been proposed that hadrons are composed of three (or possibly more) simpler components called *quarks*, and that these quarks are “glued” together by gluons which carry the strong nuclear force.

## Wave/Particle Duality: The de Broglie Relation and Wave Mechanics

The Bohr theory introduced the idea of characterising the states of electrons with integers (the quantum numbers). It is also known that integers are used in many branches of physics involving waves to characterise standing waves, interference, resonance etc. This is one of many considerations which led Louis de Broglie to postulate in 1924 the wave/particle duality expressed in his formula

$$\lambda = h/p,$$

where  $h$  is Planck’s constant described in the previous section. This relation expresses the fact that associated with any particle is a wave of wavelength  $\lambda$  which depends on the momentum  $p$  of that particle. The remarkable aspect about this relation is that when applied to electrons in the atom, due to the wave characteristics of the electron, the quantisation rules emerge naturally. The stable orbits are those in which the circumference is an integral number of wavelengths. The relation postulated by de Broglie in 1924 was verified experimentally for electrons by Davisson, Germer, and Thomson in 1927. The wave properties of atoms were demonstrated much later in 1991.

Shortly after this postulation of de Broglie, Schrödinger introduced his “wave mechanics” to characterise the de Broglie waves in 1926. Starting from the wave equation  $\nabla^2\psi + k^2\psi = 0$  where  $k = 2\pi/\lambda$ , Schrödinger replaced the wavelength by the de Broglie relation  $\lambda = h/mv$ . The wave amplitude or wave function is then given by

$$\nabla^2 \Psi + \left( \frac{4\pi^2 m^2 v^2}{h^2} \right) \Psi = 0.$$

Since the total energy of the particle  $E = \frac{1}{2}mv^2 + V$ , it follows that  $mv^2 = 2(E - V)$  and substituting in the above relation leads to

$$\nabla^2 \Psi + \left( \frac{8\pi^2 m}{h^2} \right) (E - V) \Psi = 0,$$

which is known as the Schrödinger equation. To satisfy standard boundary conditions, this equations has solutions  $\Psi$  only for particular values of the energy  $E$ . It follows that energy quantisation and the three quantum numbers follow naturally, rather than just a postulate as in Bohr's theory. The functions  $\Psi$  are also called "orbitals" to contrast with the classical orbits describing well defined trajectories. Based on de Broglie's wave/particle relation, Schrödinger considered the wave function as a physically real property of electrons.

A completely different interpretation of the wave function, which quickly gained widespread acceptance by leading physicists, was introduced by Max Born in 1926. The real novelty in his interpretation was the introduction of a probabilistic interpretation of the wave function. This was to be a subject of great controversy for many years later.

As stated above, the solution to Schrödinger's wave equation provides the quantum numbers  $n$ ,  $l$ , and  $m$ . The possible values up to  $n = 4$  (a given value of  $n$  is referred to as a shell) are given in Table 1.4.

**Table 1.4.** Possible values of the quantum numbers  $n$ ,  $l$ ,  $m$  and spectroscopic notation [1]

Shell	$n$	$l$	Orbital	$m$	Electrons in orbital	
					Max. no.	Total no.
$K$	1	0	$s$	0	2	2
$L$	2	0	$s$	0	2	8
		1	$p$	$0, \pm 1$	6	
$M$	3	0	$s$	0	2	18
		1	$p$	$0, \pm 1$	6	
		2	$d$	$0, \pm 1, \pm 2$	10	
$N$	4	0	$s$	0	2	32
		1	$p$	$0, \pm 1$	6	
		2	$d$	$0, \pm 1, \pm 2$	10	
		3	$f$	$0, \pm 1, \pm 2, \pm 3$	14	

In addition to the three quantum numbers  $n$ ,  $l$ ,  $m$ , the spin quantum number has to be added to account for the rotational motion about themselves. Finally the filling of orbital by electrons is shown Table 1.5. Arrows indicate spin and anti-parallel spin. It is then straightforward to obtain the maximum number of electrons in each shell.

This filling procedure then provides the key to classification of the elements in the periodic table.

**Table 1.5.** Filling of orbitals by electrons [1]

	1s	2s	2p <sub>x</sub>	2p <sub>y</sub>	2p <sub>z</sub>	
H	↑					1s
He	↑↓					1s <sup>2</sup>
Li	↑↓	↑				1s <sup>2</sup> 2s
Be	↑↓	↑↓				1s <sup>2</sup> 2s <sup>2</sup>
B	↑↓	↑↓	↑			1s <sup>2</sup> 2s <sup>2</sup> 2p
C	↑↓	↑↓	↑	↑		1s <sup>2</sup> 2s <sup>2</sup> 2p <sup>2</sup>
N	↑↓	↑↓	↑	↑	↑	1s <sup>2</sup> 2s <sup>2</sup> 2p <sup>3</sup>
O	↑↓	↑↓	↑↓	↑	↑	1s <sup>2</sup> 2s <sup>2</sup> 2p <sup>4</sup>
F	↑↓	↑↓	↑↓	↑↓	↑	1s <sup>2</sup> 2s <sup>2</sup> 2p <sup>5</sup>
Ne	↑↓	↑↓	↑↓	↑↓	↑↓	1s <sup>2</sup> 2s <sup>2</sup> 2p <sup>6</sup>

## Classification of the Elements

Until recently, there were 114 known chemical elements. Very recently, evidence for the existence of two new superheavy elements has been reported. Each element is characterised by atoms containing a fixed number of protons, denoted by the atomic number  $Z$ , in the nucleus and an equal number of orbital electrons to ensure electrical neutrality. In addition to protons, the nucleus contains a variable number  $N$  of electrically neutral neutrons. Atoms of an element with different numbers of neutrons but fixed number of protons are known as isotopes of that element (see inset). More than 3000 nuclides are known, but only about 10% of these are stable. The total number of protons plus neutrons is known as the mass number  $A$  of a nuclide. Nuclides with the same  $N$  and different  $Z$  are called isotones, and nuclides with the same mass number  $A$  are known as isobars. In general, an atom with atomic number  $Z$ , and neutron number  $N$  is known as a nuclide. A nuclide can be specified by the notation:

$${}^A_Z\text{X}_N,$$

where  $Z$  is the atomic (proton) number,  $N$  is the neutron number,  $A$  is the mass number ( $N + Z$ ), and  $X$  is the chemical element symbol.

Because of the relationships between  $Z$ ,  $A$ ,  $N$  ( $A = Z + N$ ) and  $X$ , a nuclide can be uniquely specified by fewer parameters. A particular chemical element is uniquely specified by its symbol  $X$  or the proton number  $Z$ . A nuclide is uniquely specified by the element name  $X$  (or proton number  $Z$ ) together with the mass number  $A$ . An example is <sup>60</sup>Co which refers to the element cobalt (chemical symbol Co) with mass number 60 (number of protons plus neutrons). A variety of ways of referring to this nuclide are in current use i.e. Co60, Co-60, Co 60, <sup>60</sup>Co, and cobalt-60.

**Nuclide,  ${}^A_Z\text{X}$** 

Refers to a particular atom or nucleus with a specific number  $N$  of neutrons and number  $Z$  of protons.  $A$  is the mass number ( $= Z + N$ ). Nuclides are either stable or radioactive. Radioactive nuclides are referred to as radionuclides.

**Atomic Number,  $Z$** 

The number of positively charged protons in the nucleus of an atom.

**Neutron Number,  $N$** 

The number of neutrons in the nucleus of an atom.

**Isotope**

One of two or more atoms of the same element that have the same number of protons (isotope) in their nucleus but different numbers of neutrons. Hydrogen  ${}^1_0\text{H}$ , deuterium  ${}^2_1\text{H}$ , and tritium  ${}^3_1\text{H}$ , are isotopes of hydrogen. Radioactive isotopes are referred to as radioisotopes.

**Isotone**

One of several different nuclides having the same number of neutrons (isotone) in their nuclei.

**Isobar**

Nuclides with the same atomic mass number  $A (= Z + N)$  but with different values of  $N$  and  $Z$  e.g.  ${}^{14}\text{B}$ ,  ${}^{14}\text{C}$ ,  ${}^{14}\text{N}$ .

**Isomer**

Atoms with the same atomic number  $Z$  and the same mass number  $A$  in different long-lived states of excitation – the higher states being metastable with respect to the ground state. For example, an isomer of  ${}^{99}\text{Tc}$  is  ${}^{99\text{m}}\text{Tc}$  where the m denotes the long-lived excited state.

## Synthesis of the Elements in Nature

The distribution of elements in nature is by no means uniform. Studies of stars reveal that hydrogen is by far the most abundant element, accounting for approximately 75% of the mass of the universe. The remaining mass is mostly in the form of helium gas with other elements contributing only to a small extent.

The hydrogen in the universe is the driving fuel for continuous change in the chemical composition. Hydrogen is being converted to helium, which is further changed into heavier elements.

The observed abundances of elements in the universe require the postulation of at least eight different processes for their formation [9]. The main processes are:

- hydrogen burning (formation of helium-4 by the fusion of hydrogen nuclei),
- helium burning (formation of carbon-12 from helium-4-nuclei),
- s processes (slow neutron capture processes, starting from iron group nuclei, close to the stability line – see section “Nuclide Charts”, Chapter 2),

- r processes (rapid neutron capture processes, starting from iron group nuclei, produce nuclei far from the line of stability),
- rp processes (similar to the r-processes, but involve successive proton absorptions),
- X processes (spallation of heavier elements into lighter elements by cosmic rays).

Light elements were probably produced in the early history of the galaxy whereas heavy elements were formed in supernovae.

According to current theory, the universe is about  $10^{10}$  years old and started as a “soup” of quarks at enormous temperatures and pressures. As the universe expanded, the temperature and pressure decreased rapidly to the point where neutrons and protons condensed out. Shortly after, nuclear fusion took place and led to the formation of deuterons followed by tritons and onto helium-3 nuclei and alpha particles (hydrogen burning), thereby giving rise to the present hydrogen to helium ratio of 3:1. In addition, some lithium-6 and lithium-7 were produced at this time. As the universe further expanded and cooled, the fusion reactions stopped and the gases condensed and eventually led to the formation of stars consisting of the primordial elements.

As a cloud of interstellar gas contracts and condenses to form a star, the temperature will rise as the gravitational potential energy is converted to kinetic energy. When the temperature increases to  $10^7$  K and beyond, fusion reactions will begin to take place and further nucleosynthesis leads to the conversion of the elements hydrogen and helium to carbon, silicon, oxygen, sulphur and heavier elements up to iron. Fusion can proceed no further than iron since this element has the high-

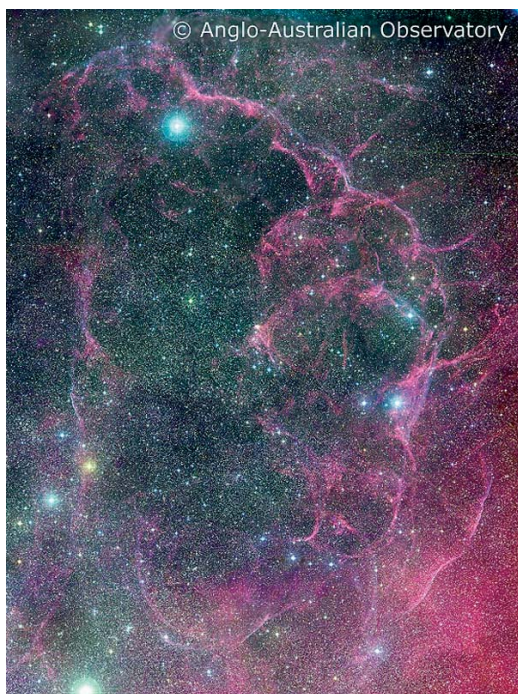


**Fig. 1.10.** Vela supernova remnant. © Anglo-Australian Observatory, photo from UK Schmidt, plates by David Malin

est binding energy. Fusion of heavier elements will consume energy rather than release it.

The synthesis of elements heavier than iron require a supernova. As stated above, the sequence of stellar burning more or less stops when the core of the star is composed of nuclei with mass numbers close to 56 (i.e. iron). At this point the central region of the star has consumed all the nuclear fuel and cannot support the star's interior against gravitational collapse into a neutron star. In this process all protons are converted into neutrons with the release of a large number of neutrinos within a short time. These neutrinos interact with the outer layers of the star resulting in a large fraction of the mass being ejected into space. In addition, large numbers of particles are produced, in particular neutrons. It is then these neutrons, which lead to the formation of heavier elements by transmutation through r(rapid)-process neutron capture events.

At least 24 elements are believed essential to living matter. The most abundant of these in the human body are, in order of importance: hydrogen, oxygen, carbon, nitrogen, calcium, phosphorus, chlorine, potassium, sulphur, sodium, magnesium, iron, copper, zinc, silicon, iodine, cobalt, manganese, molybdenum, fluorine, tin, chromium, selenium, and vanadium.

Ninety-one elements occur naturally on earth supporting the theory that heavy elements were produced during creation of the solar system. Exceptions are technetium and promethium although these are present in stars.

In the following chapter, the properties of nuclides and their constituents are described in more detail.

## 2. Nuclear Energetics

### Nuclear Units – Atomic Mass Unit and the Electron Volt

Most units used in nuclear science are based on the International System of Units or SI units (from the French “Système International d’Unités”) [1]. The base SI units are the metre (length), kilogram (mass), second (time), ampere (electric current), kelvin (temperature), candela (luminous intensity), and the mole (quantity of substance). In nuclear science, in addition to SI, two units are commonly used for mass and energy i.e. the atomic mass unit and the electron volt.

#### Mass – The Atomic Mass Unit

Masses of atomic nuclei are generally less than  $10^{-21}$  g. For this reason, it is more convenient to express the masses in so-called *atomic mass units* [2]. The atomic mass unit (abbreviated as amu or u) is defined such that the mass of a  $^{12}\text{C}$  atom is exactly 12 u. Hence,

$$1 \text{ u} = 1.6605387 \times 10^{-27} \text{ kg}.$$

#### Energy – The Electron Volt

Energies released in chemical reactions are of the order of  $10^{-19}$  J. For such reactions, it is more convenient to use the energy unit *electron volt*, eV. By definition, the electron volt is the kinetic energy gained by an electron after acceleration through a potential difference  $\Delta V$  of one volt. This kinetic energy increase of  $e\Delta V = (1.60217646 \times 10^{-19} \text{ C}) \cdot (1 \text{ V}) = 1.60217646 \times 10^{-19} \text{ J}$ . Hence

$$1 \text{ eV} = 1.60217646 \times 10^{-19} \text{ J}.$$

The energy equivalent of the atomic mass unit is

$$E = mc^2 = 931.494013 \text{ MeV}.$$

### Nuclear and Atomic Masses

Tables of masses always give *atomic* rather than *nuclear* masses. This implies that the masses given include the extra-nuclear electrons. Atomic masses are more convenient than nuclear masses since it is always atomic masses or differences between atomic

masses that are measured experimentally. This distinction is reflected in the notation used in this book: rest mass of an *atom* is denoted by  $M({}_Z^AX)$  whereas the rest mass of the *nucleus* is denoted by  $m({}_Z^AX)$ .

#### **Notation on Masses**

- rest mass of an *atom* is denoted by  $M({}_Z^AX)$
- rest mass of the *nucleus* is denoted by  $m({}_Z^AX)$

According to the above notation, the electron, neutron, and proton masses are  $m({}_{-1}^0e)$ ,  $m({}_0^1n)$ ,  $m({}_1^1H)$  respectively. For convenience, however, the notation here is simplified to  $m_e$ ,  $m_n$ ,  $m_p$ . Since combining  $Z$  electrons with the nucleus forms a neutral atom, the atomic and nuclear masses are related by

$$M({}_Z^AX) = m({}_Z^AX) + Zm_e - \frac{BE_{Ze}}{c^2},$$

where  $BE_{Ze}$  is the energy released upon binding with the nucleus. The mass change corresponding to the electron binding energy in the above relation ( $BE_{Ze}/c^2$  for hydrogen is approximately  $10^{-8}$  u) is negligible compared to the mass of the atom (hydrogen mass is about 1 u) and also the electron (about  $5.5 \times 10^{-4}$  u), such that, to a good approximation [3]

$$M({}_Z^AX) \cong m({}_Z^AX) + Zm_e.$$

## **Atomic and Molecular Weights**

The atomic weight  $\mathcal{A}$  of an atom is the ratio of the atom's mass to 1/12th of the mass of an atom of  $^{12}\text{C}$  in its ground state [3, 4]. The molecular weight of a molecule is the ratio of the molecular mass of one molecule to 1/12th of the mass of one atom of  $^{12}\text{C}$ . Both the atomic and molecular weights are dimensionless. It follows that the mass of an atom measured in atomic mass units is numerically equal to the atomic weight of that atom. The atomic mass (in u) and hence the atomic weight of a nuclide is almost equal to the atomic mass number  $A (= Z + N)$  such that  $\mathcal{A} \cong A$ .

Most naturally occurring elements consists of two or more isotopes. The isotopic abundance  $a_i$  is defined as the relative number of atoms of a particular isotope in a mixture of the isotopes of a chemical element, expressed as a fraction of all the atoms of the element. The *elemental atomic weight*  $\mathcal{A}$  is the weighted average of the atomic weights  $\mathcal{A}_i$  of the naturally occurring isotopes of the elements, weighted by the isotopic abundance  $a_i$  of each isotope i.e.

$$\mathcal{A} = \sum_i \frac{a_i}{100} \mathcal{A}_i.$$



**Atomic Weight of Magnesium**

Naturally occurring magnesium consists of three stable isotopes –  $^{24}\text{Mg}$ ,  $^{25}\text{Mg}$ ,  $^{26}\text{Mg}$  – with isotopic abundances 78.99, 10, and 11.01 atom-percent respectively. The atomic weights are 23.985041700 ( $^{24}\text{Mg}$ ), 24.98583692 ( $^{25}\text{Mg}$ ), and 25.982592929 ( $^{26}\text{Mg}$ ).

The atomic weight of magnesium  $\mathcal{A}_{\text{Mg}}$  is then:

$$\begin{aligned}\mathcal{A}_{\text{Mg}} &= \frac{a_{24}\mathcal{A}_{24} + a_{25}\mathcal{A}_{25} + a_{26}\mathcal{A}_{26}}{100} \\ &= (0.7899 \times 23.985042) + (0.1 \times 24.985837) + (0.1101 \times 25.982593) \\ &= 24.3050\end{aligned}$$

**Avogadro's Number**

A mole of a substance is defined to contain as many “elementary particles” as there are atoms in 12 g of  $^{12}\text{C}$  and is equal to  $6.0221415 \times 10^{23}$  (2002 CODATA recommended value). This number is known as Avogadro's number  $N_a$ . The mass in grams of a substance that equals the dimensionless atomic or molecular weight is called the gram atomic weight or the gram molecular weight. Hence one gram atomic weight of a substance represents one mole and contains  $N_a$  atoms or molecules.

**Basic Relation between Mass and Number of Atoms**

Consider a substance of mass  $\mathcal{M}$  (in grams). This mass corresponds to  $\mathcal{M}/\mathcal{A}$  moles and therefore contains  $(\mathcal{M}/\mathcal{A}) \cdot N_a$  atoms. Hence the basic relation between the *number of atoms* and the *mass of a substance* is given by:

$$N = \frac{\mathcal{M}}{\mathcal{A}} \cdot N_a.$$

Calculations usually involve an initial mass or an activity of a parent nuclide. The first step is then to convert this mass to a number of atoms,  $N$ , before the solutions to the decay equations is evaluated, for example.

The activity,  $A$ , is defined by  $A = kN$  where  $k$  is the decay constant  $\ln 2/\tau$  (s). Given an activity, the number of atoms is given by

$$N = \frac{A}{k} = A \cdot \frac{\tau(\text{s})}{\ln 2}$$

where  $\tau$  (s) is the half-life in seconds. The relationship between the mass and the activity is given by

$$A \cdot \frac{\tau(\text{s})}{\ln 2} = \frac{\mathcal{M}}{\mathcal{A}} \cdot N_a$$

from which it follows

$$A = \frac{\ln 2}{\tau(\text{s})} \cdot \frac{\mathcal{M}}{\mathcal{A}} \cdot N_a$$

or

$$\mathcal{M} = A \cdot \left[ \frac{\mathcal{A}}{N_a} \right] \cdot \frac{\tau(\text{s})}{\ln 2}$$

## Mass of an Atom and Atomic Number Density

With Avogadro's number, the mass of an individual atom can be evaluated. One mole of a substance, with mass of  $\mathcal{A}$  grams, contains  $N_a$  atoms. Hence, the mass of an individual atom is

$$M = \frac{\mathcal{A}}{N_a} \cong \frac{A}{N_a}$$

where the atomic weight has been approximated by the atomic mass number. That this approximation is good can be seen for the case of  $^{208}\text{Pb}$ :

Approximate relation  $M \cong A/N_a$

$$M(^{208}\text{Pb}) \cong \frac{208 \text{ g}}{6.022142 \times 10^{23}} = 3.4539 \times 10^{-22} \text{ g}.$$

Exact relation  $M = \mathcal{A}/N_a$

$$M(^{208}\text{Pb}) = \frac{207.976652 \text{ g}}{6.022142 \times 10^{23}} = 3.4535 \times 10^{-22} \text{ g}.$$

Atomic masses are expressed in atomic mass units (u), based on the definition that the mass of a neutral atom of  $^{12}\text{C}$  is exactly 12 u. All other nuclides are assigned masses relative to  $^{12}\text{C}$ . The mass of a single atom can be computed from the fact that one mole of any substance contains  $6.0221415 \times 10^{23}$  atoms and has a mass equal to the atomic mass in grams. For  $^{12}\text{C}$ , 1 mole has a mass of 12 g, hence the mass of one atom is given by:

$$M(^{12}\text{C}) = \frac{12 \text{ g}}{6.0221415 \times 10^{23}} = 1.992647 \times 10^{-23} \text{ g}.$$

The atomic mass unit, u (also known as a dalton) is then

$$1 \text{ u} = \frac{1.992647 \times 10^{-23} \text{ g}}{12} = 1.660539 \times 10^{-24} \text{ g}.$$

The energy equivalent of 1 u is  $E = mc^2 = 931.494013 \text{ MeV}$ .

## Atomic Number Density

A useful quantity in many calculations is the number density of atoms. By analogy with the basic relation between the mass and number of atoms,  $N = (\mathcal{M}/\mathcal{A}) \cdot N_a$ , the relation for the number density is given by

$$N(\text{atoms cm}^{-3}) = \frac{\rho}{\mathcal{A}} \cdot N_a$$

where  $\rho$  is the mass density (in  $\text{g cm}^{-3}$ ).

## Relativistic Mechanics and Einstein's Mass/Energy Equivalence

The fundamental relation describing motion is that the force acting on a body will result in a change of momentum i.e.

$$\mathbf{F} = \frac{d\mathbf{p}}{dt},$$

where  $\mathbf{p}$  is the linear momentum  $m\mathbf{v}$  and  $\mathbf{F}$  the force. The quantities  $\mathbf{F}$ ,  $\mathbf{p}$ , and  $\mathbf{v}$  are all vectors. In classical mechanics, the mass of a body is constant, and the above relation reduces to  $\mathbf{F} = m d\mathbf{v}/dt = m\mathbf{a}$ , the more familiar form of Newton's second law. In relativistic mechanics, the mass of a body changes with its speed  $v$  such that

$$\mathbf{F} = \frac{d}{dt}m\mathbf{v} = m \frac{d\mathbf{v}}{dt} + v \frac{dm}{dt}.$$

From conservation of energy, the work done on a particle as it moves along a path of length  $s$  must equal the change in the kinetic energy  $\Delta KE$  from the beginning to the end of the path. The work done by the force  $\mathbf{F}$  on the particle as it moves through a displacement  $ds$  is given by  $\mathbf{F} \cdot ds$ . The resulting change in the kinetic energy is then given by [3]

$$\Delta KE = \int_0^s \mathbf{F} \cdot ds = \int_0^s \frac{d\mathbf{p}}{dt} \cdot ds = \int_0^t \frac{d\mathbf{p}}{dt} \cdot \frac{ds}{dt} \cdot dt = \int_0^{mv} \mathbf{v} \cdot d\mathbf{p},$$

where it is assumed that initially the particle is at rest  $v = 0$ . Using the expression for the relativistic mass

$$m = \frac{m_0}{(1 - v^2/c^2)^{1/2}}$$

and substituting in the relation for the change in kinetic energy gives

$$\Delta KE = m_0 \int_0^v v d \left[ \frac{v}{(1 - v^2/c^2)^{1/2}} \right].$$

Differentiation of the term in square brackets leads to

$$\begin{aligned} \Delta KE &= m_0 \int_0^v v \left[ \frac{1}{(1 - v^2/c^2)^{1/2}} + \frac{v^2/c^2}{(1 - v^2/c^2)^{3/2}} \right] dv \\ &= m_0 \int_0^v \frac{v}{(1 - v^2/c^2)^{3/2}} dv = m_0 c^2 \frac{1}{(1 - v^2/c^2)^{1/2}} \Big|_0^v \\ &= \frac{m_0 c^2}{(1 - v^2/c^2)^{1/2}} - m_0 c^2 \end{aligned}$$

and finally,

$$\Delta KE = mc^2 - m_0 c^2.$$

This last expression can be rewritten in the form  $mc^2 = m_0 c^2 + \Delta KE$ . The left hand side  $mc^2$  can be regarded as the total energy of the particle consisting of the rest-mass energy  $m_0 c^2$  plus the kinetic energy of the particle. This expression for the total energy  $E$ , i.e.  $E = mc^2$  shows the equivalence of mass and energy and one of

**The energy equivalent of the rest mass of an electron is**

$$E = m_e c^2 = (5.486 \times 10^{-4} \text{ u}) \times \frac{931.49 \text{ MeV}}{\text{u}} = 0.511 \text{ MeV}.$$

An interesting example is the direct conversion of mass to energy is the electron/positron annihilation  $m_{e^-} + m_{e^+} \rightarrow 2\gamma$  in which the gamma photon each has an energy of 0.511 MeV.

**The energy equivalent of 1 amu is**

$$E = m_{\text{amu}} c^2 = (1 \text{ u}) \times \frac{931.49 \text{ MeV}}{\text{u}} = 931.49 \text{ MeV}.$$

**The energy equivalent of the rest mass of a proton is**

$$E = m_p c^2 = (1.007276 \text{ u}) \times \frac{931.49 \text{ MeV}}{\text{u}} \cong 1 \text{ GeV}.$$

the most important expressions in nuclear physics. It will be seen later that in nuclear reactions, the mass is converted into energy and vice versa. Conversion of even small amounts of mass gives rise to considerable energies.

## Binding Energy of the Nucleus

The binding energy,  $BE$ , of a nucleus is the energy which must be supplied to separate the nucleus into its constituent component nucleons. The sum of the masses of the constituents,  $m_c$ , of an isotope  ${}^A_Z X$  is given by

$$m_c = Zm_p + (A - Z)m_n,$$

where  $Z$  is the atomic number,  $A$  is the atomic mass number (number of nucleons in the nucleus),  $m_p$  is the mass of a proton atom and  $m_n$  is the mass of the neutron.

### Mass Defect

The mass defect is the difference between the mass of the constituents  $m_c$  and the actual mass of the nucleus  $m({}^A_Z X)$ , i.e.

$$\text{mass defect} = m_c - m({}^A_Z X) = Zm_p + (A - Z)m_n - m({}^A_Z X) = \frac{BE}{c^2},$$

where  $BE$  is the binding energy of the nucleus and the mass defect is equivalent of the energy required (i.e.  $BE/c^2$ ) to separate the components. It should be noted that the above expression for the mass defect involves the nuclear mass  $m({}^A_Z X)$ . Since only atomic masses are available, the above relation should be expressed in atomic masses, i.e.

$$\begin{aligned} \text{mass defect} = \frac{BE}{c^2} &= Z \left[ M({}^1_1\text{H}) - m_e + \frac{BE_{1e}}{c^2} \right] + (A - Z)m_n \\ &\quad - \left[ M({}^A_Z X) - Zm_e + \frac{BE_{Ze}}{c^2} \right] \end{aligned}$$

or

**Mass Defect and Binding Energy of  $^{17}_8\text{O}$**

Using the atomic mass data in Appendix D, the mass defect is given by

$$\begin{aligned} \text{mass defect} &= \frac{BE}{c^2} = 8M(^1_1\text{H}) + 9m_n - M(^{17}_8\text{O}) \\ &= 8(1.0078250) + 9(1.0086649) - 16.9991317 = 0.1414524 \text{ u} . \end{aligned}$$

In energy units, the binding energy  $BE$  is given by

$$BE = \text{mass defect} \times \frac{931.5 \text{ MeV}}{\text{u}} \approx 131.76 \text{ MeV} .$$

The average binding energy per nucleon  $\langle BE \rangle = BE/A$  is then

$$\langle BE \rangle = \frac{131.76}{17} = 7.75 \text{ MeV per nucleon} .$$

$$\text{mass defect} = \frac{BE}{c^2} = ZM(^1_1\text{H}) + (A - Z)m_n - M(^A_Z\text{X}) + \frac{1}{c^2} [ZBE_{1e} - BE_{Ze}] .$$

The last term,  $[ZBE_{1e} - BE_{Ze}]$ , is the difference between the binding energies of  $Z$  hydrogen electrons and the  $Z$  electrons in the atom  $^A_Z\text{X}$ . It is orders of magnitude less than nuclear binding energies and hence to a very good approximation

$$BE(^A_Z\text{X}) \cong [ZM(^1_1\text{H}) + (A - Z)m_n - M(^A_Z\text{X})]c^2 .$$

A plot of the binding energy per nucleon versus the atomic mass number shows a broad maximum in excess of 8 MeV per nucleon between mass numbers 50–100. The two dimensional plot is shown in Fig. 2.1. At lower and higher mass numbers,

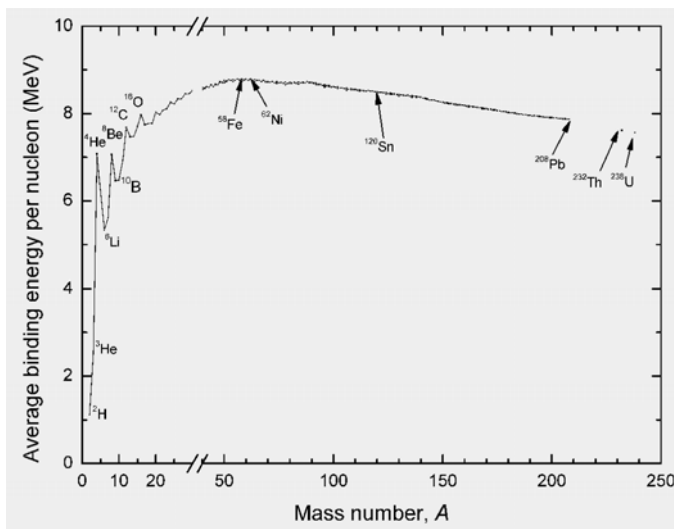


**Fig. 2.1.** Average binding energy per nucleon versus mass number for stable nuclides

the binding energy per nucleon is less. It is for this reason that energy can be released by splitting heavy elements or by fusing light elements.

Notable departures from the smooth behaviour of the binding energy per nucleon vs. the mass number are provided by  ${}^4\text{He}$ ,  ${}^{12}\text{C}$ ,  ${}^{16}\text{O}$ . The binding energies per nucleon of these isotopes are higher than their immediate neighbours indicating that they are very strongly bound. These nuclei contain respectively one, three, and four sub-units of  ${}^4\text{He}$ . This tends to suggest that nucleons form stable sub-groups of two protons and two neutrons within the nucleus.

### Mass Excess

The atomic masses are often described in terms of the mass excess  $ME$  defined by

$$ME({}_Z^AX) = M({}_Z^AX) - A,$$

where the masses are expressed in atomic mass units (u). Hence, knowing the mass excess, the mass of any nuclide can be derived. Consider the example of  ${}^{238}\text{U}$ . In the Nuclides.net database [5], the mass excess is given in units of keV, i.e.  $ME({}^{238}\text{U}) = 47308.9 \text{ keV}$ . In a first step, this must be converted to atomic mass units using  $1 \text{ u} = 931.494013 \text{ MeV}/c^2$  (see Appendix A), hence

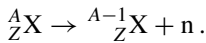
$$ME({}^{238}\text{U}) = 0.0507882 \text{ u}.$$

The mass of  ${}^{238}\text{U}$  is then given by

$$M({}^{238}\text{U}) = ME({}_Z^AX) + A = 0.0507882 \text{ u} + 238 \text{ u} = 238.0507882 \text{ u}.$$

### Nucleon Separation Energy

Another useful quantity, in addition to the binding energy, is the nucleon separation energy. Whereas the binding energy is the energy required to separate the nucleus into its constituent component nucleons, the nucleon separation is the energy required to remove a single nucleon from the nucleus according to the reaction i.e. (for a neutron removal):



The energy required to remove this neutron, denoted  $S_n({}_Z^AX)$ , is given by:

$$S_n({}_Z^AX) = [m({}_Z^{A-1}X) + m_n - m({}_Z^AX)]c^2$$

or

$$S_n({}_Z^AX) \cong [M({}_Z^{A-1}X) + m_n - M({}_Z^AX)]c^2.$$

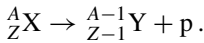
Using the relation derived earlier for the binding energy i.e.

$$BE({}_Z^AX) \cong [ZM({}_1^1\text{H}) + (A - Z)m_n - M({}_Z^AX)]c^2,$$

the neutron separation energy can also be expressed as

$$S_n({}^A_ZX) = [BE({}^A_ZX) - BE({}^{A-1}_ZX)]c^2.$$

Similarly, the energy required to remove a single proton from the nucleus according to the reaction



The energy required to remove this proton, denoted  $S_p({}^A_ZX)$ , is given by:

$$S_p({}^A_ZX) = [m({}^{A-1}_{Z-1}Y) + m_p - m({}^A_ZX)]c^2$$

or

$$S_p({}^A_ZX) \cong [M({}^{A-1}_{Z-1}Y) + M({}^1_1H) - M({}^A_ZX)]c^2.$$

Again using the relation for the binding energy, this can also be expressed as

$$S_p({}^A_ZX) = [BE({}^A_ZX) - BE({}^{A-1}_{Z-1}Y)]c^2.$$

**Table 2.1.** Comparison of the binding energy per nucleon ( $BE/A$ ) with the neutron and proton separation energies for selected nuclides

Nuclide	$BE/A$ (MeV)	$S_n$ (MeV)	$S_p$ (MeV)
${}^{16}_8\text{O}$	7.98	15.66	12.13
${}^{129}_{53}\text{I}$	8.44	8.83	6.80
${}^{99}_{43}\text{Tc}$	8.61	8.97	6.50

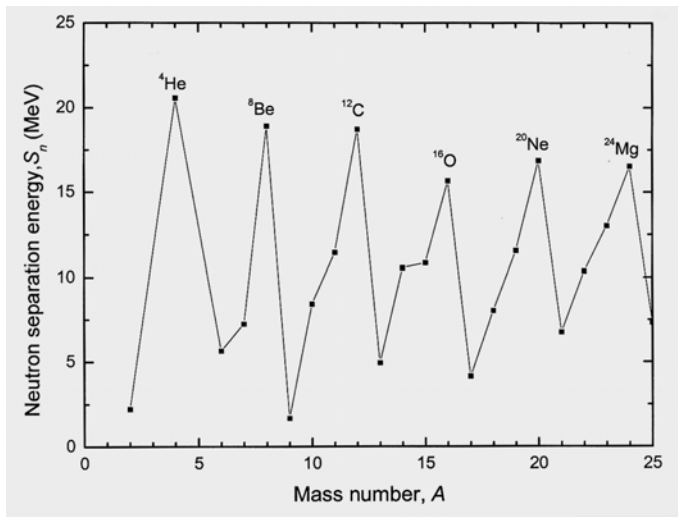


**Fig. 2.2.** The neutron separation energy as a function of the mass number

Some values of  $S_n$  and  $S_p$  are given in Table 2.1 and Fig. 2.2. The fact that the neutron and proton separation energies in  ${}^{16}_8\text{O}$  are considerably higher than the average binding energy per nucleon, implies that this nuclide is particularly stable.

### ***Q*-Value for a Reaction**

In a nuclear reaction, from conservation of energy, the total energy including the rest-mass energy must be the same before and after the reaction i.e.

$$\left( \sum_i [E_i + m_i c^2] \right)_{\text{before}} = \left( \sum_i [E_i + m_i c^2] \right)_{\text{after}},$$

where  $E_i$  and  $m_i$  are the kinetic energy and rest mass of particle respectively. Any change in the total kinetic energy before and after the reaction must be accompanied by an equivalent change in the total rest mass. Following [3], the  $Q$ -value of a reaction is defined the change in kinetic energy or rest mass in a reaction i.e.

$$Q = (\text{kinetic energy})_{\text{after}} - (\text{kinetic energy})_{\text{before}}$$

or

$$Q = (\text{rest mass})_{\text{after}} \cdot c^2 - (\text{rest mass})_{\text{before}} \cdot c^2.$$

If the kinetic energy of the products is greater than that of the reactants, the reaction is exothermic and  $Q$  is positive. If energy is required to induce a reaction, the reaction is endothermic and  $Q$  is negative. In such endothermic reactions a minimum kinetic energy of reactants is required for the reaction to proceed.

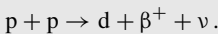
In a binary nuclear reaction  $a + X \rightarrow Y + b$ , the  $Q$ -value is given by

$$Q = (E_Y + E_b) - (E_a + E_X) = [(m_a + m_X) - (m_Y + m_b)]c^2.$$

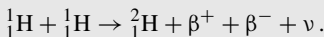
In most binary reactions, the number of protons is conserved and the same number of electron masses can be added to both sides of the above reactions. Neglecting the differences in electron binding energies, the  $Q$ -value can be expressed in terms of

#### ***Q*-Value for fusion [3]:**

Consider the fusion reaction in which two protons fuse to form a deuteron i.e.



In this reaction, the number of protons is not conserved and care is required in the evaluation of the  $Q$ -value. To obtain the  $Q$ -value in terms of the atomic masses, add two electrons to both sides of the reaction i.e.



The  $Q$ -value is then obtained from:

$$\begin{aligned} Q &= [2M({}^1_1\text{H}) - M({}^2_1\text{H}) - 2m_e - m_\nu]c^2 \\ &= (2 \times 1.007825032 - 2.014101778 - 2 \times 0.00054858) \times \frac{931.5 \text{ MeV}}{\text{u}} \\ &= 0.422 \text{ MeV}, \end{aligned}$$

where the rest mass of the neutrino has been assumed to be zero.



atomic masses i.e.

$$Q = (E_Y + E_b) - (E_a + E_X) = [(M_a + M_X) - (M_Y + M_b)]c^2.$$

In radioactive decay reactions (see Decay Energy) a parent nuclide decays to a daughter with the emission of a particle, i.e.  $P \rightarrow D + d$ .

The  $Q$ -value is given by  $Q = (E_D + E_d)$  since the parent nuclide is at rest, hence

$$Q = (E_D + E_d) = [m_P - m_D - m_d]c^2 > 0.$$

It should be noted that in some types of radioactive decay, such as beta decay and electron capture, the number of protons is not conserved. In such cases the evaluation of the  $Q$ -value using atomic masses may be inaccurate. For more information on the calculation of  $Q$ -values using atomic masses, the reader is referred to [3].

### Threshold Energy for a Nuclear Reaction

The actual amount of energy required to bring about a nuclear reaction is slightly greater than the  $Q$ -value. This is due to the fact that not only energy but also momentum must be conserved in any nuclear reaction. From conservation of momentum, a fraction  $m_a/(m_a + M_X)$  of the kinetic energy of the incident particle  $a$  must be retained by the products. This implies that only a fraction  $M_X/(m_a + M_X)$  of the incident particle is available for the reaction. It follows that the threshold energy is higher than the  $Q$ -value and is given by

$$E_{\text{th}} = -\frac{Q(m_a + M_X)}{M_X}.$$

## Energy Level Diagrams

Nuclear data can be displayed in the form of nuclear energy level diagrams. These diagrams are essentially a plot of the nuclear energy level versus the atomic number and are very useful for showing the nuclear transition corresponding to decay modes. From the basic decay data, energy level diagrams can be constructed according to the following procedure:

- The ground state of the daughter nucleus is chosen to have zero energy.
- If there is an increase in the atomic number (as in  $\beta^-$  decay), the daughter is shown to the right of the parent. The following is an example of the energy level diagram for the decay of  $^{32}_{15}\text{P}$ :

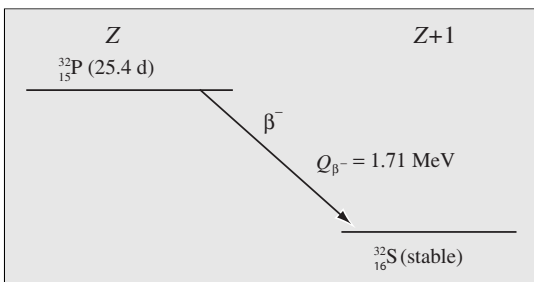


**Fig. 2.3.** Energy level diagram for the decay of  $^{32}_{15}\text{P}$

- If the radioactive decay results in a decrease of the atomic number (e.g. alpha emission, positron emission, or electron capture) the daughter is shown to the left of the parent. The following is an example of the energy level diagram for the decay of  $^{18}\text{F}$ . Since the decay energy is greater than  $2m_e c^2$  (1.022 MeV) positron emission ( $\beta^+$ ) competes with electron capture (ec) to the ground state.

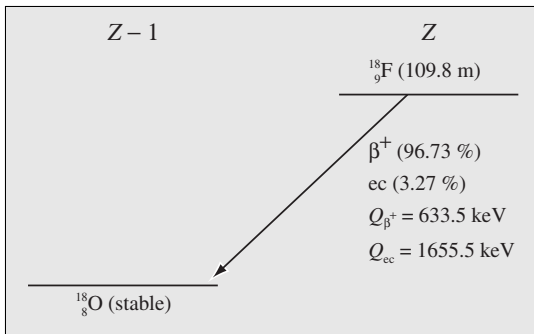


**Fig. 2.4.** Energy level diagram for the decay of  $^{18}\text{F}$

In addition to showing the decay modes and energies, these diagrams can also be used to show half-lives, branching ratios, nuclear isomerism, etc. as in the above examples.

## Nuclear Spin and Parity

Protons and neutrons have half integral spin i.e.  $+\frac{1}{2}$  or  $-\frac{1}{2}$ . Spin, which can be loosely associated with the picture of a particle spinning, is inherently quantum mechanical in nature and related to the intrinsic angular momentum associated with the sub-atomic particle. Spin is a vector quantity, with a total spin and a component of spin in a specified direction. The total spin has a spin quantum number (symbol  $s$ ) with value equal to an integer for a boson, and a half-integer for a fermion and the word ‘spin’ is often used to mean this quantum number.

The overall spin of an atomic nucleus is by virtue of the spin of each nucleon within it. The hydrogen nucleus, for example, contains one proton with a spin quan-

**Table 2.2.** Spin quantum number for various nuclei

Number of protons	Number of neutrons	Spin quantum number	Examples
Even	Even	0	$^{12}\text{C}$ , $^{16}\text{O}$ , $^{32}\text{S}$
Odd	Even	1/2	$^1\text{H}$ , $^{19}\text{F}$ , $^{31}\text{P}$
"	"	3/2	$^{11}\text{B}$ , $^{35}\text{Cl}$ , $^{79}\text{Br}$
Even	Odd	1/2	$^{13}\text{C}$
"	"	3/2	$^{127}\text{I}$
"	"	5/2	$^{17}\text{O}$
Odd	Odd	1	$^2\text{H}$ , $^{14}\text{N}$

tum number of  $\frac{1}{2}$ , and this gives rise to a spin of  $\frac{1}{2}$  for a hydrogen atom. The spin produces a magnetic moment, and this forms the basis of the technique of nuclear magnetic resonance.

Within a nucleus, nucleons (protons and neutrons) have a strong tendency to pair i.e. neutron with neutron or proton with proton so that their spins cancel (spins pair anti-parallel). Hence for all even- $Z$  even- $N$  nuclei such as  $^{12}\text{C}$ ,  $^{16}\text{O}$ ,  $^{32}\text{S}$ , the ground state spin is always zero as shown in Table 2.2.

Nuclei with an odd number of protons, neutrons, or both, will have an intrinsic nuclear spin. Although there is the tendency for nucleons to pair up spins anti-parallel to become spin-0, the total spin is not necessarily the lowest value after pairing off – some nucleons remain unpaired and result in spins as high as  $\frac{11}{2}$ .

The parity of a nucleus is the sign of the spin and is either odd (–) or even (+). Parity is important due to the fact that it is conserved in nuclear processes (in the case of weak interactions, however, such as in beta decay, parity conservation is weakly broken).

## Nuclear Isomerism

Nuclei usually exist in their ground state with the individual nucleons paired up subject to energy constraints. In some nuclides, for example resulting from radioactive decay, one or more nucleons can be excited into one or more higher spin states. These nuclei can revert back to the ground state by the emission of gamma radiation. If this emission is delayed by more than 1  $\mu\text{s}$ , the nucleus is said to be a nuclear isomer and the process of releasing energy is known as isomeric transition.

There are two very different ways that such nuclei can possess spin. Either the nucleus rotates as a whole, or several nucleons can orbit the nucleus independently in a non-collective rotation. The latter case can result in the nucleons being trapped in high spin states such that they have much higher lifetimes. Nuclides with even- $Z$  and even- $N$  (i.e. with a whole number of  $^4\text{He}$  nuclei) can also have high excess rotational spin due to alpha particles rotating independently around the nucleus. Examples here are  $^{12}\text{C}$ ,  $^{16}\text{O}$ ,  $^{20}\text{Ne}$ , and  $^{24}\text{Mg}$ .

$^{212\text{m}}\text{Po}$  is an example where the isomer has a much longer half-life than the ground state. With a spin of 18, the half-life of 45 s is very much longer than the ground state half-life of 300 ns. The isomer can be considered as two neutrons and two protons orbiting around the doubly magic  $^{208}\text{Pb}$  nucleus. The high spin state decays by alpha emission which carries off the 18 units of spin.

Other examples are  $^{178\text{n}}\text{Hf}$  (spin 16 due to 4 of the 78 nucleons orbiting the nucleus),  $^{178}\text{W}$  (spin 25 due to 8 unpaired nucleons orbiting the nucleus).

## Nuclide Charts

The origin of the nuclide chart is somewhat uncertain. In his autobiography [6], Segrè mentions the “Segrè Chart” compiled with the help of his wife at Los Alamos in 1945. After the war it was declassified and published, selling more than 50,000 copies. Segrè also mentions that the “first modest table of isotopes was published by a student in our Rome group in the 1930s”, see G. Fea [7]. One of the earliest

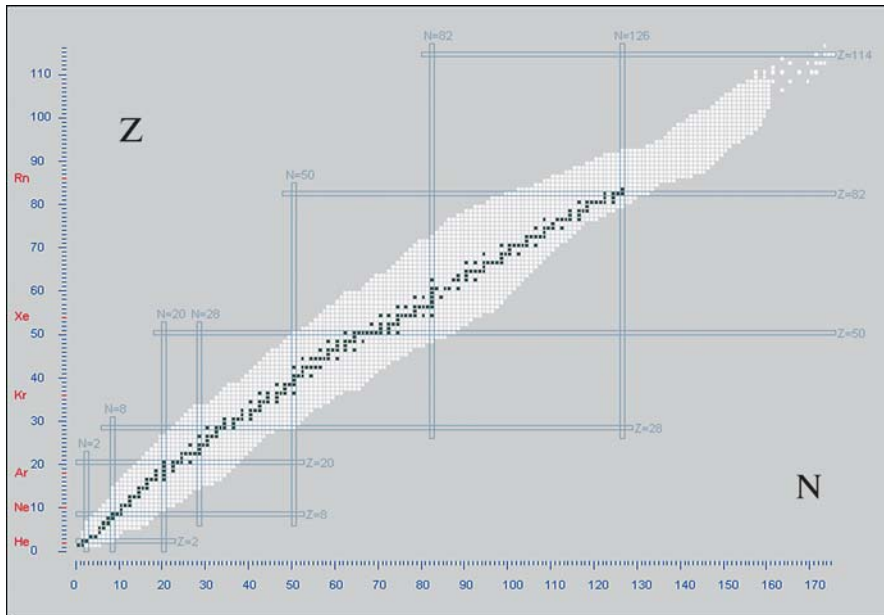


**Fig. 2.5.** Nuclide stability diagram. Stable nuclides (*black*) fall in a narrow range of neutron to proton ratio. Unstable nuclides (*white*) have neutron to proton ratios outside this range. Also shown are the proton and neutron magic numbers represented by the horizontal and vertical lines

nuclides charts was compiled by G. Friedlander and M. Perlman and published by the General Electric Company in 1946. In contrast to the earlier charts by Fea and Segrè, this chart had the proton number as the vertical axis and the neutron number as the horizontal axis. The current version of this chart is the 16th edition [8].

Nuclide charts are based upon the proton-neutron model of the nucleus and are essentially a plot of the number of protons versus the number of neutrons in stable and unstable nuclei. In these charts, the vertical and horizontal axes represent the number of protons and neutrons respectively in the nucleus as shown in Fig. 2.5.

The charts contain information on the basic nuclear properties of known nuclides. Each nuclide is represented by a box containing basic nuclear data. This data consists of the half-life, neutron cross-sections, main gamma lines etc. of that nuclide. An important characteristic of the charts is the use of colour to denote the mode of decay, half-life, or cross-sections. If the nuclide has one or more metastable states, the box is subdivided into smaller boxes for each state. The main nuclide charts in use world-wide are the Karlsruhe (Germany) [9], Strasbourg (France) [10], General Electric or KAPL (US) [8], and the JAERI (Japan) [11] charts.

It can be seen that stable isotopes lie within a relatively narrow range indicating that the neutron to proton ratio must have a certain value or range of values to be stable. Radioactive nuclei (white squares in Fig. 2.5) mostly lie outside this range. The plot also shows that for low atomic numbers, the neutron to proton ratio is unity.

At higher atomic numbers, this value increases indicating a higher ratio of neutrons to protons in heavy atoms.

The extremities of the white regions above and below the region of stability are known as the proton and neutron “drip-lines” beyond which nuclei are extremely unstable (i.e. if a nucleon is added it will “drip” out again). As nucleons are successively added to a nucleus on the stability line, the binding energy of the last nucleon decreases steadily until it is no longer bound and the nucleus decays by either neutron or proton emission.

Nuclei with even numbers of protons and neutrons are more stable than nuclei with other combinations of neutrons and protons. For uneven numbers of protons and neutrons, there are only very few stable nuclides. The stability of nuclei is extremely significant for special numbers of protons and neutrons. These (magic) numbers are 2, 8, 20, 28, 50, 82 and 126 and correspond to full shells in the shell model of the nucleus. The element tin with the proton number  $Z = 50$ , for example, has 10 stable isotopes, more than all other elements.

When the proton and neutron numbers both have magic values, the nucleus is said to be “doubly magic”. Doubly magic, stable nuclides are for example  $^4\text{He}$ , the alpha particle, as well as the nuclide  $^{208}\text{Pb}$ , which is reached in several decay processes, for example in the decay chain of  $^{232}\text{Th}$ .

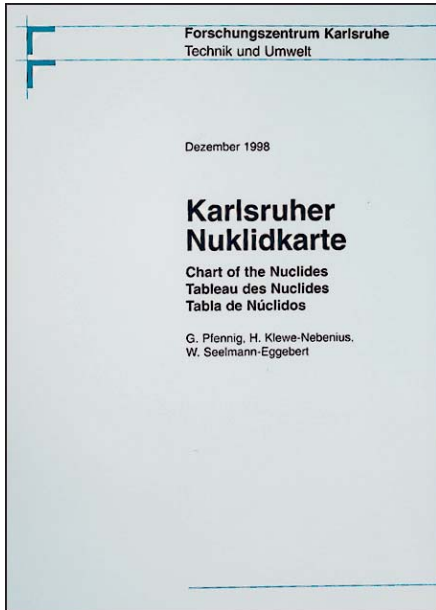
In addition to providing the most important basic nuclear data, the charts allow one to trace out radioactive decay processes and neutron reaction paths. This feature is described in more detail in the following section.

The Karlsruhe Nuclide Chart [9] is described in detail at the end of this chapter.

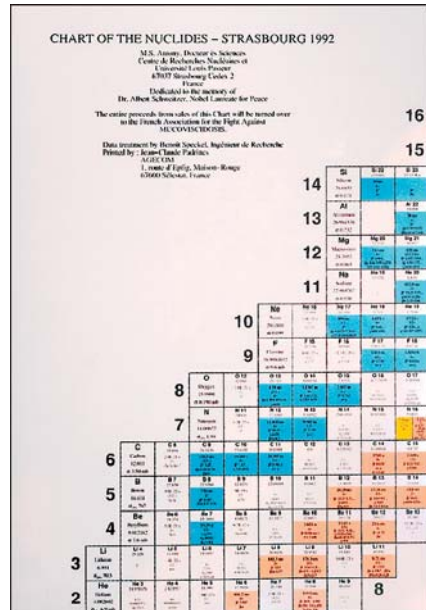
The Strasbourg Nuclide Chart [10] was developed by Dr. Mariasusai Antony from the Louis Pasteur University of Strasbourg. Approximately 5000 copies of the 1992 version were sold in more than 40 countries. This original version contained data on approximately 2550 ground states and 571 isomers. An updated version was published in 2002. The new chart displays about 2900 isotopes in the ground states and about 700 isomers. The chart is a booklet of 44 A4 formatted pages. The front cover page exhibits a stork, symbol of the region of Alsace for which Strasbourg is the capital. The colours blue, white and red (actually reddish-brown) were chosen to indicate the tri-colours of France.

Continuing a half-century tradition, Knolls Atomic Power Laboratory (KAPL) has recently published the 16th edition (2003) of its Chart of the Nuclides in both wallchart and textbook versions [8]. The first edition was published by the General Electric Company in 1946. Evaluated nuclear data is given for about 3100 known nuclides and 580 known isomers. For each nuclide the half-life, atomic mass, decay modes, relative abundances, nuclear cross-section, and other nuclear properties are detailed. The updated chart includes approximately 300 new nuclides and 100 new isomers not found in the 15th (1996) edition. There has been at least one change in more than 95% of the squares on the chart.

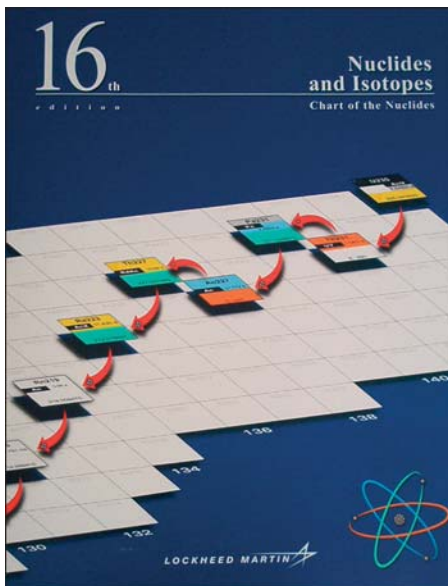
The first edition of the JAERI nuclide chart was published in February 1977. Since then the chart has been revised every 4 years, i.e. 1980, 1984, 1988, 1992, 1996, with the most recent edition appearing in 2000 [11]. In total, seven editions have been published. Approximately 2000 copies of each edition were printed, most



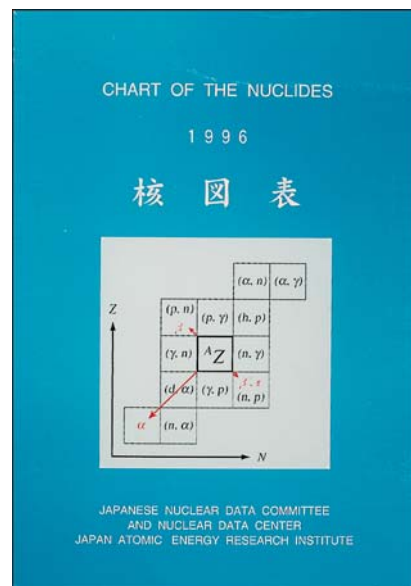
Revised 6th edition of the “Karlsruher Nuklidkarte”



Strasbourg nuclide chart



KAPL nuclide chart



Japanese (JAERI) nuclide chart

Fig. 2.6. Main paper-based nuclide charts

of which are distributed to the Japanese nuclear data community and international organisations. The chart comes as an A4-sized booklet.

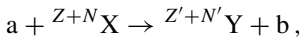
**Decay and Reaction Processes**

A small section of a nuclide chart is shown in Fig. 2.7. The central box, with co-ordinates  $Z, N$  represents a nuclide with  $Z$  protons and  $N$  neutrons. When this “parent” nuclide decays, it results in a “daughter” nuclide with co-ordinates  $Z', N'$  depending on the decay process. In Fig. 2.7, the position of the daughter nuclide is shown following decay by  $\alpha, \beta^-, \epsilon/\beta^+, n,$  and  $p$  decay processes. These decay processes are explained in detail in Chap. 4. With this information, the radioactive decay chain can be traced out. Starting with a parent nuclide, the position of the daughter can be found from the decay mode (given in the parent box) and the information given in Fig. 2.7. If the daughter is radioactive, it then becomes the parent for the next decay process etc. In this way the full decay chain may be traced out starting from a parent nuclide.

Similarly the nuclide chart may be used to trace out activation and nuclear reactions. In Fig. 2.8, a small section of the chart is shown with the nuclide  $Z, N$  at its centre.

A target nuclide of element  $X$ , with  $Z$  protons and  $N$  neutrons will transform through reaction with a particle  $a$  to an element  $Y$ , with  $Z'$  protons and  $N'$  neutrons, through the emission of a particle  $b$ .

The reaction can be written:



or more compactly in the form

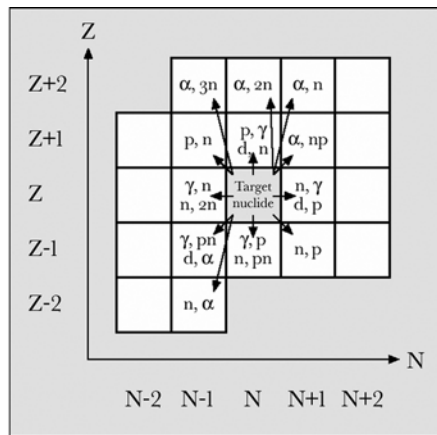
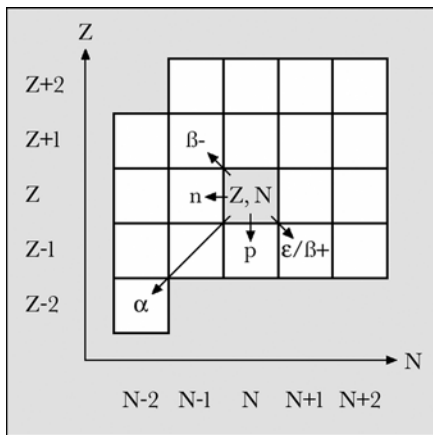
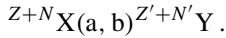


**Fig. 2.7 (left).** Nuclear decay processes on the nuclide chart. A nuclide with “co-ordinates”  $Z, N$  transforms to the nuclide  $Z', N'$  through the decay processes shown

**Fig. 2.8 (right).** Activation processes and nuclear reactions on the nuclide chart. A target nuclide with co-ordinates  $Z, N$  transforms to the nuclide  $Z', N'$  through the processes shown



The result of interaction of a variety of particles  $a$  (neutrons, alpha particles, deuterons, gamma radiation, protons etc.) with a target nuclide with co-ordinates  $Z, N$  is shown in Fig. 2.8.

### Electronic Nuclide Charts

There are a variety of “electronic” nuclide charts available on the internet. Each of these resources has its own particular tool for navigating the nuclide chart efficiently and displaying the data once a particular nuclide has been selected. These internet resources are restricted, however, to only displaying nuclear data. The main ones are shown below.

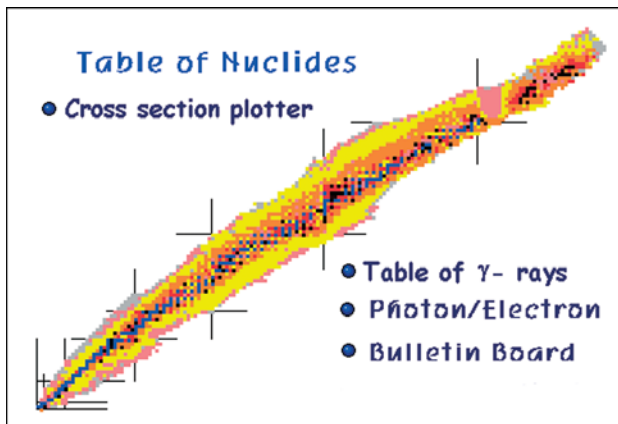


**Fig. 2.9**

*Table of Nuclides*

Korea Atomic Energy  
Research Institute  
KAERI

<http://atom.kaeri.re.kr/>

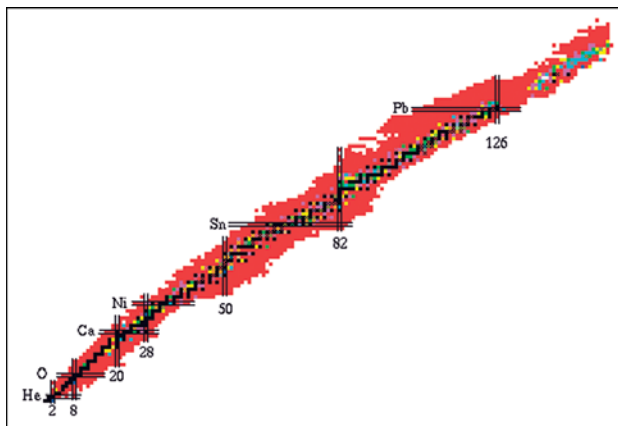


**Fig. 2.10**

*Table of the Nuclides*

Japanese Atomic  
Energy Research  
Institute (JAERI)

<http://sutekh.nd.rl.ac.uk/CoN/>

Each horizontal row represents one element; the coloured dots indicate the known isotopes of that element. A vertical column represents the nuclides with same neutron numbers. Heavy lines on the Chart occur for  $Z$  and  $N$  equal to 2, 8, 20, 28, 50, 82, and 126. These are the so-called “magic numbers”



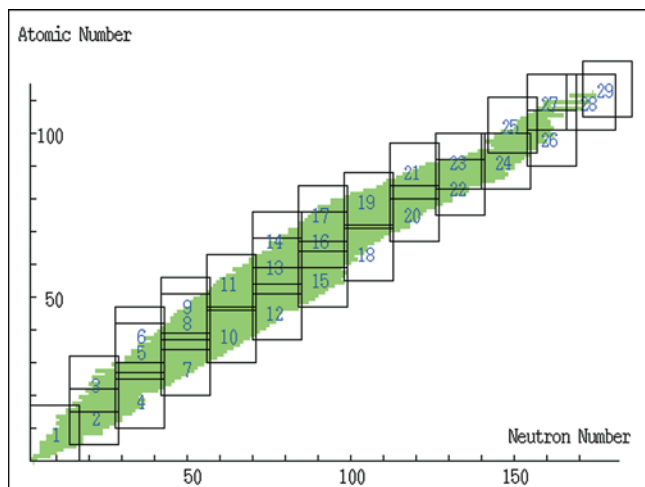


**Fig. 2.11**  
**WWW Chart**  
**of the Nuclides**  
 Japan Atomic Energy  
 Research Institute  
 (JAERI)  
<http://wwwndc.tokai.jaeri.go.jp/CN00/>

The latest version of “Chart of the Nuclides 2000” was made by T. Horiguchi, T. Tachibana, H. Koura and J. Katakura, and published by the Japanese Nuclear Data Committee (JNDC) and the JAERI Nuclear Data Center.


“WWW Chart of the Nuclides” here is based on the most recent compilation of experimental data by T. Horiguchi (Hiroshima International University) (2000)

## The Lund/LBNL Nuclear Data Search

Preliminary version (beta 1.0), 7 April 1998


**S.Y.F. Chu<sup>1</sup>, L.P. Ekström<sup>1,2</sup> and R.B. Firestone<sup>1</sup>**

<sup>1</sup> LBNL, Berkeley, USA  
<sup>2</sup> Department of Physics, Lund University, Sweden



**WWW Table of Radioactive Isotopes**

[Radiation search](#)  
[Nuclide search](#)  
[Periodic chart interface to the nuclides](#)  
[Summary drawings for A=1-277 \(PDF\)](#)  
[Nuclear charts \(PDF, 333 kbyte\)](#)  
[Database status](#)



**Table of Isotopes (ToI)**

[About this service](#)  
[ToI home page](#)

**Fig. 2.12**  
**The Lund/LBNL**  
**Nuclear Data Search**  
<http://nucleardata.nuclear.lu.se/Database/toi/>

The handbook “Table of Isotopes” has for many years been the most widely used source of information for nuclear structure and decay data. This service is intended to give convenient Web access to the Table of Isotopes data. At present only part of the decay data is implemented, but the service will eventually include search facilities, table generators, charts and drawings of all nuclear structure and decay data in the ToI book

**Nuclear Data Services**

**Welcome to the IAEA's Nuclear Data Centre**  
We offer numerical nuclear physics data with related bibliographic information:

via Web Telnat CD-ROMs Codes Atomic & Molecular Reports Data Manuals Guides Data News Search Letter Enigma Info Brazil

on this site are products of the Network of Nuclear Reaction Data Centres, the Network of Nuclear Structure and Decay development programme of the Nuclear Data Section, IAEA.

**Nuclear Databases and Files**

**General**

- [Wallet cards](#) - Ground and metastable state properties
- [NUDAT](#) - selected evaluated nuclear data
- [NSR](#) (Nuclear Science References)
- [Masses](#) (Atomic Mass Evaluation Data File)
- [Thermal neutron capture  \$\gamma\$ 's](#)

**Nuclear Structure and Decay Data**

- [ENSDF](#) - evaluated nuclear structure and decay data
- [MIRD](#) - medical internal radiation dose tables

Fig. 2.13. IAEA's Nuclear Data Centre, <http://www-nds.iaea.or.at/>

### Nuclides.net [5]

The Institute for Transuranium Elements, <http://www.nuclides.net/>

The main user interface, Nuclide Explorer, provides access to nuclide information (data on approximately 3650 ground states and isomers, from internationally recognised sources) through nuclide charts. In addition to displaying nuclear data, various applications/calculations can be launched.

There are six main applications:

- Decay Engine – a software module for decay calculations.
- Dosimetry and Shielding – a module that allows the calculation of dose rates from both unshielded and shielded point sources. A choice of 10 shield materials is available.
- Virtual Nuclides allow the user to do decay and dosimetry and shielding calculations on mixtures of nuclides.
- Fission Yield – the module gives the user access to fission products and yields for 36 fissioning nuclides (data for spontaneous fission and neutron induced fission with thermal, fast, and 14 MeV neutrons) from the main international datafiles.
- Cross-Sections give averaged neutron cross sections from the main international datafiles. Data include the cross sections for room temperature, Maxwell averaged, resonance integral, fission averaged, and 14 MeV neutrons.
- The Universal Nuclide Chart shows the most important basic data. It can also be used to simulate decay processes and reaction paths in nuclear reactors.

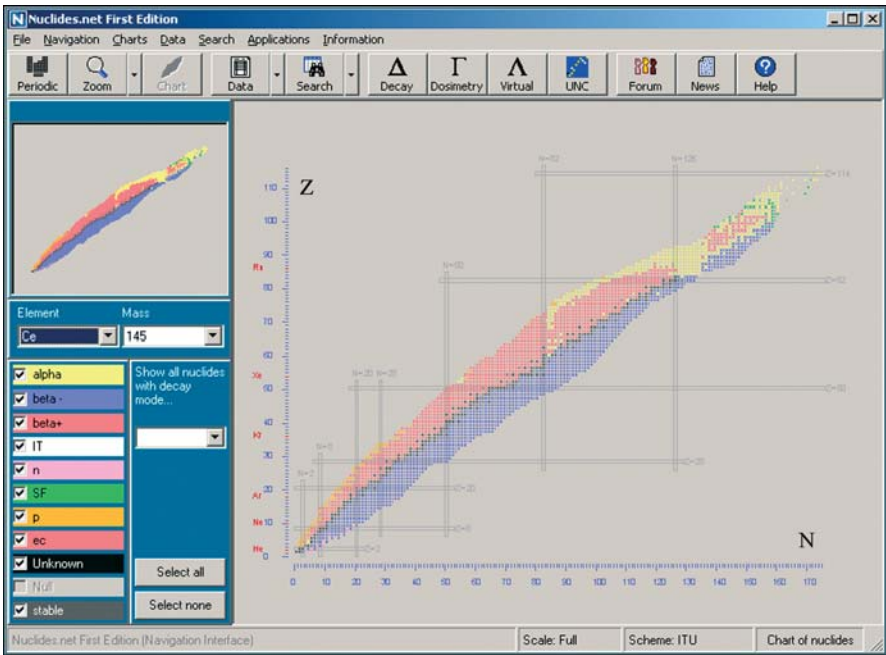


Fig. 2.14. Nuclides.net: The Nuclide Explorer

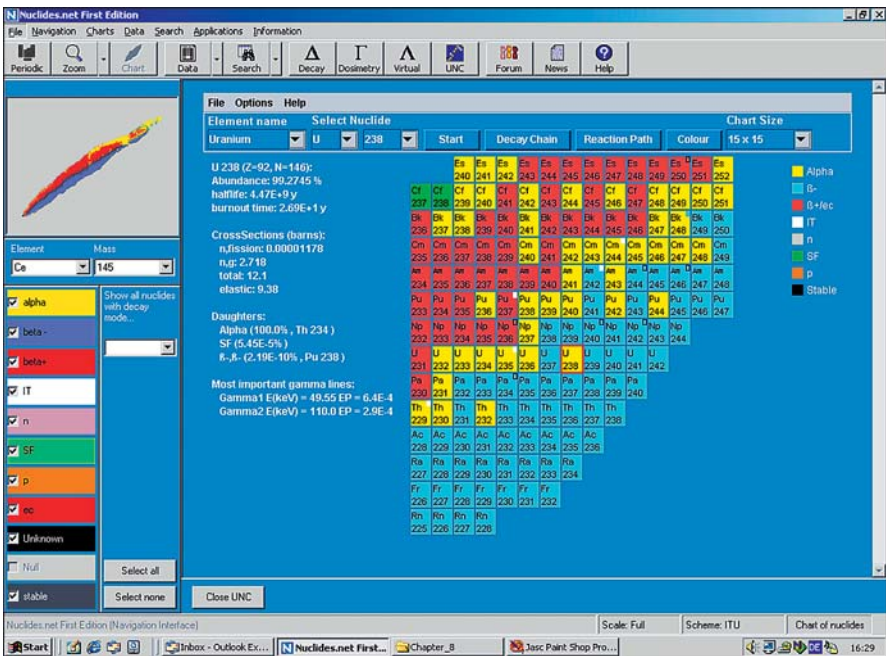


Fig. 2.15. Nuclides.net: Universal Nuclide Chart

## A Short History of the Karlsruhe Nuclide Chart

The *Karlsruhe Chart of the Nuclides* was initiated by Professor Walter Seelmann-Eggebert from the Technische Hochschule (TH) Karlsruhe to display basic nuclear data (half-lives, decay modes, particle energies, and most probable gamma energies) [9, 12]. The Karlsruhe chart of the nuclides was based on an earlier chart by G. Friedlander and M. L. Pearlman in the *General Electric Chart of the Nuclides* [13].

*1st Edition, 1958:* The first edition appeared as a wall chart in DIN A0 format. Coloured boxes were used to indicate the decay modes (black = stable nuclide, red =  $\beta^+$  decay or electron capture, blue =  $\beta^-$  decay, yellow = alpha decay, white = isomeric transition). In addition a DIN A4 version was available as a collection of sheets with an explanatory brochure for desktop use. It was prepared by W. Seelmann-Eggebert and G. Pfennig both from the Institute of Radiochemistry in the Karlsruhe Research Centre and the TH Karlsruhe. The data used in the chart was from the Nuclear Data Sheets of the National Research Council and the Table of Isotopes by D. Strominger, J. M. Hollander, G.T. Seaborg. The original chart contained data on 267 stable and 1030 unstable nuclides and more than 220 isomeric states from the, at that time, 102 known elements from hydrogen to nobelium.

*2nd Edition, 1961:* Following on the interest shown in the first edition, a second edition was published in 1961 with additional authors H. Münzel and G. Zundel – also from the Institute of Radiochemistry. A new feature was the introduction of coloured

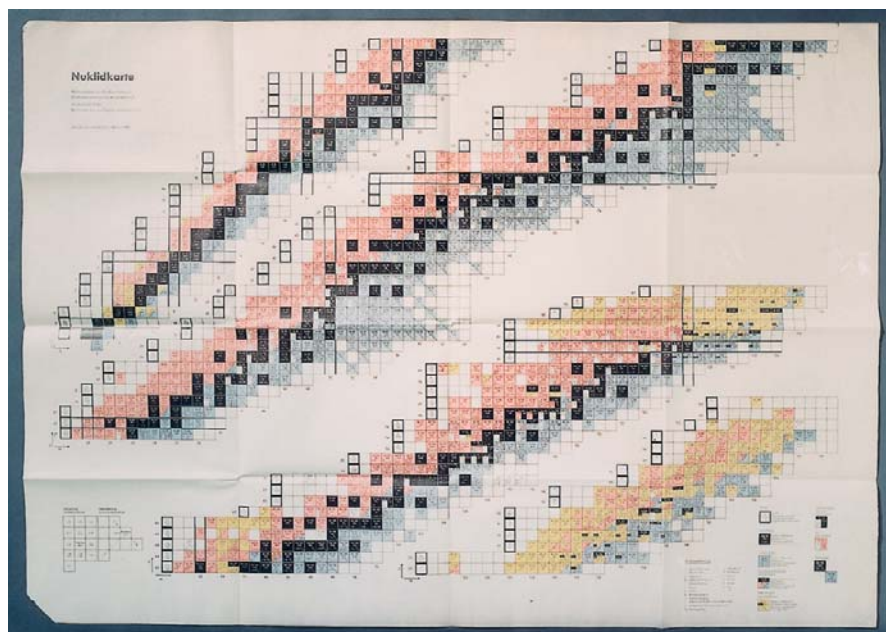


Fig. 2.16. Original Karlsruhe Chart of the Nuclides from 1958



**Fig. 2.17.** *Left:* Prof. W. Seelmann-Eggebert with the original 1st edition (1958) of the Karlsruhe Chart of the Nuclides. *Right:* The co-authors H. Klewe-Nebenius (*left*), G. Pfennig (*centre*), H. Münzel (*right*) with the revised 6th edition (1998/2001).

corners of different size to indicate the branching ratio of the decay mode. The second edition contained information on 103 elements, and data on approximately 70 new unstable nuclides.

*3rd Edition, 1968:* Due to the increasing use of the Karlsruhe chart of the nuclides worldwide, a third edition was produced in 1968 with explanatory text in four languages – German, English, French and Spanish. The colour green was introduced to indicate spontaneous fission, and atomic masses were based on  $^{12}\text{C}$ . Instead of single DIN A4 sheets, the desktop version was printed in a special arrangement in a strip folded to DIN A4 format. The third edition contained information on 105 elements and more than 1600 nuclides – an increase of 250 over the 2nd edition.

*4th Edition, 1974:* Much of the data in the 3rd edition had to be revised to reflect the higher accuracy data obtained from the use of Ge detectors. Owing to the improved experimental technique, new data had become available for many short-lived fission products. The 4th edition contained data on more than 1900 nuclides.

*5th Edition, 1981:* The fifth edition was authored by W. Seelmann-Eggebert, G. Pfennig, H. Münzel, and H. Klewe-Nebenius. New decay modes of double beta decay ( $2\beta^-$ ) and proton decay (p, colour orange) were introduced. To discriminate between direct and  $\beta$ -delayed particle emission, new notations for the latter ( $\beta\text{p}, \beta\text{n}, \beta 2\text{n}, \beta\text{sf}$ , etc.) were introduced. The 5th edition contained data on more than 2220 nuclides.

*6th Edition, 1995:* The sixth edition was published in 1995 – more than a decade after the 5th edition – by G. Pfennig and H. Klewe-Nebenius and dedicated to Professor W. Seelmann-Eggebert who died in 1988. In the meantime, four new heavy elements (108–111) had been discovered at the Gesellschaft für Schwerionenforschung (GSI) at Darmstadt. New decay modes of cluster emission e. g. C-14, O-20, Ne-24 etc. indicated by the colour violet) were added. The 6th edition contained data on approximately 2690 nuclides from 111 elements.

*Revised 6th Edition, 1998/2001:* the sixth edition was revised in 1998 to include data on the newly discovered element 112, new names for elements 104–108, new decay data for some transuranics and 150 mostly short-lived nuclides far from the line of stability.

Since the introduction of the Karlsruhe Chart of Nuclides, over 150,000 copies of the wall chart and 203,000 copies of the brochure with the folded chart have been printed. For the sixth edition more than 15,000 wall charts and 45,000 brochures were printed.

### 3. Radioactivity and Nuclear Reactions

Following the discovery of radioactivity by Henri Becquerel in 1896, two young scientists, Frederic Soddy and Ernest Rutherford then at McGill University in Canada, set about to investigate the recently discovered phenomena. In 1901, the twenty-four year-old chemist Soddy and Rutherford were attempting to identify a gas which was being released from samples of radioactive thorium oxide. They believed that this gas – they called it an “emanation” – was related to the radioactivity of the thorium sample. In order to investigate the nature of this gas, Soddy passed it over a series of powerful chemical reagents, heated white-hot. No reactions took place. Years later in his biography, he wrote [1]

I remember quite well standing there transfixed as though stunned by the colossal import of the thing and blurting out – or so it seemed at the time: “Rutherford, this is transmutation: the thorium is disintegrating and transmuted itself into argon gas”. Rutherford’s reply was typically aware of more practical implications, “For Mike’s sake, Soddy, don’t call it transmutation. They’ll have our heads off as alchemists”.



**Fig. 3.1.** Frederic Soddy (1877–1956).  
© The Nobel Foundation



**Fig. 3.2.** “The Alchemist in Search of the Philosopher’s Stone”, Joseph Wright (1734–1797) with permission from Derby Museums and Art Gallery

Following this discovery, Rutherford and Soddy published nine joint papers between 1902 and 1903 in a period of extremely productive research [2]. In 1902 they described their theory of radioactivity as a spontaneous disintegration of the radioactive element by the expulsion of particles with the result that new elements are formed. This was the ultimate step in the ancient alchemists' dream of transmutation.

### Simple Radioactive Decay: Half-life and Decay Constant

Radioactive decay is a random process. As such, one cannot state with certainty when an unstable nuclide will decay. The probability that an atom will decay during the time  $dt$  is given by  $kdt$  where  $k$  is the constant of proportionality known as the decay constant. In a system where there are  $N(0)$  atoms present initially, the number of atoms decaying in time  $dt$  is given by  $-dN = kNdt$ . In the limit of very small time intervals, this can be expressed as

$$\frac{dN}{dt} = -kN.$$

Integration with respect to time gives the number of atoms present at any time  $t$ , i.e.

$$N(t) = N(0)e^{-kt}.$$

The half-life,  $\tau$ , is used to denote the time at which the number of atoms has decreased to half the initial value, i.e.  $\frac{1}{2} = e^{-k\tau}$ . Hence the half-life is related to the decay constant through the relation

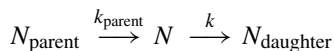
$$\tau = \frac{\ln 2}{k} \approx \frac{0.693}{k}.$$

### Activity

The number of decays per unit time interval, i.e. the activity  $A$ , is defined by

$$A = -\frac{dN}{dt} = kN.$$

It should be noted in this definition that it is assumed that  $N$  is decreasing due to decay. In general the rate equation contains a term for decay (removal) to the daughter and in-growth (production) from the parent, i.e.



for which the rate equation becomes

$$\frac{dN}{dt} = -kN + k_{\text{parent}}N_{\text{parent}}.$$

A situation could arise in which  $kN = k_{\text{parent}}N_{\text{parent}}$  and thus  $N$  is constant, i.e.  $dN/dt = 0$ . Clearly the activity is not zero. In the definition of  $A$  above only decay is considered. In the general case where decay and growth occur,  $A$  is given by  $A = kN$ . Hence  $A$  is the number of disintegrations per second even though  $N$  may be constant. The unit of activity is the Becquerel, i.e.  $1 \text{ Bq} = 1$  disintegration per second.



A technical problem arises in the evaluation of the activity in the case where the half-life is less than 1 s. The activity defined above gives the instantaneous disintegration rate. If the half-life is  $\leq 1$  s, a significant amount of the material has decayed in the first second. The above definition of the activity will then overestimate the emitted radiation. The difficulty can easily be overcome by defining the activity per integral second, i.e.

$$A_{1s} = \int_0^1 kN dt = N(0)(1 - e^{-k}),$$

where  $k = \ln 2/\tau$  (s) and  $N(0)$  is the number of atoms at time 0. For the calculation of the specific activity, denoted  $spA$ ,  $N(0)$  is the number of atoms in 1 g i.e.  $N(0) = N_a/\mathcal{A}$ . Hence

$$spA = \frac{N_a(1 - e^{-k})}{\mathcal{A}}$$

or

$$spA(\text{Bq/g}) = 6.022 \times 10^{23} \cdot \frac{1 - e^{-\frac{\ln 2}{\tau(\text{s})}}}{\mathcal{A}}.$$

### Average (Mean) Lifetime

The half-life of a nuclide is a statistical property and is a valid concept only because of the very large number of atoms involved. Any individual atom of a radionuclide may be transformed at any time, from zero to infinity. For some calculations, it is convenient to use the average life of a radionuclide. The average life is defined as the sum of the lifetimes of the individual atoms divided by the total number of atoms present originally. During a time interval from  $t$  to  $t + dt$ , the total number of transformations is  $kN dt$ . Each atom that decayed during this time interval had existed for a total lifetime  $t$ . The sum of the lifetimes of all atoms that were transformed during the time interval  $dt$ , having survived from  $t = 0$  is  $t k N dt$ . The average lifetime is then given by

$$l = \frac{1}{N(0)} \int_0^{\infty} t k N dt.$$

It is then straightforward to show that the relationship between the average or mean lifetime and the half-life is given by  $l = 1.44 \tau$ .

### Branching Ratios and Number of Decay Modes

Many nuclides have more than one decay mode. Consider a nuclide in which there are two decay modes. The probability that an atom will decay by process 1 in time  $dt$  is  $k_1 dt$ . Similarly, the probability that it will decay by process 2 in time  $dt$  is  $k_2 dt$ . Hence the equation governing the radioactive decay can be written as

$$\frac{dN}{dt} = -(k_1 + k_2)N.$$

The total decay constant for the decay of the parent nuclide is the sum of the partial decay constants i.e.  $k = k_1 + k_2$ . Hence, the branching ratios for modes 1 and 2 are defined as

$$BR_1 = \frac{k_1}{k}, \quad \text{and} \quad BR_2 = \frac{k_2}{k}.$$

In general, the branching ratio ( $BR$ ) for a particular decay mode is defined as the ratio of the number of atoms decaying by that decay mode to the number decaying in total, i.e.

$$BR_i = \frac{k_i}{(k_1 + k_2 + \dots + k_i + \dots)} = \frac{k_i}{k}.$$

Alternatively, given the total decay constant, the “partial” decay constant is given by

$$k_i = BR_i \cdot k.$$

### Number of Decay Modes

There are a number of ways in which a nuclide can decay. Usually the number of decay modes is one or two. There are nuclides, however, which have many decay modes. In Table 3.1, the seven decay modes of the nuclide  $^{11}\text{Li}$  are listed.

**Table 3.1.** Decay modes, branching ratios, and daughters of  $^{11}\text{Li}$

Decay mode	Branching ratio	Daughters
$\beta^-$	$8.07 \times 10^{-2}$	$^{11}\text{Be}$
$\beta^-, d$	$1.30 \times 10^{-4}$	$^9\text{Li}$
$\beta^- \alpha$	$1.00 \times 10^{-2}$	$^7\text{He}$
$\beta^- n$	$8.49 \times 10^{-1}$	$^{10}\text{Be}$
$\beta^- 3n$	$1.90 \times 10^{-2}$	$^8\text{Be}$
$\beta^- t$	$1.40 \times 10^{-4}$	$^8\text{Li}$
$\beta^- 2n$	$4.10 \times 10^{-4}$	$^9\text{Be}$

### Decay Chains

It is very often the case that the daughter product of a nuclear decay is also radioactive. In such cases one speaks of radioactive decay “chains”. As an example, consider the decay chain  $N_1 \rightarrow N_2 \rightarrow N_3 \rightarrow \dots$  in which the starting or “parent” nuclide  $N_1$  decays to the “daughter”  $N_2$ . This daughter in turn is radioactive and decays to  $N_3$ . More generally each nuclide in the decay chain  $N_i$  can “branch”, with branching ratio  $k_{N_i, N_j}$ , to more than one daughter. In addition, there may be an external source term  $S_i$  for the production of  $N_i$  (apart from the decay of the parent).

The situation for successive radioactive decay is shown schematically in Fig. 3.3. This general process of radioactive decay was first investigated systematically by Bateman [3].

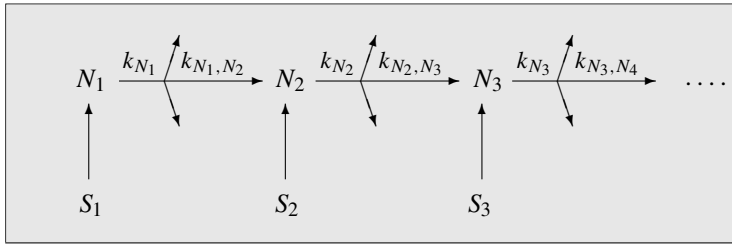


**Fig. 3.3.** Successive radioactive decay with branching and source terms

The differential equations governing the above processes can be written as:

$$\begin{aligned}\frac{dN_1}{dt} &= S_1 - k_{N_1} \cdot N_1, \\ \frac{dN_2}{dt} &= S_2 + k_{N_1, N_2} \cdot N_1 - k_{N_2} \cdot N_2, \\ \frac{dN_i}{dt} &= S_i + k_{N_{i-1}, N_i} \cdot N_{i-1} - k_{N_i} \cdot N_i, \\ \frac{dN_n}{dt} &= S_n + k_{N_{n-1}, N_n} \cdot N_{n-1} - k_{N_n} \cdot N_n,\end{aligned}$$

where  $N_n$  is the number of atoms of species  $n$  present at time  $t$ ,  $k_n$  is the decay constant (total removal constant) for species  $n$  ( $k = \ln 2/\tau$ ),  $k_{n, n+1}$  is the partial decay constant (partial removal constant) and is related to the branching ratio  $BR_{n, n+1}$  through the relation  $k_{n, n+1} = BR_{n, n+1} \cdot k_n$ . The solution to this system of equations is [4]

$$N_n(t) = \sum_{i=1}^{i=n} \left[ \left( \prod_{j=1}^{j=n-1} k_{j, j+1} \right) \times \sum_{j=i}^{j=n} \left( \frac{N_i(0) e^{-k_j t}}{\prod_{\substack{p=i \\ p \neq j}}^{p=n} (k_p - k_j)} + \frac{S_i (1 - e^{-k_j t})}{k_j \prod_{\substack{p=i \\ p \neq j}}^{p=n} (k_p - k_j)} \right) \right] \quad (3.1)$$

for the particular case (of most interest) one is interested in the decay chain starting from a single parent nuclide with no source term  $S$ . In this case the above relation reduces to:

$$N_n(t) = \prod_{j=1}^{j=n-1} k_{j, j+1} \sum_{j=i}^{j=n} \frac{N_i(0) e^{-k_j t}}{\prod_{\substack{p=i \\ p \neq j}}^{p=n} (k_p - k_j)} \quad (3.2)$$

It is of interest to construct the first few terms, i.e.



**Fig. 3.4.** H. Bateman.  
 © 2002 University of St. Andrews; <http://www-gap.dcs.st-and.ac.uk/~history/Mathematicians/Bateman.html>

*Mr Bateman, Solution of a system of differential equations, etc. 423*

*The solution of a system of differential equations occurring in the theory of radio-active transformations. By H. BATEMAN, M.A., Trinity College.*

[Read 21 February 1910.]

1. It has been shown by Prof. Rutherford\* that the amounts of the primary substance and the different products in a given quantity of radio-active matter vary according to the system of differential equations,

$$\left. \begin{aligned} \frac{dP}{dt} &= -\lambda_1 P \\ \frac{dQ}{dt} &= \lambda_1 P - \lambda_2 Q \\ \frac{dR}{dt} &= \lambda_2 Q - \lambda_3 R \\ \frac{dT}{dt} &= \lambda_3 R - \lambda_4 T \\ &\dots\dots\dots \end{aligned} \right\} \dots\dots\dots(1).$$

where  $P, Q, R, S, T, \dots$  denote the number of atoms of the primary substance and successive products which are present at time  $t$ .

Prof. Rutherford has worked out the various cases in which there are only two products in addition to the primary substance, and it looks at first sight as if the results may be extended to any number of products without much labour.

Unfortunately the straightforward method is unsymmetrical and laborious, and as the results of the calculations are needed in some of the researches which are being carried on in radio-activity the author has thought it worth while to publish a simple and symmetrical method of obtaining the required formulae.

2. Let us introduce a set of auxiliary quantities  $p(x), q(x), r(x), \dots$  depending on a variable  $x$  and connected with the quantities  $P(t), Q(t), R(t), \dots$  by the equations,

$$p(x) = \int_0^\infty e^{-xt} P(t) dt, \quad q(x) = \int_0^\infty e^{-xt} Q(t) dt \dots\dots(2).$$

It is easily seen that

$$\int_0^\infty e^{-xt} \frac{dP}{dt} dt = -P(0) + x \int_0^\infty e^{-xt} P(t) dt \dots\dots(3),$$

$= -P_0 + xp,$

\* *Radio-activity, 2nd edition, p. 581.*

**Fig. 3.5.** An extract from Bateman's original publication from 1910 [3]

$$\begin{aligned} N_1 &= N_1(0) e^{-k_1 t} \\ N_2 &= k_{1,2} \left\{ \frac{N_1(0) e^{-k_1 t}}{k_2 - k_1} + \frac{N_1(0) e^{-k_2 t}}{k_1 - k_2} \right\} \\ N_3 &= k_{1,2} k_{2,3} \left\{ \frac{N_1(0) e^{-k_1 t}}{(k_2 - k_1)(k_3 - k_1)} + \frac{N_1(0) e^{-k_2 t}}{(k_1 - k_2)(k_3 - k_2)} \right. \\ &\quad \left. + \frac{N_1(0) e^{-k_3 t}}{(k_1 - k_3)(k_2 - k_3)} \right\} \end{aligned} \tag{3.3}$$

...

These relations allow one to update the numbers of atoms from time  $t = 0$  to time  $t$ . It is also of interest to calculate the numbers at various times in the range  $0, t$  (for example for plotting purposes). This can be done by specifying the total time  $t$  over which the calculation is to be made, and the number of time-steps  $L$  to reach  $t$ . The time interval for each calculation is then  $\Delta t = t/L$ . For  $L = 1$ , the numbers

are evaluated at the time  $t$ . For  $L = 2$ , the numbers are evaluated at  $t/2$ , and  $t$ . For  $L = 3$ , the  $N$ s are evaluated at  $t/3, 2t/3, t$  etc. From above, the relation to be used is then

$$N_n((l + 1)\Delta t) = \sum_{j=1}^{j=n} \left[ \left( \prod_{j=1}^{j=n-1} k_{j,j+1} \right) \sum_{j=1}^{j=n} \frac{N_i(l\Delta t)e^{-k_j\Delta t}}{\prod_{\substack{p=n \\ p=j}} (k_p - k_j)} \right] \tag{3.4}$$

for  $l = 1, 2, 3, \dots L$ .

### Convergent and Divergent Branches

The solution to the differential equations given in equations (3.1–3.4) is valid for the various species produced in series, i.e. in a chain. If branching occurs, as indicated in Figs. 3.3 and 3.6, the solution (e.g. equation 3.2) must be applied to all possible chains. As an example, consider the radioactive decay of  $^{225}\text{Ac}$ . The schematic decay is shown in Fig. 3.6 together with the various paths by which  $^{225}\text{Ac}$  can decay. The breakdown into “linear chains” is shown in Fig. 3.6b. Equations (3.1–3.4) must be applied to each of these three chains. In the evaluation of the total quantities of any species, care is required not to count the same decay more than once.

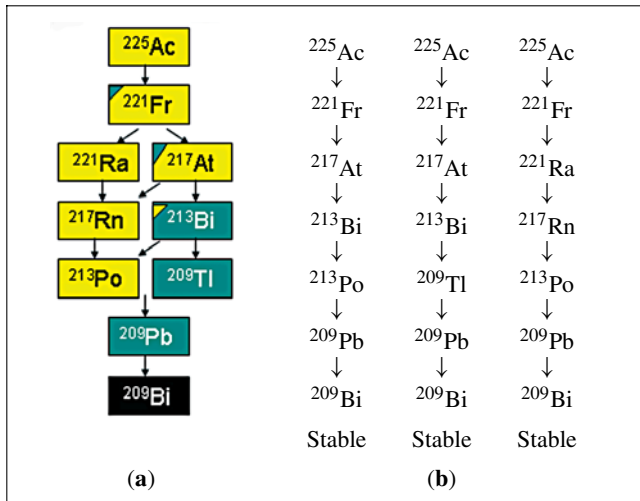


**Fig. 3.6.** (a) Schematic decay of  $^{225}\text{Ac}$ . The colours used indicate the type of decay (yellow: alpha emission, blue: beta emission, black: stable), (b) the three main “linear chains” for the decay of  $^{225}\text{Ac}$  giving the various paths by which the nuclide can decay

### Radioactive Equilibria

Consider a simplified radioactive decay process involving only three nuclides,  $N_1$ ,  $N_2$ , and  $N_3$ . The nuclide 1 decays into nuclide 2 which in turn decays to nuclide 3.

Nuclide 1 is the parent of nuclide 2 (or nuclide 2 is the daughter of nuclide 1). From the relations given above, the number of atoms of nuclide 2 is given by equation (3.3) [5]

$$\begin{aligned} N_2 &= \frac{k_1}{k_2 - k_1} \cdot N_1(0) \cdot (e^{-k_1 t} - e^{-k_2 t}) \\ &= \frac{k_1}{k_2 - k_1} \cdot N_1 \left(1 - e^{-(k_1 - k_2)t}\right) \end{aligned} \quad (3.5)$$

From Eq. (3.5) it can be seen that the time required to reach equilibrium depends on the half-life of both the parent and the daughter. Three cases can be distinguished:

1.  $\tau_1 \gg \tau_2$ . The half-life of the parent is much longer than that of the daughter.
2.  $\tau_1 > \tau_2$ . The half-life of the parent is longer than that of the daughter.
3.  $\tau_1 < \tau_2$ . The half-life of the parent is shorter than that of the daughter.

These will be discussed in more detail in the following sections.

### Secular Equilibrium: ( $\tau_1 \gg \tau_2$ )

In secular equilibrium, the half-life of the parent is much longer than that of the daughter, i.e.  $\tau_1 \gg \tau_2$  ( $k_1 \ll k_2$ ). In this case Eq. (3.5) reduces to

$$N_2 = \frac{k_1}{k_2} \cdot N_1(0) \cdot (1 - e^{-k_2 t})$$

For times  $t \gg \tau_1$ , radioactive equilibrium is established and the following relation holds:

Secular Equilibrium:  $\frac{N_2}{N_1} = \frac{k_1}{k_2} = \frac{\tau_2}{\tau_1}$ , and  $A_1 = A_2$ ,

where  $A$  is the activity defined by  $k \cdot N$ . Hence in radioactive equilibrium the ratio of the numbers, and the masses are constant whereas the activities are equal as shown in Fig. 3.7.

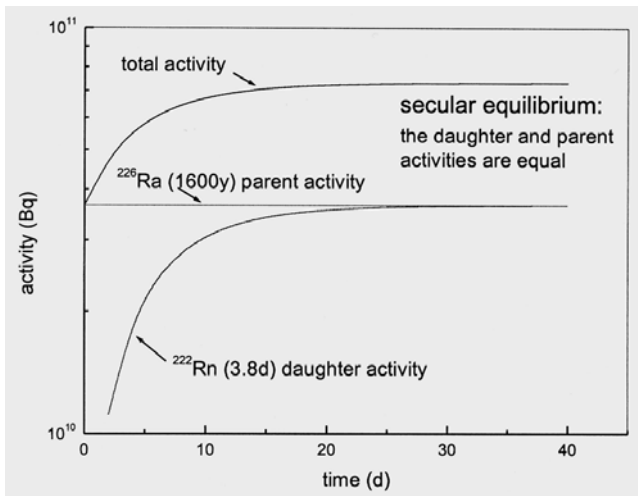


**Fig. 3.7.** Schematic illustration of secular equilibrium between a parent <sup>226</sup>Ra and its daughter <sup>222</sup>Rn (Radon gas): buildup of short-lived daughters from a long-lived parent

**Transient Equilibrium: ( $\tau_1 \geq \tau_2$ )**

In transient equilibrium the half-life of the daughter is of the same order but smaller than that of the parent, i.e.  $\tau_1 > \tau_2$  ( $k_1 < k_2$ ). The general equation for the daughter is from equation (3.5)

$$N_2 = \frac{\tau_2}{\tau_2 - \tau_1} \cdot N_1(0) \cdot \left( e^{-k_1 t} - e^{-k_2 t} \right).$$

As an example, consider the decay of  $^{140}\text{Ba}$  as shown in Fig. 3.8. For times  $t \ll \tau_1$  (12.75 d), the first exponential term is very close to 1 and  $N_2$  increases according to  $(1 - e^{-k_2 t})$  (rising part of activity of  $^{140}\text{La}$  in Fig. 3.8). For times  $t \gg \tau_2$  (1.68d), the second exponential becomes smaller than the first one with  $N_2$  decreasing according to  $e^{-k_1 t}$  (see Fig. 3.8). For this decreasing part of the curve, one obtains

Transient Equilibrium: 
$$N_2 = \frac{\tau_2}{\tau_2 - \tau_1} \cdot N_1$$

where the relation  $N_1 = N_1(0)e^{-k_1 t}$  has been used. This is the condition for transient equilibrium.

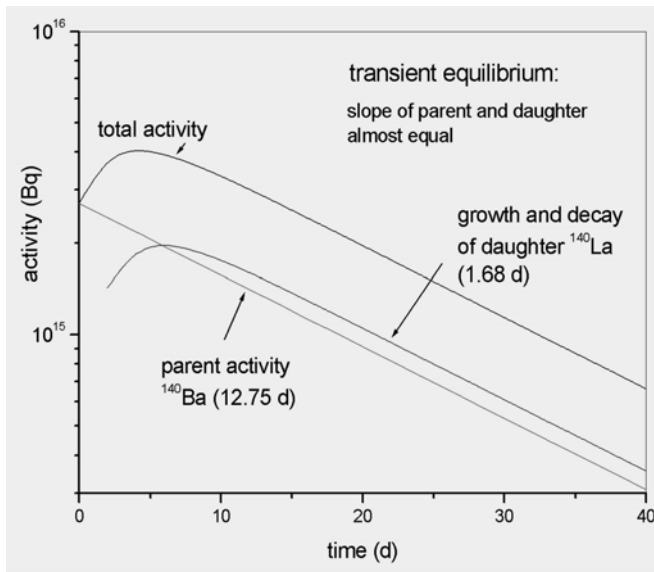


**Fig. 3.8.** Schematic illustration of transient equilibrium between a parent  $^{140}\text{Ba}$  and its daughter  $^{140}\text{La}$ : daughter and parent activities are approximately equal but change with time

**No-Equilibrium: ( $\tau_1 < \tau_2$ )**

In the case of no equilibrium, the half-life of the parent is shorter than that of the daughter. When the parent has a shorter half-life than that of the daughter, the daughter activity grows to some maximum and then decays with its own characteristic half-life. An example is shown in Fig. 3.9 for  $^{146}\text{Ce}$ .

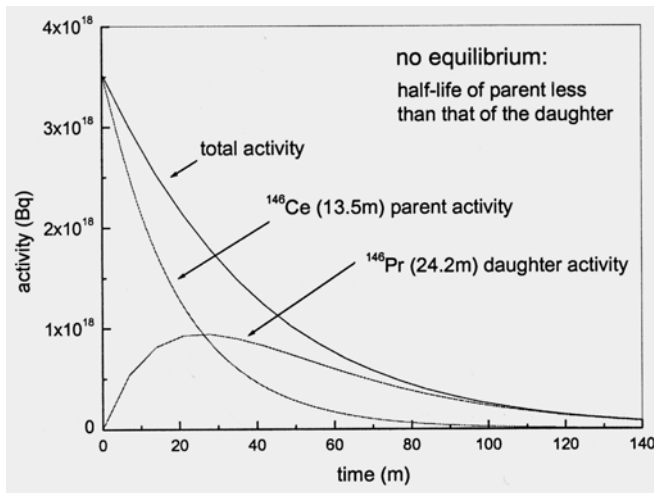
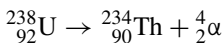


**Fig. 3.9.** Schematic illustration of ‘no-equilibrium’ between a parent  $^{146}\text{Ce}$  and its daughter  $^{146}\text{Pr}$ : total activity approaches the daughter activity with time

## Decay Energy

The decay energy is the total energy released in a radioactive decay. A radioactive decay reaction is a special case of a binary nuclear reaction  $a + X \rightarrow Y + b$  (see section *Q-Value for a Reaction*) in which there is no particle  $a$  and  $X$  is at rest. The decay energy is just the  $Q$ -value for this type of reaction.

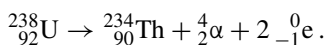
Consider the radioactive decay of  $^{238}\text{U}$  is commonly written in the form:



and the  $Q$  value for this reaction as:

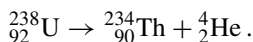
$$Q = M(^{238}\text{U}) - M(^{234}\text{Th}) - m_{\alpha}.$$

However, it should be noted that in all nuclear reactions, total charge must be conserved. In the above reaction, the number of electrons is not conserved. On the left hand side, the uranium atom has 92 electrons. On the right, the thorium atom has 90 electrons and the alpha particle no electrons. Before proceeding, care is required to balance the electron number. This can be done by noting that, when an alpha particle is emitted from the uranium atom, the emission of the alpha particle must be accompanied by the emission of two orbital electrons from the thorium atom. The correct reaction should be written as:



Conceptually the two electrons can be combined with the alpha particle to produce a He atom with two electrons (the binding energy of the two electrons in the helium atom is neglected) i.e.





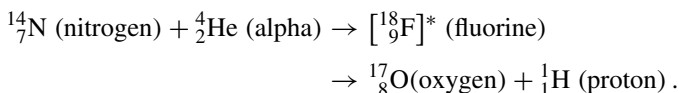
The  $Q$ -value can now be expressed in terms of the atomic masses as:

$$\begin{aligned} Q &= M({}_{92}^{238}\text{U}) - M({}_{90}^{234}\text{Th}) - M({}_2^4\text{He}) \\ &= (238.050788 \text{ u}) - (234.043601 \text{ u}) - (4.002603 \text{ u}) \\ &= 0.004584 \text{ u} = 4.27 \text{ MeV}. \end{aligned}$$

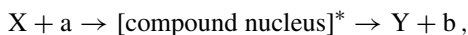
Alternatively, the decay energy can be obtained for the emitted alpha particles together with the recoil energy of the thorium atom. About 77% of the  $\alpha$  particles emitted have a kinetic energy of 4.20 MeV and 23% have an energy of 4.15 MeV. The 4.20 MeV transition results in the ground state of  ${}^{234}\text{Th}$ . The 4.15 MeV transition gives rise to an excited state which then decays by the emission of a 0.05 MeV photon to the ground state. Thus the total decay energy is 4.20 MeV plus the recoil energy of the thorium nucleus. From conservation of momentum, the momentum  $p$  of the alpha particle and the thorium nucleus must be equal. Since the energy  $E$  is related to the momentum by  $E = p^2/2M$ , it follows that the energy of the recoiling thorium nucleus is  $E_{\text{Th}} = (4/234) \times E_{\alpha} = 0.07 \text{ MeV}$ . Hence the total decay energy  $Q$  is 4.27 MeV.

## Nuclear Reactions

During his investigations on the scattering of alpha particles by nuclei, Rutherford noticed that certain light elements could be disintegrated by these alpha particles. In 1919, he placed an alpha particle source inside a box that could be filled with various gases. A zinc sulphide screen was placed outside the box to detect scintillations. When the box was filled with nitrogen, scintillations were seen on the screen. These scintillations could not have been produced by alpha particles since the distance between the source and the screen was greater than the range of alpha particles in the gas. Rutherford concluded that the particles were protons ejected by the impact of the alpha particles on nitrogen nuclei. This, now famous, nuclear reaction can be written



This transmutation of nitrogen into oxygen was the first artificially induced nuclear reaction (notice that radioactive decay is also a nuclear reaction but it occurs naturally). Nuclear reactions involve the absorption of a bombarding particle by the nucleus of the target material. Absorption of the bombarding particle first produces an excited compound nucleus (fluorine in the above example) which then decays to yield the final products. The main interactions of interest occur when the bombarding particles are alpha particles, protons, deuterons, neutrons, light nuclei, and photons. The nuclear reaction can be represented as



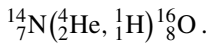
where X is the target nucleus, a the bombarding particle, Y the product nucleus, and b the emitted particle. In condensed form this reaction can be written as

Target (projectile, emission) Product

or

$X(a, b)Y$ .

Since the total charge  $Z$  and the total number of nucleons must be the same before and after the reaction, it is customary to include these in the reaction as shown in the transmutation reaction with nitrogen above. In condensed form, this reaction can be written



### Cross-sections

The likelihood of an interaction between a bombarding particle and a nucleus is described by the concept of cross-section denoted by the Greek letter  $\sigma$ . There is no guarantee that a particular bombarding projectile will interact with the target nucleus to bring about a given reaction –  $\sigma$  provides only a measure of the probability that it will occur. The cross-section depends on the properties of the target nuclei and the incident projectile.

If a target is irradiated by particles or photons, then the reduction in flux of the particles or photons after passing through the target is given by

$$-\frac{d\phi}{dx} = \sigma N\phi$$

where  $\phi$  is the flux of projectiles,  $N$  is the number of target atoms per unit volume, and  $\sigma$ , the cross-section, is the constant of proportionality. From this relation, the units of cross-section are  $\text{m}^2$  or  $\text{cm}^2$ . Cross-sections are usually in the range of  $10^{-24} \text{ cm}^2$ . Nuclear physicists use the unit of barn, abbreviated b, where:

$$1 \text{ b} = 10^{-24} \text{ cm}^2.$$

Cross-sections are defined for all types of reaction resulting from the interaction of an incident particle and a nucleus. In the case of an absorption reaction, the de-excitation of the compound nucleus may involve the emission of an alpha particle, electrons, positrons, protons,  $\gamma$ -rays or, in the case of fission, fission fragments. All the different decay “paths” can be referred to by a specific cross-section such as  $\sigma_\alpha$  for  $\alpha$  emission,  $\sigma_\beta$  for  $\beta$  emission,  $\sigma_f$  for fission cross-section, etc.

To represent a particular reaction (see Table 3.2), the abbreviated symbol of the incident and emitted particles within parenthesis is used, e.g. alpha-proton ( $\alpha, p$ ), alpha-neutron ( $\alpha, n$ ), neutron-proton ( $n, p$ ), gamma-proton ( $\gamma, p$ ), proton-gamma ( $p, \gamma$ ), neutron-fission ( $n, f$ ), etc. The corresponding cross-sections are abbreviated the same way e.g. the neutron-fission cross-section is noted  $\sigma_{(n,f)}$ .

**Table 3.2.** Examples of nuclear reactions [6, 7]

Reaction type	Reaction	Description
( $\alpha, p$ )	${}^4_2\text{He} + {}^{14}_7\text{N} \rightarrow {}^{17}_8\text{O} + {}^1_1\text{H}$ or ${}^{14}_7\text{N}(\alpha, p){}^{17}_8\text{O}$	The first nuclear reaction reported by Rutherford in 1919. By bombarding nitrogen with alpha particles he observed the production of protons. This transmutation of nitrogen was the first artificially induced nuclear reaction.
( $\alpha, n$ )	${}^4_2\text{He} + {}^9_4\text{Be} \rightarrow {}^{12}_6\text{C} + {}^1_0\text{n}$ or ${}^9_4\text{Be}(\alpha, n){}^{12}_6\text{C}$ $\alpha + {}^9\text{Be} \rightarrow {}^{12}\text{C} + \text{n}$	The neutron was discovered by Chadwick in 1932 by bombarding beryllium with alpha particles.
( $\gamma, n$ )	$\gamma + {}^2_1\text{H} \rightarrow {}^1_1\text{H} + {}^1_0\text{n}$ or ${}^2_1\text{H}(\gamma, n){}^1_1\text{H}$	Highly energetic (gamma) photons can knock neutrons directly out of the nucleus. In this case, photon irradiation of deuterium results in hydrogen with the generation of neutrons.
( $p, \gamma$ )	${}^1_1\text{H} + {}^7_3\text{Li} \rightarrow {}^8_4\text{Be} + \gamma$ or ${}^7_3\text{Li}(p, \gamma){}^8_4\text{Be}$	Protons can induce nuclear reactions. In the radiative capture of a proton, the nucleus enters into a higher energy state and de-excites with the emission of a photon. The product nucleus decays immediately into two alpha particles.
( $\gamma, \alpha n$ )	$\gamma + {}^{17}_8\text{O} \rightarrow {}^{12}_6\text{C} + {}^4_2\text{He} + {}^1_0\text{n}$ or ${}^{17}_8\text{O}(\gamma, \alpha n){}^{12}_6\text{C}$	High energy photon can split oxygen into carbon, an alpha particle and a neutron.
( $n, p$ )	${}^1_0\text{n} + {}^{16}_8\text{O} \rightarrow {}^{16}_7\text{N} + {}^1_1\text{p}$ or ${}^{16}_8\text{O}(n, p){}^{16}_7\text{N}$	High energy neutrons (in a fast reactor) can interact with oxygen to produce nitrogen and a proton.
( $n, f$ )	${}^1_0\text{n} + {}^{235}_{92}\text{U} \rightarrow \text{fission products}$	Neutron induced fission
( $d, n$ )	${}^2_1\text{H} + {}^3_1\text{H} \rightarrow {}^4_2\text{He} + {}^1_0\text{n}$ or $\text{D} + \text{T} \rightarrow \text{He} + \text{n}$ , or $\text{T}(d, n)\text{He}$	Fusion reaction
( $n, nT$ )	$\text{n} + {}^7\text{Li} \rightarrow {}^3\text{H} + \text{n}$	Tritium (denoted by T or ${}^3\text{H}$ ) production
( $n, p$ )	$\text{n} + {}^{14}\text{N} \rightarrow {}^{14}\text{C} + \text{p}$	Cosmogenic production of ${}^{14}\text{C}$ by cosmic ray protons

## Neutron Reactions

A special class of nuclear reactions involves neutrons. Due to the fact that they have no charge, neutrons are very effective in penetrating the nucleus producing nuclear reactions. Nuclear reactors and so-called “spallation” sources produce very high fluxes of neutrons. A list of the main neutron reactions is given in Table 3.3.

**Table 3.3.** Main neutron induced nuclear reactions

	n,4n	n,t
Elastic	n,p	n, <sup>3</sup> He
Inelastic	n,2p	n,α
n,γ	n,np	n,nα
n,fission	n,nd	n,n2α
n,2n	n,nt	n,2nα
n,3n	n,d	n,t2α

The most common neutron reaction is radiative capture. In this process the excitation energy induced by the neutron is released by the emission of a gamma photon. The process is denoted by (n,γ) as shown in the table. In this process the mass number of the nucleus increases by one but the charge remains unchanged. Hence the process of radiative capture produces a new isotope of the target element. This new isotope may be short-lived, in which case it will decay to a new chemical element through the emission of an alpha particle etc.

Another important reaction is neutron induced fission denoted by (n,fission) in the table. In this process, the excitation energy induced by the neutron causes the nucleus to break up or “fission” into lighter elements.

## Burnout Time

The half-life of a radioactive nuclide,  $\tau$ , is defined as the time it takes for half of the atoms of a radioactive source to undergo transformation. If one takes the standard decay equation:

$$\frac{dN(t)}{dt} = -kN,$$

where  $N(t)$  is the number of atoms at the time  $t$ , and  $k$  is the decay constant, the solution is  $N(t) = N(0) \exp(-kt)$ . It follows that  $\frac{1}{2} = \exp(-k\tau)$  and hence  $\tau = \ln 2/k$ . In a reactor, the rate of disappearance of a nuclide is given by

$$\frac{dN(t)}{dt} = -\sigma_a N \Phi,$$

where  $N(t)$  is the number of atoms at the time  $t$ ,  $\sigma_a$  the absorption cross-section and  $\Phi$  the neutron flux of the reactor. The absorption cross-section is the sum of the capture and fission cross-sections i.e.  $\sigma_a = \sigma_{n,\gamma} + \sigma_{n,\text{fission}}$ .

Similarly to the definition of the half-life, a “burnout time”  $\tau_{bo}$  can be defined as the time it takes for half the atoms to transform to the heavier isotope i.e.  $\tau_{bo} = \ln 2 / (\sigma_a \cdot \phi)$ . The above relations can be combined to give a relation for the overall rate of change due to decay and reaction of a nuclide in a neutron flux i.e.:

$$\frac{dN(t)}{dt} = -kN - \sigma_a N \Phi = - \left( \frac{\ln 2}{\tau} + \frac{\ln 2}{\tau_{bo}} \right) N .$$

In this equation, when  $\tau \gg \tau_{bo}$  (long half-life, short burnout time), one can neglect the decay process as the absorption of a neutron occurs much faster than the decay, and when  $\tau_{bo} \gg \tau$  (long burnout time and short half-life), one can neglect the nuclear reaction as the nuclide has decayed long before a neutron is absorbed.

In the case of a  $^{238}\text{U}$  nucleus in a reactor, the  $^{238}\text{U}$  will transform mainly by neutron absorption to give  $^{239}\text{U}$ , since the burnout time for  $^{238}\text{U}$  (26.9 y) is much shorter than its half-life of  $4.47 \times 10^9$  years. This  $^{239}\text{U}$  then decays to  $^{239}\text{Np}$  since the half-life of  $^{239}\text{U}$  (23.4 minutes) is shorter than its burnout time. The  $^{239}\text{Np}$  then decays to  $^{239}\text{Pu}$  as its half-life of 2.35 days is much shorter than its burnout time (for a standard neutron flux of  $3 \times 10^{14}$  neutrons  $\text{cm}^{-2} \text{s}^{-1}$ ) of 2.0 years. The  $^{239}\text{Pu}$  then absorbs neutrons and goes on to  $^{240}\text{Pu}$  and  $^{241}\text{Pu}$  which have a half-life of several years, so that the burnout time is much shorter and the neutron reaction takes place. The reaction path for  $^{238}\text{U}$  in a thermal neutron flux of  $3 \times 10^{14}$  neutrons  $\text{cm}^{-2} \text{s}^{-1}$  is shown in Fig. 3.10.

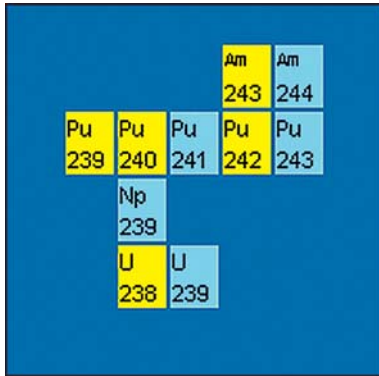


**Fig. 3.10.** First 9 steps of reaction path of  $^{238}\text{U}$  (from the “Universal Nuclide Chart”, App. E) [8]

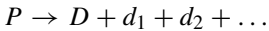
One has to be careful with neglecting a particular process. If the half-life and the burnout time for the standard neutron flux of  $3 \times 10^{14}$  neutrons  $\text{cm}^{-2} \text{s}^{-1}$  are not very different, only a small change in the neutron flux will change the behaviour of the nuclide.

Changing the neutron flux can change the reaction path. This can be illustrated with the nuclide  $^{233}\text{Pa}$ . This nuclide has a half-life of 26.9 days and a burnout time of 1.8 years. In this case, the  $^{233}\text{Pa}$  decays to  $^{233}\text{U}$ . But if the neutron flux is increased to  $8 \times 10^{15}$  neutrons  $\text{cm}^{-2} \text{s}^{-1}$ , the burnout time decreases to 25 days, so that the probability for the neutron reaction is higher than for the decay. This means that  $^{233}\text{Pa}$  absorbs a neutron and gives  $^{234}\text{Pa}$  more often than decaying to  $^{233}\text{U}$ .

## 4. Types of Radioactive Decay

### Decay Modes

Radioactive decay is a spontaneous nuclear transformation which results in the formation of new elements. In this process, an unstable “parent” nuclide  $P$  is transformed into a more stable “daughter” nuclide  $D$  through various processes. Symbolically the process can be described as follows:



where the light products  $d_1 + d_2 + \dots$  are the emitted particles. The process is usually accompanied by the emission of gamma radiation. If the daughter nuclide is also unstable, the radioactive decay process continues further in a decay chain until a stable nuclide is reached. Radioactive nuclides decay spontaneously by the following processes:

- Alpha ( $\alpha$ ) decay
- Beta-minus ( $\beta^-$ ) decay
- Gamma emission ( $\gamma$ )
- Isomeric transitions (IT)
- Beta-plus ( $\beta^+$ ) decay
- Electron capture ( $\epsilon$  or  $ec$ )
- Spontaneous fission (SF)
- Proton decay (p)
- Special beta-decay processes ( $\beta^-n$ ,  $\beta^+\alpha$ ,  $\beta^+p$ )
- Heavy-ion radioactivity ( $^{14}\text{C}$ ,  $^{24}\text{Ne}$ , etc.)
- Decay of bare nuclei-bound beta decay

Radioactive decay is a nuclear process and is largely independent of the chemical and physical states of the nuclide. The actual process of radioactive decay depends on the neutron to proton ratio and on the mass-energy relationship of the parent, daughter, and emitted particle(s). As with any nuclear reactions, the various conservation laws must hold.

A summary of the pure and mixed modes is given in Tables 4.1 and 4.2 [1]. There are 8 known pure decay modes ( $\alpha$ ,  $\beta^-$ ,  $\beta^+$ ,  $ec$ , SF, n, p, CE). In addition to the pure decay modes listed, there are mixed modes, listed in Table 4.2, ranging from special

beta decay processes such as beta delayed neutron, alpha, or proton emission to more exotic decay modes such as two-proton (2p) emission and “cluster” emission. Cluster emission is a generic term covering a variety of rare decay processes – they are grouped together with the mixed decay modes in Table 4.2. A description of pure decay modes is given in Table 4.3.

**Table 4.1.** Pure decay modes

Mode	Symbol
Alpha	$\alpha$
Beta minus	$\beta^-$
Beta plus	$\beta^+$
Electron capture	ec
Spontaneous fission	SF
Neutron	n
Proton	p
Cluster emission	CE

**Table 4.2.** Mixed decay modes

$(\beta^-)$	$(\beta^+/ec)$	(IT)	CE
$2\beta^-$	$2\beta^+$	IT, $\alpha$	$^{12}\text{C}$
$\beta^-,d$	$\beta^+,xa^\dagger$		$^{14}\text{C}$
$\beta^-,t$	$\beta^+,\alpha$	(proton)	$^{20}\text{O}$
$\beta^-,x\alpha^\dagger$	$\beta^+,2\alpha$	2p	$^{23}\text{F}$
$\beta^-, \alpha$	$\beta^+,3\alpha$		$^{24}\text{Ne}$
$\beta^-,2\alpha$	$\beta^+,SF$	(neutron)	$^{28}\text{Mg}$
$\beta^-,3\alpha$	$\beta^+,xp^\dagger$	n, $xn^\dagger$	$^{30}\text{Mg}$
$\beta^-, xn^\dagger$	$\beta^+,p$	2n (n,n)	$^{32}\text{Si}$
$\beta^-,n$	$\beta^+,2p$	3n (n,2n)	$^{34}\text{Si}$
$\beta^-,2n$	$\beta^+,3p$	4n (n,3n)	
$\beta^-,3n$	$\beta^+,ec$		$^{24}\text{Ne}+^{26}\text{Ne}$
$\beta^-,4n$	ec, $\alpha$		$^{24}\text{Ne}+^{25}\text{Ne}$
$\beta^-,SF$	ec,p		$^{28}\text{Mg}+^{30}\text{Mg}$

$^\dagger$  Denotes multiple particle emission

**Table 4.3.** Summary of different types of radioactive decay. The parent nuclide is denoted by  $P$  and the daughter nuclide by  $D$ .

Decay type	Reaction	Description
Alpha ( $\alpha$ )	${}^A_Z P \rightarrow {}^A_{Z-2} D + \alpha$	In proton rich nuclides, an alpha particle ( ${}^4_2\text{He}$ ) can be emitted – the daughter nucleus contains two protons and two neutrons less than the parent.
Beta-minus ( $\beta^-$ )	${}^A_Z P \rightarrow {}^A_{Z+1} D + \beta^- + \bar{\nu}$	In neutron rich nuclides, a neutron in the nucleus can decay to a proton – thereby an electron ( $\beta^-$ ) is emitted together with an anti-neutrino ( $\bar{\nu}$ ).
Beta-plus ( $\beta^+$ )	${}^A_Z P \rightarrow {}^A_{Z-1} D + \beta^+ + \nu$	In proton rich nuclides, a proton in the nucleus changes to a neutron – thereby a positron ( $\beta^+$ ) is emitted together with a neutrino ( $\nu$ ).
Electron capture ( $\epsilon$ or $ec$ )	${}^A_Z P + e^- \rightarrow {}^A_{Z-1} D^* + \nu$	An orbital electron is “captured” by the nucleus and results in a proton being converted to a neutron and a neutrino ( $\nu$ ). The daughter nucleus is usually left in an excited state.
Gamma ( $\gamma$ )	${}^A_Z P^* \rightarrow {}^A_Z P + \gamma$	An atom in an excited state decays through the emission of a photon.
Isomeric transition (IT)	${}^A_m P \rightarrow {}^A_Z P + \gamma$	Isomeric transition occurs in long-lived metastable states (isomers) of parent nuclei.
Internal conversion (IC)	${}^A_Z P^* \rightarrow [{}^A_Z P]^+ + e^-$	A nucleus in an excited state ejects an orbital (usually a $K$ -shell) electron.
Proton (p)	${}^A_Z P \rightarrow {}^A_{Z-1} D + p$	A proton is ejected from the nucleus.
Neutron (n)	${}^A_Z P \rightarrow {}^A_{Z-1} D + n$	A neutron is ejected from the nucleus.
Spontaneous fission (SF)	${}^A_Z P \rightarrow D_H + D_L + \nu n$	In this process, the parent nucleus splits into heavy and light fragment daughter nuclei ( $D_H$ , $D_L$ ) with mass and charge roughly half that of the parent, and several neutrons $\nu n$ .
Special beta-decay processes $\beta^-n$ , $\beta^+\alpha$ , $\beta^+p$	${}^A_Z P \rightarrow {}^A_{Z+1} D^* + \beta^- + \bar{\nu}$ ${}^A_{Z+1} D^* \rightarrow {}^A_{Z+1} D + n$	Particle (neutron, alpha, proton) emission immediately follows beta decay.
Heavy-ion radioactivity	${}^A_Z P \rightarrow D_H + D_L$	A heavy parent decays by the emission of a light ion.



### Alpha ( $\alpha$ ) Decay

In alpha decay, the parent atom  ${}^A_Z P$  emits an alpha particle  ${}^4_2\alpha$  and results in a daughter nuclide  ${}^{A-4}_{Z-2} D$ . Immediately following the alpha particle emission, the daughter atom still has the  $Z$  electrons of the parent – hence the daughter atom has two electrons too many and should be denoted by  ${}^{A-4}_{Z-2} D^{2-}$ . These extra electrons are lost soon after the alpha particle emission leaving the daughter atom electrically neutral. In addition, the alpha particle will slow down and lose its kinetic energy. At low energies

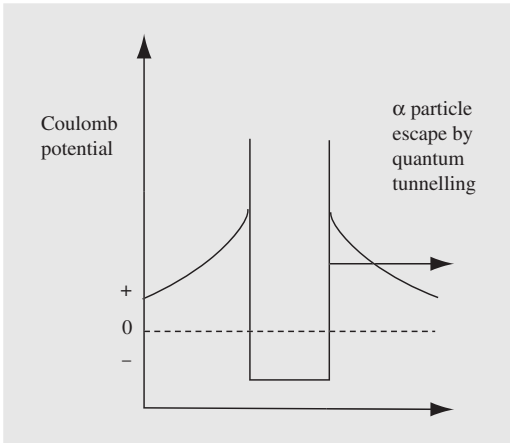
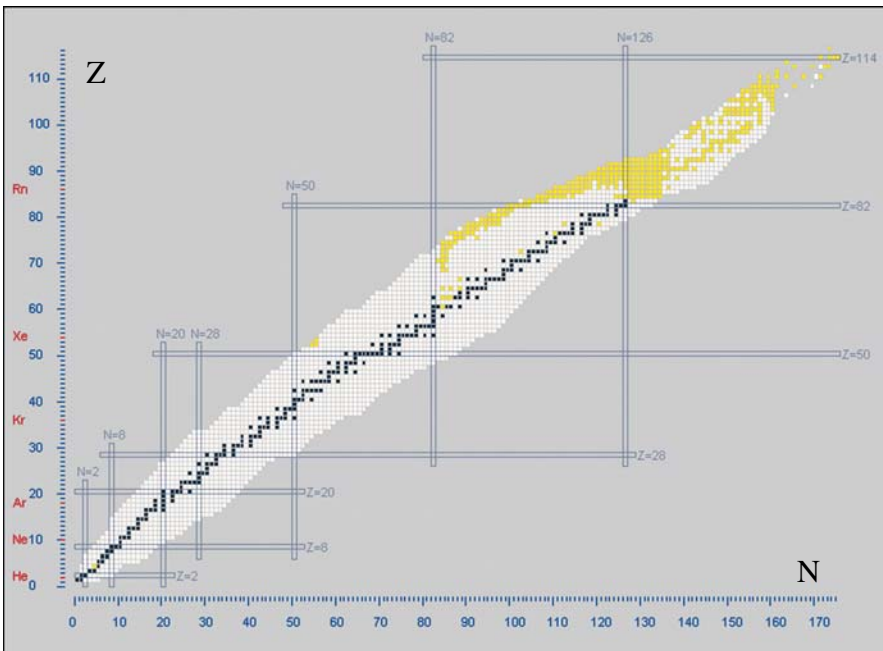
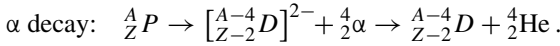


**Fig. 4.1.** Potential barrier near nucleus

**Fig. 4.2 (below).** Alpha emitters (yellow) in Nuclides.net [1]



the alpha particle will acquire two electrons to become a neutral helium atom. The alpha decay process is described by:



The process of alpha decay is found mainly in proton rich, high atomic number nuclides due to the fact that electrostatic repulsive forces increase more rapidly in heavy nuclides than the cohesive nuclear force. In addition, the emitted particle must have sufficient energy to overcome the potential barrier in the nucleus as shown in Fig. 4.1. The height of the potential barrier is about 25 MeV. Nevertheless, alpha particles can escape this barrier by the process of quantum tunnelling.

The known alpha emitters are shown in yellow in Fig. 4.2. There are in total 815 alpha emitting nuclides listed in the Nuclides.net [1] database.

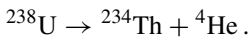
### Decay Energy

From Chap. 3, the  $Q$ -value for alpha decay is given by

$$\begin{aligned} \frac{Q_\alpha}{c^2} &= M({}^A_Z P) - [M({}^{A-4}_{Z-2} D)^{2-}) + m({}^4_2\alpha)] \\ &\cong M({}^A_Z P) - [M({}^{A-4}_{Z-2} D) + 2m_e + m({}^4_2\alpha)] \\ &\cong M({}^A_Z P) - [M({}^{A-4}_{Z-2} D) + M({}^4_2\text{He})]. \end{aligned}$$

In the above reactions, the binding energy of the two electrons on the daughter atom, as well as in the helium atom is of the order of a few eV and hence negligible in comparison to the  $Q$ -value which is of the order MeV. The  $Q$ -value in the above is now expressed in terms of tabulated atomic masses.

As an example of alpha particle emission, we consider the alpha decay from  ${}^{238}\text{U}$ , i.e.



In this reaction, the neutron to proton ratio increases from 1.59 for  ${}^{238}\text{U}$  to 1.6 for  ${}^{234}\text{Th}$ . It is of interest to evaluate the  $Q$ -value and to determine the energy distribution among the reactions products. Hence, using the atomic masses listed in Appendix D,

$$\begin{aligned} \frac{Q_\alpha}{c^2} &= M({}^{238}\text{U}) - M({}^{234}\text{Th}) - M({}^4\text{He}) \\ &= (238.050788 \text{ u}) - (234.043601 \text{ u}) - (4.002603 \text{ u}) \\ &= 0.004584 \text{ u} \hat{=} 4.27 \text{ MeV}. \end{aligned}$$

From conservation of energy and momentum, it follows that

$$\begin{aligned} E_\alpha &= Q_\alpha \cdot \frac{M(\text{Th})}{[M(\text{Th}) + M(\text{He})]} \\ &\cong 4.27 \text{ MeV} \cdot \left(\frac{234}{238}\right) = 4.2 \text{ MeV} \end{aligned}$$

and

$$E_{\text{Th}} = Q_{\alpha} \cdot \frac{M(\text{He})}{[M(\text{Th}) + M(\text{He})]}$$

$$\cong 4.27 \text{ MeV} \cdot \left( \frac{4}{238} \right) = 0.07 \text{ MeV}$$

where it can be seen that the lighter alpha particle transports most of the kinetic energy.

### Energy Level Diagram

The energy level diagram for the alpha decay from  $^{238}\text{U}$  is shown in Fig. 4.3.

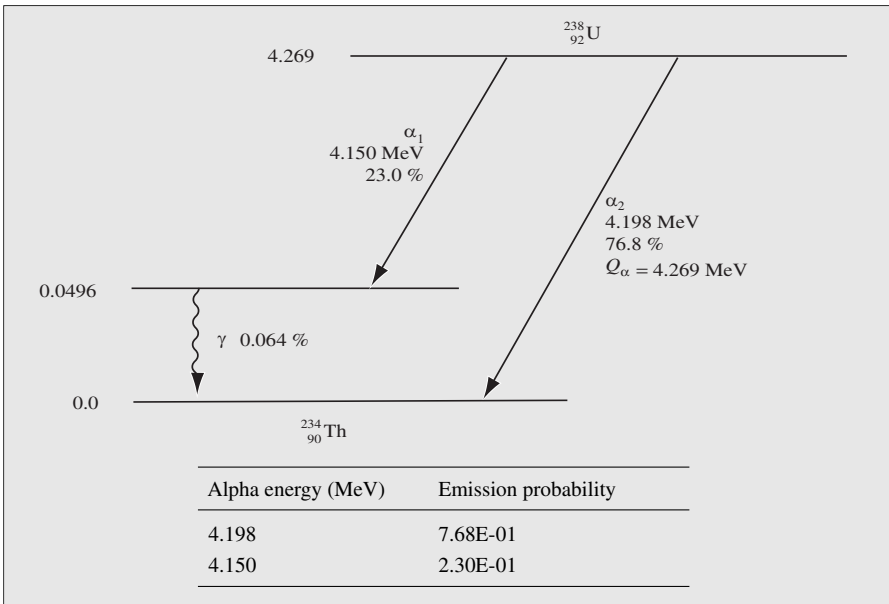


**Fig. 4.3.** Energy levels for alpha decay of  $^{238}\text{U}$  showing the main  $\alpha$  and associated  $\gamma$  emissions

In their interaction with matter, the alpha particles give up their energy and become neutral helium atoms. Their range in solids and liquids is very short – of the order of micrometres. In air the range is typically a few centimetres. Because of this short range, they do not normally constitute a hazard to humans. They are absorbed in the outer layers of the skin before they cause injury. If the alpha emitters are taken internally, for example by ingestion or inhalation, they are very toxic because of the large amount of energy released in a short distance within living tissue. This property can be used for killing cancer cells in such processes as alpha-immunotherapy (see Chap. 7).

### Beta-minus ( $\beta^-$ ) Decay

$\beta^-$  radioactivity occurs when a nucleus emits a negative electron from an unstable radioactive nucleus. This happens when the nuclide has an excess of neutrons. The-

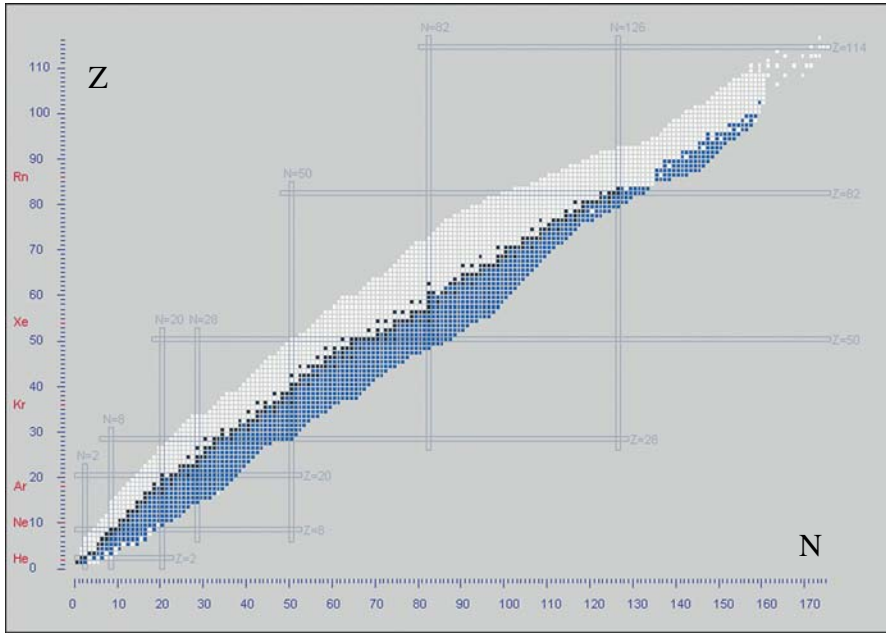
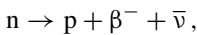


**Fig. 4.4.**  $\beta^-$  emitters (blue) in Nuclides.net [1]

oretical considerations (the fact that there are radionuclides which decay by both positron and negatron emission and the de Broglie wavelength of MeV electrons is much larger than nuclear dimensions), however, do not allow the existence of a negative electron in the nucleus. For this reason the beta particle is postulated to arise from the nuclear transformation of a neutron into a proton through the reaction



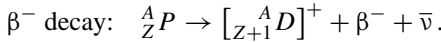
where  $\bar{\nu}$  is an antineutrino. The ejected high energy electron from the nucleus and denoted by  $\beta^-$  to distinguish it from other electrons denoted by  $e^-$ .

Beta emission differs from alpha emission in that beta particles have a continuous spectrum of energies between zero and some maximum value, the endpoint energy, characteristic of that nuclide. The fact that the beta particles are not monoenergetic but have a continuous energy distribution up to a definite maximum energy, implies that there is another particle taking part i.e. the neutrino  $\nu$ .

This endpoint energy corresponds to the mass difference between the parent nucleus and the daughter as required by conservation of energy. The average energy of the beta particle is approximately  $\frac{1}{3}$  of the maximum energy.

More precisely, the “neutrino” emitted in  $\beta^-$  decay is the anti-neutrino (with the neutrino being emitted in  $\beta^+$  decay). The neutrino has zero charge and almost zero mass. The maximum energies of the beta particles range from 10 keV to 4 MeV. Although beta minus particles have a greater range than alpha particles, thin layers of water, glass, metal, etc. can stop them. There are 1281  $\beta^-$  emitters in the Nuclides.net database [1] (shown in Fig. 4.4).

The  $\beta^-$  decay process can be described by:



Immediately following the decay by beta emission, the daughter atom has the same number of orbital electrons as the parent atom and is thus positively charged. Very quickly, however, the daughter atom acquires an electron from the surrounding medium to become electrical neutral.

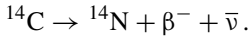
Beta radiation can be an external radiation hazard. Beta particles with less than about 200 keV have limited penetration range in tissue. However, beta particles give rise to Bremsstrahlung radiation which is highly penetrating.

### Decay Energy

From Chap. 3, the  $Q$ -value for  $\beta^-$  decay is given by

$$\begin{aligned} \frac{Q_{\beta^-}}{c^2} &= M({}_Z^A P) - [M({}_{Z+1}^A D)^+ + m_{\beta^-} + m_{\bar{\nu}}] \\ &\cong M({}_Z^A P) - [M({}_{Z+1}^A D) - m_e + m_{\beta^-} + m_{\bar{\nu}}] \\ &\cong M({}_Z^A P) - M({}_{Z+1}^A D), \end{aligned}$$

where the  $Q$ -value is now expressed in terms of the atomic masses. As an example of  $\beta^-$  emission, we consider the beta decay of  ${}^{14}\text{C}$ , i.e.



From the atomic masses listed in Appendix D, the decay energy is given by

$$\begin{aligned} \frac{Q_{\beta^-}}{c^2} &= M({}^{14}\text{C}) - M({}^{14}\text{N}) = 14.003242 \text{ u} - 14.003074 \text{ u} \\ &= 0.000168 \text{ u} \cong 0.1565 \text{ MeV}. \end{aligned}$$

### Energy Level Diagram

The energy level diagram for the decay of  ${}^{14}\text{C}$  is shown in Fig. 4.5. A more complicated example is shown in Fig. 4.6 for the decay of  ${}^{38}\text{Cl}$ . In this case, the daughter  ${}^{38}\text{Ar}$  can be produced in an excited state following  $\beta^-$  decay. From the figure it can be seen that the  ${}^{38}\text{Cl}$  parent can decay to both the ground state and two excited states.

The decay energy to the ground state is given by

$$\begin{aligned} \frac{Q_{\beta^-}}{c^2} &= M({}^{38}\text{Cl}) - M({}^{38}\text{Ar}) = 37.968010 \text{ u} - 37.962732 \text{ u} \\ &= 0.005278 \text{ u} \cong 4.917 \text{ MeV}. \end{aligned}$$

To evaluate the decay energy or  $Q$ -value to an energy state higher than the ground state, the mass of the daughter atom  $M({}_{Z+1}^A D)$  must be replaced by the mass of the excited daughter i.e.  $M({}_{Z+1}^A D^*) \cong M({}_{Z+1}^A D) + E^*/c^2$ . Hence the decay energy to the excited state with energy  $E^*$  above the ground state is

$$\frac{Q_{\beta^-}}{c^2} = M({}_Z^A P) - M({}_{Z+1}^A D) - \frac{E^*}{c^2}.$$

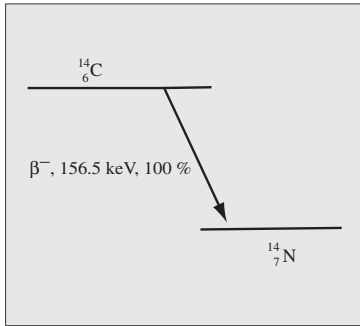


**Fig. 4.5.** Energy levels for beta decay of  $^{14}\text{C}$  showing the main  $\beta^-$  emission

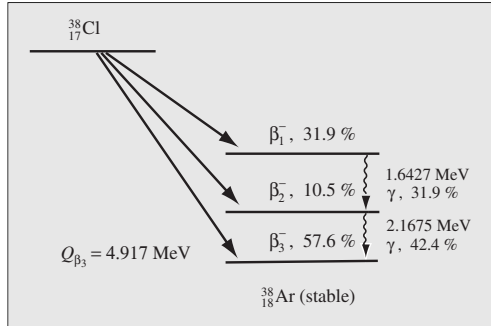


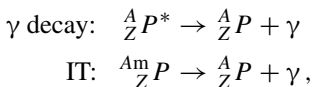
**Fig. 4.6.** Energy levels for beta decay of  $^{38}\text{Cl}$ . Three groups of  $\beta^-$  particles are emitted [2]

## Gamma Emission and Isomeric Transition (IT)

Gamma emission is not a primary decay process but usually accompanies alpha and beta decay. Typically this type of radiation arises when the daughter product resulting from alpha or beta decay is formed in an excited state. This excited state returns very rapidly ( $< 10^{-9}$  s) to the ground state through the emission of a gamma photon. Instead of having a well-defined range like alpha and beta particles, gamma rays lose characteristically a certain fraction of their energy per unit distance through matter. Gamma rays are highly penetrating and can result in considerable organic damage. Gamma emitting sources require heavy shielding and remote handling.

In contrast to normal gamma emission that occurs by dipole radiation, isomeric transitions must occur by higher order multipole transitions that occur on a longer time-scale. If the lifetime for gamma emission exceeds about one nanosecond, the excited nucleus is defined to be in a metastable or isomeric state (denoted by m). The decay process from this excited state is known as an isomeric transition (IT).

The gamma decay or isomeric transition process can be described by:



where the asterisk \* denotes the excited state and m the isomeric or metastable state.

### Decay Energy

From conservation of energy

$$M({}^A_Z P) = M({}^A_Z P^*) - \frac{E^*}{c^2},$$

where  $E^*$  is the excitation energy of the nucleus. On de-excitation the energy  $E^*$  is shared between the energy of the gamma photon  $E_\gamma$  and the recoil energy of the atom  $E_P$ .

The decay energy or  $Q$ -value for the gamma transition is given by

$$Q_{\gamma,IT} = E^* = E_{\gamma} + E_P .$$

From conservation of energy and momentum, it can be shown that

$$E_{\gamma} = Q_{\gamma,IT} \cdot \left[ 1 + \frac{E_{\gamma}}{2M_P c^2} \right]^{-1} .$$

Since the photon energy has a maximum value of approximately 10 MeV, and  $2M_P c^2 > 4000$  MeV, it follows that  $E_{\gamma} \cong Q_{\gamma,IT} = E^*$  such that in gamma emission or isomeric transition, the kinetic energy of the recoil nucleus is negligible in comparison to the energy of the gamma photon.

There are 473 nuclides which decay by isomeric transition in the Nuclides.net [1] database.

## Internal Conversion (IC)

Alternative to gamma emission, the excited nucleus may return to the ground state by ejecting an orbital electron. This is known as internal conversion and results in the emission of an energetic electron and X-rays due to electrons cascading to lower energy levels. The ratio of internal conversion electrons to gamma emission photons is known as the internal conversion coefficient. Conversion electrons are monoenergetic.

The internal conversion process can be described by:

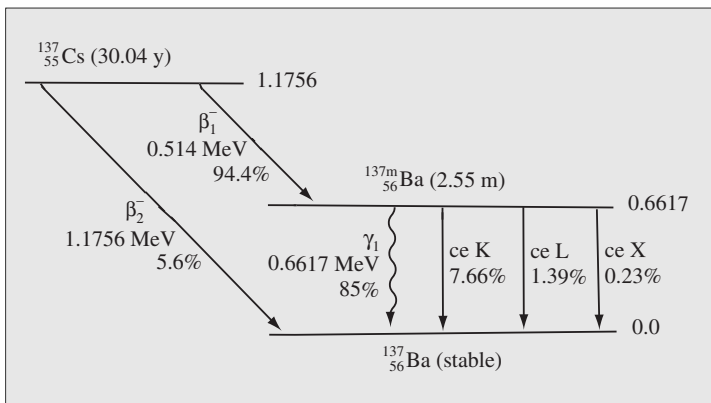
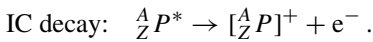


**Fig. 4.7.** Gamma emission and internal conversion (ce) of  ${}^{137m}\text{Ba}$  in the transformation of  ${}^{137}\text{Cs}$  to  ${}^{137}\text{Ba}$  [2]

### Decay Energy

The  $Q$ -value for internal conversion is given by

$$\begin{aligned} \frac{Q_{IC}}{c^2} &= M({}_Z^A P^*) - [M({}_Z^A P^+) + m_{e^-}] \\ &\cong \left[ M({}_Z^A P) + \frac{E^*}{c^2} \right] - \left[ \left\{ M({}_Z^A P) - m_e + \frac{BE_e}{c^2} \right\} + m_e \right] \\ &= \frac{[E^* - BE_e]}{c^2}. \end{aligned}$$

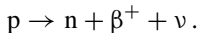
From conservation on energy and momentum, this energy is shared between the daughter ion and IC electron as follows:

$$\begin{aligned} E_e &= \left[ \frac{M({}_Z^A P)}{M({}_Z^A P) + m_e} \right] [E^* - BE_e] \cong E^* - BE_e \\ E_{ion} &= \left[ \frac{m_e}{M({}_Z^A P) + m_e} \right] [E^* - BE_e] \cong 0. \end{aligned}$$

Consider the decay of the isomeric state  $^{137m}\text{Ba}$ . This nuclide emits a 0.661 MeV photon which undergoes internal conversion in 11% of the transitions. These conversion electrons are seen in the beta spectrum of  $^{137}\text{Cs}$ . Following the internal conversion, outer orbital electrons fill the deeper energy levels and result in characteristic X-ray emission. These X-rays can in turn lead to the ejection of outer electrons through an internal photoelectric effect. The low energy ejected electrons are known as Auger electrons.

### Beta-plus ( $\beta^+$ ) Decay (Positron Emission)

In nuclides where the neutron to proton ratio is low, and alpha emission is not energetically possible, the nucleus may become more stable by the emission of a positron (a positively charged electron). Within the nucleus a proton is converted into a neutron, a positron, and a neutrino i.e.



Similarly to the  $\beta^-$ , the positron  $\beta^+$  is continuously distributed in energy up to a characteristic maximum energy. The positron, after being emitted from the nucleus, undergoes strong electrostatic attraction with the atomic electrons. The positron and negative electrons annihilate each other and result in two photons (gamma rays) each with energy of 0.511 MeV moving in opposite directions.

There are 1496  $\beta^+$  emitters in the Nuclides.net database (shown in Fig. 4.8). The radiation hazard from positrons is similar to that from  $\beta^-$  particles. In addition, the gamma radiation resulting from the positron-electron annihilation presents an external radiation hazard.



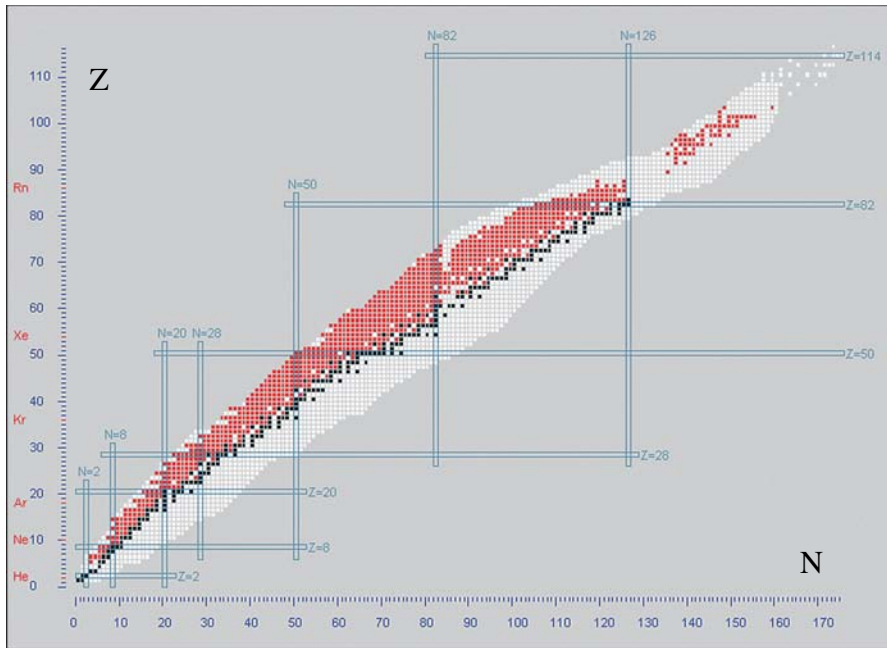
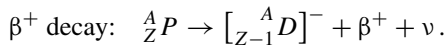


**Fig. 4.8.**  $\beta^+$  emitters (*red*) in the Nuclides.net database

The  $\beta^+$  decay process can be described by:



Immediately following the decay by positron emission, the daughter atom has the same number of orbital electrons as the parent atom and is thus negatively charged. Very quickly, however, the daughter atom loses the electron from the surrounding medium to become electrically neutral.

### Decay Energy

From Chapter 3, the  $Q$ -value for  $\beta^+$  decay is given by

$$\begin{aligned} \frac{Q_{\beta^+}}{c^2} &= M({}_Z^A P) - [M([{}_{Z-1}^A D]^-) + m_{\beta^+} + m_{\nu}] \\ &\cong M({}_Z^A P) - [M([{}_{Z-1}^A D] + m_e) + m_{\beta^+} + m_{\bar{\nu}}] \\ &= M({}_Z^A P) - M({}_{Z-1}^A D) - 2m_e, \end{aligned}$$

where the  $Q$ -value is now expressed in terms of the atomic masses and the electron mass (binding energy of the electron to the daughter ion has been neglected).

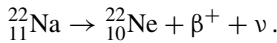
The daughter is often produced in an excited state and the decay energy is given by

$$\frac{Q_{\beta^+}}{c^2} = M({}_Z^A P) - M({}_{Z-1}^A D) - 2m_e - \frac{E^*}{c^2},$$

where  $E^*$  is the excitation energy. Since the daughter is much heavier, the positron carries most of the kinetic energy.

**Energy Level Diagram**

An example is the decay of  ${}^{22}\text{Na}$ :



From the atomic masses listed in Appendix D, the decay energy is given by

$$\begin{aligned} \frac{Q_{\beta^+}}{c^2} &= M({}^{22}\text{Na}) - M({}^{22}\text{Ne}) - 2m_e \\ &= 21.994436 \text{ u} - 21.991385 \text{ u} - 2(0.000549 \text{ u}) \hat{=} 1.82 \text{ MeV}. \end{aligned}$$

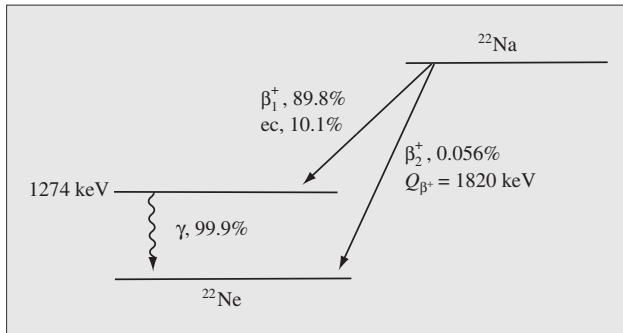
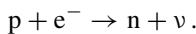


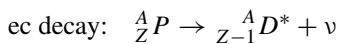
**Fig. 4.9.** Energy levels for beta decay of  ${}^{22}\text{Na}$  showing the main  $\beta^+$  emissions [2]

**Electron Capture ( $\epsilon$  or  $ec$ )**

Neutron deficient nuclides can also attain stability by capturing an electron from the inner  $K$  or  $L$  shells of the atomic orbits. As a result, a proton in the nucleus transforms to a neutron i.e.



The process is similar to  $\beta^+$  decay in that the charge of the nucleus decreases by 1. The  $ec$  decay process can be described by:



and the daughter is usually produced in an excited state. The resulting nucleus is unstable and decays by the ejection of an unobservable neutrino ( $\nu$ ) and the emission of a characteristic X-ray when the electron vacancy in the  $K$  or  $L$  shell is filled by outer orbital electrons. The Nuclides.net database lists 162 nuclides (shown in Fig. 4.10) which undergo electron capture.

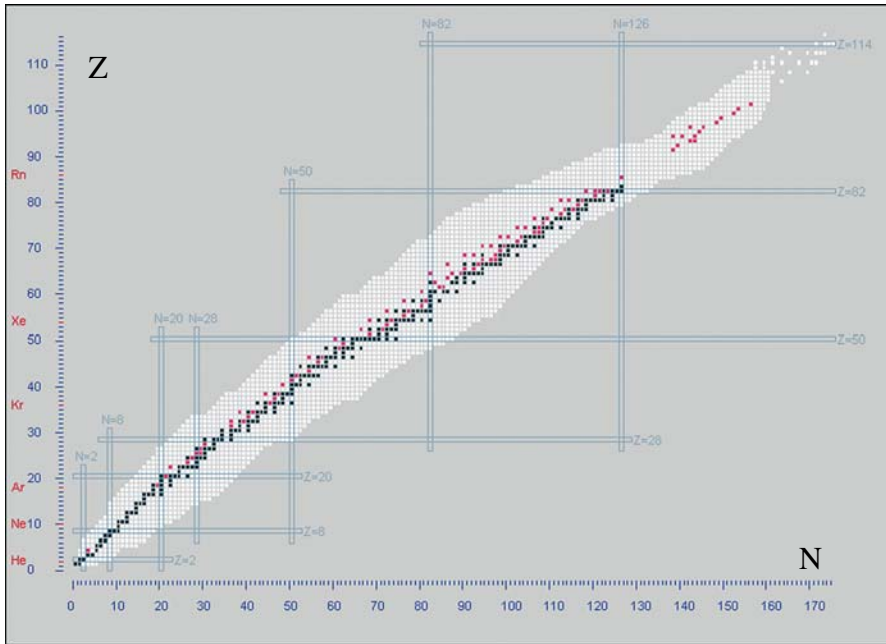


**Fig. 4.10.** Nuclides which undergo electron capture (*red*) in the Nuclides.net database

### Decay Energy

The  $Q$ -value for ec decay is given by

$$\begin{aligned}\frac{Q_{ec}}{c^2} &= M({}_Z^A P) - [M({}_{Z-1}^A D) + m_\nu] \\ &\cong M({}_Z^A P) - M({}_{Z-1}^A D)\end{aligned}$$

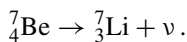
If the daughter is produced in an excited state, the decay energy is given

$$\frac{Q_{ec}}{c^2} = M({}_Z^A P) - M({}_{Z-1}^A D) - \frac{E^*}{c^2}$$

where  $E^*$  is the excitation energy.

### Energy Level Diagram

An example is the electron capture process in beryllium-7 i.e.



From the atomic masses listed in Appendix D, the decay energy is given by

$$\frac{Q_{ec}}{c^2} = M({}^7\text{Be}) - M({}^7\text{Li}) = 7.016929 \text{ u} - 7.016004 \text{ u} \cong 861.6 \text{ keV}$$

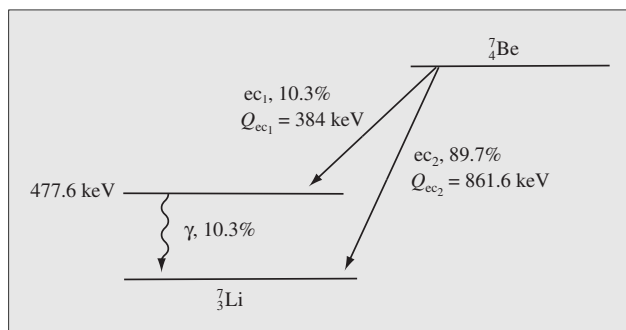


**Fig. 4.11.** Energy levels for decay of  ${}^7\text{Be}$  showing the main electron captures [2]

## Spontaneous Fission (SF)

The discovery of fission by neutrons is credited to Hahn and Strassmann [3], and to Meitner and Frisch [4] for their explanation of the phenomena and introduction of the term *nuclear fission*. Spontaneous fission was discovered in 1940 by Petrzak and Flerov [5].

Although the alpha emitting properties of  ${}^{238}\text{U}$  were well known by that time, the much less common spontaneous fission had been “masked” due to its very small branching ratio of about one SF in  $2 \times 10^6$  alpha emissions. With the exception of  ${}^8\text{Be}$  (which decays into two alpha particles), SF has not been detected in any elements lighter than thorium. In the 1960s, sources of  ${}^{252}\text{Cf}$  became available and detailed measurement of the fissioning of this system contributed much to our understanding of the process.

Actinides (Ac, Th, Pu, U, Pu, Am, Np, Cm, etc.) and trans-actinides can undergo radioactive decay by spontaneous fission. In this process the nucleus splits into two fragment nuclei, with mass and charge roughly half that of the parent, and several neutrons.

The spontaneous fission (SF) decay process can be described qualitatively by:

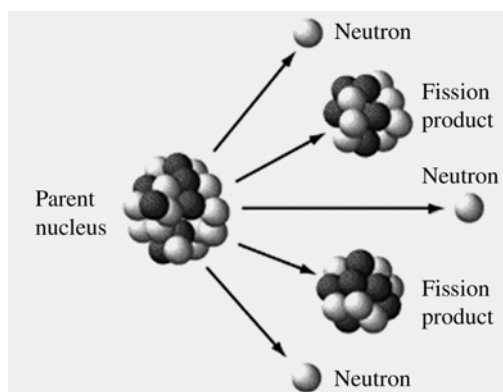
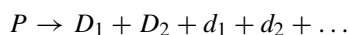
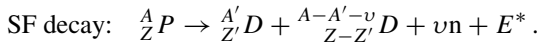


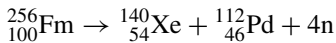
**Fig. 4.12.** Spontaneous fission of heavy nuclides (AJ Software & Multimedia. Used by permission. All rights reserved. [www.atomicarchive.com](http://www.atomicarchive.com))

and in more detail by



The process is shown schematically in Fig. 4.12. A “parent” nuclide  ${}^A_Z P$  splits into two “daughter” nuclides  ${}^{A'}_{Z'} D$  and  ${}^{A-A'-\nu}_{Z-Z'} D$  together with the release of  $\nu$  prompt neutrons and energy  $E^*$ . Typically  $\nu$  ranges from 2–4 and  $E^*$  is approximately 200 MeV. Additionally, so-called delayed neutrons may be emitted by the primary fission products. The daughter nuclides or fission products have in general different mass numbers  $A$  and atomic numbers  $Z$ .

Since there are more than two decay products, the products and their energies cannot be uniquely identified. In the case of the spontaneous fission of fermium-256, one such reaction is:



(this reaction represents only one of many fission product combinations). The kinetic energy release in this process, due mainly to large electrostatic repulsion of the fragments, is approximately 190 MeV.

The distribution of the energy released in fission is shown in Table 4.4. The Nuclides.net database currently lists 127 spontaneously fissioning nuclides (shown in Fig. 4.13 and Table 4.5).

About 87% of the total energy is emitted promptly with the fission fragments. Most of the neutrons released are prompt neutrons and are released within  $10^{-14}$  s of fissioning. Some neutrons are released on a much longer timescale and are associated with the fission decay chains. Since the discovery of this process, the identification of the mass and the nuclear charge of the fission products has always been an important part of fission investigations and experiments. In the early days of fission product yields exploration, initiated by nuclear physicists such as Anderson and Fermi, radiochemical methods were used. These are being progressively replaced by more sophisticated physical methods for the determination of the yields [6–8].

**Table 4.4.** Energy released resulting from spontaneous fission of  ${}^{235}\text{U}$

Products	Emitted energy (MeV)
Prompt energy:	
Fission fragments	168
Fission neutrons	5
$\gamma$ emission	7
Radioactivity:	
$\beta$ decay (electrons)	8
$\beta$ decay (neutrinos)	12
$\gamma$ emission	7
Total	207

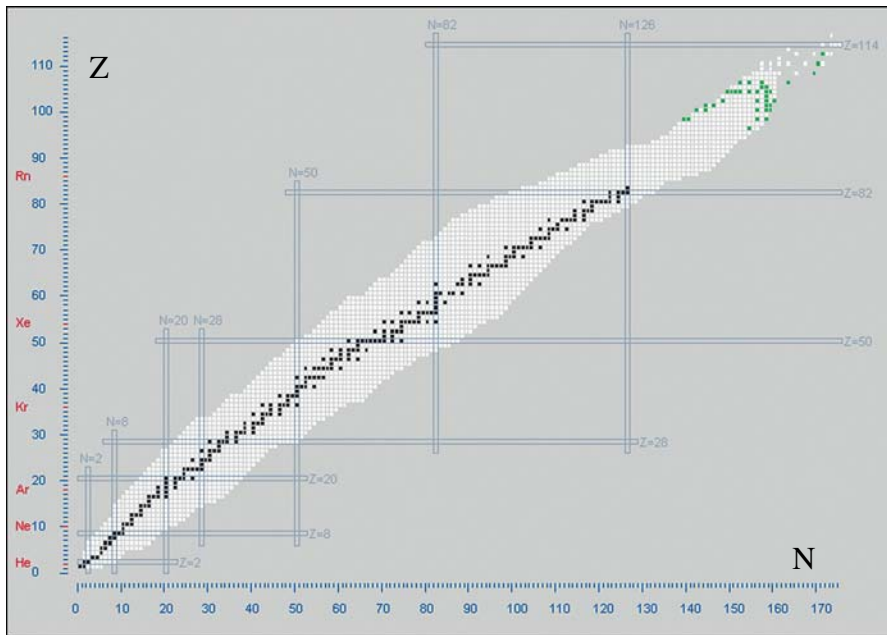


**Fig. 4.13.** Nuclides (green) in which spontaneous fission is the *main* decay mode

Although mass yield distributions have been measured with sufficient precision for most fission reactions of technical importance, the distribution of independent yields is still not completely known. The reason for this is that the mass distribution of fission products does not change with time after the fission reaction, if the small effect due to delayed neutron emission is neglected. Independent yields, however, describe the elemental distribution of fission products and undergo a rapid change after fission because of the predominance of short-lived  $\beta^-$ -unstable nuclides.

Therefore, the methods of measuring independent yields differ from those for the measurement of chain yields, and thus require more advanced technology.

On the other hand, only a small fraction of yields, independent and/or cumulative, of approximately 900 primary products have been measured for any fission reaction. About 25% of the fission products have been measured, at best, for the fissioning systems of technical importance and usually about 1% or less for the other fission reactions. Therefore, most of the independent and cumulative yields must be estimated.

Fission yield distributions are interesting from two standpoints a) they provide information on the nature of large collective motion of nuclear matter in different energy ranges and b) low energy fission yield distributions are important for the control of nuclear reactors.

In the framework of nuclear technologies (reactor technology, safeguards, etc.), there is an even more important need of nuclear data. The cumulative fission product distribution is of great interest for practical purposes such as waste storage, control of nuclear reactors, etc. Independent yields are of importance for the fundamental

**Table 4.5.** Spontaneously fissioning nuclides in the Nuclides.net database

Nuclides	Half-life	Nuclides	Half-life	Nuclides	Half-life	Nuclides	Half-life
<sup>230</sup> <sub>90</sub> Th	7.5E4 y	<sup>247</sup> <sub>97</sub> Bk	1.4E3 y	<sup>259</sup> <sub>100</sub> Fm	1.5 s	<sup>257</sup> <sub>104</sub> Rf	4.7 s
<sup>232</sup> <sub>90</sub> Th	1.4E10 y	<sup>249</sup> <sub>97</sub> Bk	320 d	<sup>245</sup> <sub>101</sub> Md	900 μs	<sup>258</sup> <sub>104</sub> Rf	12 ms
<sup>231</sup> <sub>91</sub> Pa	3.3E4 y	<sup>237</sup> <sub>98</sub> Cf	2.1 s	<sup>247</sup> <sub>101</sub> Md	270 ms	<sup>259</sup> <sub>104</sub> Rf	2.7 s
<sup>234</sup> <sub>91</sub> Pa	6.7 h	<sup>238</sup> <sub>98</sub> Cf	21 ms	<sup>247m</sup> <sub>101</sub> Md	1.12 s	<sup>260</sup> <sub>104</sub> Rf	20.1 ms
<sup>234m</sup> <sub>91</sub> Pa	1.17 m	<sup>240</sup> <sub>98</sub> Cf	1.06 m	<sup>255</sup> <sub>101</sub> Md	27 m	<sup>261</sup> <sub>104</sub> Rf	1.08 m
<sup>230</sup> <sub>92</sub> U	20.8 d	<sup>242</sup> <sub>98</sub> Cf	3.49 m	<sup>257</sup> <sub>101</sub> Md	5.52 h	<sup>262</sup> <sub>104</sub> Rf	2.06 s
<sup>232</sup> <sub>92</sub> U	68.95 y	<sup>246</sup> <sub>98</sub> Cf	1.49 d	<sup>258m</sup> <sub>101</sub> Md	57 m	<sup>262m</sup> <sub>104</sub> Rf	47 ms
<sup>233</sup> <sub>92</sub> U	1.6E5 y	<sup>248</sup> <sub>98</sub> Cf	3.3E2 d	<sup>259</sup> <sub>101</sub> Md	1.6 h	<sup>263</sup> <sub>104</sub> Rf	10 m
<sup>234</sup> <sub>92</sub> U	2.5E5 y	<sup>249</sup> <sub>98</sub> Cf	3.5E2 y	<sup>260</sup> <sub>101</sub> Md	27.8 d	<sup>255</sup> <sub>105</sub> Db	1.7 s
<sup>235</sup> <sub>92</sub> U	7.0E8 y	<sup>250</sup> <sub>98</sub> Cf	13.09 y	<sup>250</sup> <sub>102</sub> No	250 μs	<sup>256</sup> <sub>105</sub> Db	3 s
<sup>236</sup> <sub>92</sub> U	2.3E7 y	<sup>252</sup> <sub>98</sub> Cf	2.65 y	<sup>251</sup> <sub>102</sub> No	800 ms	<sup>257</sup> <sub>105</sub> Db	1.4 s
<sup>238</sup> <sub>92</sub> U	4.5E9 y	<sup>254</sup> <sub>98</sub> Cf	60.5 d	<sup>252</sup> <sub>102</sub> No	2.3 s	<sup>258</sup> <sub>105</sub> Db	4.6 s
<sup>237</sup> <sub>93</sub> Np	2.1E6 y	<sup>255</sup> <sub>98</sub> Cf	1.42 h	<sup>253</sup> <sub>102</sub> No	1.7 m	<sup>260</sup> <sub>105</sub> Db	1.52 s
<sup>236</sup> <sub>94</sub> Pu	2.86 y	<sup>256</sup> <sub>98</sub> Cf	12.3 m	<sup>254</sup> <sub>102</sub> No	55 s	<sup>261</sup> <sub>105</sub> Db	1.8 s
<sup>238</sup> <sub>94</sub> Pu	87.76 y	<sup>247</sup> <sub>99</sub> Es	4.55 m	<sup>256</sup> <sub>102</sub> No	2.91 s	<sup>262</sup> <sub>105</sub> Db	34 s
<sup>239</sup> <sub>94</sub> Pu	2.4E4 y	<sup>253</sup> <sub>99</sub> Es	20.47 d	<sup>258</sup> <sub>102</sub> No	1.2 ms	<sup>263</sup> <sub>105</sub> Db	29 s
<sup>240</sup> <sub>94</sub> Pu	6.6E3 y	<sup>254</sup> <sub>99</sub> Es	2.8E2 d	<sup>259</sup> <sub>102</sub> No	58 m	<sup>258</sup> <sub>106</sub> Sg	3.3 ms
<sup>241</sup> <sub>94</sub> Pu	14.36 y	<sup>254m</sup> <sub>99</sub> Es	1.64 d	<sup>260</sup> <sub>102</sub> No	106 ms	<sup>259</sup> <sub>106</sub> Sg	580 ms
<sup>242</sup> <sub>94</sub> Pu	3.7E5 y	<sup>255</sup> <sub>99</sub> Es	39.8 d	<sup>262</sup> <sub>102</sub> No	5 ms	<sup>260</sup> <sub>106</sub> Sg	3.8 ms
<sup>244</sup> <sub>94</sub> Pu	8.1E7 y	<sup>242</sup> <sub>100</sub> Fm	800 μs	<sup>252</sup> <sub>103</sub> Lr	1 s	<sup>261</sup> <sub>106</sub> Sg	230 ms
<sup>241</sup> <sub>95</sub> Am	4.3E2 y	<sup>243</sup> <sub>100</sub> Fm	210 ms	<sup>253</sup> <sub>103</sub> Lr	1.5 s	<sup>263</sup> <sub>106</sub> Sg	800 ms
<sup>242m</sup> <sub>95</sub> Am	1.4E2 y	<sup>244</sup> <sub>100</sub> Fm	3.3 ms	<sup>254</sup> <sub>103</sub> Lr	13 s	<sup>265</sup> <sub>106</sub> Sg	16 s
<sup>242n</sup> <sub>95</sub> Am	14 ms	<sup>245</sup> <sub>100</sub> Fm	4.2 s	<sup>255</sup> <sub>103</sub> Lr	22 s	<sup>266</sup> <sub>106</sub> Sg	20 s
<sup>243</sup> <sub>95</sub> Am	7.4E3 y	<sup>246</sup> <sub>100</sub> Fm	1.1 s	<sup>256</sup> <sub>103</sub> Lr	28 s	<sup>269</sup> <sub>106</sub> Sg	22 s
<sup>240</sup> <sub>96</sub> Cm	27 d	<sup>248</sup> <sub>100</sub> Fm	36 s	<sup>257</sup> <sub>103</sub> Lr	646 ms	<sup>261</sup> <sub>107</sub> Bh	13 ms
<sup>242</sup> <sub>96</sub> Cm	1.6E2 d	<sup>250</sup> <sub>100</sub> Fm	30 m	<sup>259</sup> <sub>103</sub> Lr	6.3 s	<sup>262</sup> <sub>107</sub> Bh	102 ms
<sup>243</sup> <sub>96</sub> Cm	29.12 y	<sup>252</sup> <sub>100</sub> Fm	1.06 d	<sup>260</sup> <sub>103</sub> Lr	3 m	<sup>262m</sup> <sub>107</sub> Bh	8 ms
<sup>244</sup> <sub>96</sub> Cm	18.11 y	<sup>254</sup> <sub>100</sub> Fm	3.24 h	<sup>261</sup> <sub>103</sub> Lr	39 m	<sup>277</sup> <sub>108</sub> Hs	11 m
<sup>245</sup> <sub>96</sub> Cm	8.5E3 y	<sup>255</sup> <sub>100</sub> Fm	20.07 h	<sup>253</sup> <sub>104</sub> Rf	13 ms	<sup>266</sup> <sub>109</sub> Mt	6 ms
<sup>246</sup> <sub>96</sub> Cm	4.7E3 y	<sup>256</sup> <sub>100</sub> Fm	2.63 h	<sup>254</sup> <sub>104</sub> Rf	23 μs	<sup>280</sup> <sub>110</sub> Ds	7.5 s
<sup>248</sup> <sub>96</sub> Cm	3.4E5 y	<sup>257</sup> <sub>100</sub> Fm	1.0E2 d	<sup>255</sup> <sub>104</sub> Rf	1.5 s	<sup>283</sup> <sub>112</sub> Uub	12.7 s
<sup>250</sup> <sub>96</sub> Cm	9.0E3 y	<sup>258</sup> <sub>100</sub> Fm	360 μs	<sup>256</sup> <sub>104</sub> Rf	6.7 ms		

understanding of the corresponding nuclear reactions, but also for short-term practical purposes in reactor operation.

In the fission process, the probability of measuring the production of an isotope or a nuclide is generally expressed as the yield (given in units of production per unit fission or in percent).

### Proton Decay

As one moves further to the left of the line of stability, the proton to neutron ratio increases with increasing distance (see Fig. 4.14) and the nuclides are increasingly proton rich. In such proton rich nuclides, positron ( $\beta^+$ ) decay is usually energetically more favourable. However, as the binding energy of these protons decreases further, there comes a point in which proton emission becomes energetically possible. More often, proton emission follows positron emission in a two-stage process i.e.  $\beta^+$  decay results in a daughter in an excited state which then de-excites by proton emission.

A review of the early theoretical speculations on the subject of proton emission has been given by Goldansky in 1966 [9]. The first observation of proton emission was reported by Jackson et al. in 1970 [10] with the nuclide  $^{53m}\text{Co}$ . This decay process, is exhibited by the metastable state of cobalt-53, i.e.

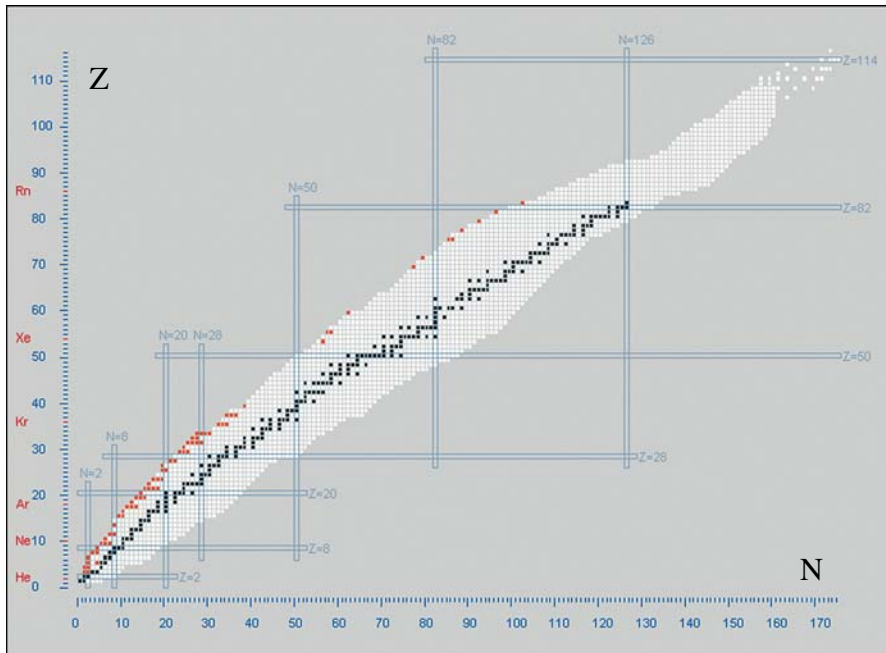
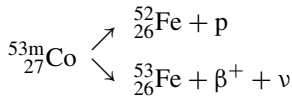


Fig. 4.14. Proton emitters (brown) in the Nuclides.net database



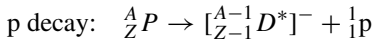
**Table 4.6.** Proton emitters in the Nuclides.net database

Nuclide	Half-life	Nuclide	Half-life	Nuclide	Half-life
${}^4_3\text{Li}$	9.1E-14 ns	${}^{45}_{25}\text{Mn}$	70 ns	${}^{109}_{53}\text{I}$	100 $\mu\text{s}$
${}^5_3\text{Li}$	3.0E-13 ns	${}^{45}_{26}\text{Fe}$	350 ns	${}^{112}_{55}\text{Cs}$	500 $\mu\text{s}$
${}^5_4\text{Be}$		${}^{48}_{27}\text{Co}$		${}^{113}_{55}\text{Cs}$	17 $\mu\text{s}$
${}^7_5\text{B}$	3.5E-13 ns	${}^{49}_{27}\text{Co}$	35 ns	${}^{117}_{57}\text{La}$	500 ms
${}^9_5\text{B}$	8.0E-10 ns	${}^{53\text{m}}_{27}\text{Co}$	247 ms	${}^{121}_{59}\text{Pr}$	600 ms
${}^{10}_7\text{N}$		${}^{52}_{29}\text{Cu}$		${}^{128}_{61}\text{Pm}$	800 ms
${}^{11}_7\text{N}$	5.0E-13 ns	${}^{53}_{29}\text{Cu}$	300 ns	${}^{132}_{63}\text{Eu}$	400 ms
${}^{14}_9\text{F}$		${}^{54}_{29}\text{Cu}$	75 ns	${}^{138}_{65}\text{Tb}$	400 ms
${}^{15}_9\text{F}$	4.6E-13 ns	${}^{55}_{29}\text{Cu}$	200 ns	${}^{142}_{67}\text{Ho}$	300 ms
${}^{16}_9\text{F}$	1.1E-11 ns	${}^{56}_{31}\text{Ga}$		${}^{146}_{69}\text{Tm}$	235 ms
${}^{18}_{11}\text{Na}$		${}^{57}_{31}\text{Ga}$		${}^{146\text{m}}_{69}\text{Tm}$	72 ms
${}^{19}_{11}\text{Na}$	40 ns	${}^{58}_{31}\text{Ga}$		${}^{147}_{69}\text{Tm}$	580 ms
${}^{21}_{13}\text{Al}$	35 ns	${}^{58\text{m}}_{31}\text{Ga}$		${}^{150}_{71}\text{Lu}$	35 ms
${}^{24}_{15}\text{P}$		${}^{59}_{31}\text{Ga}$		${}^{151\text{m}}_{71}\text{Lu}$	85 ms
${}^{25}_{15}\text{P}$	30 ns	${}^{60}_{33}\text{As}$		${}^{156}_{73}\text{Ta}$	144 ms
${}^{28}_{17}\text{Cl}$		${}^{60\text{m}}_{33}\text{As}$		${}^{156\text{m}}_{73}\text{Ta}$	360 ms
${}^{29}_{17}\text{Cl}$	20 ns	${}^{61}_{33}\text{As}$		${}^{160}_{75}\text{Re}$	790 $\mu\text{s}$
${}^{30}_{17}\text{Cl}$	30 ns	${}^{62}_{33}\text{As}$		${}^{161}_{75}\text{Re}$	
${}^{30}_{18}\text{Ar}$	20 ns	${}^{63}_{33}\text{As}$		${}^{165}_{77}\text{Ir}$	1 $\mu\text{s}$
${}^{32}_{19}\text{K}$		${}^{67}_{35}\text{Br}$		${}^{165\text{m}}_{77}\text{Ir}$	300 $\mu\text{s}$
${}^{33}_{19}\text{K}$	25 ns	${}^{68}_{35}\text{Br}$	1.2 $\mu\text{s}$	${}^{166}_{77}\text{Ir}$	10.5 ms
${}^{34}_{19}\text{K}$	40 ns	${}^{69}_{35}\text{Br}$	24 ns	${}^{166\text{m}}_{77}\text{Ir}$	15.1 ms
${}^{34}_{20}\text{Ca}$	35 ns	${}^{71}_{37}\text{Rb}$		${}^{167}_{77}\text{Ir}$	35.2 ms
${}^{36}_{21}\text{Sc}$		${}^{72}_{37}\text{Rb}$	1.2 $\mu\text{s}$	${}^{167\text{m}}_{77}\text{Ir}$	30 ms
${}^{37}_{21}\text{Sc}$		${}^{72\text{m}}_{37}\text{Rb}$		${}^{171}_{79}\text{Au}$	10 $\mu\text{s}$
${}^{38}_{21}\text{Sc}$	300 ns	${}^{73}_{37}\text{Rb}$	< 30 ns	${}^{171\text{m}}_{79}\text{Au}$	1.02 ms
${}^{38\text{m}}_{21}\text{Sc}$		${}^{77}_{39}\text{Y}$	1.2 $\mu\text{s}$	${}^{172}_{79}\text{Au}$	4.7 ms
${}^{39}_{21}\text{Sc}$	300 ns	${}^{81}_{41}\text{Nb}$	800 ms	${}^{177}_{81}\text{Tl}$	1 $\mu\text{s}$
${}^{40}_{23}\text{V}$		${}^{85}_{43}\text{Tc}$	500 ms	${}^{177\text{m}}_{81}\text{Tl}$	
${}^{41}_{23}\text{V}$		${}^{104}_{51}\text{Sb}$	470 ms	${}^{185}_{83}\text{Bi}$	2 ms
${}^{42}_{23}\text{V}$	55 ns	${}^{105}_{51}\text{Sb}$	1.12 s	${}^{185\text{m}}_{83}\text{Bi}$	44 $\mu\text{s}$
${}^{44}_{25}\text{Mn}$	105 ns	${}^{108}_{53}\text{I}$	36 ms		

with branching ratios of 1.5% (p mode) and 98.5% ( $\beta^+$  mode). Proton radioactivity from a ground state, i.e.  $^{151}\text{Lu}$ , was first reported by Hofmann et al. in 1981 [11]. In the following three years, three more proton emitters were observed in the region of nuclei near  $^{151}\text{Lu}$  with  $^{147}\text{Tm}$ ,  $^{147\text{m}}\text{Tm}$ ,  $^{150}\text{Lu}$ , and two in the region near  $^{100}\text{Sn}$  i.e.  $^{113}\text{Cs}$  and  $^{109}\text{I}$ . This work is summarised in the review article by Hofmann in 1995 [12]. More recently, due to various experimental improvements, proton transitions have been found in nuclei near to  $N = 82$  ( $^{146}\text{Tm}$ ,  $^{146\text{m}}\text{Tm}$ ,  $^{156}\text{Ta}$ ,  $^{160}\text{Re}$ ) and also in  $^{165,166,167}\text{Ir}$ ,  $^{171}\text{Au}$ ,  $^{185}\text{Bi}$  and  $^{105}\text{Sb}$ . As of 1995, 21 proton transitions have been established definitively. Since then more proton emitters have been either claimed or identified. The Nuclides.net database contains 95 proton emitters (shown in Fig. 4.14 and Table 4.6).

The phenomena of two-proton radioactivity has been discussed by Brown [13]. In total there are 13 two-proton emitters in the Nuclides.net database.

The proton decay process can be described by:



following emission of the proton, the daughter atom has an extra electron which is rapidly ejected to the surrounding media in order to balance the charge.

### Decay Energy

The  $Q$ -value for proton decay is given by

$$\begin{aligned} \frac{Q_p}{c^2} &= M({}^A_Z P) - \left\{ M([{}^{A-1}_{Z-1} D^*]^-) + m_p \right\} \\ &\cong M({}^A_Z P) - \left\{ [M({}^{A-1}_{Z-1} D^*) + m_e] + m_p \right\} \\ &\cong M({}^A_Z P) - \left\{ [M({}^{A-1}_{Z-1} D) + \frac{E^*}{c^2} + m_e] + m_p \right\} \\ &\cong M({}^A_Z P) - M({}^{A-1}_{Z-1} D) - M({}^1_1 \text{H}) - \frac{E^*}{c^2} \end{aligned}$$

For proton decay to the ground state

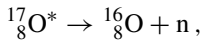
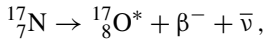
$$\frac{Q_p}{c^2} = M({}^A_Z P) - M({}^{A-1}_{Z-1} D) - M({}^1_1 \text{H})$$

### Special Beta-Decay Processes

To the right of the line of stability, the nuclides are neutron rich and neutron emission can be expected in this region by analogy with proton emission from proton rich nuclides. Neutron emission from a ground state nuclide has not been observed although it is energetically possible for some nuclides.

### Neutron Emission

Neutron emission immediately following  $\beta^-$  emission (beta delayed neutron emission denoted  $\beta^-n$ ) has been observed in many neutron-rich nuclides. The phenomena of delayed neutron emission is very important in the control of nuclear reactors since neutron emission occurs on a timescale much longer than that associated with fission – this allows a response time long enough to move control rods and thereby control the fission reactor. An example of this type of emission is given by  $^{17}\text{N}$  i.e.



where the asterisk denotes the short-lived intermediate excited states of oxygen-17. The effective half-life for this process is 4.17 s. There are 279 ( $\beta^-n$ ) emitters in the Nuclides.net database. The delayed neutron emission from the  $\beta^-$  decay of  $^{87}\text{Br}$  is shown in Fig. 4.15.

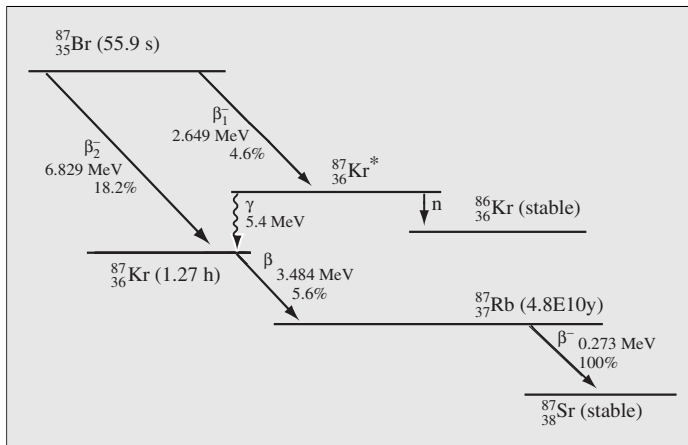
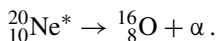
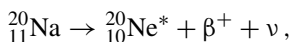


**Fig. 4.15.** Decay scheme of  $^{87}\text{Br}$  showing the delayed neutron emission from  $^{87}_{36}\text{Kr}^*$  [2]

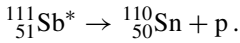
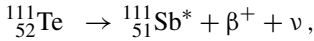
### Alpha and Proton Emission

Some positron emitters in the light-element region beta decay partly to excited states that are unstable with respect to emission of an alpha particle ( $\beta^+\alpha$ ). Both the positron decay from boron-8 and negatron decay from lithium-8 ( $\beta^-2\alpha$ ) are beta-delayed alpha emission, because ground as well as excited states of beryllium-8 are unstable with respect to breakup into two alpha particles. Another example is the decay of  $^{20}\text{Na}$ , i.e.



There are 39  $\beta^+\alpha$  emitters listed in the Nuclides.net database.

In a few cases, positron decay leads to an excited nuclear state not able to bind a proton. In these cases, proton radiation appears with the half-life of the beta transition. One example of this is the decay of  $^{111}\text{Te}$ , i.e.



There are 177  $\beta^+$  p in the Nuclides.net database. An example of proton emission following the  $\beta^-$  decay of  $^{73}\text{Kr}$  is shown in Fig. 4.16.

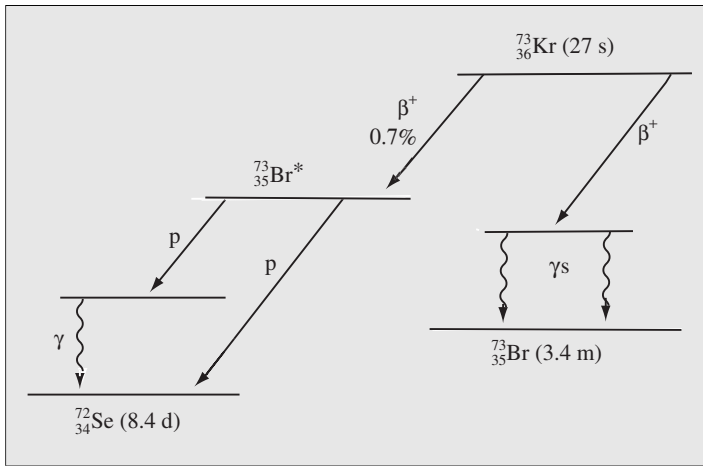
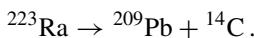


**Fig. 4.16.** Proton emission in the decay of  $^{73}\text{Kr}$  in which 0.7% of the  $\beta^+$  transitions are to the metastable state  $^{73}\text{Br}^*$  which then decay by proton emission [2]

## Heavy-Ion or Cluster Radioactivity

In 1984, Rose and Jones [14] at Oxford University announced the discovery of a new rare type of radioactive decay in the nuclide  $^{223}\text{Ra}$ . Their article entitled “A new kind of natural radioactivity” was published in *Nature*. The possibility that such a decay process, intermediate between alpha decay and spontaneous fission, may exist was postulated by A. Sandulescu, D. N. Poenaru, and W. Greiner a few years earlier in 1980. Rose and Jones showed that part of the  $^{223}\text{Ra}$  parent nuclide decays directly to  $^{209}\text{Pb}$  by the emission of a 30 MeV  $^{14}\text{C}$  ion i.e.



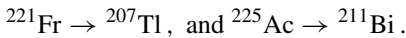
It is of interest to calculate value of the decay energy for this process i.e.

$$\begin{aligned} \frac{Q_p}{c^2} &= M(^{223}\text{Ra}) - M(^{209}\text{Pb}) - M(^{14}\text{C}) \\ &= 223.018502 \text{ u} - 208.981090 - 14.003241 \text{ u} \hat{=} 31.8 \text{ MeV}. \end{aligned}$$

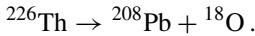
This calculated value of the decay energy is in agreement with the observed kinetic energy of the carbon ion.

Observations also have been made of carbon-14 from radium-222, radium-224, and radium-226, as well as neon-24 from thorium-230, protactinium-231, and uranium-232. Such heavy-ion radioactivity, like alpha decay and spontaneous fission, involves quantum-mechanical tunnelling through the potential-energy barrier. Shell effects play a major role in this phenomenon and in all cases observed to date the heavy partner of carbon-14 or neon-24 is close to doubly magic lead-208, a region of higher stability.

The ratio of carbon-14 decay to alpha decay is about  $5.5 \times 10^{-10}$ . This low value explains why the spontaneous decay mode had not been observed earlier. Since the probability of cluster emission is expected to be greatest when the daughter nuclide configuration is close to that of a full shell, attempts have been made to observe the phenomenon with parent nuclides near  $Z = 88$  ( $Z = 82$  corresponds to a magic proton line). Hence the search has concentrated on the elements francium and actinium with potential daughter of thallium and bismuth, e.g.



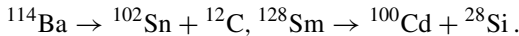
Oxygen cluster emission was discovered by Hussonois et al. [15] in the decay of thorium, i.e.



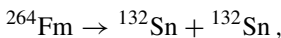
Similarly,  $^{34}\text{Si}$  cluster should result from the decay of  $^{241}\text{Am}$  and  $^{240}\text{Pu}$ .

## Magic Radioactivity

The discovery of trans-tin cluster emitters may confirm the idea of “magic radioactivity” proposed by Sandulescu in 1989 [16]. Magic numbers in the trans-tin region are at  $N = 50$  and  $82$  and  $Z = 50$ . The doubly magic closed shell nuclides  $^{132}\text{Sn}$  and  $^{100}\text{Sn}$  lie far from the line of stability as can be seen in Fig. 4.17. In the proton rich region around Ba–Sm cluster emission would lead to nuclides close to the doubly magic  $^{100}\text{Sn}$ . Expected cluster emission reactions could be



Sandulescu has also proposed the idea of cold fission as a special case of cluster radioactivity where the fission fragments lie in the  $Z = 50$  region. An example is the decay of fermium i.e.



in which the neutron rich fermium splits into two identical doubly magic tin fragments with a probability comparable to that of alpha decay.

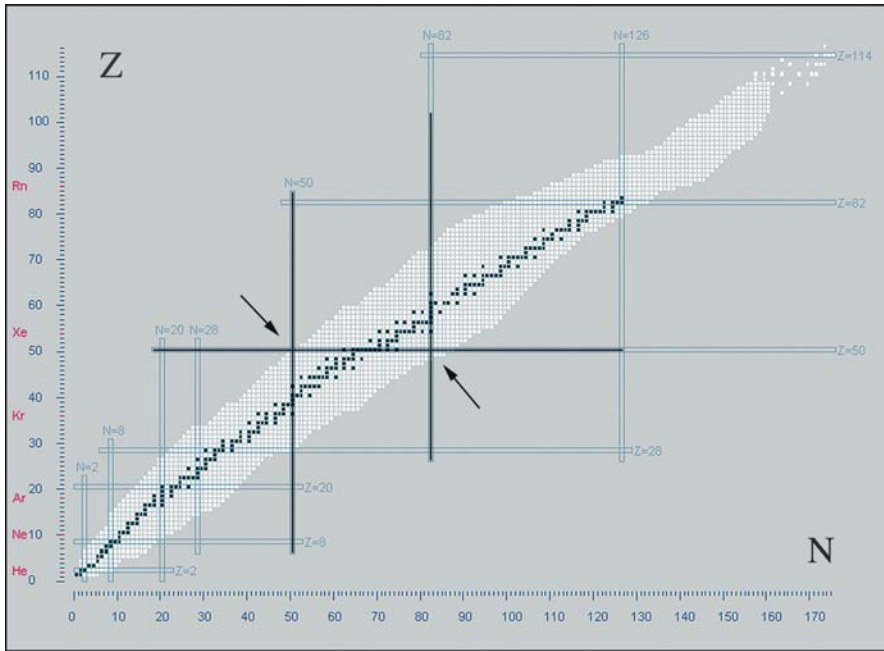


**Fig. 4.17.** Magic numbers in the trans-tin region are at  $N = 50$  and  $82$  and  $Z = 50$ . The location of doubly magic tin nuclides  $^{132}\text{Sn}$  and  $^{100}\text{Sn}$  are indicated

## Decay of Bare Nuclei – Bound Beta Decay

The effect of external physical conditions on the nuclear decay rate has been of interest for many decades (see “How Constant is the Decay Constant?” in Chapter 5). Many attempts have been made to alter the decay rate by varying the temperature, pressure, chemical environment etc. [17] but only small effects have been observed. This situation has now changed with the observation that the half-lives of highly charged ions can be increased from 10% to 670% [18].

When a stable atom is fully ionised, the resulting ion may be unstable. These nuclei give rise to a special kind of  $\beta^-$  emission in which an electron is liberated from the nucleus, through transformation of a neutron to a proton, and captured into one of the empty energy shells of the atom (Figs. 4.18, 4.19 [19]). This “bound beta decay” was predicted in 1947 by the French physicists Daudel et al. [20] but was observed for the first time only in 1992 [21] at the Institute of Heavy Ion Research (GSI) at Darmstadt.

A bound beta isotope, denoted  $\beta_b$ , is an isotope which is (nearly) stable as a neutral atom, but which decays by  $\beta_b$  decay when fully ionized. There are now four such isotopes known in nature:  $^{163}\text{Dy}$ ,  $^{187}\text{Re}$ ,  $^{193}\text{Ir}$ , and  $^{205}\text{Tl}$ . The isotope  $^{187}\text{Re}$  is included because of its extremely long beta decay half-life (43 Gy).

Bound beta decay was first observed with highly ionised ions of the stable nuclide  $^{163}\text{Dy}$  [21] and  $^{187}\text{Re}$  [23] provided by the synchrotron and stored in the storage

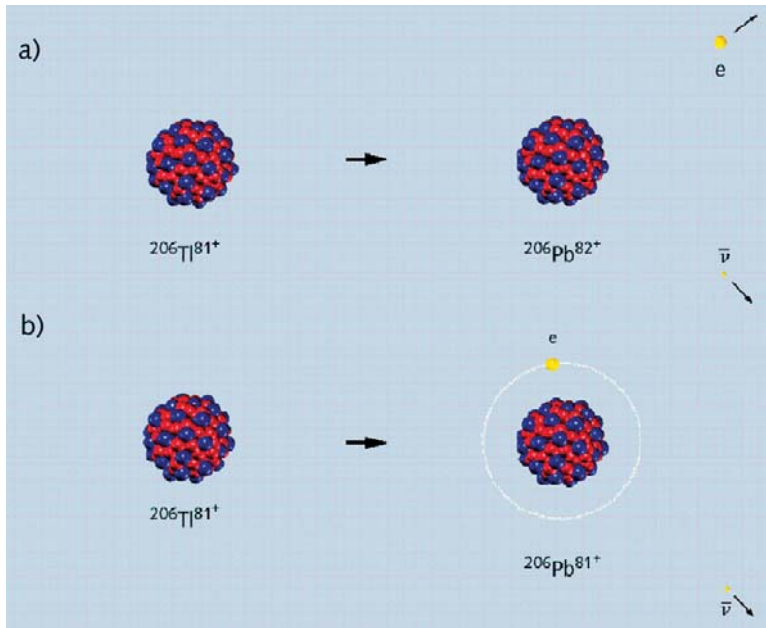


**Fig. 4.18.** While in usual  $\beta^-$  decay the electron goes into a continuum state (a), it is captured and bound in an inner atomic shell in bound beta decay  $\beta_b^-$  (b). (Courtesy GSI [19])

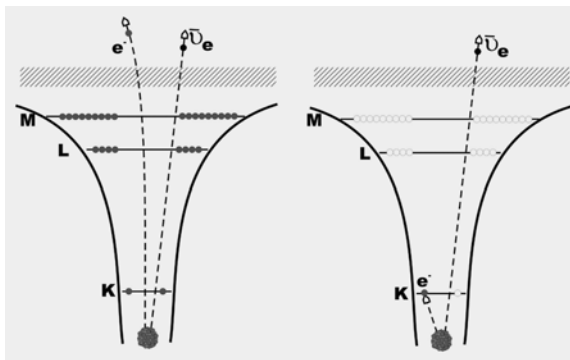


**Fig. 4.19.** Energy level diagrams for the bare (left) and bound beta decay (right) for highly charged ions (HCI). (Courtesy F. Bosch, GSI Darmstadt [22])

cooler ring at GSI [24, 25]. The ionised  $^{163}\text{Dy}^{66+}$  is observed to decay with a half-life of 47 d by  $\beta^-$  emission to  $^{163}\text{Ho}$ . For the almost stable  $^{187}\text{Re}$ , the fully ionised  $^{187}\text{Re}^{75+}$  ion shows a decrease in the half-life of 9 orders of magnitude. In addition to the  $^{163}\text{Dy}/^{163}\text{Ho}$  transmutation under extreme conditions, other such reactions pairs are  $^{205}\text{Tl}/^{205}\text{Pb}$  and  $^{193}\text{Ir}/^{193}\text{Pt}$  and these may have an impact in stellar nucleosynthesis where terrestrial and stellar half-lives may be different.

Through the recent developments in high intensity lasers, it may become possible to investigate such reactions which until now could only be studied in a very limited way in terrestrial laboratories (see section on “Laser Transmutation” in Chapter 5).

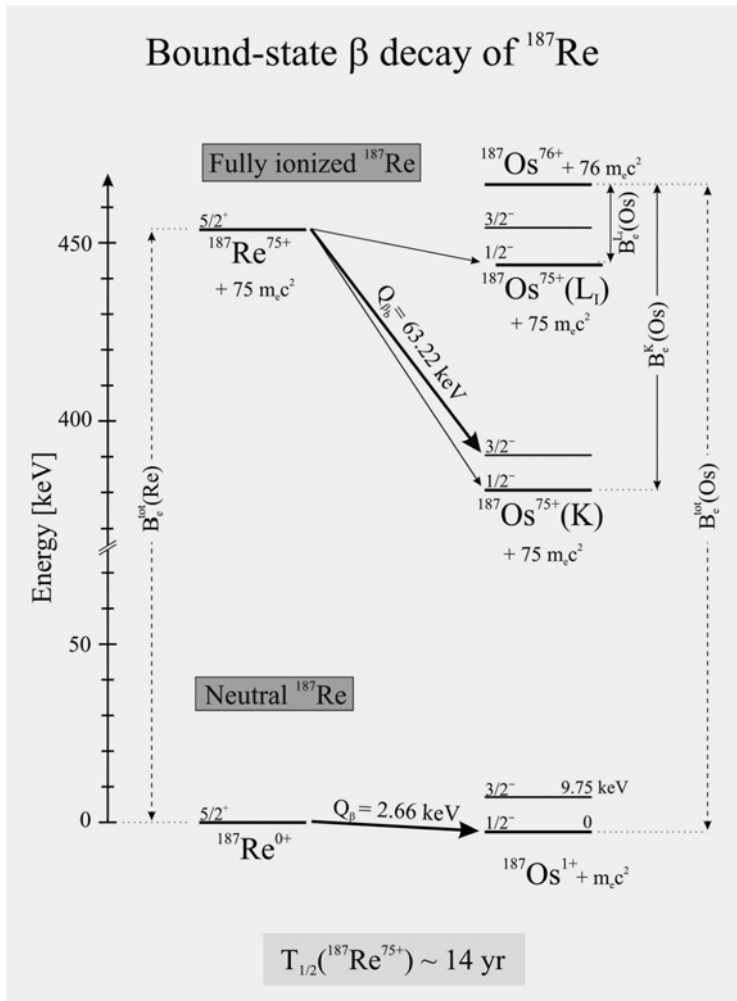


**Fig. 4.20.** Energy level diagram for the decay of bare and neutral  $^{187}\text{Re}$ . The half-life of bare  $^{187}\text{Re}$  has been determined to be only 33 ns, i.e. by more than 9 orders of magnitude shorter than in the neutral charge state. (Courtesy F. Bosch, GSI Darmstadt)

**Table 4.7.** Measured half-lives for bare isomers. The hindrance factors  $T_{1/2}(\text{bare})/T_{1/2}(\text{neutral})$  are shown in the last column

Isomer	$T_{1/2}$ bare, s	$T_{1/2}$ neutral, s	Hindrance factor
$^{151\text{m}}\text{Er}$	19(3)	0.58(2)	33(5)
$^{149\text{m}}\text{Dy}$	11(1)	0.49(2)	22(2)
$^{144\text{m}}\text{Tb}$	12(2)	4.25(15)	2.8(5)



Very recently quite the opposite effect has been demonstrated [18] in that instead of the nuclear decay process being accelerated in bare atoms, it has been hindered in bare isomers. The main decay channel of the isomeric states of neutral atoms is internal conversion. The results, showing an increase of the half-life by up to a factor 30, are shown in Table 4.7 for the bare isomers  $[^{151m}\text{Er}]^{68+}$ ,  $[^{149m}\text{Dy}]^{75+}$ , and  $[^{144m}\text{Tb}]^{65+}$ .

## Halo Nuclides

For most nuclides, the density of nucleons in the nucleus is more or less uniform. However near the neutron dripline, some neutrons are only weakly bound to the inner core nucleus. In this recently discovered phenomena, the nuclei consist of a normal nucleus surrounded by a halo of extra neutrons with a diameter very much larger than the core nucleus. The halo neutrons are mostly outside the region of the strong nuclear force between the nucleons. Typically half-lives of these nuclei are around 100 ms.

One such example of a halo nuclide is  $^{11}\text{Li}$ . It consists of a  $^9\text{Li}$  core surrounded by a halo of two loosely bound neutrons requiring only 0.3 MeV to remove them. The  $^{11}\text{Li}$  nucleus is similar in size to that of  $^{48}\text{Ca}$  which has a neutron binding energy

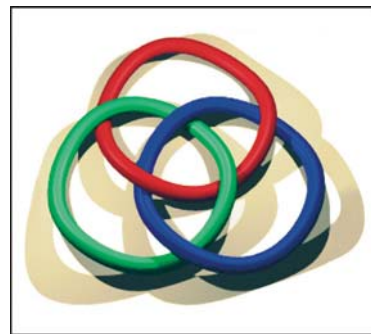
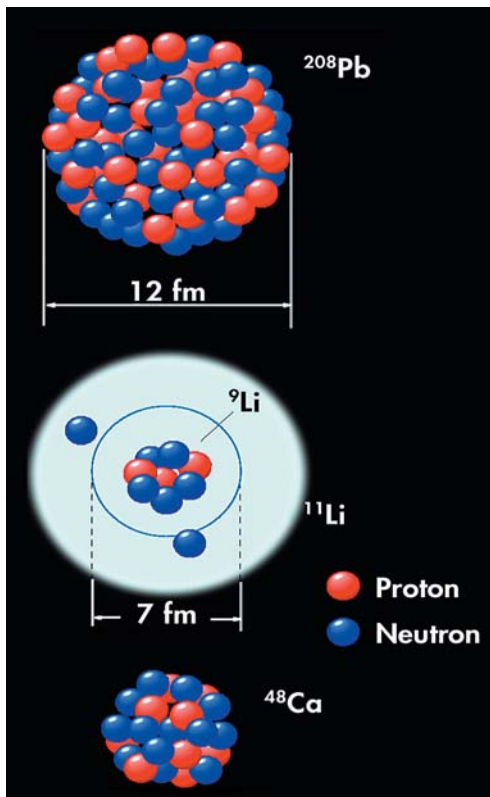


**Fig. 4.22** (above)

The Borromean rings provide an analogy for the structure of halo nuclei in which the removal of any one of the three major components breaks the whole system. Courtesy Wilton Catford, from the SIRIUS Science Booklet [26]

**Fig. 4.21** (left)

The neutron halo in  $^{11}\text{Li}$  extends to fill the volume equivalent to  $^{208}\text{Pb}$ , with very dilute, pure neutron matter. Courtesy Wilton Catford, from the SIRIUS Science Booklet [26]

of about 8 MeV. Other examples of halo nuclei are  ${}^6\text{He}$  ( ${}^4\text{He} + 2n$ ),  ${}^8\text{He}$  ( ${}^4\text{He} + 4n$ ),  ${}^{11}\text{Be}$  ( ${}^{10}\text{Be} + 1n$ ),  ${}^{14}\text{Be}$ ,  ${}^{17}\text{B}$  and  ${}^{19}\text{Ca}$ .

Proton halo nuclides may also exist for nuclei near the proton dripline. Possible nuclides are  ${}^8\text{B}$ ,  ${}^{13}\text{N}$ , and  ${}^{17}\text{F}$ .

### **Borromean Nuclei**

In Borromean nuclei, three separate parts of the nucleus are bound together in such a way that if any one is removed, the remaining two become unbound. The expression originates from the Borromean Rings which consist of interlocking rings.

${}^{12}\text{C}$ , in its excited state, is one example of a Borromean nucleus. It consists of three sub-units of  ${}^4\text{He}$ . If one is removed, the result is  ${}^8\text{Be}$  which is not bound. Other examples are  ${}^6\text{He}$ ,  ${}^{11}\text{Li}$ ,  ${}^{14}\text{Be}$ , and  ${}^{22}\text{C}$ .

## CHAPTER 6

# *Absorption of Nuclear Radiation*

### Contents

6.1.	Survey of absorption processes	125
6.2.	Absorption curves	126
6.3.	Absorption of protons and heavier ions	130
6.4.	Absorption of electrons	134
6.4.1.	Ionization	135
6.4.2.	Bremsstrahlung	136
6.4.3.	Čerenkov radiation	137
6.4.4.	Positron annihilation	138
6.4.5.	Absorption curves and scattering of $\beta$ -particles	140
6.5.	Absorption of $\gamma$ -radiation	141
6.5.1.	Attenuation coefficient	141
6.5.2.	Partial absorption processes	142
6.6.	Absorption of neutrons	147
6.7.	Radiation shielding	147
6.8.	Analytical applications of radiation absorption	149
6.8.1.	SIMS (Secondary Ion Mass Spectrometry)	150
6.8.2.	PIXE (Proton or Particle Induced X-ray Emission)	150
6.8.3.	ESCA (Electron Spectrometry for Chemical Analysis)	152
6.8.4.	XFS (X-ray Fluorescence Spectrometry)	152
6.8.5.	Mössbauer effect	154
6.9.	Technical applications of radiation sources	157
6.9.1.	Radionuclide gauges	158
6.9.2.	Radiography	161
6.9.3.	Radionuclide power generators	162
6.10.	Exercises	163
6.11.	Literature	165

Our understanding of the nature of nuclear particles is based on their mode of interaction with matter. Knowledge about this interaction is essential in a variety of areas of nuclear science, such as the proper utilization and construction of detection and measuring devices for radiation, the design of radiation shielding, the medical and biological applications of radiation, radiochemical synthesis, etc.

The term *nuclear radiation* is used to include all elementary particles, both uncharged (e.g. photons) and charged, having energies in excess of approximately 100 eV whether the particles have been produced through nuclear reactions (spontaneous or induced) or have acquired their energy in electrostatic accelerators. This lower energy limit is very high in

TABLE 6.1. *Survey of nuclear radiation absorption processes*  
 The reaction cross-sections ( $\sigma$ ) give only order of magnitude at about 1 MeV in  $Z \approx 20$

	Reacting particles and fields	Type of reaction	$\sigma$ (barns)	Name of process
1	<i>Protons and heavier ions</i> react with			
1a	orbital electrons	Particle energy loss through atomic excitation and ionization	$\geq 10^5$	Ionization, (atomic) excitation
1b	atomic nucleus	Particle elastically scattered	$\leq 10$	Nuclear scattering
1c		Particle inelastically scattered	$< 1$	Nuclear (coulomb) excitation
1d		Particle captured, formation of compound nucleus ( $E_p > E_{\alpha}(\text{min})^{(c)}$ )	$\leq 0.1$	Nuclear transmutation
2	<i>Electrons</i> ( $e^-$ , $\beta^-$ , $\beta^+$ ) react with			
2a	orbital electrons	Particle energy loss through atomic excitation and ionization	$> 10^2$	Ionization, (atomic) excitation
2b		Slow $\beta^+$ annihilated, 2-3 photons formed	(100%)	Positron annihilation
2c	electric field of nucleus	Particle scattered with energy loss, continuous emission of $h\nu$ ( $E_e > 1 \text{ MeV}$ )	$> 1$	Bremsstrahlung
3	<i>Photons</i> ( $\gamma$ ) react with			
3a	field of orbital electrons	$\gamma$ scattered without energy loss	$\leq 0.01$	Coherent scattering
3b	free (outer) electrons	$\gamma$ scattered with energy loss, ionization	$\leq 10^{(a)}$	Compton effect
3c	bound (inner) electrons	$\gamma$ completely absorbed, one electron knocked out		Photo effect
3d	field of nuclear force	$\gamma$ annihilated, formation of positron-negatron pair ( $E_\gamma > 1.02 \text{ MeV}$ )		Pair formation
3e	atomic nucleus	$\gamma$ scattered without energy loss	$\leq 10^{-3}$	Mössbauer effect
3f		$\gamma$ scattered with energy loss		Nuclear excitation
3g		$\gamma$ absorbed by nucleus, nuclear transmutation ( $E_\gamma > 5 \text{ MeV}$ ) <sup>(c)</sup>		Nuclear photo effect
4	<i>Neutrons</i> react with			
4a	atomic nucleus	n scattered with energy loss	$\leq 10$	Neutron moderation
4b		n captured, nuclear transformation	$\leq 10^4$	Neutron capture

<sup>(a)</sup> See Fig. 6.17;  $\sigma$  increases strongly with decreasing energy.

<sup>(b)</sup> Threshold energy for  $\text{Be}(\gamma, \alpha)^4\text{He}$  1.6 MeV,  $\text{D}(\gamma, n)\text{H}$  2.2 MeV.

<sup>(c)</sup>  $E_{\alpha}(\text{min})$  is the Coulomb barrier energy, eqn. (12.18).

comparison to ionization energies (usually  $< 15$  eV) and to the energies involved in chemical bonds (normally  $1 - 5$  eV). Therefore, nuclear radiation can cause ionization in its passage through matter; this is reflected in the common name *ionizing radiation*. Neutrons of energies  $< 100$  eV are included because their absorption (capture) by nuclei results in emission of nuclear radiation with energies  $\gg 100$  eV.

The passage of such high energy radiation through matter results in the transfer of energy to the atoms and molecules of the absorber material. This transfer of energy continues until the impinging particle of the radiation has reached the same average kinetic energy as the atoms comprising the material; i.e. until *thermal equilibrium* is obtained.

In considering the absorption of nuclear radiation it is appropriate to view the overall process from two aspects: (1) processes occurring to the nuclear particles themselves as their energies are reduced to the thermal equilibrium value; such *absorption processes* are the principal consideration of this chapter; (2) processes in the absorbing material due to the effect of the transfer of energy. This transfer results initially in excitation and ionization which cause physical and chemical changes. The study of these effects is the domain of *radiation chemistry* and is considered in Chapter 7.

### 6.1. Survey of absorption processes

The reduction in the intensity of a beam of ionizing particles can be caused either by reaction with the nuclei of the absorbing material (nuclear reactions) or with the atomic electrons (electron collision). In Table 6.1 the most important processes involved in the absorption of nuclear radiation in matter are listed along with the probability for each process. Comparison shows that the probability of interactions with electrons is considerably greater than that of a nuclear reaction; the only exception to this is the case of neutron absorption. In fact the principal mode of interaction between the particle and the atoms of the absorbing material involves the electromagnetic fields of the particle and the atomic electrons. Since neutrons are neutral particles, in order for them to transfer energy it is necessary that they experience a collision with a nucleus. Consequently for all particles except neutrons, nuclear reactions can be neglected in considering the processes involved in the reduction of the intensity of the particle beam.

As nuclear radiation passes the atoms of an absorber, it can transfer some of its energy to the atoms. If the amount of energy transferred is sufficient, ionization of the atom results. The positive ion and the electron thus formed are known as an *ion pair*. Frequently the electrons from this primary ionization have sufficiently high kinetic energy to cause *secondary ionization* in other atoms. The number of electrons produced in secondary ionization is often larger than that of the primary ionization but the average kinetic energies of the secondary electrons are lower than those of the primary electrons. In many interactions the initial radiation transfers insufficient energy for ionizations; instead an electron is raised to a higher, excited energy level of the atom. These *excited atoms* rapidly return to lower energy states by emission of electromagnetic radiation such as X-rays, visible light, etc. For neutrons the absorption process involving the capture of the neutron (cf. §§4.5 and 10.6) imparts sufficient recoil energy to cause ionization and excitation.

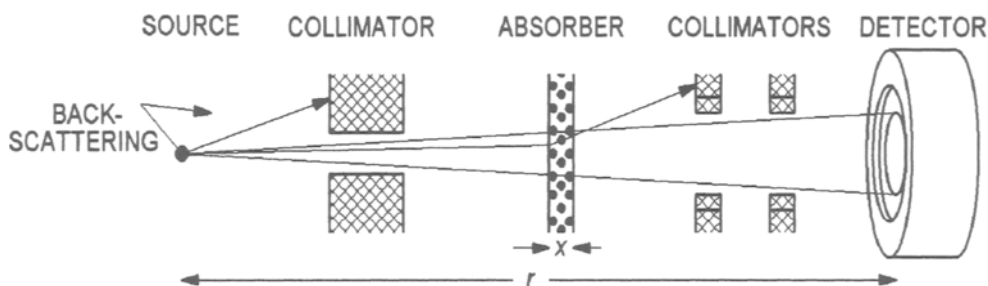


FIG. 6.1. Geometrical arrangement for measuring absorption curves.

## 6.2. Absorption curves

In order to measure the absorption of nuclear radiation, the experiments must be performed in such a manner as to eliminate as many of the interfering factors as possible. Usually a well-collimated beam is used. This is illustrated in Figure 6.1 for a point radioactive source. The relation between the disintegration rate  $A$  and the count rate  $R$  is given by (4.45):

$$R = \psi A$$

The *counting efficiency*  $\psi$  includes a number of factors:

$$\psi = \psi_{\text{sample}} \psi_{\text{abs}} \psi_{\text{det}} \psi_{\text{geom}} \quad (6.1)$$

If conditions were ideal, there would be no self-absorption or scattering in the sample (in which case  $\psi_{\text{sample}} = 1$ ), no absorption of radiation between the sample and the detector window ( $\psi_{\text{abs}} = 1$ ), and the detector would have a 100% efficiency (sensitivity) to a "count" for each particle reaching its window ( $\psi_{\text{det}} = 1$ ).

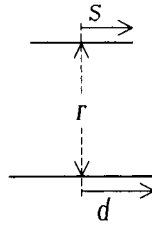
The geometric efficiency  $\psi_{\text{geom}}$ , is 1 for  $4\pi$ -geometry, i.e. for a spherical detector subtending a  $360^\circ$  solid angle about the sample. Although such detectors exist (Ch. 8), more commonly the sample is counted outside the detector at some distance  $r$ , as indicated in Figure 6.1. If the detector window offers an area of  $S_{\text{det}}$  perpendicular to the radiation, the geometrical efficiency is approximated by (for small  $\psi_{\text{geom}}$ )

$$\psi_{\text{geom}} \approx S_{\text{det}} / (4\pi r^2) \quad (6.2)$$

If a detector with a circular window of radius  $s$  is at a distance  $r$  from a source of radius  $d$ , the geometrical efficiency is given by

$$\psi_{\text{geom}} = \frac{1}{2} [1 - (1 + s^2/r^2)^{-1/2}] k \quad (6.3)$$

When the sample is a point source,  $k = 1$ , else  $k$  can be read from the series of curves in Figure 6.2.



The activity measured is proportional to the particle flux  $\phi$  reaching the detector

$$R = k_{\text{det}} \phi \quad (6.4)$$

where  $k_{\text{det}} = S_{\text{det}} \psi_{\text{det}}$  and

$$\phi = \psi_{\text{abs}} \phi_0 \quad (6.5)$$

and

$$\phi_0 = \psi_{\text{sample}} nA/(4\pi r^2) \quad (6.6)$$

$\phi_0$  is the flux of particles (particles  $\text{m}^{-2} \text{s}^{-1}$ ) which reach the detector from the source when  $\psi_{\text{abs}} = 1$ , and  $n$  is the number of particles emitted per decay ( $n > 1$  only for  $\gamma$  following  $\alpha$ - and  $\beta$ -decays). Thus if every  $\beta$ -decay yields  $2\gamma$  (in cascade) and  $\gamma$  is the measured radiation, then  $n_\gamma = 2$ , and  $\phi_0 = n_\gamma A_\beta / (4\pi r^2)$   $\gamma$ -quanta  $\text{m}^{-2} \text{s}^{-1}$ . In branched decay  $n$  will not be an integer. Equation (6.6) is the so called  $1/r^2$ -law since the measured flux varies as the inverse of the square of the distance to the source.

These equations are valid as long as the conditions at the source and at the detector, as well as  $r$ , are kept constant. When an absorber is inserted between the source and detector (Fig. 6.1),  $\psi_{\text{abs}}$  depends on the absorber thickness  $x$  (m). For zero absorber thickness,  $\psi_{\text{abs}} = 1$  in accurate measurements. There is a small absorption due to the air between the sample and detector unless the measurement is done in a vacuum.

Absorption curves relate the variation of either  $R$  or  $\phi$  to the thickness of the absorbing material. In Figure 6.3 the relative transmission  $\phi/\phi_0$  is plotted as a function of absorber thickness for different kinds of radiation. For charged particles, i.e. electrons, protons, and heavier ions,  $\phi/\phi_0$  reaches zero at a certain  $x$ -value ( $x_{\text{max}}$ ); this is referred to as the maximum range,  $R$ , of the particles. The range can be expressed by either the *average range* ( $x = C_1$  for heavy ions and  $C_3$  for electrons) or the *maximum* (or extrapolated) *range* ( $C_2$  and  $C_4$ , respectively, in Fig. 6.3). The loss of energy involves collisions with atomic electrons, and the energy loss per collision and the number of collisions varies from one ionizing particle to the next, resulting in a slight *straggling* in the range. The average range is the meaningful one.

Figure 6.4 shows an absorption curve for  $^{32}\text{P}$ . The radioactivity  $R$  has been measured as a function of aluminum absorber thickness in *linear density*,  $\text{kg m}^{-2}$  or more commonly  $\text{mg cm}^{-2}$ . The low activity "tail" ( $C_4$  in Fig. 6.4) is the background activity  $R_b$ , which has to be subtracted from the measured value  $R_m$  to obtain the true value for the radiation (e.g.  $^{32}\text{P}$ ):  $R = R_m - R_b$ . The extrapolation of  $R$  to a value equal to  $R_b$  (i.e.  $C_3$ ) gives the range.

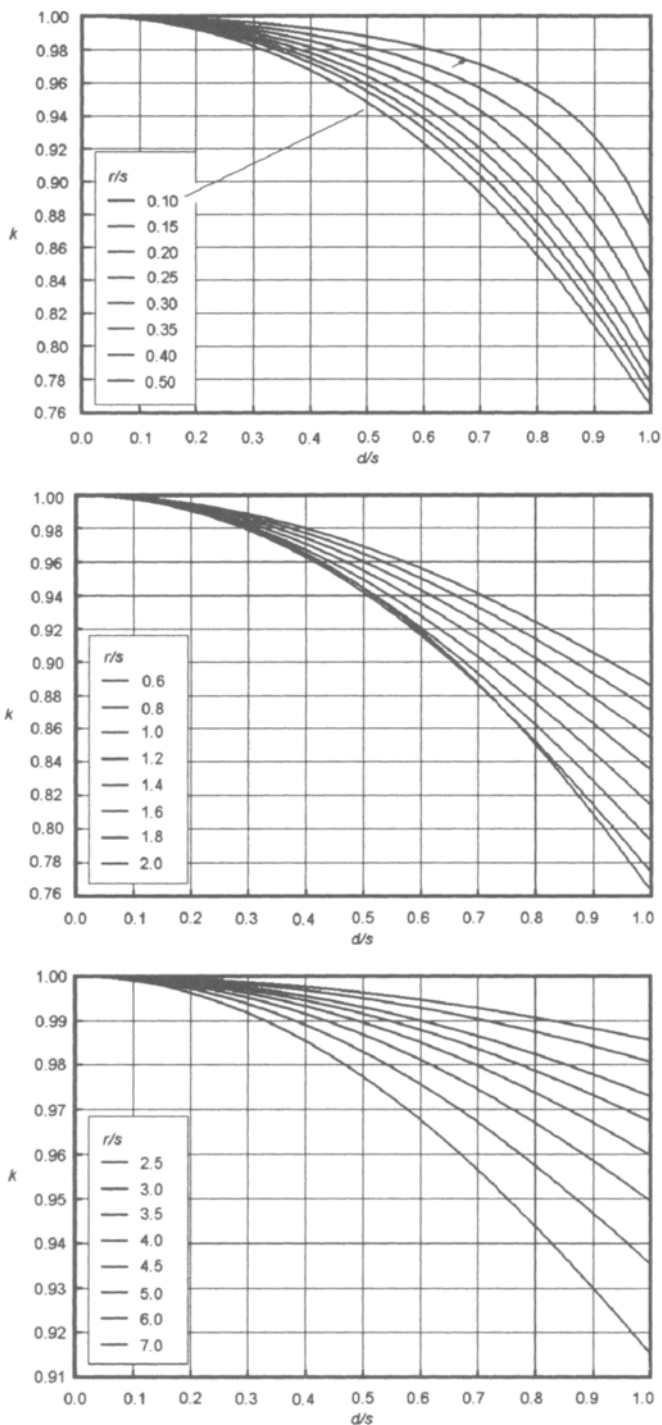


FIG. 6.2. Correction factor for finite source radius, eqn. (6.3).



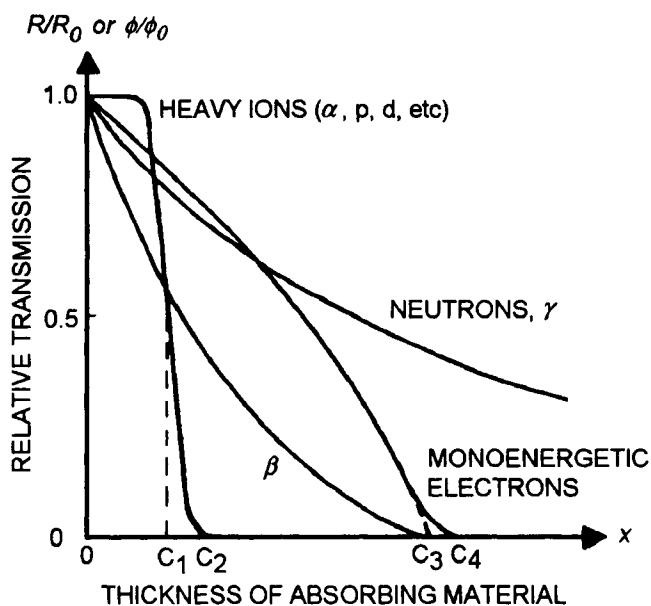


FIG. 6.3. Curves showing relative transmission  $\phi/\phi_0$  (or  $R/R_0$ ) as function of absorber thickness  $x$ .  $C_1$  and  $C_3$  are average,  $C_2$  and  $C_4$  maximum range.

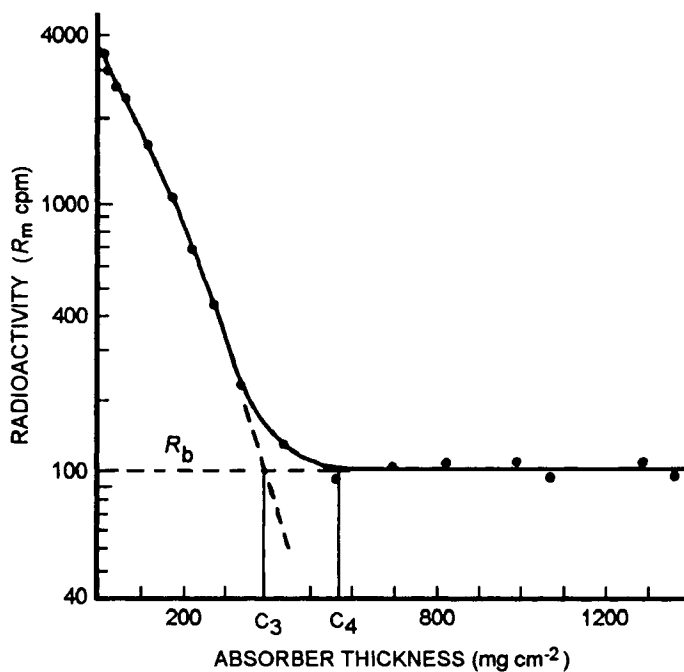


FIG. 6.4. Absorption curve for  $^{32}\text{P}$   $\beta$ -radiation showing extrapolated ( $C_4$ ) and average ( $C_3$ ) ranges. The dashed curve is obtained after subtraction of background.

Whereas it is possible to specify maximum ranges for charged particles, this is not possible for neutral particles such as neutrons and  $\gamma$ -quanta. If the absorber is not too thick, these particles undergo only one collision, or at the most a few, before they are absorbed. As a result the absorption curve has an exponential form.

$$\phi = \phi_0 e^{-\mu x} \quad (6.7)$$

where  $\mu$  is the *total attenuation coefficient*. Thus for  $n$  and  $\gamma$  we have

$$\psi_{\text{abs}}(x) = e^{-\mu x} \quad (6.8)$$

The reduction in intensity of a beam can occur by two mechanisms. One involves the deflection or scattering of the particles from the direct line of path between the source and the detector and is described by the *scattering coefficient*  $\mu_s$ . The second mode of reduction is the complete transfer of the projectile energy to the absorbing material (the particles are "captured" ) and is designated by the (*energy*) *absorption coefficient*  $\mu_a$ . The (total) attenuation coefficient in (6.7) is the sum of both these modes.

$$\mu = \mu_s + \mu_a \quad (6.9)$$

Both  $\mu_s$  and  $\mu_a$  can be measured independently. The (total) attenuation coefficient is of primary interest in radiation shielding, while the (energy) absorption coefficient is important in considering radiation effects on matter.

### 6.3. Absorption of protons and heavier ions

The mode of interaction of protons and heavier charged particles with the atoms of the absorbing material can be illustrated by considering the absorption of  $\alpha$ -particles. With rare exception,  $\alpha$ -particles emitted by radioactive nuclides have energies between 4 and 9 MeV. Since the  $\alpha$ -particles are so much heavier than electrons, they are deflected very slightly when their Coulomb fields interact with atoms or molecules to form ion pairs. As a result,  $\alpha$ -particles travel in a straight line as they pass through matter, which explains the straight paths observed for  $\alpha$ -particles in cloud chamber photographs (Fig. 6.5). This is in contrast to the very curved or irregular paths of the secondary electrons emitted in the formation of the ion pair. For a 5 MeV  $\alpha$ -particle the maximum energy of the secondary electrons is 2.7 keV. However only a small fraction of the secondary electrons actually receive this much energy; the average energy of the secondary electrons is closer to 100 eV. The ionization caused by more energetic secondary electrons is usually referred to as  *$\delta$ -tracks* (cf. §7.2).

In solids and liquids the total path length for  $\alpha$ -particles from radioactive decay is quite short. However, in gases at standard temperature and pressure the paths are several centimeters long (Table 6.2). The range in air for  $\alpha$ -particles with an initial energy  $E_\alpha$  MeV can be calculated by the empirical equation ( $\rho_{\text{air}} = 1.293 \text{ kg m}^{-3}$ ):

$$\hat{R}_{\text{air}} = 0.31 E_\alpha^{3/2} \text{ (cm)} = 0.40 E_\alpha^{3/2} \text{ (mg cm}^{-2}\text{)} \quad (6.10)$$

The range  $\hat{R}_z$  in other materials can be approximated roughly by

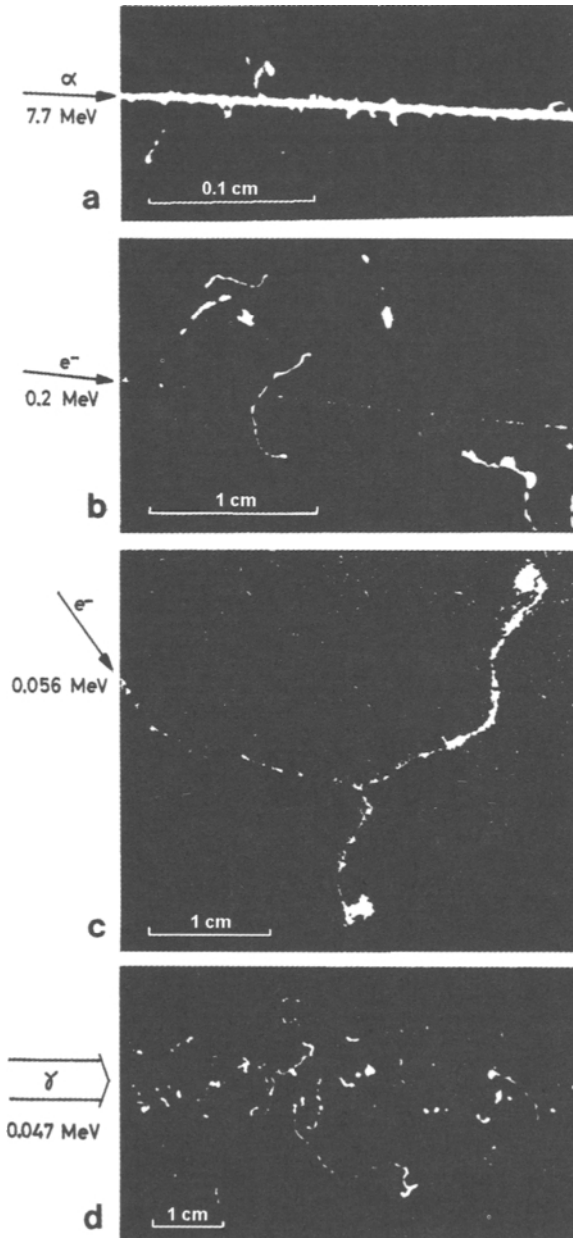


FIG. 6.5. Cloud chamber tracks of  $\alpha$ ,  $\beta$ , ( $e^-$ ) and  $\gamma$ -rays at 1 bar in air ((a), (b), and (c)) and in methane (d). (From W. Gentner, H. Maier-Leibnitz, and H. Bothe.)

$$\hat{R}_z = 0.173 E_\alpha^{3/2} A_z^{1/3} \text{ (mg cm}^{-2}\text{)} \quad (6.11)$$

TABLE 6.2. Range in water, and average linear energy transfer (LET) values for different radiation

Radiation	Energy (MeV)	Maximum range		Average LET value in water (keV/ $\mu\text{m}$ )
		cm air	mm water	
Electron	1	405	4.1	0.24
	3	1400	15	0.20
	10	4200	52	0.19
Proton	1	2.3	0.023	43
	3	14	0.014	21
	10	115	1.2	8.3
Deuteron	1	1.7	—	—
	3	8.8	0.088	34
	10	68	0.72	14
Helium	1	0.57	0.0053	190
	3	1.7	0.017	180
	10	10.5	0.11	92
Fiss. fragment	100	2.5	0.025	3300
$^{226}\text{Ra}$ ( $\alpha$ )	$E_\alpha$ 4.80	3.3	0.033	145
$^{210}\text{Po}$ ( $\alpha$ )	$E_\alpha$ 5.30	3.8	0.039	136
$^{222}\text{Rn}$ ( $\alpha$ )	$E_\alpha$ 5.49	4.0	0.041	134
$^3\text{H}$ ( $\beta$ )	$E_{\text{max}}$ 0.018	0.65	0.0055	1.1
$^{35}\text{S}$ ( $\beta$ )	$E_{\text{max}}$ 0.167	31	0.32	0.17
$^{90}\text{Sr}$ ( $\beta$ )	$E_{\text{max}}$ 0.544	185	1.8	0.10
$^{32}\text{P}$ ( $\beta$ )	$E_{\text{max}}$ 1.71	770	7.9	0.07
$^{90}\text{Y}$ ( $\beta$ )	$E_{\text{max}}$ 2.25	1020	11	0.07
$^{137}\text{Cs}$ ( $\gamma$ )	$E_\gamma$ 0.66	$x_{1/2} = 8.1$ cm $\text{H}_2\text{O}$		0.39
$^{60}\text{Co}$ ( $\gamma$ )	$E_\gamma$ 1.20-1.30	$x_{1/2} = 11.1$ cm $\text{H}_2\text{O}$		0.27

where  $A_z$  is the atomic weight of the absorber. Figure 6.6 shows the range of various charged particles in an aluminum absorber. The range of a 5 MeV  $\alpha$  is  $6 \text{ mg cm}^{-2}$ ; thus  $\hat{R}_{\text{Al}} = 6 \times 10^{-3} / \rho_{\text{Al}} \text{ cm} = 0.002 \text{ mm}$ . Alpha-particles from radioactive decay are easily stopped even by the thickness of a sheet of paper.

When the absorber consists of a composite material, containing the weight fractions  $w_1, w_2, w_3$ , etc of elements 1, 2, 3, etc with ranges  $\hat{R}_1, \hat{R}_2, \hat{R}_3$ , etc, the range  $\hat{R}_{\text{comp}}$  in the absorber is obtained from the relation

$$1/\hat{R}_{\text{comp}} = w_1/\hat{R}_1 + w_2/\hat{R}_2 + w_3/\hat{R}_3 + \dots \quad (6.12)$$

The number of ion pairs formed per millimeter of range for  $\alpha$ -particles, protons, and electrons are shown in Figure 6.7a. The larger *specific ionization* of the  $\alpha$ -particles compared to the protons is related to the fact that the former are doubly charged. In general the specific ionization increases with the ionic charge of the particle for the same kinetic energy. Fission fragments that initially have very large energies also have very large ionic charges leading to quite high specific ionization in their absorption in matter; their range is 2-3 cm in air and 2-3  $\text{mg cm}^{-2}$  in aluminum.

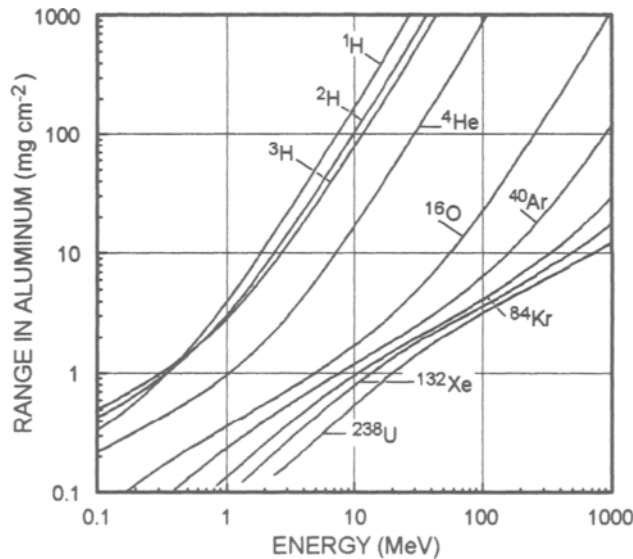


FIG. 6.6. Range of some energetic particles in an aluminum absorber.

A quantum-mechanical and relativistic analysis of the interaction between a fast moving positive ion of atomic number  $z$  and the electrons in the absorber leads to the following expression for the energy loss per unit distance,  $dE/dx$  (J/m), traveled in an absorber

$$-dE/dx = \left\{ (4\pi\gamma^2 z^2 e^4 NZ) / (m_e v^2) \right\} \left[ \ln \left\{ (2m_e v^2) / I \right\} - \ln(1 - \beta^2) - \beta^2 \right] \quad (6.13)$$

where  $\gamma z e$  is the charge of the ion moving at velocity  $v$  ( $\beta = v/c$ ) through an absorber containing  $N$  atoms of atomic number  $Z$  per volume unit and having an effective ionization potential  $I$ . For a completely stripped ion,  $\gamma = 1$ . The range,  $R$ , of an ion may be calculated by integrating the energy loss expression

$$R = \int_{E_0}^0 (dE/dx)^{-1} dE \quad (6.14)$$

from the initial energy  $E_0$  to zero.

Charged particles decrease in velocity as they lose their energy in traversing an absorber. As a result they spend progressively longer times in the vicinity of any particular atom, which results in an increase in the probability of interaction with that atom. Consequently there is a steady increase in the number of ion pairs formed along the path of the particle rather than a constant density of ion pairs. Near the end of the range for heavy charged particles a maximum is observed for the number of ion pairs formed per unit path length (the *Bragg peak*) (Fig. 6.7b). At a distance just beyond the Bragg peak maximum the kinetic energy of the particles is comparable to those of the orbital electrons of the absorber. As a result, the particle can acquire electrons,  $\gamma < 1$  in (6.13), finally becoming uncharged,  $\gamma = 0$ , and thereby losing its ability to cause further ionization.

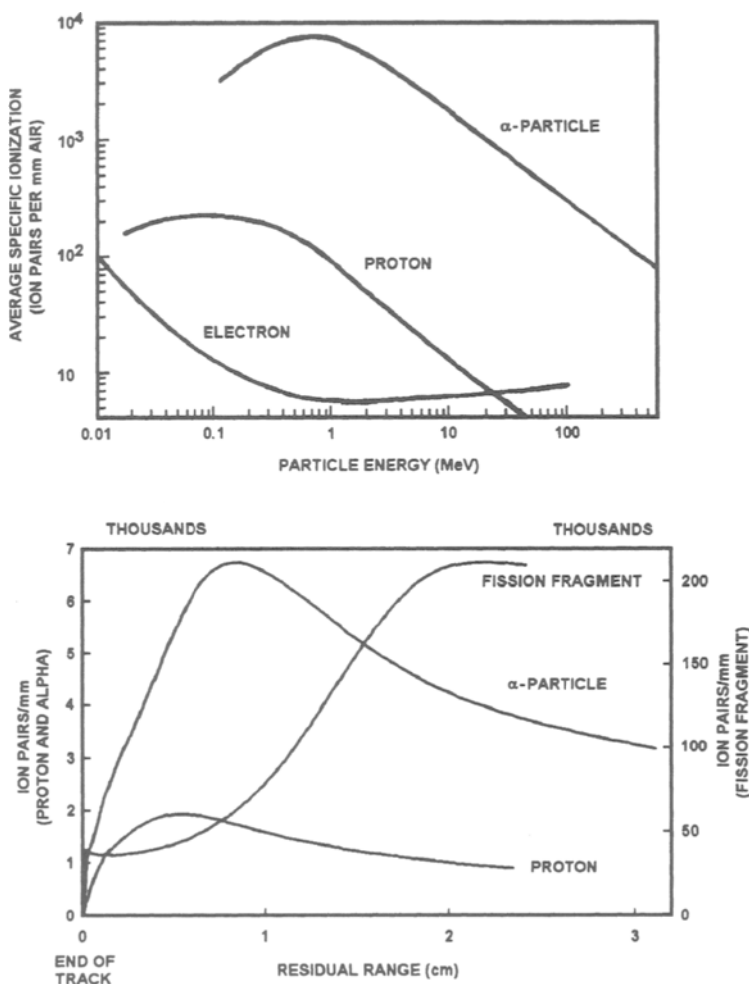


FIG. 6.7. Number of ion pairs formed per mm air at STP as function of particle energy. (a) average specific ionization at maximum particle energy, (b) same for residual range. (From H. A. C. McKay.)

#### 6.4. Absorption of electrons

Absorption of high energy electron beams occurs through interaction with the orbital electrons and the electromagnetic field at the atom. The processes are summarized in Table 6.1 and Figure 6.8. In order to distinguish between electrons from accelerators and those from  $\beta$ -decay we refer to the latter as  $\beta$ -particles.

## 6.4.1. Ionization

Beta-particles lose their energy primarily by the same mechanism as  $\alpha$ -particles (Fig. 6.7a and b); however, there are several important differences. Since the masses of the  $\beta$ -particles and of the orbital electrons are the same at non-relativistic velocities, the  $\beta$ -particles can lose a large fraction of their energy in a single collision. The  $\beta$ -particle undergoes a wide angle deflection in such collisions and consequently  $\beta$ -particles are scattered out of the beam path all along the length. The secondary electrons ionized from the atom have such high energies that they cause extensive secondary ionization which provides 70-80% of the total ionization in  $\beta$ -absorption processes (Fig. 6.5b). Approximately half of the total

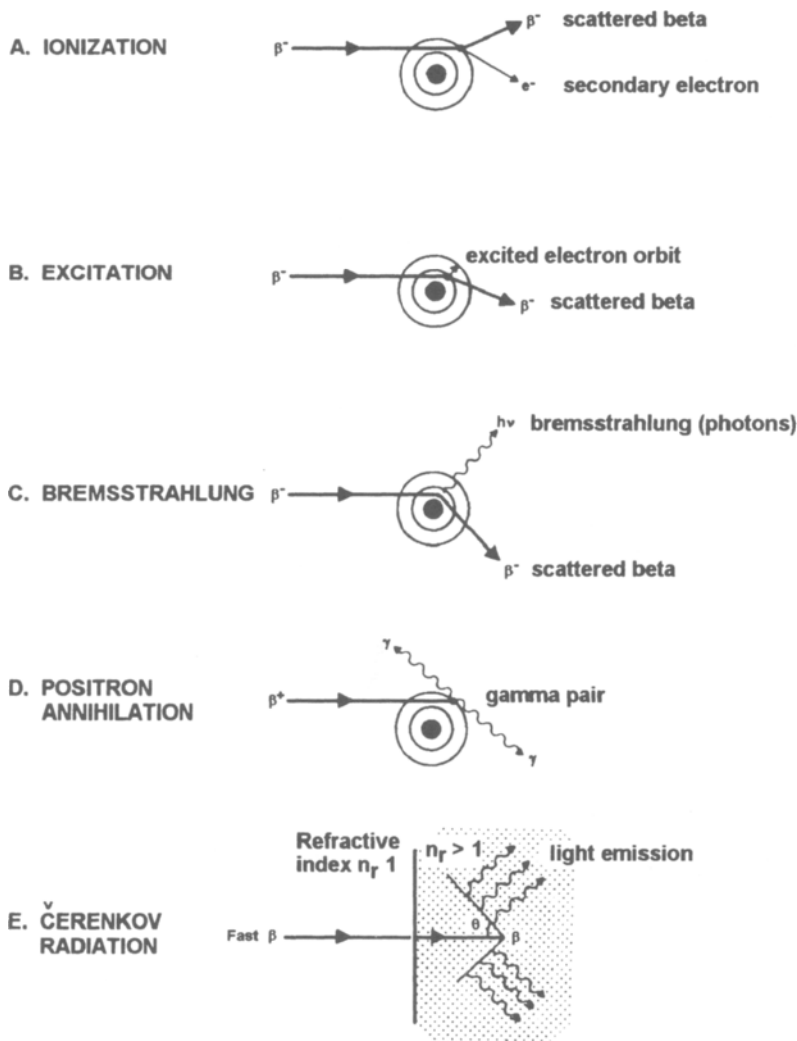


FIG. 6.8. Schematic description of the five processes accounting for  $\beta$ -particle absorption.

energy of the  $\beta$ -particle is lost by ionization and half by excitation. The track formed is further discussed in §7.2.

The specific ionization from a  $\beta$ -particle is much lower than that from a heavy ion as can be seen in Figure 6.7a. This is due to the fact that for the same initial energy,  $\beta$ -particles have much greater velocity than have  $\alpha$ -particles or protons because their mass is very much smaller than the mass of the heavy particles. This greater velocity results in a correspondingly lower ionization and gives a much longer range to  $\beta$ -particles. The erratic path observed for  $\beta$ -particles in Figure 6.5c is a result of the large energy transfer and the resulting large deflections involved in the encounters with the orbital electrons. However, at very high energies the  $\beta$ -particles have straight paths as a result of the fact that very energetic  $\beta$ -particles have a momentum considerably in excess of that of the orbital electron.

#### 6.4.2. Bremsstrahlung

As a  $\beta$ -particle approaches an atomic nucleus, it is attracted by the positive field of the nucleus and deflected from its path. The deflection results in an acceleration that, according to classical electrodynamics, leads to emission of electromagnetic radiation (Fig. 6.8c). Therefore the encounter with the positive charge of the nuclear field decreases the energy of the  $\beta$ -particle by an amount exactly equal to the amount of electromagnetic radiation emitted. This radiation is known as *bremstrahlung* (braking radiation). The loss of energy by emission of bremsstrahlung radiation increases with the  $\beta$  energy and with the atomic number of the absorber material (Fig. 6.9). In aluminum approximately 1% of the energy of a 1 MeV electron is lost by bremsstrahlung radiation and 99% by ionization whereas in lead the loss by radiation is about 10%. For electrons of greater than 10 MeV energy,

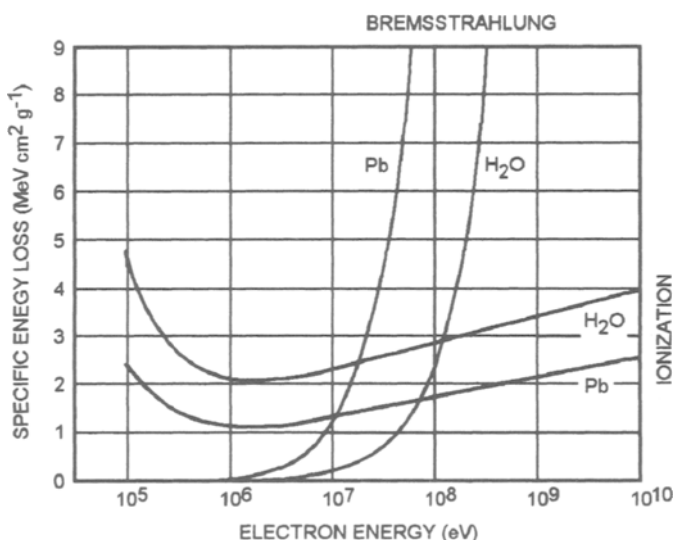


FIG. 6.9. Energy loss of fast electrons by ionization and bremsstrahlung. (From Gentner, Maier-Leibnitz, and Bothe.)



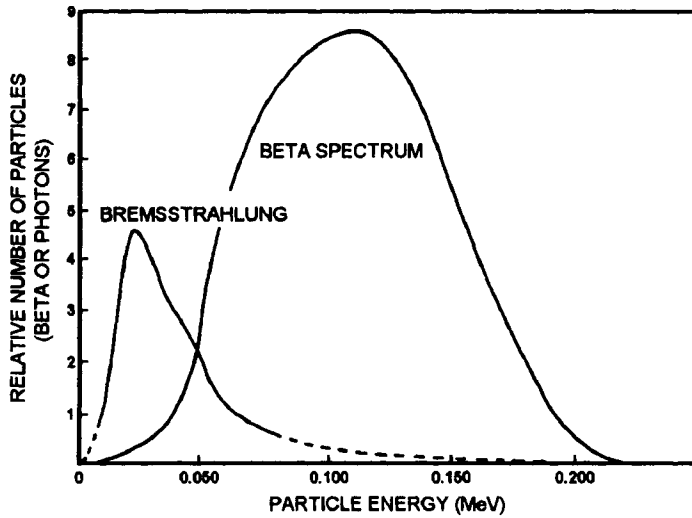


FIG. 6.10. Beta-spectrum (right curve) and bremsstrahlung spectrum in aluminum for  $^{147}\text{Pm}$ . The ordinate of the bremsstrahlung spectrum is enlarged about 100 times.

bremsstrahlung emission is the predominant mode of energy loss in lead. However, for the energies in radioactive decay, bremsstrahlung can usually be neglected - particularly for absorption processes in material of low atomic weight. The ratio of *specific energy loss* ( $dE/dx$ ) through bremsstrahlung to that through collision (i.e. all other processes) is approximately:

$$(dE/dx)_{\text{brems}} / (dE/dx)_{\text{coll}} \approx E_e Z / 800 \quad (6.15)$$

where  $E_e$  is kinetic energy of the electron (MeV) and  $Z$  the atomic number of the absorber atoms.

Figure 6.10 shows the bremsstrahlung spectrum obtained in aluminum for  $\beta$ -particles emitted by  $^{147}\text{Pm}$ . In this case a very small fraction of the  $\beta$ -energy is converted into radiation. The bremsstrahlung spectrum is always of much lower energy than that of the  $\beta$ -spectrum. Bremsstrahlung sources of a wide variety of energies are commercially available. Recently special electron accelerators have been designed for the sole purpose of producing bremsstrahlung radiation to be used for (analytical) X-ray excitation and for medical irradiation purposes; see Ch. 13.

#### 6.4.3. Čerenkov radiation

The velocity of light in matter  $c$  depends on the refractive index  $n_r$

$$c = c n_r^{-1} \quad (6.16)$$

In water  $n_r = 1.33$ , in plexiglass 1.5.  $\beta$ -particles with energies  $> 0.6$  MeV move faster than light in water. When the particle velocity ( $v_p$ )  $> c$ , electromagnetic radiation is

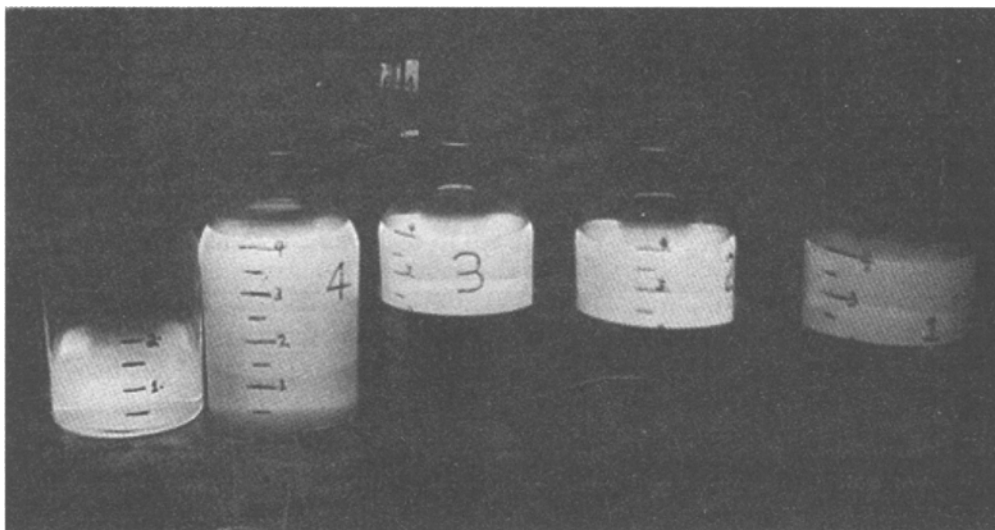


FIG. 6.11. Bottles containing highly radioactive  $^{90}\text{Sr}$  solutions glow in the dark due to Čerenkov radiation from daughter  $^{90}\text{Y}$  ( $E_{\text{max}}$  2.3 MeV).

emitted coherently in a cone whose axis is the direction of the moving particle (Fig. 6.8e). The angle of the cone  $\theta$  is obtained from

$$\sin \theta = c/v_p \quad (6.17)$$

This Čerenkov radiation is the source of the bluish light observed in highly radioactive solutions (Fig. 6.11) and around reactor fuel elements submerged in water. The radiation can be used for detecting  $\beta$ -particles and for measuring high particle energies (from  $\theta$ ). For a fast electron the energy loss through Čerenkov radiation is  $\leq 0.1\%$  of the energy loss through other processes. Čerenkov detectors are described in Ch. 8.

#### 6.4.4. Positron annihilation

Positrons interact with matter through ionization, excitation, emission of bremsstrahlung, and Čerenkov radiation in the same manner as negative electrons. As the kinetic energy of the positron decreases in the absorber, there is an increase in probability of direct interaction between the positron and an electron (Fig. 6.8d) in which both the positron and electron are annihilated. The energy of the two electron masses is converted into electromagnetic radiation. This process, known as *positron annihilation*, is a characteristic means of identification of positron emission. Since an electron mass is equivalent to 0.51 MeV, and the kinetic energy of the particles of annihilation is essentially zero, the total energy for the annihilation process is 1.02 MeV. In order to conserve momentum the photons must be emitted with equal energy and in exactly opposite direction in case of only two photons (the dominating case). These photons of 0.51 MeV each are referred to as *annihilation radiation*. The presence of  $\gamma$ -rays at 0.51 MeV in the electromagnetic spectrum

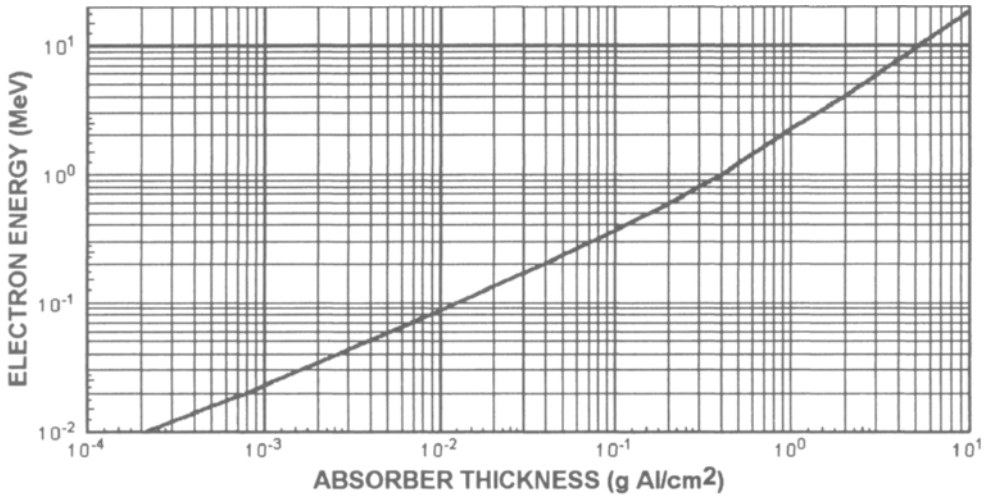


FIG. 6.12. Empirical relation for the maximum range of  $\beta$ -particles in aluminum.

of a radionuclide is strong evidence for the presence of positron emission by that nuclide.

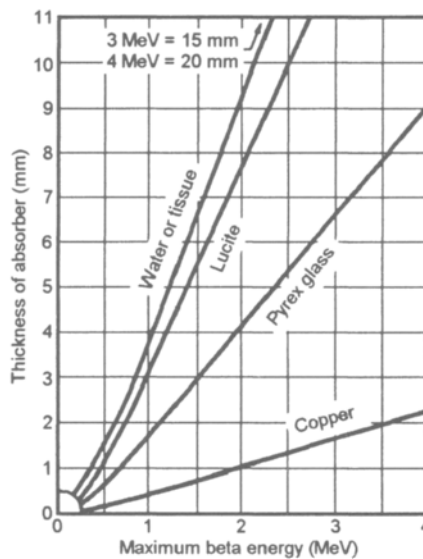


FIG. 6.13. Thickness of various materials needed to completely stop  $\beta$ -particles.

#### 6.4.5. Absorption curves and scattering of $\beta$ -particles

An absorption curve for  $\beta$ -particles has a quite different shape than it has for  $\alpha$ -particles (cf. Fig. 6.3). The continuous spectrum of energies in radioactive  $\beta$ -decay plus the extensive wide angle scattering of the  $\beta$ -particles by the absorber atoms account for the fact that range curves for  $\beta$ -particles continuously decrease. Even for a beam of initially mono-energetic electrons, the continuous removal of electrons from the beam path by wide angle deflection results in a plot showing a continuous decrease in the numbers of electrons with distance, with approximately 95% of the original  $\beta$ -particles stopped in the first half of the range. It is more common to speak of the absorber thickness necessary to stop 50% of the particles than to speak of the range itself. This *half-thickness value* is much easier to ascertain experimentally than is an apparent range. It should be remembered that the energy deposited at complete  $\beta$ -absorption is  $E_{\text{abs}} \approx E_{\text{max}}/3$  (Ch. 4).

The absorption curve for  $\beta$ -particles formed in radioactive decay can be described with fair approximation by the relationship (6.7). This is due to the continuous energy spectrum resulting in an exponential relationship for the range curve. In the  $E_{\text{max}}$  range 0.7-3 MeV the range in aluminum closely follows the relation (*Feather's rule*)

$$\hat{R}(\text{g Al cm}^{-2}) = 0.543 E_{\text{max}}(\text{MeV}) - 0.160 \quad (6.18)$$

This is the range  $C_3$  in Figure 6.4.

Figure 6.12 shows an empirical relationship between the maximum energy of  $\beta$ -particles and the extrapolated range in aluminum. Compared to  $\alpha$ -radiation,  $\beta$ -radiation has a much longer range. For example, the range of an  $\alpha$ -particle of 5 MeV is 3.6 cm in air while that of a  $\beta$ -particle of 5 MeV is over 17 m. A comparison of the range in air and water for electrons and heavy particles is given in Table 6.2. Figure 6.13 is useful for a rapid estimate of the absorber thickness needed to protect against  $\beta$ -particles.

An additional complication in the experimental measurements of absorption curves for  $\beta$ -particles is found in the fact that a certain fraction of  $\beta$ -particles which are not originally emitted in the direction of the detector may be deflected to the detector by the large angle

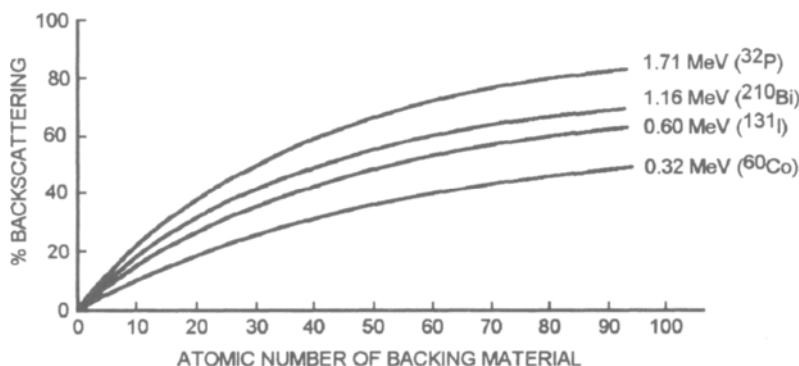


FIG. 6.14. Backscattering of  $\beta$ -particles of different energy as function of the atomic number of thick backing materials.

scattering. This process is known as *backscattering*, since the *backing* (or *support*) for radioactive samples may cause scattering of a certain fraction of the particles through as much as  $180^\circ$ . The fraction of back-scattered  $\beta$ -radiation depends on the geometry of the measuring system, the energy of the  $\beta$ -particles, and the thickness and electron density of the backing material. In Figure 6.14 the percent backscattering as a function of the atomic number of the backing material is shown for four  $\beta$ -energies ( $E_{\max}$ ); the radioactive sample is considered infinitely thin (i.e. no self-absorption). From the curve for  $^{32}\text{P}$  on platinum ( $Z = 78$ ) we see that about 40% of the measured radiation is due to back-scattered radiation ( $0.8/(1.0 + 0.8) = 0.4$ ). Backscattering increases with the thickness of the backing material up to a saturation value which is reached when the thickness of the backing is about one-fifth of the extrapolated range of the  $\beta$ -particles in that material.

## 6.5. Absorption of $\gamma$ -radiation

The absence of charge and rest mass for  $\gamma$ -rays results in little interaction with the absorbing atoms and in long ranges. The number of ion pairs produced in a given path length by  $\gamma$ -rays is only 1-10% of that produced by  $\beta$ -particles of the same energy (Fig. 6.5); e.g. a 1 MeV  $\gamma$ -ray produces only about one ion pair per centimeter of air. As a consequence of this low specific ionization of  $\gamma$ -rays, the ionization is almost completely secondary in nature resulting from the action of a few high energy primary ion pairs.

### 6.5.1. Attenuation coefficient

Unlike heavy particles and electrons which lose their energy as a result of many collisions,  $\gamma$ -rays are completely stopped in one or, at most, a few interactions. For thin absorbers the attenuation of  $\gamma$ -rays follows relation (6.7), where  $\phi$  is the number of photons  $\text{m}^{-2} \text{s}^{-1}$ . The proportionality factor  $\mu$  is called the (*total*) *attenuation coefficient*. When it has the dimension of  $\text{m}^{-1}$  and the thickness  $x$  is expressed in meters,  $\mu$  is referred to as the *linear* attenuation coefficient. The attenuation coefficient can be expressed in other ways:

$$\mu_m = \mu/\rho = \sigma_a N_A / M = \sigma_e Z N_A / M \quad (6.19)$$

where  $\rho$  is the density,  $M$  the average atomic weight, and  $Z$  the average atomic number of the absorber.  $N_A \rho / M$  can be replaced by  $N_v$ , by which we can define a *macroscopic absorption cross-section*  $\Sigma$  (cf. §14.1).  $\Sigma^{-1}$  is the mean free path or *relaxation length* of the radiation in the absorbing material.  $\mu_m$  (in  $\text{cm}^2 \text{g}^{-1}$  when  $x$  is in centimeters) is the *mass attenuation coefficient*;  $\sigma_a$  is the probability of reaction between a  $\gamma$ -ray and the electron cloud of the absorber atom (*atomic reaction cross-section*,  $\text{m}^2 \text{atom}^{-1}$ );  $\sigma_e$  is the probability of the reaction of a  $\gamma$ -ray with a single electron of the absorber (*electron reaction cross-section*,  $\text{m}^2 \text{electron}^{-1}$ ).  $\sigma_a$  and  $\sigma_e$  are analogous to the nuclear reaction cross-sections discussed later. In Table 6.1 only the equivalent nuclear and atomic reaction cross-sections are given.

Since a  $\gamma$ -ray may be removed from the beam in the first few Ångströms of its entrance into the absorber or may travel several centimeters with no interaction at all and then be

removed, it is not possible to apply the range concept to  $\gamma$ -rays in the way that it is applied to charged particles. However, it is experimentally easy to measure the thickness of absorber necessary to remove half of the initial  $\gamma$ -rays (half thickness value) from a beam, or reduce it to 1/10, 1/100, etc. Figure 6.15 shows the required thickness of concrete and lead necessary to reduce  $\gamma$ -rays of different energies by factors of 10 (shielding thicknesses are further discussed in §6.7). The half-thickness value is

$$x_{1/2} = \ln(2)/\mu \quad (6.20)$$

and the 1/10 value

$$x_{1/10} = \ln(10)/\mu \quad (6.21)$$

### 6.5.2. Partial absorption processes

Gamma-ray absorption occurs as illustrated in Figure 6.16 by four different processes: coherent scattering, photoelectric effect, Compton effect, and pair production. For each of these processes, a partial coefficient can be expressed:

$$\mu = \mu_{\text{coh}} + \mu_{\text{phot}} + \mu_{\text{Comp}} + \mu_{\text{pair}} \quad (6.22)$$

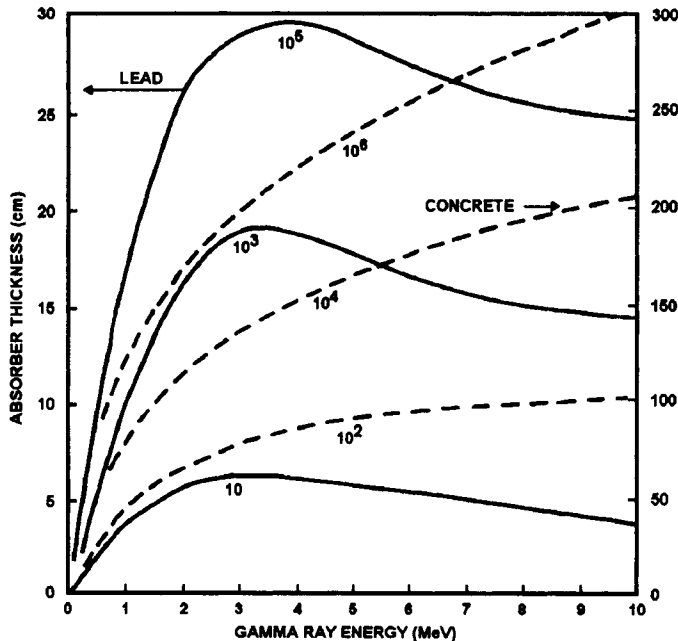


FIG. 6.15. Thickness of lead and concrete reducing  $\gamma$ -ray flux by different powers of 10, as function of  $\gamma$ -ray energy. The curves are for thick absorbers and include build-up factors.

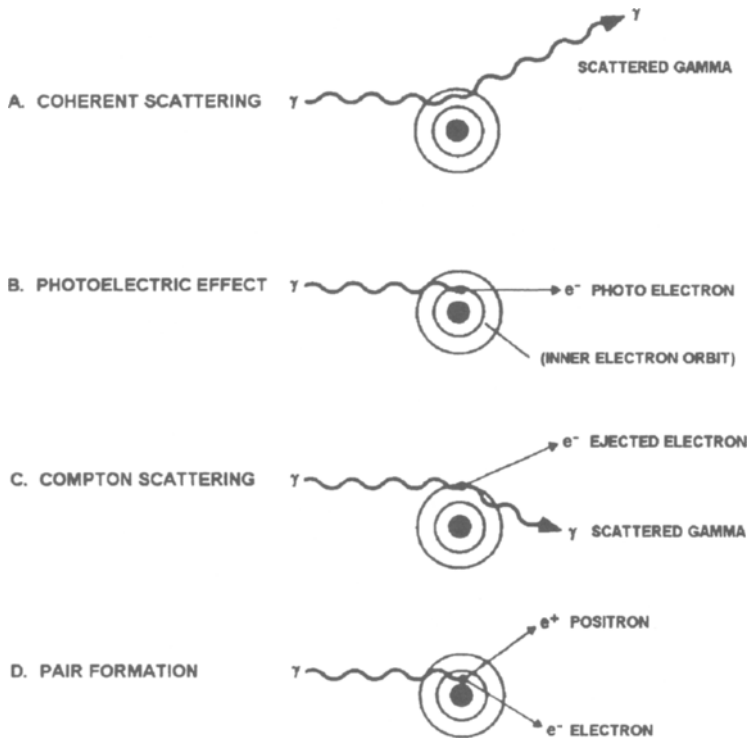
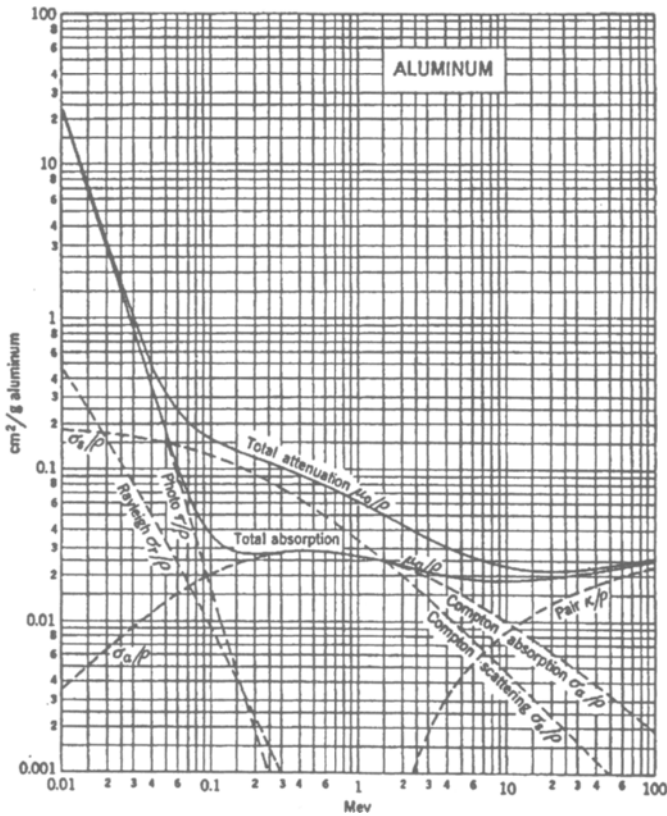
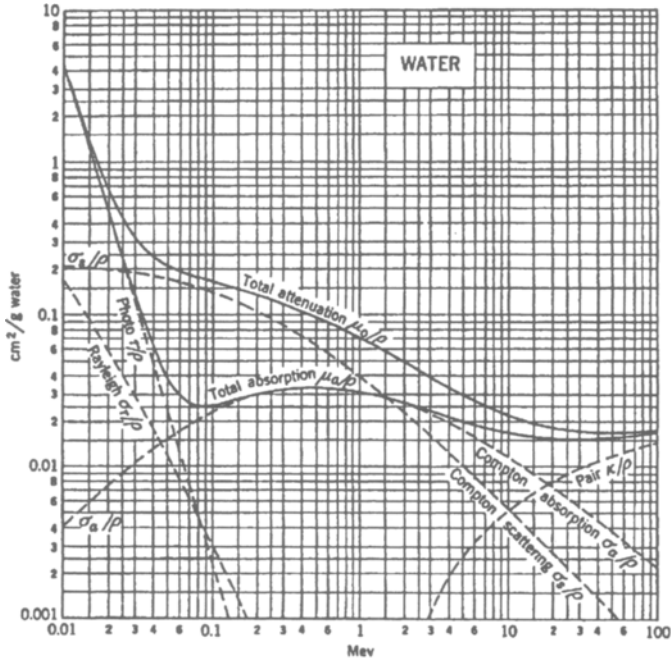


FIG. 6.16. Schematic description of the four main processes accounting for  $\gamma$ -ray interaction and absorption.

Comparing with (6.9),  $\mu_{\text{phot}}$  and  $\mu_{\text{pair}}$  are absorption processes, while  $\mu_{\text{coh}}$  is all scattering;  $\mu_{\text{Comp}}$  contributes to both the  $\mu_{\text{s}}$  and the  $\mu_{\text{a}}$  terms. In Figure 6.17 the total attenuation, absorption, and the partial coefficients are given for water, aluminum, and lead as a function of the  $\gamma$ -ray energy. The corresponding linear coefficients are obtained by multiplying with  $\rho$  (for aluminum 2.7, for lead 11.3). It should be noted that the aluminum curves also can be used for absorption in concrete.

In *coherent scattering* (also called Bragg or Rayleigh scattering, denoted  $\sigma_r$  in Fig. 6.17) the  $\gamma$ -ray is absorbed and immediately re-emitted from the atom with unchanged energy but in a different direction. Coherently scattered radiation can give interference patterns, so the process is used for structural analysis of absorbing material in the same way as X-rays are. The probability for coherent scattering increases with the square of atomic number of the absorber and decreases with  $\gamma$ -ray energy. In lead, coherent scattering amounts to about 20% of the total attenuation for  $\gamma$ -energies of 0.1 MeV but decreases in importance for higher energy  $\gamma$ -rays.

In absorption of  $\gamma$ -rays by the *photoelectric effect* (denoted  $\tau$  in Fig. 6.17) the photons are absorbed completely by the atom. This absorption results in excitation of the atom above the binding energy of some of its orbital electrons with the result that an electron is ejected and an ion pair formed. The energy  $E_e$  of the emitted photoelectron is the difference between the energy of the  $\gamma$ -ray and the binding energy for that electron in the atom





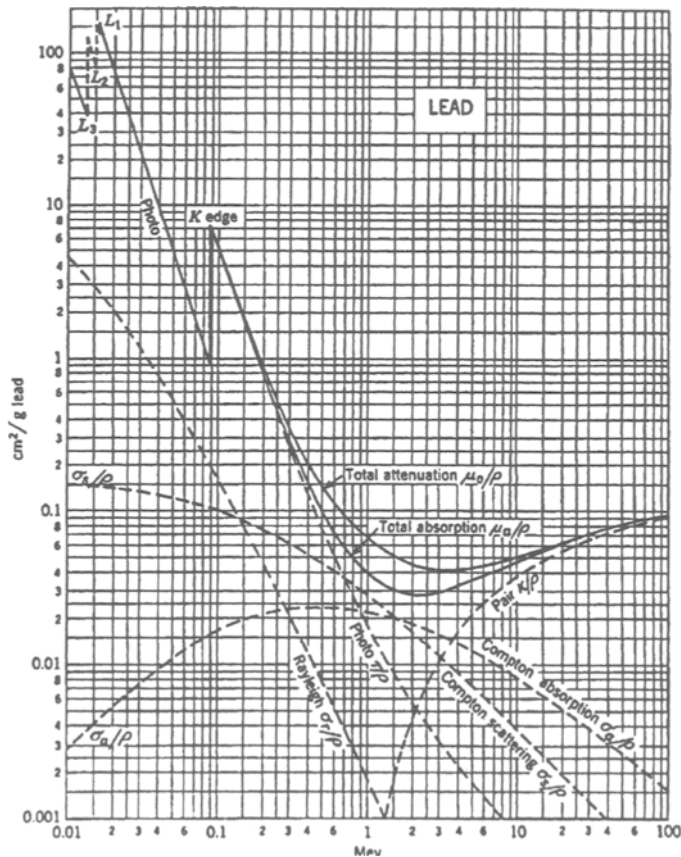


FIG. 6.17. Total and partial mass absorption and attenuation coefficients for  $\gamma$ -rays in water, aluminum and lead. (From R. D. Evans.)

$$E_e = E_\gamma - E_{be} \quad (6.23)$$

If the photoelectron originates from an inner electronic orbital, an electron from a higher orbital moves to fill the vacancy. The difference in binding energy of the higher and the lower energy orbital causes emission of X-rays and of low energy *Auger electrons*. The process of electron cascade, accompanied by X-ray and Auger electron emission, continues until the atom is reduced to its ground state energy. The photoelectron as well as the Auger electrons and the X-rays cause extensive secondary ionization by interacting with the absorber atoms.

The probability for the photoelectric effect decreases with increasing  $\gamma$ -ray energy. It is largest for the most tightly bound electrons and thus the absorption coefficient for the photoelectric effect increases in the order of electron shells  $K > L > M > \dots$ . In Figure 6.17 we see that in lead it is the dominating mode of absorption up to about 0.7 MeV. Discontinuities observed in the graph of  $\mu$  vs  $E_\gamma$  are related to the differences in binding energies of the electrons in the different shells as the increasing  $\gamma$ -ray energy allows more

tightly bound electrons to be emitted. These discontinuities coincide with the K, L, etc., edges observed in X-ray absorption.

Gamma-rays of higher energy, rather than interacting with the field of the whole atom as in the photoelectric effect, interact with the field of one electron directly. This mode of interaction is called the *Compton effect* after its discoverer, A. H. Compton. In the Compton effect an electron is ejected from an atom while the  $\gamma$ -ray is deflected with a lower energy. The energy of the scattered  $\gamma$ -ray,  $E_\gamma'$ , is expressed by the equation

$$E_\gamma' = E_\gamma - E_e \quad (6.24)$$

where  $E_e$  is the kinetic energy of the Compton electron. The probability for Compton scattering increases with target  $Z$  and decreases with  $E_\gamma$ . Since the Compton interaction occurs only with the most weakly bound electrons and high energy  $\gamma$ -rays, the binding energy of the electron is negligible compared to  $E_\gamma$ . The Compton electrons and scattered  $\gamma$ -rays have angles and energies which can be calculated from the relationships between the conservation of energy and momentum, correcting for the relativistic mass of the electrons at these kinetic energies. The scattered  $\gamma$ -ray may still have sufficient energy to interact further by the Compton effect, the photoelectric effect or pair production. Again, emission of X-rays and Auger electrons usually accompanies Compton interaction and extensive secondary ionization follows. Since the Compton electron can have a spread of values, the scattered  $\gamma$ -rays exhibit a broad spectrum. The Compton electrons, as in the case of photoelectrons, are eventually stopped by the processes described for  $\beta$ -particles.

Figure 6.17 shows the division of energy between the scattered Compton  $\gamma$  and the Compton electron as a function of  $\gamma$ -ray energy. Only the energy of the electron is deposited in the absorber as the scattered  $\gamma$ -ray has a high probability of escape. Thus Compton electrons contribute to the (*energy*) *absorption coefficient*  $\mu_a$  while the Compton  $\gamma$  contributes to the *total attenuation coefficient*  $\mu$  through the scattering coefficient  $\mu_s$  in (6.9).

The fourth mode of interaction for  $\gamma$ -rays with an absorber involves conversion in the Coulomb field of the nucleus of a  $\gamma$ -ray into an electron and a positron (Fig. 6.18). This process is termed *pair production* since a pair of electrons, one positive and one negative, is produced. The process can be considered as the inverse phenomenon of positron annihilation. Since the rest mass of an electron corresponds to 0.51 MeV, the  $\gamma$ -ray must have a minimum value of 1.02 MeV to interact by pair production. As the energy of the  $\gamma$ -ray is increased beyond this value, the probability of pair production increases (see Fig. 6.17, where  $\mu_{\text{pair}}$  is denoted  $\kappa$ ). The excess energy (above the 1.02 MeV) appears as the kinetic energy of the electron pair.

$$E_\gamma = 1.02 + E_{e^-} + E_{e^+} \quad (6.25)$$

The pair of electrons are absorbed as described in §6.4. The annihilation of positrons produce 0.51 MeV  $\gamma$ 's, which are absorbed by the processes described previously.

Figure 6.19 summarizes the domains of interaction of the main  $\gamma$ -ray absorption processes as a function of  $\gamma$ -ray energy and absorber  $Z$ -value.

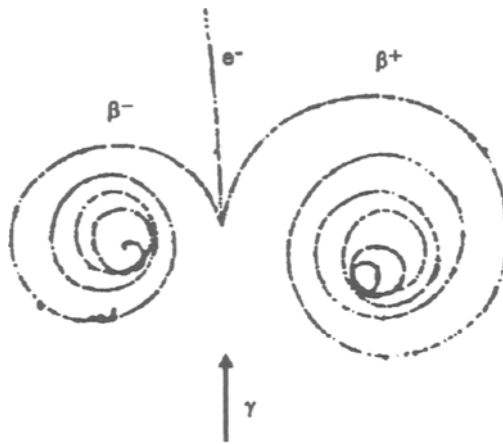


FIG. 6.18. Tracks of electron pair in a  $H_2$  bubble chamber in a strong magnetic field perpendicular to the plane of the tracks. (Courtesy Lawrence Radiation Laboratory.)

## 6.6. Absorption of neutrons

A beam of collimated neutrons is attenuated in a thin absorber through scattering and absorption processes in a similar manner to the attenuation of  $\gamma$ -rays; these processes are described in previous §'s. In a thick absorber the neutrons are slowed from incident energy at the absorber face to thermal energies if the absorber is thick enough. The ultimate fate of the neutron is capture by an absorber atom. Because of the spread in neutron energy and the energy dependency of the capture cross-sections, no simple relation can be given for the attenuation of the neutron beam (cf. next section).

## 6.7. Radiation shielding

The absorption properties of nuclear radiation in material must be known in order to design shielding to avoid unwanted radiation effects on the surroundings by nuclear radiation sources.

For charged particles the shielding is usually slightly thicker than that required for the maximum range of projectiles in the material. Absorption thicknesses of 0.2 mm are adequate to completely absorb the particles from  $\alpha$ -decay. By contrast 15 mm of materials of low  $Z$  such as water, plastic, etc., are required for absorption of  $\beta$ -radiation with energies up to 3 MeV. Radiation shielding constructed from materials of higher atomic number require correspondingly thinner thicknesses. The data in Table 6.2 and the curves in Figs. 6.6 and 6.13 provide information on the thickness of absorber material required for the energy of various types of radiation.

Since  $\gamma$ -rays and neutrons have no definite range but exhibit a logarithmic relation between thickness and intensity, only a partial reduction of the radiation can be obtained. Combining (6.6) and (6.7)

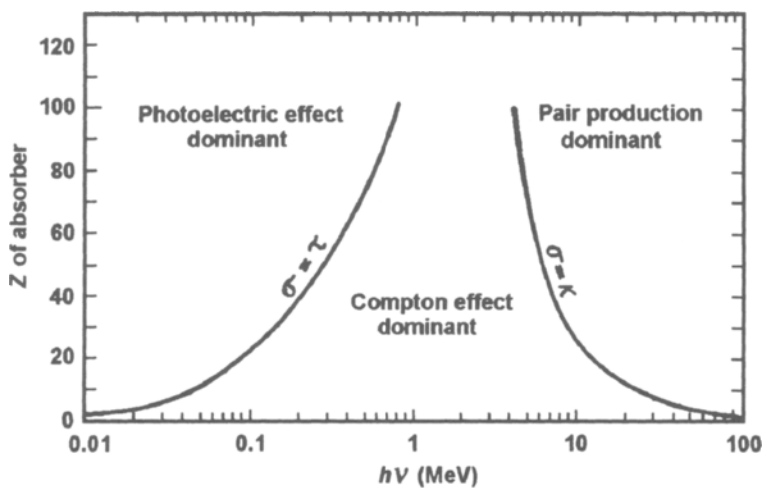


FIG. 6.19. Dominance regions for the three  $\gamma$ -ray absorption processes.

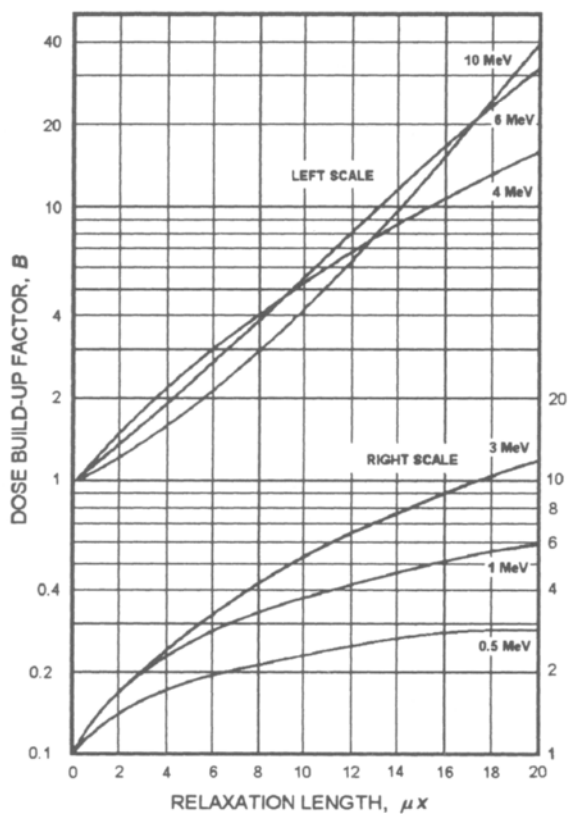


FIG. 6.20. Dose build-up factors in lead for a point isotropic source. Upper curves have scale to the left, lower curves to the right. (From *Radiological Health Handbook*.)

$$\phi = (nA/(4\pi r^2))e^{-\mu x} \quad (6.26)$$

it is seen that the intensity from a point source of radiation can be decreased by increasing either the distance from the source  $r$  or the thickness  $x$  of the absorber. Alternately, an absorber with a higher absorption coefficient,  $\mu$ , can be chosen to reduce the thickness required.

Equation (6.26) is valid only for point sources with ideal geometry, i.e. no back or multiple scattering, etc. For  $\gamma$ -radiation the thicker the absorber the higher is the percentage of radiation which may be scattered backwards through secondary (mainly Compton) scattering. The effect of geometry and absorber thickness can be taken into account by including a constant  $B$  in the absorption equation:

$$\phi = B\phi_0 e^{-\mu x} \quad (6.27)$$

The "*dose build-up*" factor  $B$  not only takes into account multiple Compton and Rayleigh scattering but also includes correction for positron formation at high  $\gamma$ -energies and subsequent annihilation. Since for thick radiation shielding and high  $\gamma$ -energies the factor  $B$  may reach several powers of 10, it is quite important to be considered in designing biological shielding for radiation. Calculation of  $B$  is difficult and empirical data are most commonly used. Figure 6.20 gives  $B$ -values for a lead shield. The thickness of the shielding is given in relaxation lengths  $\mu x$ . This value is obtained from diagrams like Figure 6.17; e.g. for a 3 MeV  $\gamma$ ,  $\mu_m$  is found to be  $0.046 \text{ cm}^2 \text{ g}^{-1}$ . If the absorber is 0.1 m thick the linear density is  $10\rho_{\text{Pb}} = 113 \text{ g cm}^{-2}$  and the relaxation length becomes 5.2. With Figure 6.20 this gives (for the 3 MeV  $\gamma$ -line) a dose build-up factor  $B$  of 3. Thus the lead shield transmits three times more radiation than is expected by the simple relation (6.26). The flux reduction values for concrete and lead shielding in Figure 6.15 have been adjusted to take the dose build-up into consideration.

Equation (6.27) is not directly applicable for neutrons. For an estimate of required shielding we can use diagrams like that in Figure 6.21, which shows the attenuation of neutrons of three different energies in concrete and water, the most common neutron-shielding materials. It is necessary also to take into account the  $\gamma$ -rays emitted in neutron capture, which increases the shielding thickness required.

## 6.8. Analytical applications of radiation absorption

In previous sections of this chapter we have shown how different particles emitted in nuclear reactions are stopped in matter without causing nuclear reactions (nuclear reactions are treated later in this book). If the property of the particle is well defined (e.g. mass, charge, energy, etc) its interaction with the absorbing material can be well predicted, provided the composition of the absorbing material also is well defined. Conversely, the composition of the absorbing material (a "sample") can be determined from studying the absorption process (the "irradiation"). For example, atoms of the absorber (sample) may be knocked out and can be collected for analyses. When electrons are knocked out from the atomic shells of the absorber (sample) atoms, either the energy of these electrons may be analyzed, or the energy of the electromagnetic radiation emitted when the shells are refilled.

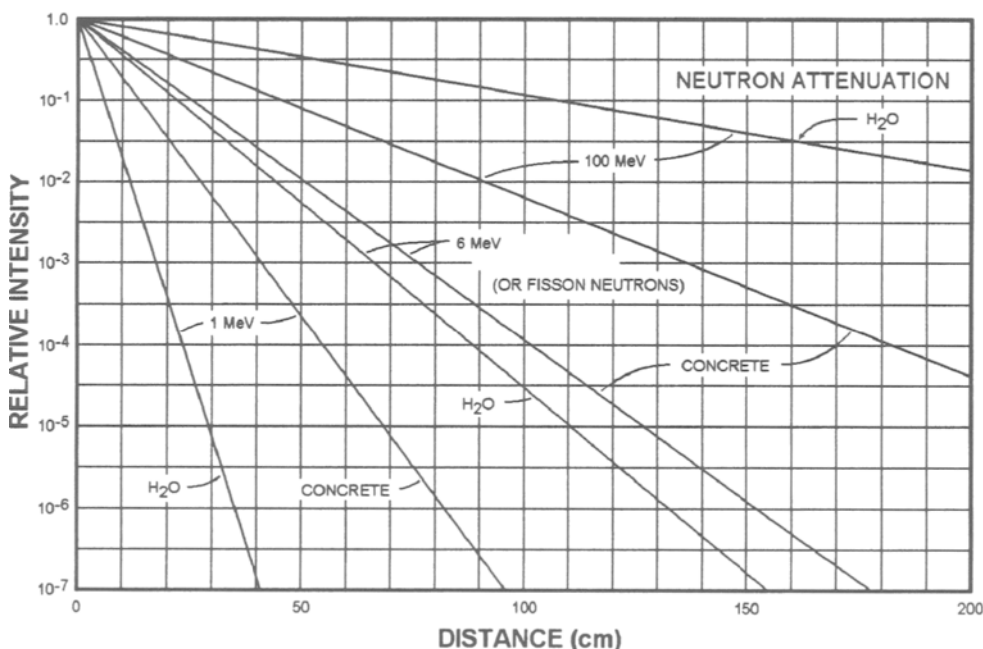


FIG. 6.21. Shielding thickness necessary to reduce a neutron beam in water and concrete. The 6 MeV lines can be used for fission neutrons. (From *Nuclear Data Tables*.)

These energies are characteristic of the sample and can thus be used for its identification. There are many analytical applications based on these principles, the most important ones will be described in this Section.

#### 6.8.1. SIMS (Secondary Ion Mass Spectrometry)

When heavy ions of energy largely exceeding the chemical binding energies, but with energies much lower than needed to cause nuclear reactions, hit a surface then atoms of this surface are *sputtered* out. These atoms, or actually ions, can be introduced in a mass spectrometer to determine the exact masses and mass/charge ratios, from which the element is identified. This is the basis for the SIMS analytical method for studying surfaces, particularly semiconductor surfaces. By bombarding with  $O^{2+}$  or  $Cs^+$  of  $\leq 10$  keV most surface elements can be detected (in fortunate cases down to the ppb range) with a resolution of the order 100 – 200 Å.

#### 6.8.2. PIXE (Proton or Particle Induced X-ray Emission)

In the PIXE technique high energy protons (or heavier ions) are used to irradiate a thin sample (say 0.1 mg/cm<sup>2</sup>). The probability for expulsion of an electron followed by the

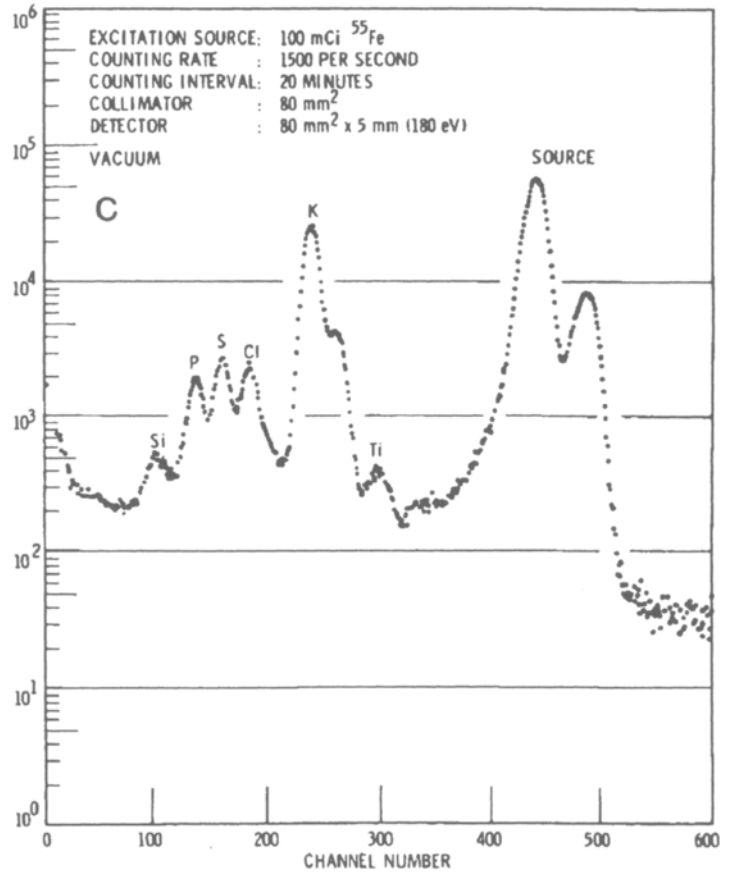
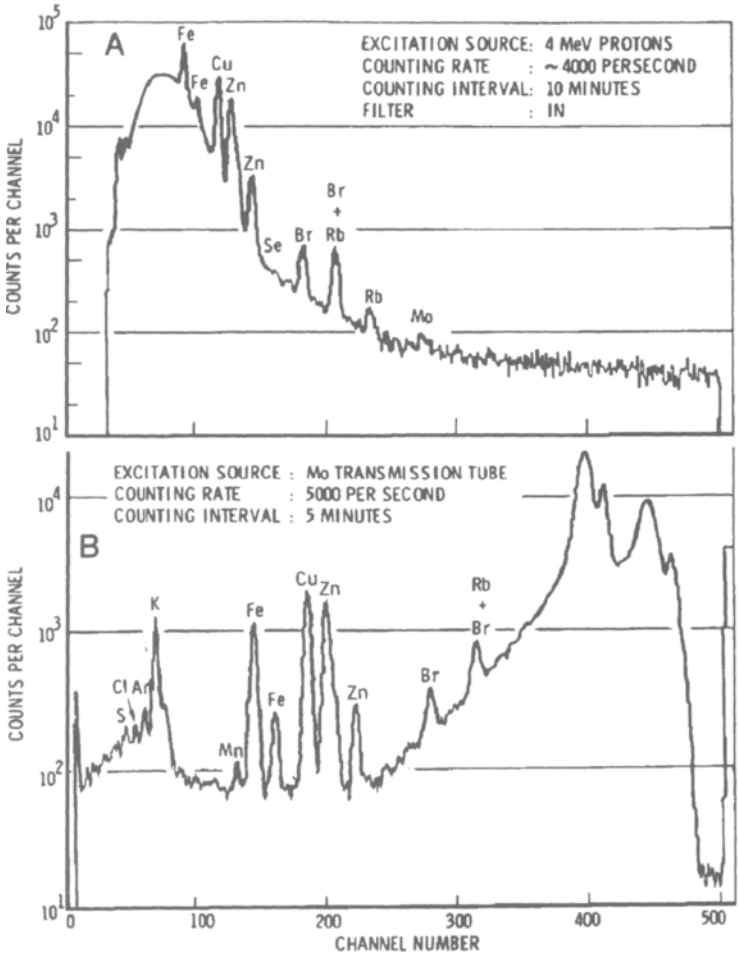


FIG. 6.22. PIXE analysis of trace elements in environmental and biological samples.

emission of a K-x-ray decreases with increasing  $Z$  of the sample; e.g. for 5 MeV protons the reaction cross section is ca.  $10^{-25} \text{ m}^2$  for  $Z = 10$  to 20 and about  $10^{-28} \text{ m}^2$  (1 barn) for  $Z = 50$ ; cf. Table 6.1. It can be shown that the reaction probability has a maximum when the incident particle has a velocity equal to the Bohr orbital velocity of the electron. Though the sensitivity decreases with  $Z$  elements up to Pb can be determined. The technique has primarily been used to determine trace elements in environmental and biological samples, see Figure 6.22(a).

### 6.8.3. ESCA (*Electron spectrometry for chemical analysis*)

High resolution  $\beta$ -spectroscopy can be used to determine chemical properties. A sample is irradiated with mono-energetic photons of  $E_{h\nu}$ , leading to the emission from the sample surface of photoelectrons. The relevant equation is

$$E_{h\nu} = E_{\text{be}}(X, Y) + E_e \quad (6.28)$$

where  $E_e$  is the kinetic energy of the emitted electrons, which can be determined very accurately (presently to about 0.01 eV) in the magnetic spectrograph; *photoelectron spectroscopy*. This sensitivity is much greater than chemical binding energies,  $E_{\text{be}}(X, Y)$ , where  $X$  refers to an atom in compound  $Y$ . The probability for ejection of photoelectrons increases with decreasing photon energy (Fig. 6.16 and 6.19) and therefore low energy X-rays are used as a source.

Although it is the outermost (or most weakly bound) electrons which form the valency orbitals of a compound, this does not leave the inner orbitals unaffected. An outer electron (which we may refer to as  $e_L$ ) of an atom  $X_1$  which takes part in bond formation with another atom  $X_2$  decreases its potential, which makes the inner electrons (which we may call  $e_K$ ) more strongly bound to  $X_1$ . Thus  $E_{\text{be}}(e_K)$  increases by an amount depending on  $E_{\text{be}}(e_L)$ . Although this is a somewhat simplified picture, it leads to the practical consequence that the binding energy of  $e_K$ , which may be in the 100 – 1000 eV range, depends on the chemical bond even if its orbital is not involved directly in the bond formation. Figure 6.23 shows the ESCA spectrum of trifluoroacetate. Since the largest chemical shift, relative to elementary carbon, is obtained for the most electronegative atoms, the peaks refer to the carbon atoms in the same order as shown in the structure.

### 6.8.4. XFS (*X-ray fluorescence analysis*)

If a sample containing atoms of a particular element (e.g. Ag) is irradiated with photons of energy high enough to excite an inner electron orbital (e.g. the  $K_\alpha$  orbital in Ag at 22.1 keV), X-rays are emitted in the de-excitation. If the photon source is an X-ray tube with a target made of some element (Ag in our example), the probability is very high that the  $K_\alpha$  X-ray emitted from the source would be absorbed by the sample atoms and re-emitted (*fluorescence*). (This is an "electron shell resonance absorption" corresponding to the Mössbauer effect, although the width of the X-ray line is so large that recoil effects can be neglected.) The spectrum of the scattered X-radiation (or, more correctly, photon radiation



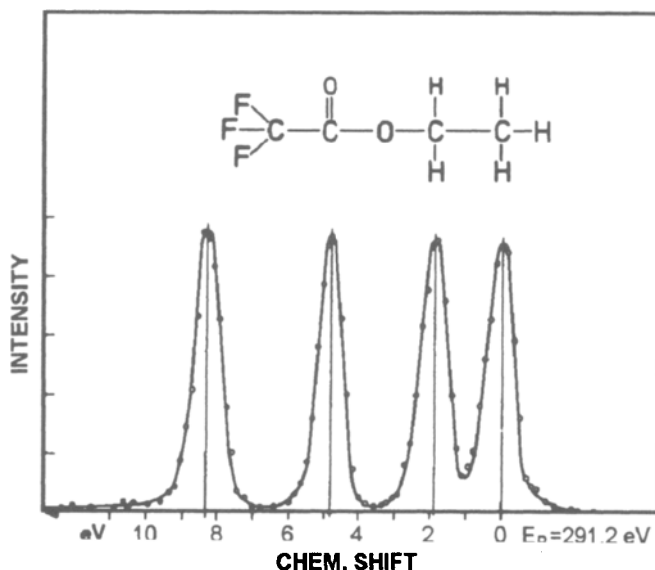


FIG. 6.23. ESCA spectrum of trifluoroacetate.

emitted from the sample) is referred to as the *X-ray fluorescence spectrum*. It contains lower energy radiation including  $K_{\alpha}$  radiation emitted by atoms of lower atomic number. The height of these other peaks is lower because of a lower reaction cross-section (Fig. 6.24). Figure 6.22(B) illustrates an XFS analysis of a biological sample.

X-ray fluorescence analysis using vacuum tube sources have become a well-established analytical technique in the last decade. Nuclear interest stems partly from the possibility of using radioactive sources for stimulating X-ray fluorescence in a sample. These sources can be classified depending on the mode of production of the X-rays:

(i)  $\gamma$ -ray sources: decay between closely located nuclear energy levels, e.g. a 59.5 keV  $\gamma$  emitted in the  $\alpha$ -decay of  $^{241}\text{Am}$ ; also "broad spectrum"  $\gamma$ -sources like  $^{125}\text{I}$  are used.

(ii) x-ray sources: (a) radiation emitted in rearrangement of electron orbitals following  $\alpha$ - or  $\beta$ -decay (primary X-rays), e.g. 11.6-21.7 keV uranium L-X-rays from  $^{238}\text{U}$  formed in the  $\alpha$ -decay of  $^{242}\text{Pu}$ , or 41.3-47.3 keV europium K-X-rays from  $\beta$ -decay of  $^{153}\text{Gd}$ ; (b) irradiation of a target with  $\alpha$ -,  $\beta$ -, or  $\gamma$ -radiation leading to ionization and excitation of the target atoms and its de-excitation by X-ray emission.

(iii) Bremsstrahlung sources, e.g. T in titanium, or  $^{147}\text{Pm}$  in aluminum (Fig. 6.10).

An important advantage of radioactive X-ray fluorescence sources is that very small instruments requiring no (X-ray) high voltage or current can be designed for field applications. Such instruments are used in geological investigations (bore holes, mineral samples, etc.), in-line mineral analysis (Zn, Cu, and other ores in flotation cycles, Ca in cement raw-material, etc.), on-line analysis of surface depositions (Zn on iron sheets, Ag in photographic emulsions, etc.). Figure 6.22 shows fluorescent spectra obtained on bovine liver with three different excitation sources: (A) 4 MeV protons (PIXE), (B) (conventional) molybdenum transmission tube, and (C) radioactive  $^{55}\text{Fe}$ .

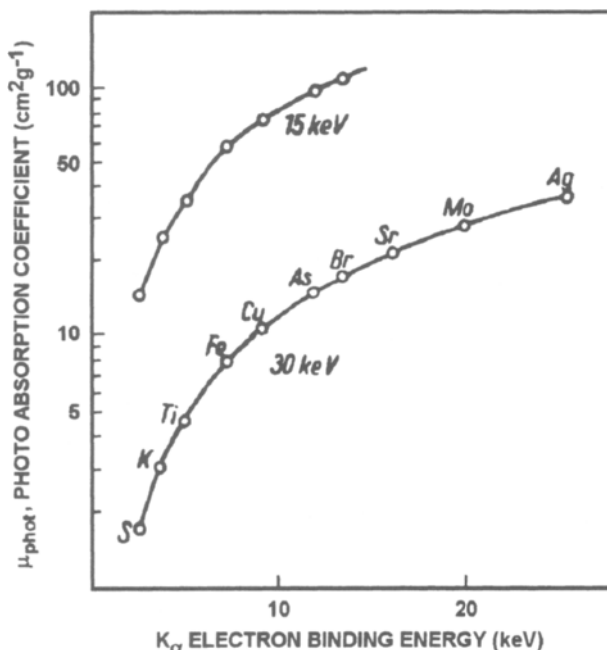


FIG. 6.24. Photoelectron absorption coefficients at  $K_{\alpha}$  edges for 10 and 30 keV  $\gamma$ -rays as function of absorber material. The photo effect is the dominating absorption mode.

### 6.8.5. Mössbauer effect

According to the wave model of the atom, electrons in the innermost orbitals have a finite probability of existence within the nucleus. These electrons interact with the nuclear charge distribution, and thereby affect the nuclear energy levels (cf. §11.3.3). The extent of the effect depends on the exact properties of the electron orbitals involved, which vary with different chemical compounds. Therefore a  $\gamma$ -ray emitted from an isomeric state of an atom bound in one chemical compound may have a slightly different energy than from the same atom bound in another compound. This difference, referred to as the *isomer (energy) shift*, is extremely small, only about  $10^{-10}$  of the energy of the emitted  $\gamma$ . Nevertheless, it can be measured by a technique developed by R. Mössbauer. The fundamental physics involved and technique used is well illustrated by Mössbauer's original experiment. Mössbauer placed an  $^{191}\text{Os}$  source about a half-meter from a  $\gamma$ -ray detector A as shown in Figure 6.25. An iridium foil absorber was placed between the source and detector so that some of the photons of 129 keV energy from the  $^{191}\text{Os}$  were absorbed by the iridium atoms in the foil, exciting these atoms from the ground state ( $3/2+$ ) to the  $5/2+$  state. Because of the short half-life of the latter state it immediately decayed, re-emitting the  $\gamma$ -ray. The emission was isotropic, i.e., occurs in all directions. The result was a reduction in intensity measured by detector A but an increase in the count rate in detector B.

The conditions for such a *nuclear resonance absorption* are very stringent. Using the Heisenberg relationship (4.66) we can estimate the half-value width of the 129 keV peak to be  $5 \times 10^{-6}$  eV. We can also use relation (4.34) to calculate the iridium atom recoil energy to be  $46 \times 10^{-3}$  eV. Thus the  $\gamma$ -ray leaves the source with an energy of  $(129 \times 10^3$

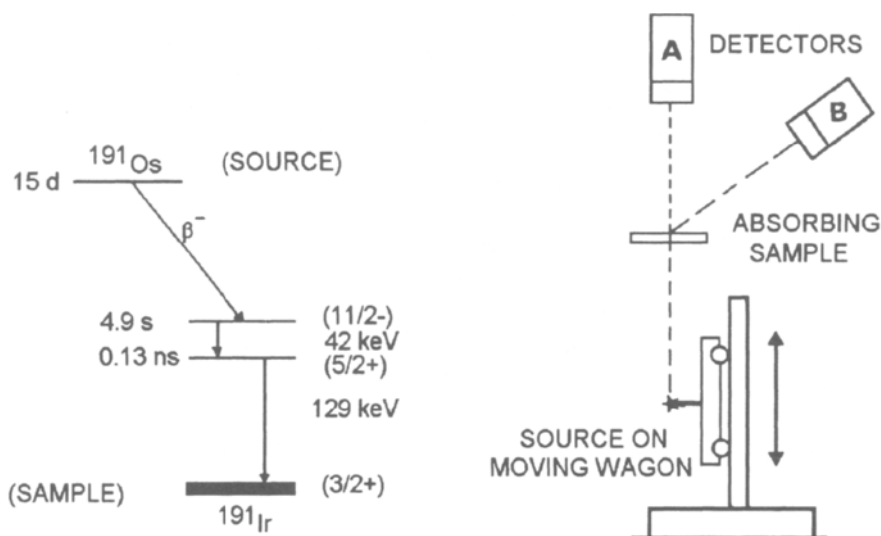


FIG. 6.25. Decay scheme of  $^{191}\text{Os}$  and principle of a Mössbauer experiment.

$-46 \times 10^{-3}$  eV). Also, in order for the 129 keV  $\gamma$ -ray to be absorbed in  $^{191}\text{Ir}$ , it must arrive with an excess energy of  $46 \times 10^{-3}$  eV to provide for the conservation of momentum of the absorbing atom. Thus there is a deficit of  $2 \times 46 \times 10^{-3}$  eV, which is very different from the value of the very narrow energy width of the  $\gamma$ -ray. Consequently, no resonance absorption can take place.

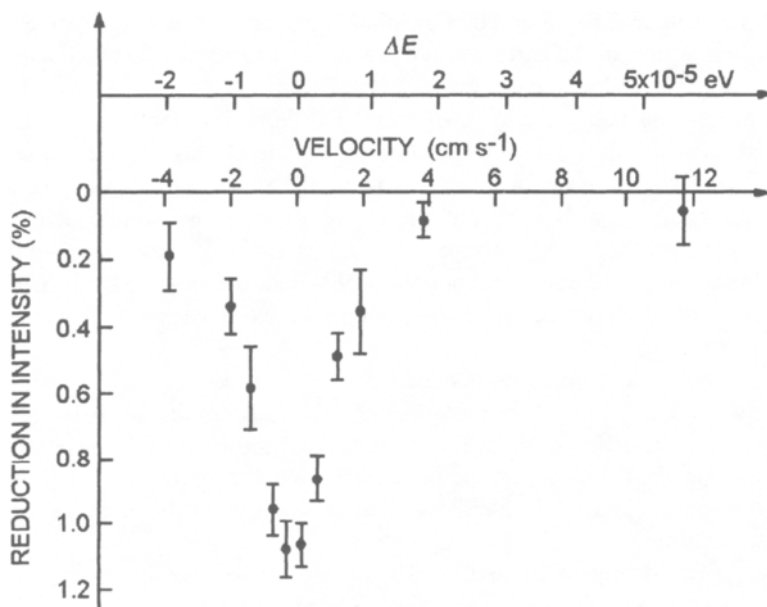


FIG. 6.26. Mössbauer spectrum of  $^{191}\text{Ir}$  metal. (From R. Mössbauer.)

The limitation posed by the recoil phenomenon can be circumvented. If the source and absorber atoms are fixed in a crystal, the recoil energy may be insufficient to cause bond breakage. The energy is absorbed as an atomic vibration in the crystal, provided the quantization of the vibrational states agree exactly with the recoil energy. If not, which is often the case, the absorber atom stays rigid in the lattice, and the recoil energy is taken up by the whole crystal. In this case it is necessary to use the mass of the crystal in (4.34) rather than the mass of a single atom. Under these circumstances the recoil energy becomes infinitesimally small for the emitting as well as the absorbing atom; this is called *recoilless absorption*. The probability for recoilless absorption is improved if the source and absorber are cooled to low temperatures.

The data of Figure 6.26 were obtained by recoilless absorption in osmium metal containing  $^{191}\text{Os}$  (source) and Ir metal, both cooled in cryostats. By slowly moving the source (with velocity  $v$ ) towards or away from the absorber (see Fig. 6.25), some kinetic energy  $\Delta E_\gamma$  is added or subtracted from the source energy  $E_\gamma$  as "detected" by the absorber (Doppler effect). The energy and velocity relationship is given by the Doppler equation

$$\Delta E_\gamma / E_\gamma = v/c \quad (6.29)$$

The velocity is shown in the Figure, where a value of  $v$  of  $1 \text{ cm s}^{-1}$  corresponds to  $4.3 \times 10^{-6} \text{ eV}$ . The half-value of the  $\gamma$ -peak is found to be about  $20 \times 10^{-6} \text{ eV}$ , i.e. a factor 4 times higher than calculated by the Heisenberg relationship. This is due to Doppler broadening of the peak as a consequence of some small atomic vibrations. Although the Mössbauer method can be used for measurements of  $\gamma$ -line widths, the results are subject to considerable errors.

One of the most striking uses of the extreme energy resolution obtainable by the Mössbauer effect was achieved by R. V. Pound and G. A. Rebka, who measured the emission of photons in the direction towards the earth's center, and in the opposite direction from the earth's center. They found that the photon increased its energy by one part in  $10^{16}$  per meter when falling in the earth's gravitational field. This can be taken as a proof that the photon of  $E_{h\nu} > 0$  does have a mass.

When a "Mössbauer pair" (like  $^{191}\text{Os}/\text{Ir}$ , or  $^{57}\text{Co}/\text{Fe}$ ,  $^{119\text{m}}\text{Sn}/\text{Sn}$ ,  $^{169}\text{Er}/\text{Tm}$ , etc.) have source and absorber in different chemical states, the nuclear energy levels differ for the two Mössbauer atoms by some amount  $\Delta E_\gamma$ . By using the same technique as in Figure 6.25, resonance absorption can be brought about by moving the source with a velocity corresponding to  $\Delta E_\gamma$ . In this manner, a characteristic *Mössbauer spectrum* of the compound (relative to a reference compound) is obtained; the location of the peaks (i.e. the absorption maxima) with respect to a non-moving source (the *isomer shift*) is usually given in  $\text{mm s}^{-1}$ .

Figure 6.27 shows the isomer shifts obtained for a number of actinide compounds. The positions of the isomer shifts show the effect of valence states due to different population of the  $5f$  orbitals. The different shifts for compounds of the same valence state is a measure of the variation in the covalency of the bonding. The compounds on the left are metallic. The shifts reflects the contributions of conduction electrons to the electron density at the nucleus of neptunium.

Mössbauer spectroscopy is limited to the availability of suitable sources. About 70 Mössbauer pairs are now available. The technique provides a useful method for studying

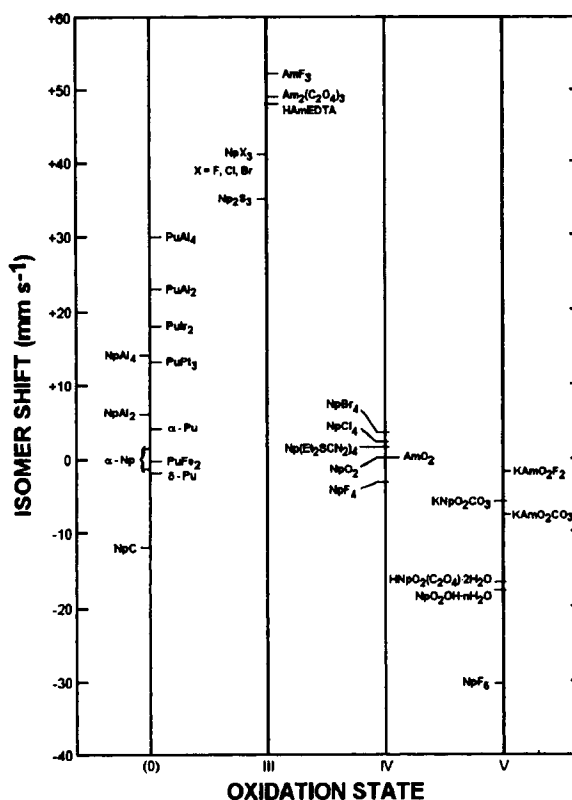


FIG. 6.27. Isomer shifts for some actinide metals and actinide compounds.

chemical compounds in the solid state, especially compounds which are nontransparent to light and chemically or radioactively unstable.

### 6.9. Technical applications of radiation sources

Nuclear radiation absorption methods have many technical applications. These methods are not to be confused with radioisotope tracer methods, although radioisotopes may be used as radiation sources. In the tracer method the chemical properties of the radionuclide are important while in the applications discussed in this section only the type and energy of radiation emitted are important.

As a *source* of radiation in such technical applications, either accelerators or radiation from radionuclides can be used. Interchangeable radionuclides have the advantage over accelerators as radiation sources in that they can cover a larger energy range from high energy  $\gamma$ -rays to low energy  $\beta$ -rays in a much simpler way. This makes it possible to select the type and energy of radiation which have the most advantageous properties for a particular use. An additional advantage of radionuclides is that the sources can usually be made much smaller than X-ray sources, enabling them to be used in places where larger equipment is inconvenient or impossible to place. The fact that radionuclides require neither

electric power nor cooling also renders them more suitable for field applications. Further, their independence from effects of temperature, pressure, and many other factors results in higher reliability compared to X-ray generators. Finally, and, perhaps as important as any of the other factors, they are in general much less expensive than accelerators.

To counterbalance these advantages is the disadvantage of the inability to turn off the radiation from radionuclides. This often requires that the radiation source be well shielded, adding to its weight and cost. An additional drawback to the use of radionuclides is that they have to be replaced after a few half-lives. The seriousness of this disadvantage depends upon the lifetime of the particular nuclide and is unimportant in cases where longlived sources can be used.

The extensive use of radionuclides in industry is illustrated by Table 6.3, which summarizes the various studies undertaken by I.C.I., UK, in "a typical year".

### 6.9.1. Radionuclide gauges

*Radionuclide gauges* are a measurement system consisting of two parts, a radioactive source and a detector, fixed in some geometry to each other. They are used mainly for control in industrial processes but can also be applied for specific analyses. The gauges come in two types. In one type the radiation source and the detector are on opposite sides of the technical arrangement to be measured; these are known as transmission or absorption instruments. In the second type, known as reflection or back-scattering instruments, the radiation source and the detector are on the same side. The instruments are also classified with respect to the kind of radiation involved. For example,  $\gamma$ -transmission,  $\beta$ -reflection, secondary X-ray instruments, etc. These radioisotope gauges are used for measurements of thicknesses, densities, etc.

TABLE 6.3. Radioisotope based studies undertaken annually by a large chemical company

Technique <sup>(a)</sup>	Number of applications
Level and interface measurements:	
$\gamma$ -ray absorption	210
Neutron backscatter	480
$\gamma$ -ray backscatter (storage cavities)	71
Blockage detection and deposition:	
$\gamma$ -ray absorption	132
Neutron backscatter	129
Entrainment and voidage:	
$\gamma$ -ray absorption	86
Thickness and corrosion measurements	15
Distillation column scans	108
Flow measurements:	
Pulse velocity	483
Dilution techniques	84
Leak detection	90
Residence-time studies	21
Carry-over studies (tracer)	6

<sup>(a)</sup> Less commonly used techniques have not been included.

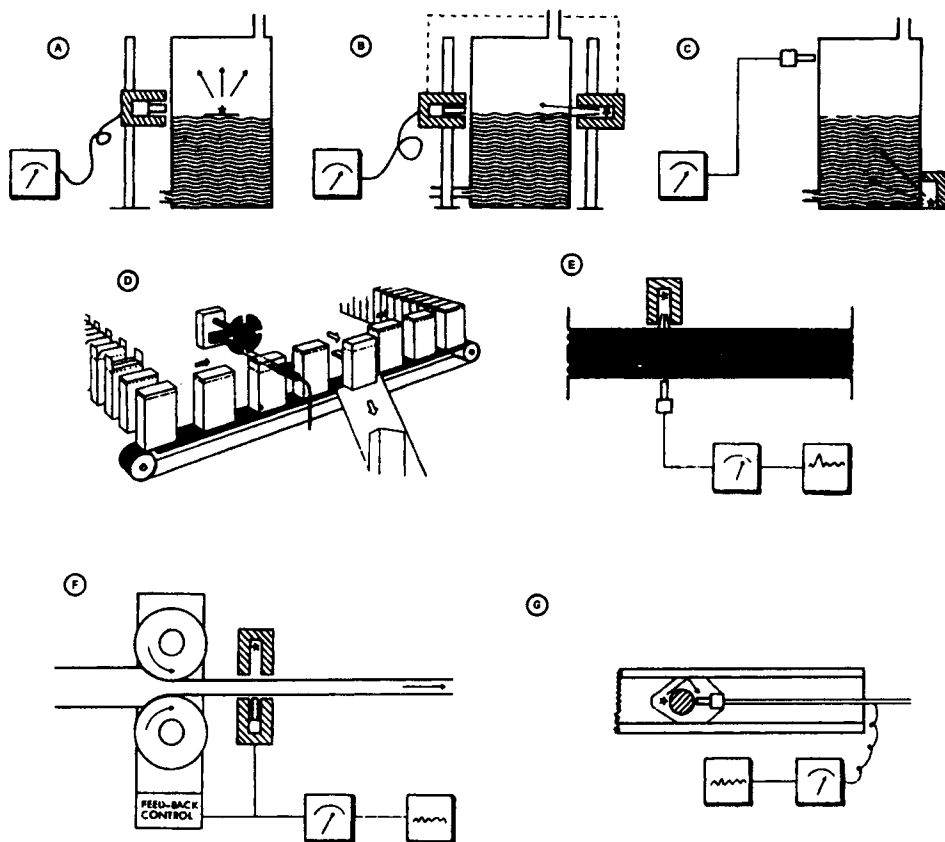


FIG. 6.28. Radionuclide gauges for: A-C level measurements in tanks, D control of package filling, E flow density measurements, F thickness control, and G wall material in pipes and bore holes.

In Figure 6.28 a number of types of application for transmission instruments are illustrated. Illustrations A – C show measurements of level control. Type A can be used only for liquids while B and C can be used for all kinds of material. The latter instruments are uniquely suitable for application to large storage containers for grain, wood chips, oil, sand, cement, etc., and for material under extreme conditions such as molten glass and metal, explosives, etc. Level gauges are also used in the control of the filling of packages, cans, etc. in industry as illustrated in D.

Let us consider a somewhat unusual application of this type of instrument. In the manufacture of titanium it is important to keep liquid  $\text{TiCl}_4$  at a particular high temperature and pressure in a vessel.  $\text{TiCl}_4$  has a triple point (i.e. the pressure and temperature conditions at which all three phases - solid, liquid, and vapor - of a substance are at equilibrium) in the neighborhood of the particular technical conditions. By using a  $\gamma$ -density gauge it is possible to detect when the triple point is exceeded because of the disappearance of the vapor-liquid interface. This allows a simple method of control of the process conditions in the vessel.

The use of radioisotope gauges in density measurements is dependent upon (6.26) in which  $r$  and  $x$  are constant while the absorption coefficient is density dependent (i.e. dependent on the average atomic composition of the absorber). A practical arrangement is illustrated in Figure 6.28, E, where the density of a medium in a pipeline is measured. This medium may be a mixture of gas and liquid such as water and water liquids with different composition and different amounts of dissolved substances as, for example, oil, salts or acids in water, process solutions in general or sludges, and emulsions such as fruit juices, latex emulsions, etc. From the variation in density the concentration and composition may be determined. Such density gauges are also used for control in filling of soft drink bottles and cans and submerged in rivers and lakes for measuring the depth of the bottom silt, etc. Density gauges are used in the production and the fabrication of such diverse products as automobile tires and cigarette packages.

Thickness gauges are the most common type of instrument using the absorption technique. In this case  $x$  in (6.26) is varied. Measurements can be carried out on all kinds of materials with thicknesses of  $\leq 100 \text{ g cm}^{-2}$  and is independent of the temperature and of whether the material is stationary or in motion. Figure 6.29, F, illustrates the application of a thickness gauge in a rolling mill where material of constant thickness is produced by using the signal from the detector for control purposes. Thickness gauges are used in the fabrication of glass, metal, paper, plastic, rubber, candy bars, etc. They have been used for measuring the thickness of snow in polar regions, icing on airplane wings, and other applications in which it is necessary to use remote operation.

In order to measure very thin layers of material such as coatings of paint, wax, and plastic films on papers or other material, two thickness gauges are used with a differential coupling so that one detector measures the uncovered and the other the covered or treated portion of the material. Thickness gauges also are used in industry to measure the degree of wear in industrial machinery. For surface measurements of thicknesses  $\leq 0.8 \text{ g cm}^{-2}$  most thickness gauges use radiation sources with  $\beta$ -emitters while for thicknesses of  $0.8\text{--}5 \text{ g cm}^{-2}$  bremsstrahlung radiation sources are most suitable. For even thicker materials  $\gamma$ -emitters are used.

Use of reflection gauges depends on the fact that the intensity of the scattered radiation under conditions of constant geometry depends on the thickness of the scattering material and its electron density (if  $\beta$ - or  $\gamma$ -sources are used). If neutrons are used the mass number of the scattering material is of prime importance. The electron density of the scattering material varies with the particular element and the chemical composition. Frequently, it is possible to determine the thickness and the nature of a surface layer by means of  $\beta$ -scattering. Reflection gauges have been applied to on-line analysis of tin-covered iron plates, metal coatings on plastics, paint layers, and to measuring the protective coating inside pipelines (Fig. 6.29, G). In some instances  $\gamma$ -radiation sources are preferred over  $\beta$ -emitters in measurements of material with greater wall thicknesses, particularly when transmission measurements are not feasible. Steel thickness from 1 to 20 cm has been measured with 5% accuracy using backscattering from  $^{60}\text{Co}$  or  $^{137}\text{Cs}$  sources of  $20 \mu\text{Ci}$  intensity.

Scattering and reflection are dependent on the electron density of the absorber, which is approximately proportional to the value of  $Z/A$ . Backscattering of  $\beta$ -particles from organic compounds is therefore very dependent on the hydrogen concentration ( $Z/A = 1$ ) but fairly independent of the concentration of C, N, and O ( $Z/A = 0.5$ ). This has led to the development of sensitive instruments for hydrogen analysis for various organic and



water-containing materials. In an instrument using 10 mCi  $^{90}\text{Sr}$ , the hydrogen concentration in a 10 ml sample can be determined in 20 min with 0.03% accuracy. This is not only superior to other conventional analytical methods, it also has the advantage of being a nondestructive technique.

Neutrons are slowed down most effectively by light elements (§12.6). As a consequence, neutron scattering can be used for the analyses of light elements, particularly hydrogen. In one type of instrument the radiation source consists of  $^{252}\text{Cf}$  which produces fast neutrons (from spontaneous fission), while the detector is sensitive only to slow neutrons. This system is used for studies of ground water and analysis of bore holes in wells (Fig. 6.29, G). These analyses are usually combined with density determinations using a  $\gamma$ -source, thereby making it possible to identify strata of water, oil, coal, etc.

Some properties and uses of commercial radionuclide gauges are listed in Table 6.4.

### 6.9.2. Radiography

Radiography is a photographic technique in which nuclear radiation is used instead of light. Medical examination and nondestructive industrial testing using X-rays generated by high-vacuum tubes are the most important areas. A number of suitable sources of radioactive nuclides for producing radiograms are given in Table 6.4.

Beta-radiography is only suitable for thin objects and not widely applied. On the other hand,  $\gamma$ -radiography is a common nondestructive test technique in which normally  $^{137}\text{Cs}$  or  $^{60}\text{Co}$  has been used.  $\gamma$ -radiography has advantages in field use and in detection of sensitive objects. The radiation source can be  $^{60}\text{Co}$ , which is normally kept in a portable radiation shielding of 30–60 kg of lead and situated at the end of a rod so that it can be pushed out of the shielding for use. The photographic film is located in a cassette surrounded by amplifying screens.

TABLE 6.4. Some commercially available radionuclide gauges and  $\gamma$ -sources for radiography (France)

Radiation	Source	$t_{1/2}$	Application
$\alpha$	U or Ra	Long	Thickness control in manufacturing paper, aluminum; $\leq 60 \text{ g/m}^2$
Soft $\beta$	$^{147}\text{Pm}$ (0.2 MeV)	2.6 y	Thickness control; $\leq 400 \text{ g/m}^2$
$\beta$ , soft $\gamma$	$^{204}\text{Tl}$ (0.8 MeV)	3.8 y	Thickness: 1.10 mm steel, 3-50 mm glass; 8-100 $\text{kg/m}^2$
Hard $\beta$	$^{144}\text{Ce}$ (3 MeV)	0.78 y	Thickness $\leq 1 \text{ mm steel}$ ; $\leq 10 \text{ kg/m}^2$
X	$^{109}\text{Cd}$ (88 keV)	1.24 y	Detection of S-content in hydrocarbons
n, $\gamma$	RaBe, $^{137}\text{Cs}$	30 y	Moisture-density meter for civil engineering and agriculture
$\gamma$	$^{60}\text{Co}$ (1.3 MeV)	5.3 y	4 MBq source for backscatter on $\leq 20 \text{ mm steel}$ , 0.4 - 40 GBq for remote level indication
Soft $\gamma$	$^{192}\text{Ir}$ (0.3 MeV)	74 d	400 GBq, 26 kg: $\leq 40 \text{ mm steel radiography}$
Medium $\gamma$	$^{137}\text{Cs}$ (0.7 MeV)	30 y	400 GBq, 45 kg: $\leq 70 \text{ mm steel pipeline inspection}$
Hard $\gamma$	$^{60}\text{Co}$ (1.3 MeV)	5.3 y	10 TBq, 900 kg: $\leq 180 \text{ mm steel radiography}$

The exposure  $At$  (GBq hours) required for an optical density ( $\hat{D} = \log$  (incident light/transmitted light))  $\sim 2$  at an absorber (object) thickness  $x$  (cm) using a typical industrial X-ray film and a  $^{60}\text{Co}$   $\gamma$ -ray source positioned at a distance of 1 m from the film can be estimated by the expressions

$$\begin{aligned} \log(At) &= 1.068 + 0.135x && \text{for an iron absorber} \\ \log(At) &= 1.068 + 0.040x && \text{for a concrete absorber} \end{aligned}$$

Exercise 6.14 is an example of the use of these expressions.

Gamma-radiography has been used for determining the number of reinforced iron bars in concrete construction, cavities in various kinds of castings (as explosives, plastics or metals), cracks or other defects in turbine blades in airplane parts, detonators in unexploded bombs, welded joints in pressure vessels, distillation towers and pipes, corrosion inside pipes and furnaces, and medical field X-rays, to mention only a few applications. Gamma-radiography is used throughout the world for product control leading to improved working safety and economy.

Because  $\gamma$ -absorption occurs through interaction with the electrons, objects of high atomic numbers show the strongest absorption. By using neutrons instead of  $\gamma$ -rays, the opposite effect is achieved, i.e. low  $Z$  objects are most effective in removing neutrons from a beam. This is used in *neutron radiography* in which both reactor neutrons and neutrons from  $^{252}\text{Cf}$  sources are applied. Because of the higher neutron flux from the reactor than from  $^{252}\text{Cf}$  sources of normal size (i.e.  $\leq 1$  mg) the exposure time at the reactor is much shorter. On the other hand, the small size of the  $^{252}\text{Cf}$  source offers other conveniences.

### 6.9.3. Radionuclide power generators

The absorption of radiation leads to an increase in the temperature of the absorber. An example of this is the absorption of the kinetic energy of fission products in nuclear reactor fuel elements which is a main source of the heat production in reactors. The absorption of decay energy of radioactive nuclides in appropriate absorbing material can be used in a similar - albeit more modest - way as an energy source.

Figure 6.29 shows the principles of two different radioisotope power generators, the larger (to the left) is of SNAP-7 type and produces  $\sim 60$  W, the smaller one produces  $\sim 10$  mW. The radiation source for the larger generator consists of 15 rods (A) clad with hastelloy and containing approximately 7 kg of  $\text{SrTiO}_3$  which has approximately 225 000 Ci of  $^{90}\text{Sr}$ . This heat source is surrounded by 120 pairs of lead telluride thermoelements (B) and a radiation shield of 8 cm of depleted uranium (C). The whole arrangement is surrounded by a steel cover with cooling fins. The weight of this generator is 2.3 t with dimensions of 0.85 m in length and 0.55 m in diameter. It is estimated that the lifetime of such an energy source is at least 5 y, although the half-life of  $^{90}\text{Sr}$  (30 y) promises a longer period. Radionuclide generators in unmanned lighthouses, navigation buoys, automatic weather stations, etc., in sizes up to about 100 W, have been in use in a number of countries, e.g. Japan, Sweden, the UK, the USA, etc. Since no moving parts are involved, these generators need a minimum of service. Their reliability makes them valuable in remote areas like the Arctic regions where several such generators have been installed.

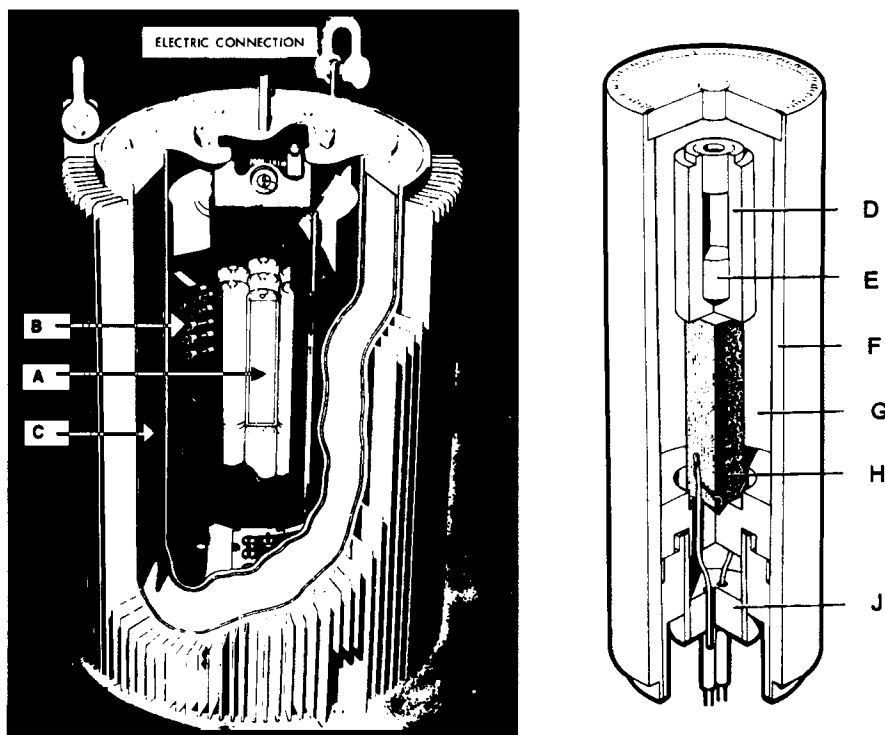


FIG. 6.29. A -  $^{90}\text{SrTiO}_3$ ; B - thermocouples; C - radiation shield (depleted U); D - capsule; E -  $^{238}\text{Pu}$ ; F - secondary containment; G - thermal insulation; H - thermopile; J - insulator.

$^{90}\text{Sr}$  is the preferred radionuclide for terrestrial uses. Its power density is relatively high,  $0.93 \text{ W g}^{-1}$ , as compared to some other possible radionuclides as  $^{137}\text{Cs}$  ( $0.26 \text{ W g}^{-1}$ ) and  $^{238}\text{Pu}$  ( $0.55 \text{ W g}^{-1}$ ), but it is lower than  $^{244}\text{Cm}$  ( $2.8 \text{ W g}^{-1}$ ) and  $^{245}\text{Cm}$  ( $121 \text{ W g}^{-1}$ ). Recently  $^{60}\text{Co}$  has come into use; the heating mainly comes from absorption of the  $\gamma$ 's in a uranium shielding.

$^{238}\text{Pu}$  has been used as an energy source in space. Several satellites with radioisotope generators of 25 W have been placed in space, and the Apollo project employed a generator "SNAP-27" containing  $^{238}\text{Pu}$  with a total weight of 14 kg and producing 50 W power. The Viking landers on the planet Mars used  $^{238}\text{Pu}$  as the main energy source. It was used also to power the Pioneer vehicles which gave us the first close pictures of the planet Jupiter and in the Voyager missions to the outer planets (in August 1989 one of them passed Neptunus at  $\sim 5000 \text{ km}$  altitude, taking remarkable close-up pictures) where the  $^{238}\text{Pu}$  power source produced 450 W. One will reach the star Sirius in about 300 000 years!

## 6.10. Exercises

6.1. In §6.3 two equations are given for calculating the range of  $\alpha$ -particles in air and in other material from the particle energy as well as a curve for the range in aluminum. How different are the values from the equations and from the curve for a 5 MeV  $\alpha$ ?

6.2. What is the minimum energy that an  $\alpha$ -particle must have to be detected by a GM tube having a mica (the density is approximately equal to aluminum) window of  $1.5 \text{ mg cm}^{-2}$ ?

6.3. For an irradiation experiment it is necessary to extract a beam of deuterons from an accelerator. The projectile energy is  $22 \text{ MeV D}^+$ . For this purpose the beam is deflected and permitted to pass through a thin titanium foil (density  $4.5 \text{ g cm}^{-3}$ ). Assuming that  $R_1 \rho_1 M_1^{-1/2} = R_2 \rho_2 M_2^{-1/2}$  (Bragg-Kleiman rule), what is the maximum thickness of the foil? Give the answer in millimeters.

6.4. Make a rough estimate of the range in air for a  $1 \text{ MeV } \alpha$ ,  $1 \text{ MeV H}^+$  and  $1 \text{ MeV e}^-$  using the plot in Fig.

6.7. The energy to form an ion pair in air is  $14.6 \text{ eV}$  but assume that twice as much energy is lost through excitation.

6.5. What is the range of a  $6.3 \text{ MeV } \alpha$ -particle in (a) aluminum, (b) nickel, (c) platinum?

6.6. What is the  $\gamma$ -ray flux from a  $3.7 \text{ GBq } ^{60}\text{Co}$  source at a distance of  $3 \text{ m}$ ? Assume  $\psi_{\text{sample}} = 1$ .

6.7. What is the maximum range in millimeters of  $\beta$ -particles from T,  $^{14}\text{C}$ ,  $^{32}\text{P}$  and  $^{90}\text{Sr}$  in a photographic emulsion if its absorption efficiency is assumed to be the same as aluminum? The density of the emulsion is assumed to be  $1.5 \text{ g cm}^{-3}$ .

6.8. The  $E_{\text{max}}$  of  $^{32}\text{P}$   $\beta$ -particles is  $1.71 \text{ MeV}$ . To what electron velocity does this correspond?

6.9. In a laboratory an irradiation area must be designed for  $\gamma$ -radiography using a  $3.7 \times 10^{11} \text{ Bq } ^{60}\text{Co}$  source. For this purpose a cubic building is erected with an interior side length of  $2 \text{ m}$ . The desired flux reduction is  $10^6$ . How thick must the wall be and how much will the shielding material cost (i.e. not including labor costs) if it is made of (a) concrete? (b) lead? Assume lead blocks cost  $\$1.50$  per kg and concrete  $\$40$  per  $\text{m}^3$ .

6.10. An experiment is done with  $^{60}\text{Co}$  which emits  $0.05860 \text{ MeV } \gamma$ . The detector used is a NaI crystal. What photo peaks will be observed if the electron binding energies in sodium are K  $1072$  and L  $63 \text{ eV}$ , and in iodine K  $33170$  and L  $4800 \text{ eV}$ ?

6.11. A human body may be considered as consisting of water. Radiation from  $^{137}\text{Cs}$  is absorbed by a  $15 \text{ cm}$  thick body. How much is the  $\gamma$ -ray flux reduced by the body, and how much of the beam energy ( $\beta$  plus  $\gamma$ ) is absorbed?

6.12. For iron the mass attenuation coefficients are: at  $0.5 \text{ MeV } \gamma$ ,  $0.083$ ; at  $1.0 \text{ MeV}$ ,  $0.059$ ; at  $1.5 \text{ MeV}$ ,  $0.047 \text{ cm}^2 \text{ g}^{-1}$ . Calculate the corresponding one-tenth values.

6.13. An absorption curve of a sample emitting  $\beta$ - and  $\gamma$ -rays was taken with aluminum absorber using a gas-flow proportional counter. The data obtained were:

Absorber thickness ( $\text{g cm}^{-2}$ )	Activity (counts $\text{min}^{-1}$ )	Absorber thickness ( $\text{g cm}^{-2}$ )	Activity (counts $\text{min}^{-1}$ )
0	5800	0.700	101
0.070	3500	0.800	100
0.130	2200	1.00	98
0.200	1300	2.00	92
0.300	600	4.00	80
0.400	280	7.00	65
0.500	120	10.00	53
0.600	103	14.00	40

(a) Estimate the maximum energy of the  $\beta$ -spectrum. (b) Find the energy of the  $\gamma$ -ray.

6.14. A 40-story high modern business building is supported by  $0.9 \text{ m}$  thick pillars of reinforced concrete. The insurance company must check that the number of iron bars are as many as required, and therefore they want to investigate the pillars by  $\gamma$ -radiography. What exposure times are required for (a) a small  $200 \text{ GBq } ^{60}\text{Co}$  source, (b) for a large  $150 \text{ TBq}$  source? Use the same film data as in 6.9.2.

6.15. A swimming-pool reactor produces a flux of  $3 \times 10^{16}$  thermal neutrons  $\text{m}^{-2} \text{ s}^{-1}$  at  $1 \text{ m}$  from the reactor center. Assuming a parallel beam of neutrons diffusing up to the surface of the pool where the neutron flux is measured to be  $10^8 \text{ n m}^{-2} \text{ s}^{-1}$ , calculate the thickness ( $x \text{ m}$ ) of the water layer required. For thermal neutrons the flux is reduced exponentially with the exponent  $xL^{-1}$ , where  $L$  is the diffusion length ( $2.75 \text{ cm}$  in  $\text{H}_2\text{O}$ ).

6.16. In a sample of  $10.4 \text{ TBq}$  of old fission products, the average  $\gamma$ -ray energy is  $0.5 \text{ MeV}$  and on the average  $0.4 \gamma$ 's are emitted per  $\beta$ -decay. (a) What is the lead shielding required to reduce the  $\gamma$  flux to  $10^2 \gamma \text{ cm}^{-2} \text{ s}^{-1}$

at 1.5 m from the source assuming only exponential absorption? (b) What is the relaxation length? (c) What is the build-up factor?

### 6.11. Literature

- B. T. PRICE, C. C. HORTON, and K. T. SPINNEY, *Radiation Shielding*, Pergamon Press, Oxford, 1957.
- S. FLÜGGE (ed.), *Handbuch der Physik*, Band 34, 1958, and 38/2, 1959, Springer-Verlag.
- R. L. MÖSSBAUER, Recoilless nuclear resonance absorption, *Ann. Rev. Nucl. Sci.* **12** (1962) 1.
- J. C. ROCKLEY, *An Introduction to Industrial Radiology*, Butterworths, London, 1964.
- C. S. FADLEY, S. B. M. HAGSTRÖM, J. M. HOLLANDER, M. P. KLEIN, and D. A. SHIRLEY, Chemical bonding information from photoelectron spectroscopy, *Science* **157** (1967) 1571.
- D. A. SHIRLEY, Chemical tools from nuclear physics, *Science* **161** (1968) 745.
- IAEA, *Nuclear Well Logging in Hydrology*, Tech. Report 126, Vienna, 1971.
- IAEA, *Commercial Portable Gauges for Radiometric Determination of the Density and Moisture Content of Building Materials*, Tech. Report 130, Vienna, 1971.
- G. M. BANCROFT, *Mössbauer Spectroscopy*, J. Wiley, 1973.
- J. A. COOPER, Comparison of particle and photon excited X-ray fluorescence applied to trace element measurements on environmental samples, *Nucl. Instr. Methods* **106** (1973) 525.
- H. W. THUMMEL, Stand und Entwicklungstendenzen auf dem Gebiet der Isotopen und Strahlenanalytik. Physikalische Analysenverfahren mit Radionukliden, *Isotopenpraxis* **11** (1975) 1, 41, 87, 117, 172.
- C. H. WANG, D. H. WILLIS, and W. D. LOVELAND, *Radiotracer Methodology in the Biological, Environmental and Physical Sciences*, Prentice Hall, 1975.
- W. D. EHMANN, and D. E. VANCE, *Radiochemistry and Nuclear Methods of Analysis*, Wiley Interscience, 1991.
- G. FURLAN, P. CASSOLA GUIDA, and C. TUNIZ (Ed.), *New Paths in the Use of Nuclear Techniques for Art and Archeology*, World Scientific Pub., Singapore, 1986.
- M. J. RYCROFT (ed.), *The Cambridge Encyclopedia of Space*, Cambridge University Press, 1990

# Chapter 4

---

## General Properties of Radiation Detectors

**B**efore discussing the different types of radiation detectors individually, we first outline some general properties that apply to all types. Included will be some basic definitions of detector properties, such as efficiency and energy resolution, together with some general modes of operation and methods of recording data that will be helpful in categorizing detector applications.

### I. SIMPLIFIED DETECTOR MODEL

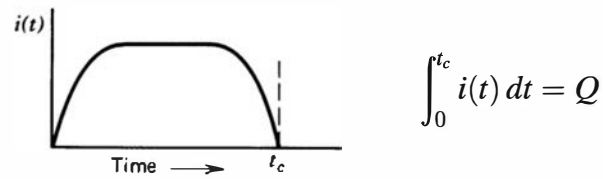
We begin with a hypothetical detector that is subject to some type of irradiation. Attention is first focused on the interaction of a *single* particle or quantum of radiation in the detector, which might, for example, be a single alpha particle or an individual gamma-ray photon. In order for the detector to respond at all, the radiation must undergo interaction through one of the mechanisms discussed in Chapter 2. As indicated by Eq. (2.3), the interaction or stopping time is very small (typically a few nanoseconds in gases or a few picoseconds in solids). In most practical situations, these times are so short that the deposition of the radiation energy can be considered instantaneous.

The net result of the radiation interaction in a wide category of detectors is the appearance of a given amount of electric charge within the detector active volume.<sup>†</sup> Our simplified detector model thus assumes that a charge  $Q$  appears within the detector at time  $t = 0$  resulting from the interaction of a single particle or quantum of radiation. Next, this charge must be collected to form the basic electrical signal. Typically, collection of the charge is accomplished through the imposition of an electric field within the detector, which causes the positive and negative charges created by the radiation to flow in opposite directions. The time required to fully collect the charge varies greatly from one detector to another. For example, in ion chambers the collection time can be as long as a few milliseconds, whereas in semiconductor diode detectors the time is a few nanoseconds. These times reflect both the mobility of the charge carriers within the detector active volume and the average distance that must be traveled before arrival at the collection electrodes.

We therefore begin with a model of a prototypical detector whose response to a single particle or quantum of radiation will be a current that flows for a time equal to the charge collection time. The sketch below illustrates one example for the time dependence the detector current might assume, where  $t_c$  represents the charge collection time.

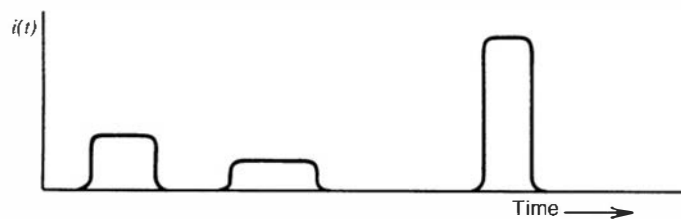
---

<sup>†</sup>Strictly true only for detectors such as ion chambers, proportional tubes, G-M tubes, or semiconductor diode detectors. The discussion is also useful for detector types in which the charge is formed indirectly, as from a photomultiplier tube used with a scintillation crystal.



The time integral over the duration of the current must simply be equal to  $Q$ , the total amount of charge generated in that specific interaction.

In any real situation, many quanta of radiation will interact over a period of time. If the irradiation rate is high, situations can arise in which current is flowing in the detector from more than one interaction at a given time. For purposes of the present discussion, we assume that the rate is low enough so that each individual interaction gives rise to a current that is distinguishable from all others. The magnitude and duration of each current pulse may vary depending on the type of interaction, and a sketch of the instantaneous current flowing in the detector might then appear as shown in the sketch below.



It is important to recall that, because the arrival of radiation quanta is a random phenomenon governed by Poisson statistics, the time intervals between successive current pulses are also randomly distributed.

## II. MODES OF DETECTOR OPERATION

We can now introduce a fundamental distinction between three general modes of operation of radiation detectors. The three modes are called *pulse mode*, *current mode*, and *mean square voltage mode* (abbreviated MSV mode, or sometimes called *Campbell mode*). Pulse mode is easily the most commonly applied of these, but current mode also finds many applications. MSV mode is limited to some specialized applications that make use of its unique characteristics. Although the three modes are operationally distinct, they are interrelated through their common dependence on the sequence of current pulses that are the output of our simplified detector model.

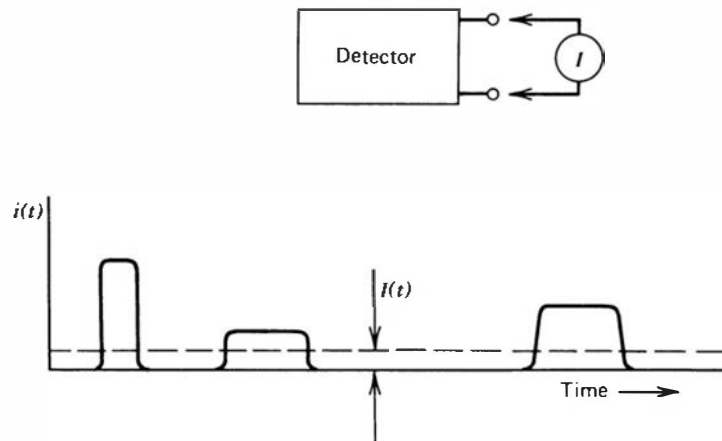
In pulse mode operation, the measurement instrumentation is designed to record each individual quantum of radiation that interacts in the detector. In most common applications, the time integral of each burst of current, or the total charge  $Q$ , is recorded since the energy deposited in the detector is directly related to  $Q$ . All detectors used to measure the energy of individual radiation quanta must be operated in pulse mode. Such applications are categorized as *radiation spectroscopy* and are the subject of much of the remainder of this text.

In other circumstances, a simpler approach may suit the needs of the measurement: All pulses above a low-level threshold are registered from the detector, regardless of the value of  $Q$ . This approach is often called *pulse counting*, and we will show various examples later in this text. It can be useful in many applications in which only the intensity of the radiation is of interest, rather than the incident energy distribution of the radiation.

At very high event rates, pulse mode operation becomes impractical or even impossible. The time between adjacent events may become too short to carry out an adequate analysis, or the current pulses from successive events may overlap in time. In such cases, one can revert to alternative measurement techniques that respond to the time average taken over many individual events. This approach leads to the remaining two modes of operation: current mode and MSV mode.

### A. Current Mode

In the sketch below, we show a current-measuring device (an ammeter or, more practically, a picoammeter) connected across the output terminals of a radiation detector.



If we assume that the measuring device has a fixed response time  $T$ , then the recorded signal from a sequence of events will be a time-dependent current given by

$$I(t) = \frac{1}{T} \int_{t-T}^t i(t') dt' \quad (4.1)$$

Because the response time  $T$  is typically long compared with the average time between individual current pulses from the detector, the effect is to average out many of the fluctuations in the intervals between individual radiation interactions and to record an average current that depends on the product of the interaction rate and the average charge per interaction. In current mode, this time average of the individual current bursts serves as the basic signal that is recorded.

At any instant of time, however, there is a statistical uncertainty in this signal due to the random fluctuations in the arrival time of the event. In many ways, the integration time  $T$  is analogous to the measurement time discussed in the statistical analysis of Chapter 3. Thus, the choice of large  $T$  will minimize statistical fluctuations in the signal but will also slow the response to rapid changes in the rate or nature of the radiation interactions.

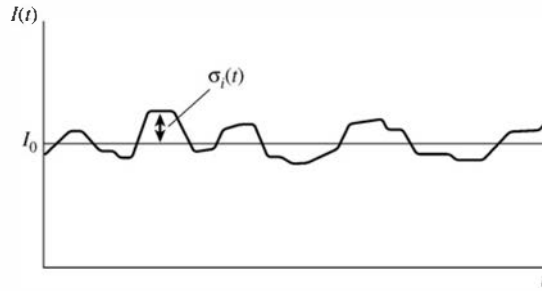
The *average* current is given by the product of the event rate and the average charge produced per event.

$$I_0 = rQ = r \frac{E}{W} q \quad (4.2)$$



where  $r$  = event rate  
 $Q = Eq/W$  = charge produced for each event  
 $E$  = average energy deposited per event  
 $W$  = average energy required to produce a unit charge pair (e.g., electron-ion pair)  
 $q = 1.6 \times 10^{-19}\text{C}$

For steady-state irradiation of the detector, this average current can also be rewritten as the sum of a constant current  $I_0$  plus a time-dependent fluctuating component  $\sigma_i(t)$ , as sketched below.



Here  $\sigma_i(t)$  is a random time-dependent variable that occurs as a consequence of the random nature of the radiation events interacting within the detector.

A statistical measure of this random component is the variance or mean square value, defined as the time average of the square of the difference between the fluctuating current  $I(t)$  and the average current  $I_0$ . This mean square value is given by

$$\overline{\sigma_I^2(t)} = \frac{1}{T} \int_{t-T}^t [I(t') - I_0]^2 dt' = \frac{1}{T} \int_{t-T}^t \sigma_i^2(t') dt' \tag{4.3}$$

and the standard deviation follows as

$$\overline{\sigma_I(t)} = \sqrt{\overline{\sigma_I^2(t)}} \tag{4.4}$$

Recall from Poisson statistics that the standard deviation in the number of recorded events  $n$  over a given observation period is expected to be

$$\sigma_n = \sqrt{n} \tag{4.5}$$

Therefore, the standard deviation in the number of events occurring at a rate  $r$  in an effective measurement time  $T$  is simply

$$\sigma_n = \sqrt{rT} \tag{4.6}$$

If each pulse contributes the same charge, the *fractional* standard deviation in the measured signal due to random fluctuations in pulse arrival time is given by

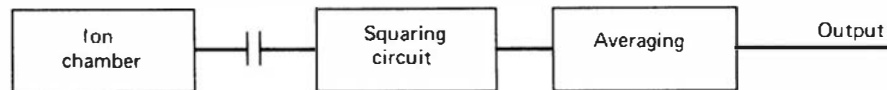
$$\frac{\overline{\sigma_I(t)}}{I_0} = \frac{\sigma_n}{n} = \frac{1}{\sqrt{rT}} \tag{4.7}$$

Here  $\overline{\sigma_I(t)}$  is the time average of the standard deviation in the measured current,  $T$  is the response time of the picoammeter and  $I_0$  is the average current read on the meter. This result is useful in estimating the uncertainty associated with a given current mode measurement.

It should be noted that, in the derivation of Eq. (4.7), the charge produced in each event ( $Q$ ) is assumed to be constant. Therefore, the result accounts for only the random fluctuations in pulse arrival time, but not for fluctuations in pulse amplitude. In some applications, however, this second source of variance in the signal is small in comparison with the first, and the general character of the results given remains applicable.<sup>1</sup>

## B. Mean Square Voltage Mode

An extension of this discussion of the statistical properties of the signal in current mode leads us to the next general mode of operation: the mean square voltage (MSV) mode. Suppose that we send the current signal through a circuit element that blocks the average current  $I_0$  and only passes the fluctuating component  $\sigma_i(t)$ . By providing additional signal-processing elements, we now compute the time average of the squared amplitude of  $\sigma_i(t)$ . (The details of these circuits are not important here; for further discussion see Ref. 2.) The processing steps are illustrated below:



The result corresponds to the quantity  $\overline{\sigma_I^2(t)}$  defined previously in Eq. (4.3). Combining Eqs. (4.2) and (4.7), we predict the magnitude of the signal derived in this way to be

$$\overline{\sigma_I^2(t)} = \frac{rQ^2}{T} \quad (4.8)$$

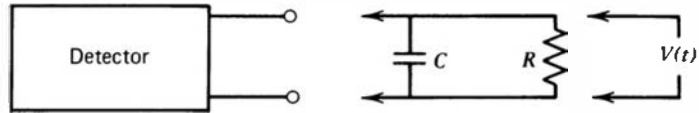
We see that this mean square signal is directly proportional to the event rate  $r$  and, more significantly, proportional to the *square of the charge  $Q$  produced in each event*. An analysis of this mode of operation was first given by Campbell,<sup>3</sup> and the term *Campbelling mode* is therefore substituted for *MSV mode* in some usage.

The MSV mode of operation is most useful when making measurements in mixed radiation environments when the charge produced by one type of radiation is much different than that from the second type. If simple current mode operation is chosen, the measured current will linearly reflect the charges contributed by each type. In MSV mode, however, the derived signal is proportional to the *square* of the charge per event. This operational mode will therefore further weight the detector response in favor of the type of radiation giving the larger average charge per event. As one example of the useful application of the MSV mode, in Chapter 14 we describe its use with neutron detectors in reactor instrumentation to enhance the neutron signal compared with the response due to smaller-amplitude gamma-ray events.

## C. Pulse Mode

In reviewing various applications of radiation detectors, we find that current mode operation is used with many detectors when event rates are very high. Detectors that are applied to radiation dosimetry are also normally operated in current mode for reasons that will be discussed in Chapter 5. MSV mode is useful in enhancing the relative response to large-amplitude events and finds widespread application in reactor instrumentation. Most applications, however, are better served by preserving information on the amplitude and timing of individual events that only pulse mode can provide. Consequently, the remainder of this chapter deals with various aspects of pulse mode operation.

The nature of the signal pulse produced from a single event depends on the input characteristics of the circuit to which the detector is connected (usually a preamplifier). The equivalent circuit can often be represented as shown below.



Here  $R$  represents the input resistance of the circuit, and  $C$  represents the equivalent capacitance of both the detector itself and the measuring circuit. For example, if a preamplifier is attached to the detector, then  $R$  is its input resistance and  $C$  is the summed capacitance of the detector, the cable used to connect the detector to the preamplifier, and the input capacitance of the preamplifier itself. In most cases, the time-dependent voltage  $V(t)$  across the load resistance is the fundamental signal voltage on which pulse mode operation is based. Two separate extremes of operation can be identified that depend on the relative value of the time constant of the measuring circuit. From simple circuit analysis, this time constant is given by the product of  $R$  and  $C$ , or  $\tau = RC$ .

**CASE 1. SMALL RC** ( $\tau \ll t_c$ )

In this extreme the time constant of the external circuit is kept small compared with the charge collection time, so that the current flowing through the load resistance  $R$  is essentially equal to the instantaneous value of the current flowing in the detector. The signal voltage  $V(t)$  produced under these conditions has a shape nearly identical to the time dependence of the current produced within the detector as illustrated in Fig. 4.1b. Radiation detectors are sometimes operated under these conditions when high event rates or timing information is more important than accurate energy information.

**CASE 2. LARGE RC** ( $\tau \gg t_c$ )

It is generally more common to operate detectors in the opposite extreme in which the time constant of the external circuit is much larger than the detector charge collection time. In this

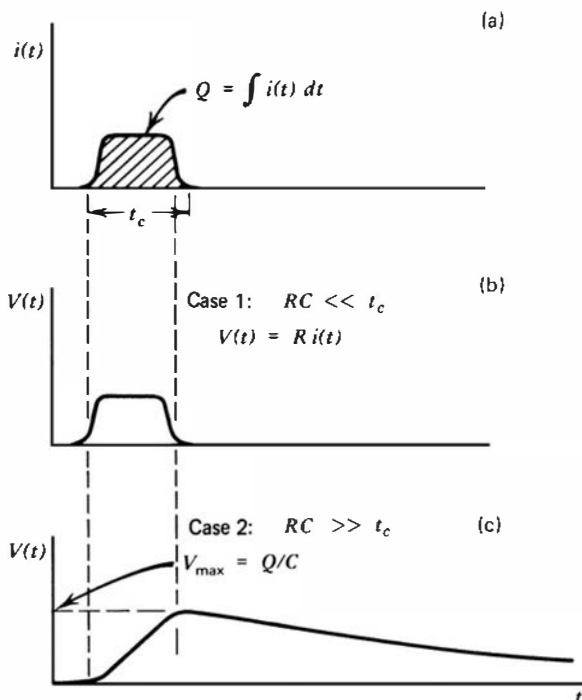


**Figure 4.1** (a) The assumed current output from a hypothetical detector. (b) The signal voltage  $V(t)$  for the case of a small time constant load circuit. (c) The signal voltage  $V(t)$  for the case of a large time constant load circuit.

case, very little current will flow in the load resistance during the charge collection time and the detector current is momentarily integrated on the capacitance. If we assume that the time between pulses is sufficiently large, the capacitance will then discharge through the resistance, returning the voltage across the load resistance to zero. The corresponding signal voltage  $V(t)$  is illustrated in Fig. 4.1c.

Because the latter case is by far the most common means of pulse-type operation of detectors, it is important to draw some general conclusions. First, the time required for the signal pulse to reach its maximum value is determined by the charge collection time within the detector itself. No properties of the external or load circuit influence the rise time of the pulses. On the other hand, the decay time of the pulses, or the time required to restore the signal voltage to zero, is determined only by the time constant of the load circuit. The conclusion that the leading edge is detector dependent and the trailing edge circuit dependent is a generality that will hold for a wide variety of radiation detectors operated under the conditions in which  $RC \gg t_c$ . Second, the amplitude of a signal pulse shown as  $V_{\max}$  in Fig. 4.1c is determined simply by the ratio of the total charge  $Q$  created within the detector during one radiation interaction divided by the capacitance  $C$  of the equivalent load circuit. Because this capacitance is normally fixed, *the amplitude of the signal pulse is directly proportional to the corresponding charge generated within the detector* and is given by the simple expression

$$V_{\max} = Q/C \quad (4.9)$$

Thus, the output of a detector operated in pulse mode normally consists of a sequence of individual signal pulses, each representing the results of the interaction of a single quantum of radiation within the detector. A measurement of the rate at which such pulses occur will give the corresponding rate of radiation interactions within the detector. Furthermore, the amplitude of each individual pulse reflects the amount of charge generated due to each individual interaction. We shall see that a very common analytical method is to record the distribution of these amplitudes from which some information can often be inferred about the incident radiation. An example is that set of conditions in which the charge  $Q$  is directly proportional to the energy of the incident quantum of radiation. Then, a recorded distribution of pulse amplitudes will reflect the corresponding distribution in energy of the incident radiation.

As shown by Eq. (4.9), the proportionality between  $V_{\max}$  and  $Q$  holds only if the capacitance  $C$  remains constant. In most detectors, the inherent capacitance is set by its size and shape, and the assumption of constancy is fully warranted. In other types (notably the semiconductor diode detector), the capacitance may change with variations in normal operating parameters. In such cases, voltage pulses of different amplitude may result from events with the same  $Q$ . In order to preserve the basic information carried by the magnitude of  $Q$ , a type of preamplifier circuit known as a *charge-sensitive* configuration has come into widespread use. As described in Chapter 17, this type of circuit uses feedback to largely eliminate the dependence of the output amplitude on the value of  $C$  and restores proportionality to the charge  $Q$  even in cases in which  $C$  may change. For this preamplifier configuration, the simple  $RC$  representation shown in the sketch at the start of this section is no longer accurate, but the principle of collecting the current pulse across a capacitance that is discharged through a resistance remains valid.

Pulse mode operation is the more common choice for most radiation detector applications because of several inherent advantages over current mode. First, the sensitivity that is achievable is often many factors greater than when using current or MSV mode because each individual quantum of radiation can be detected as a distinct pulse. Lower limits of detectability are then normally set by background radiation levels. In current mode, the minimum detectable current may represent an average interaction rate in the detector that is many times greater. The second and more important advantage is that each pulse amplitude carries some information that is often a useful or even necessary part of a particular application.

In both current and MSV mode operations, this information on individual pulse amplitudes is lost and all interactions, regardless of amplitude, contribute to the average measured current. Because of these inherent advantages of pulse mode, the emphasis in nuclear instrumentation is largely in pulse circuits and pulse-processing techniques.

### III. PULSE HEIGHT SPECTRA

When operating a radiation detector in pulse mode, each individual pulse amplitude carries important information regarding the charge generated by that particular radiation interaction in the detector. If we examine a large number of such pulses, their amplitudes will not all be the same. Variations may be due either to differences in the radiation energy or to fluctuations in the inherent response of the detector to monoenergetic radiation. The pulse amplitude distribution is a fundamental property of the detector output that is routinely used to deduce information about the incident radiation or the operation of the detector itself.

The most common way of displaying pulse amplitude information is through the *differential pulse height distribution*. Figure 4.2a gives a hypothetical distribution for purposes of example. The abscissa is a linear pulse amplitude scale that runs from zero to a value larger than the amplitude of any pulse observed from the source. The ordinate is the differential number  $dN$  of pulses observed with an amplitude within the differential amplitude increment  $dH$ , divided by that increment, or  $dN/dH$ . The horizontal scale then has units of pulse

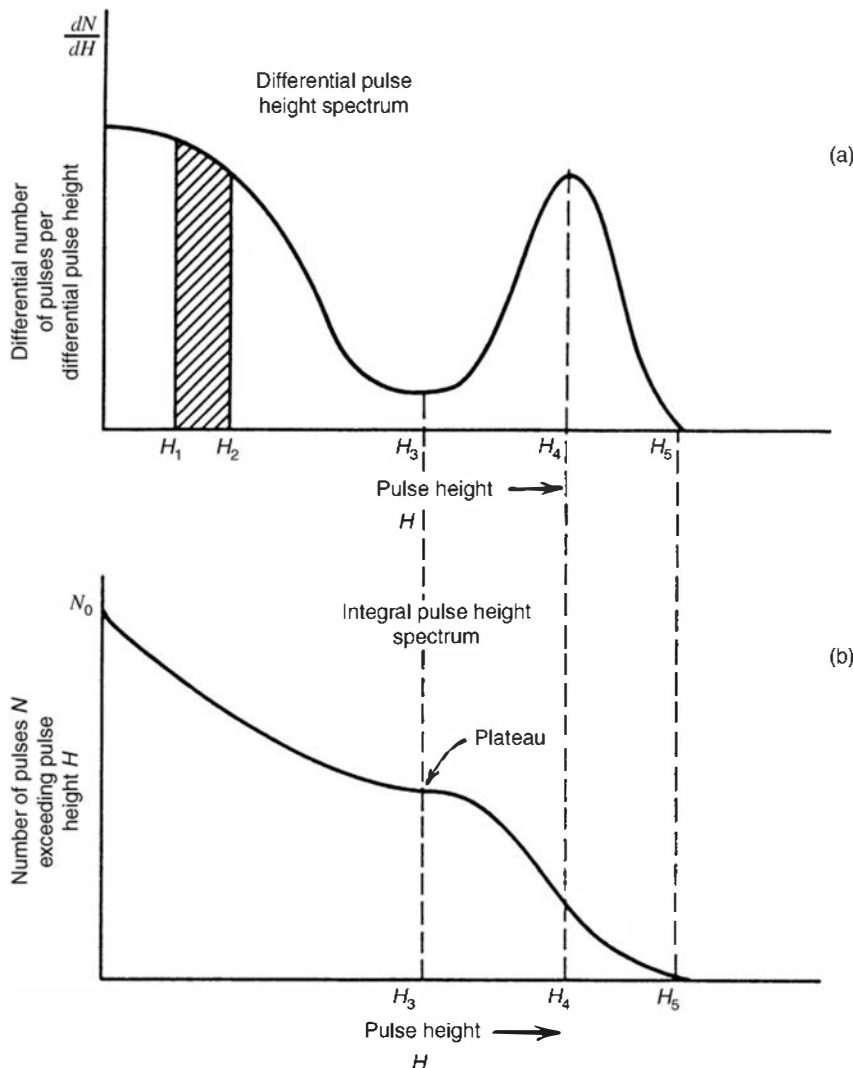


**Figure 4.2** Examples of differential and integral pulse height spectra for an assumed source of pulses.

amplitude (volts), whereas the vertical scale has units of inverse amplitude (volts<sup>-1</sup>). The number of pulses whose amplitude lies between two specific values,  $H_1$  and  $H_2$ , can be obtained by integrating the area under the distribution between those two limits, as shown by the cross-hatched area in Fig. 4.2a:

$$\text{number of pulses with amplitude between } H_1 \text{ and } H_2 = \int_{H_1}^{H_2} \frac{dN}{dH} dH \quad (4.10)$$

The total number of pulses  $N_0$  represented by the distribution can be obtained by integrating the area under the entire spectrum:

$$N_0 = \int_0^{\infty} \frac{dN}{dH} dH \quad (4.11)$$

Most users of radiation instrumentation are accustomed to looking at the shape of the differential pulse height distribution to display significant features about the source of the pulses. The maximum pulse height observed ( $H_5$ ) is simply the point along the abscissa at which the distribution goes to zero. Peaks in the distribution, such as at  $H_4$ , indicate pulse amplitudes about which a large number of pulses may be found. On the other hand, valleys or low points in the spectrum, such as at pulse height  $H_3$ , indicate values of the pulse amplitude around which relatively few pulses occur. The physical interpretation of differential pulse height spectra always involves *areas* under the spectrum between two given limits of pulse height. The value of the ordinate itself ( $dN/dH$ ) has no physical significance until multiplied by an increment of the abscissa  $H$ .

A less common way of displaying the same information about the distribution of pulse amplitudes is through the *integral pulse height distribution*. Figure 4.2b shows the integral distribution for the same pulse source displayed as a differential spectrum in Fig. 4.2a. The abscissa in the integral case is the same pulse height scale shown for the differential distribution. The ordinate now represents the number of pulses whose amplitude exceeds that of a given value of the abscissa  $H$ . The ordinate  $N$  must always be a monotonically decreasing function of  $H$  because fewer and fewer pulses will lie above an amplitude  $H$  that is allowed to increase from zero. Because all pulses have some finite amplitude, the value of the integral spectrum at  $H = 0$  must be the total number of pulses observed ( $N_0$ ). The value of the integral distribution must decrease to zero at the maximum observed pulse height ( $H_5$ ).

The differential and integral distributions convey exactly the same information and one can be derived from the other. The amplitude of the differential distribution at any pulse height  $H$  is given by the absolute value of the slope of the integral distribution at the same value. Where peaks appear in the differential distribution, such as  $H_4$ , local maxima will occur in the magnitude of the slope of the integral distribution. On the other hand, where minima appear in the differential spectrum, such as  $H_3$ , regions of minimum magnitude of the slope are observed in the integral distribution. Because it is easier to display subtle differences by using the differential distribution, it has become the predominant means of displaying pulse height distribution information.

## IV. COUNTING CURVES AND PLATEAUS

When radiation detectors are operated in pulse counting mode, a common situation often arises in which the pulses from the detector are fed to a counting device with a fixed discrimination level. Signal pulses must exceed a given level  $H_d$  in order to be registered by the counting circuit. Sometimes it is possible to vary the level  $H_d$  during the course of the measurement to provide information about the amplitude distribution of the pulses. Assuming that  $H_d$  can be varied between 0 and  $H_5$  in Fig. 4.2, a series of measurements can be carried out in which the

number of pulses  $N$  per unit time is measured as  $H_d$  is changed through a sequence of values between 0 and  $H_5$ . This series of measurements is just an experimental determination of the integral pulse height distribution, and the measured counts should lie directly on the curve shown in Fig. 4.2b.

In setting up a pulse counting measurement, it is often desirable to establish an operating point that will provide maximum stability over long periods of time. For example, small drifts in the value of  $H_d$  could be expected in any real application, and one would like to establish conditions under which these drifts would have minimal influence on the measured counts. One such stable operating point can be achieved at a discrimination point set at the level  $H_3$  in Fig. 4.2. Because the slope of the integral distribution is a minimum at that point, small changes in the discrimination level will have minimum impact on the total number of pulses recorded. In general, regions of minimum slope on the integral distribution are called *counting plateaus* and represent areas of operation in which minimum sensitivity to drifts in discrimination level are achieved. It should be noted that plateaus in the integral spectrum correspond to valleys in the differential distribution.

Plateaus in counting data can also be observed with a different procedure. For a particular radiation detector it is often possible to vary the gain or amplification provided for the charge produced in radiation interactions. This variation could be accomplished by varying the amplification factor of a linear amplifier between the detector and counting circuit, or in many cases more directly by changing the applied voltage to the detector itself. Figure 4.3 shows the differential pulse height distribution corresponding to three different values of voltage gain applied to the same source of pulses. Here the value of gain can be defined as the ratio of the voltage amplitude for a given event in the detector to the same amplitude before some parameter (such as amplification or detector voltage) was changed. The highest voltage gain will result in the largest maximum pulse height, but in all cases the area under the differential

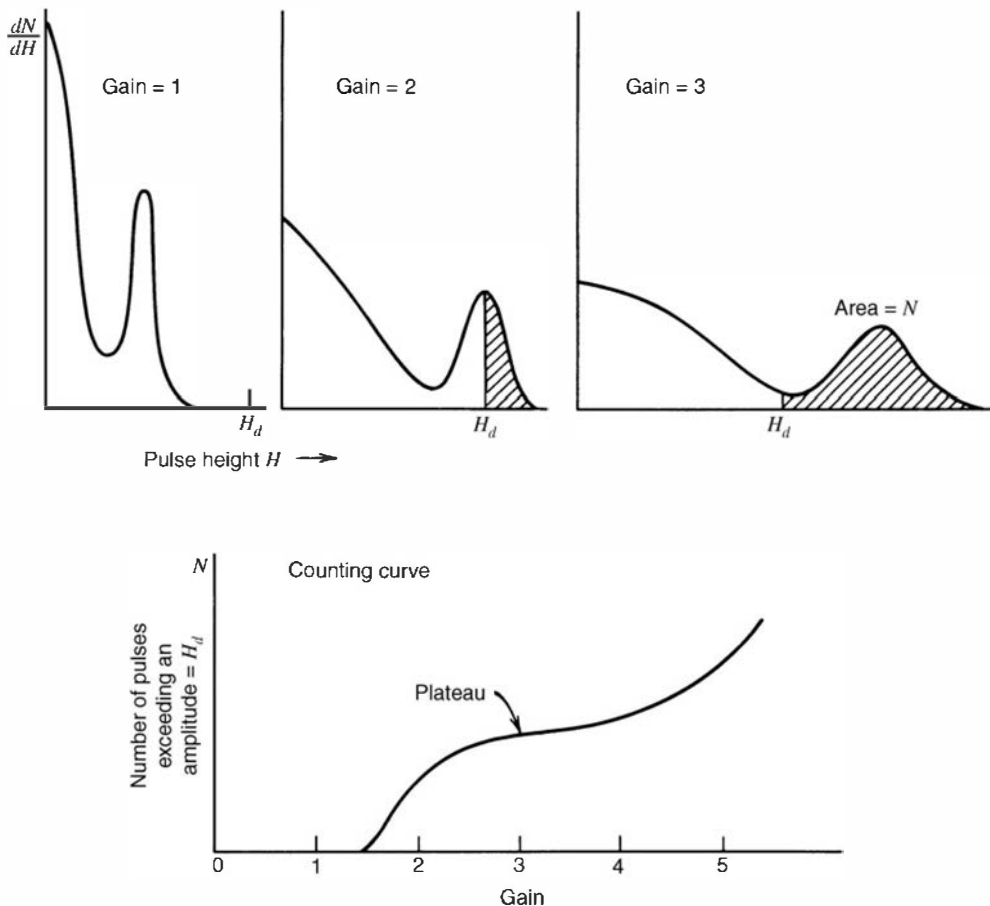


**Figure 4.3** Example of a counting curve generated by varying gain under constant source conditions. The three plots at the top give the corresponding differential pulse height spectra.

distribution will be a constant. In the example shown in Fig. 4.3, no counts will be recorded for a gain  $G = 1$  because under those conditions all pulses will be smaller than  $H_d$ . Pulses will begin to be recorded somewhere between a gain  $G = 1$  and  $G = 2$ . An experiment can be carried out in which the number of pulses recorded is measured as a function of the gain applied, sometimes called the *counting curve*. Such a plot is also shown in Fig. 4.3 and in many ways resembles an integral pulse height distribution. We now have a mirror image of the integral distribution, however, because small values of the gain will record no pulses, whereas large values will result in counting nearly all the pulses. Again, plateaus can be anticipated in this counting curve for values of the gain in which the effective discrimination pulse height  $H_d$  passes through minima in the differential pulse height distribution. In the example shown in Fig. 4.3, the minimum slope in the counting curve should correspond to a gain of about 3, in which case the discrimination point is near the minimum of the valley in the differential pulse height distribution.

In some types of radiation detectors, such as Geiger–Mueller tubes or scintillation counters, the gain can conveniently be varied by changing the applied voltage to the detector. Although the gain may not change linearly with voltage, the qualitative features of the counting curve can be traced by a simple measurement of the detector counting rate as a function of voltage. In order to select an operating point of maximum stability, plateaus are again sought in the counting curve that results, and the voltage is often selected to lie at a point of minimum slope on this counting curve. We shall discuss these plateau measurements more specifically in Chapters 6 and 7 in connection with proportional counters and Geiger–Mueller detectors.

## V. ENERGY RESOLUTION

In many applications of radiation detectors, the object is to measure the energy distribution of the incident radiation. These efforts are classified under the general term *radiation spectroscopy*, and later chapters give examples of the use of specific detectors for spectroscopy involving alpha particles, gamma rays, and other types of nuclear radiation. At this point we discuss some general properties of detectors when applied to radiation spectroscopy and introduce some definitions that will be useful in these discussions.

One important property of a detector in radiation spectroscopy can be examined by noting its response to a monoenergetic source of that radiation. Figure 4.4 illustrates the differential pulse height distribution that might be produced by a detector under these conditions. This distribution is called the *response function* of the detector for the energy used in the determination. The curve labeled “Good resolution” illustrates one possible distribution around an average pulse height  $H_0$ . The second curve, labeled “Poor resolution,” illustrates the response of a detector with inferior performance. Provided the same number of pulses are recorded in both cases, the areas under each peak are equal. Although both distributions are centered at the same average value  $H_0$ , the width of the distribution in the poor resolution case

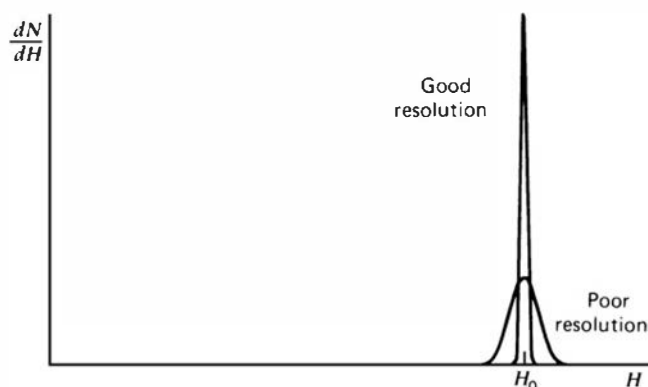


**Figure 4.4** Examples of response functions for detectors with relatively good resolution and relatively poor resolution.



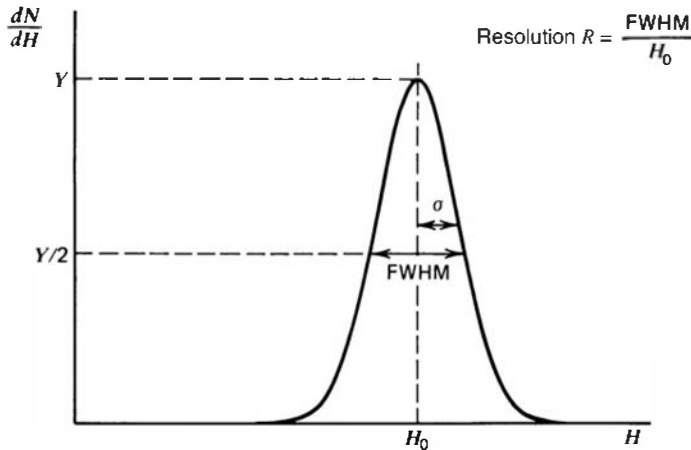


**Figure 4.5** Definition of detector resolution. For peaks whose shape is Gaussian with standard deviation  $\sigma$ , the FWHM is given by  $2.35\sigma$ .

is much greater. This width reflects the fact that a large amount of fluctuation was recorded from pulse to pulse even though the same energy was deposited in the detector for each event. If the amount of these fluctuations is made smaller, the width of the corresponding distribution will also become smaller and the peak will approach a sharp spike or a mathematical delta function. The ability of a given measurement to resolve fine detail in the incident energy of the radiation is obviously improved as the width of the response function (illustrated in Fig. 4.4) becomes smaller and smaller.

A formal definition of detector *energy resolution* is shown in Fig. 4.5. The differential pulse height distribution for a hypothetical detector is shown under the same assumption that only radiation for a single energy is being recorded. The full width at half maximum (FWHM) is illustrated in the figure and is defined as the width of the distribution at a level that is just half the maximum ordinate of the peak. This definition assumes that any background or continuum on which the peak may be superimposed is negligible or has been subtracted away. The energy resolution of the detector is conventionally defined as the FWHM divided by the location of the peak centroid  $H_0$ . The energy resolution  $R$  is thus a dimensionless fraction conventionally expressed as a percentage. Semiconductor diode detectors used in alpha spectroscopy can have an energy resolution less than 1%, whereas scintillation detectors used in gamma-ray spectroscopy normally show an energy resolution in the range of 3–10%. It should be clear that the smaller the figure for the energy resolution, the better the detector will be able to distinguish between two radiations whose energies lie near each other. An approximate rule of thumb is that one should be able to resolve two energies that are separated by more than one value of the detector FWHM.

There are a number of potential sources of fluctuation in the response of a given detector that result in imperfect energy resolution. These include any drift of the operating characteristics of the detector during the course of the measurements, sources of random noise within the detector and instrumentation system, and statistical noise arising from the discrete nature of the measured signal itself. The third source is in some sense the most important because it represents an irreducible minimum amount of fluctuation that will always be present in the detector signal no matter how perfect the remainder of the system is made. In a wide category of detector applications, the statistical noise represents the dominant source of fluctuation in the signal and thus sets an important limit on detector performance.

The statistical noise arises from the fact that the charge  $Q$  generated within the detector by a quantum of radiation is not a continuous variable but instead represents a discrete number of charge carriers. For example, in an ion chamber the charge carriers are the ion pairs produced by the passage of the charged particle through the chamber, whereas in a scintillation counter they are the number of electrons collected from the photocathode of the photomultiplier tube. In all cases the number of carriers is discrete and subject to random fluctuation from event to event even though exactly the same amount of energy is deposited in the detector.

An estimate can be made of the amount of inherent fluctuation by assuming that the formation of each charge carrier is a Poisson process. Under this assumption, if a total number  $N$  of charge carriers is generated on the average, one would expect a standard deviation of  $\sqrt{N}$  to characterize the inherent statistical fluctuations in that number [see Eq. (3.29)]. If this were the only source of fluctuation in the signal, the response function, as shown in Fig. 4.5, should have a Gaussian shape, because  $N$  is typically a large number. In this case, the Gaussian function introduced in Chapter 3 is most conveniently written

$$G(H) = \frac{A}{\sigma\sqrt{2\pi}} \exp\left(-\frac{(H - H_0)^2}{2\sigma^2}\right) \quad (4.12)$$

The width parameter  $\sigma$  determines the FWHM of any Gaussian through the relation  $\text{FWHM} = 2.35\sigma$ . (The remaining two parameters,  $H_0$  and  $A$ , represent the centroid and area, respectively.)

The response of many detectors is approximately linear, so that the average pulse amplitude  $H_0 = KN$ , where  $K$  is a proportionality constant. The standard deviation  $\sigma$  of the peak in the pulse height spectrum is then  $\sigma = K\sqrt{N}$  and its FWHM is  $2.35K\sqrt{N}$ . We then would calculate a limiting resolution  $R$  due only to statistical fluctuations in the number of charge carriers as

$$R \Big|_{\text{Poisson limit}} \equiv \frac{\text{FWHM}}{H_0} = \frac{2.35K\sqrt{N}}{KN} = \frac{2.35}{\sqrt{N}} \quad (4.13)$$

Note that this limiting value of  $R$  depends only on the number of charge carriers  $N$ , and the resolution improves ( $R$  will decrease) as  $N$  is increased. From Eq. (4.13) we see that in order to achieve an energy resolution better than 1%, one must have  $N$  greater than 55,000. An ideal detector would have as many charge carriers generated per event as possible, so that this limiting resolution would be as small a percentage as possible. The great popularity of semiconductor detectors stems from the fact that a very large number of charge carriers are generated in these devices per unit energy lost by the incident radiation.

Careful measurements of the energy resolution of some types of radiation detectors have shown that the achievable values for  $R$  can be lower by a factor as large as 3 or 4 than the minimum predicted by the statistical arguments given above. These results would indicate that the processes that give rise to the formation of each individual charge carrier are not independent, and therefore the total number of charge carriers cannot be described by simple Poisson statistics. The *Fano factor* has been introduced in an attempt to quantify the departure of the observed statistical fluctuations in the number of charge carriers from pure Poisson statistics and is defined as

$$F \equiv \frac{\text{observed variance in } N}{\text{Poisson predicted variance}(= N)} \quad (4.14)$$

Because the variance is given by  $\sigma^2$ , the equivalent expression to Eq. (4.13) is now

$$R \Big|_{\text{Statistical limit}} = \frac{2.35K\sqrt{N}\sqrt{F}}{KN} = 2.35\sqrt{\frac{F}{N}} \quad (4.15)$$

Although the Fano factor is substantially less than unity for semiconductor diode detectors and proportional counters, other types such as many scintillation detectors appear to show a limiting resolution consistent with Poisson statistics and the Fano factor would, in these cases, be unity.

The fact that Fano factors of less than one are observed for some detectors can be considered to be a consequence of the partitioning process of the original energy carried in

by the incident particle. A simple argument<sup>4</sup> suffices to show that one would expect to observe a Fano factor of less than unity in the outcome for sampling experiments of a general nature in which there is a constraint on the total quantity that is subject to sampling. In the case of an ionizing particle losing its energy in the detector material, a “sample” represents the amount of energy that goes into creating a charge carrier, and the assumption is made that this energy is subject to sample-to-sample variation. This variation reflects differing amounts of energy that are lost to thermal processes as individual charge carriers are formed along the particle track. Adding the constraint that the sum of all energy losses must equal the initial particle energy, it is then predicted that the number of charge carriers produced will fluctuate with a variance that is less than that of a Poisson distribution.

Any other source of fluctuations in the signal chain will combine with the inherent statistical fluctuations from the detector to give the overall energy resolution of the measuring system. It is sometimes possible to measure the contribution to the overall FWHM due to a single component alone. For example, if the detector is replaced by a stable pulse generator, the measured response of the remainder of the system will show a fluctuation due primarily to electronic noise. If there are several sources of fluctuation present and each is symmetric and independent, statistical theory predicts that the overall response function will always tend toward a Gaussian shape, even if the individual sources are characterized by distributions of different shape. As a result, the Gaussian function given in Eq. (4.12) is widely used to represent the response function of detector systems in which many different factors may contribute to the overall energy resolution. Then the total FWHM will be the quadrature sum of the FWHM values for each individual source of fluctuation:

$$(\text{FWHM})_{\text{overall}}^2 = (\text{FWHM})_{\text{statistical}}^2 + (\text{FWHM})_{\text{noise}}^2 + (\text{FWHM})_{\text{drift}}^2 + \dots$$

Each term on the right is the square of the FWHM that would be observed if all other sources of fluctuation were zero.

## VI. DETECTION EFFICIENCY

All radiation detectors will, in principle, give rise to an output pulse for each quantum of radiation that interacts within its active volume. For primary charged radiation such as alpha or beta particles, interaction in the form of ionization or excitation will take place immediately upon entry of the particle into the active volume. After traveling a small fraction of its range, a typical particle will form enough ion pairs along its path to ensure that the resulting pulse is large enough to be recorded. Thus, it is often easy to arrange a situation in which a detector will see every alpha or beta particle that enters its active volume. Under these conditions, the detector is said to have a counting efficiency of 100%.

On the other hand, uncharged radiations such as gamma rays or neutrons must first undergo a significant interaction in the detector before detection is possible. Because these radiations can travel large distances between interactions, detectors are often less than 100% efficient. It then becomes necessary to have a precise figure for the detector efficiency in order to relate the number of pulses counted to the number of neutrons or photons incident on the detector.

It is convenient to subdivide counting efficiencies into two classes: *absolute* and *intrinsic*. Absolute efficiencies are defined as

$$\epsilon_{\text{abs}} = \frac{\text{number of pulses recorded}}{\text{number of radiation quanta emitted by source}} \quad (4.16)$$

and are dependent not only on detector properties but also on the details of the counting geometry (primarily the distance from the source to the detector). The intrinsic efficiency is

defined as

$$\epsilon_{\text{int}} = \frac{\text{number of pulses recorded}}{\text{number of radiation quanta incident on detector}} \quad (4.17)$$

and no longer includes the solid angle subtended by the detector as an implicit factor. The two efficiencies are simply related for isotropic sources by  $\epsilon_{\text{int}} = \epsilon_{\text{abs}} \cdot (4\pi/\Omega)$ , where  $\Omega$  is the solid angle of the detector seen from the actual source position. It is much more convenient to tabulate values of intrinsic rather than absolute efficiencies because the geometric dependence is much milder for the former. The intrinsic efficiency of a detector usually depends primarily on the detector material, the radiation energy, and the physical thickness of the detector in the direction of the incident radiation. A slight dependence on distance between the source and the detector does remain, however, because the average path length of the radiation through the detector will change somewhat with this spacing.

Counting efficiencies are also categorized by the nature of the event recorded. If we accept all pulses from the detector, then it is appropriate to use *total* efficiencies. In this case all interactions, no matter how low in energy, are assumed to be counted. In terms of a hypothetical differential pulse height distribution shown in Fig. 4.6, the entire area under the spectrum is a measure of the number of all pulses that are recorded, regardless of amplitude, and would be counted in defining the total efficiency. In practice, any measurement system always imposes a requirement that pulses be larger than some finite threshold level set to discriminate against very small pulses from electronic noise sources. Thus, one can only approach the theoretical total efficiency by setting this threshold level as low as possible. The *peak* efficiency, however, assumes that only those interactions that deposit the full energy of the incident radiation are counted. In a differential pulse height distribution, these full energy events are normally evidenced by a peak that appears at the highest end of the spectrum. Events that deposit only part of the incident radiation energy then will appear farther to the left in the spectrum. The number of full energy events can be obtained by simply integrating the total area under the peak, which is shown as the cross-hatched area in Fig. 4.6. The total and peak efficiencies are related by the *peak-to-total* ratio  $r$

$$r = \frac{\epsilon_{\text{peak}}}{\epsilon_{\text{total}}} \quad (4.18)$$

which is sometimes tabulated separately. It is often preferable from an experimental standpoint to use only peak efficiencies, because the number of full energy events is not sensitive to some perturbing effects such as scattering from surrounding objects or spurious noise. Therefore, values for the peak efficiency can be compiled and universally applied to a wide variety of laboratory conditions, whereas total efficiency values may be influenced by variable conditions.

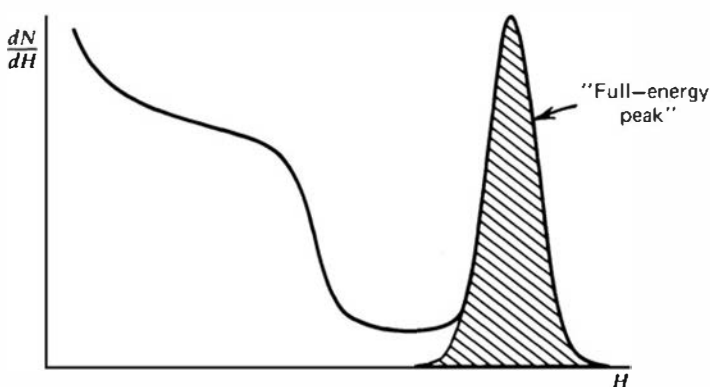


**Figure 4.6** Example of the full-energy peak in a differential pulse height spectrum.

To be complete, a detector efficiency should be specified according to both of the above criteria. For example, the most common type of efficiency tabulated for gamma-ray detectors is the *intrinsic peak efficiency*.

A detector with known efficiency can be used to measure the absolute activity of a radioactive source. In the following discussion, we assume that a detector with an intrinsic peak efficiency  $\epsilon_{ip}$  has been used to record  $N$  events under the full-energy peak in the detector spectrum. For simplicity, we also assume that the source emits radiation isotropically and that no attenuation takes place between the source and detector. From the definition of intrinsic peak efficiency, the number of radiation quanta  $S$  emitted by the source over the measurement period is then given by

$$S = N \frac{4\pi}{\epsilon_{ip}\Omega} \tag{4.19}$$

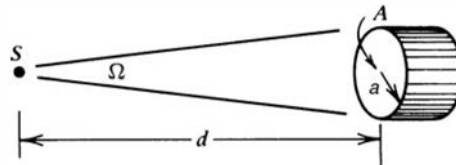
where  $\Omega$  represent the solid angle (in steradians) subtended by the detector at the source position. The solid angle is defined by an integral over the detector surface that faces the source, of the form

$$\Omega = \int_A \frac{\cos \alpha}{r^2} dA \tag{4.20}$$

where  $r$  represents the distance between the source and a surface element  $dA$ , and  $\alpha$  is the angle between the normal to the surface element and the source direction. If the volume of the source is not negligible, then a second integration must be carried out over all volume elements of the source. For the common case of a point source located along the axis of a right circular cylindrical detector,  $\Omega$  is given by

$$\Omega = 2\pi \left( 1 - \frac{d}{\sqrt{d^2 + a^2}} \right) \tag{4.21}$$

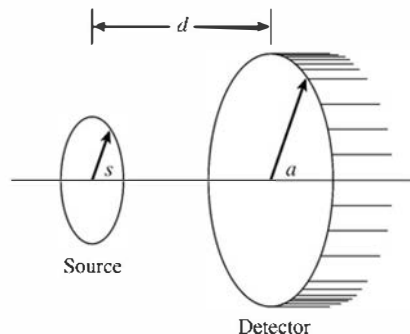
where the source–detector distance  $d$  and detector radius  $a$  are shown in the sketch below:



For  $d \gg a$ , the solid angle reduces to the ratio of the detector plane frontal area  $A$  visible at the source to the square of the distance:

$$\Omega \cong \frac{A}{d^2} = \frac{\pi a^2}{d^2} \tag{4.22}$$

Another commonly encountered circumstance, shown in the sketch below, involves a uniform circular disk source emitting isotropic radiation aligned with a circular disk detector, both positioned perpendicular to a common axis passing through their centers:



In terms of the dimensions shown on the sketch, it can be shown<sup>5</sup> that the effective solid angle averaged over the surface of the source is given by solving the integral

$$\Omega = \frac{4\pi a}{s} \int_0^\infty \frac{\exp(-dk)J_1(sk)J_1(ak)}{k} dk$$

where the  $J_1(x)$  are Bessel functions of  $x$ . This integral does not have an analytic solution, so it can only be solved using numerical techniques. A useful approximate solution is

$$\begin{aligned} \Omega &\cong 2\pi \left[ 1 - \frac{1}{(1+\beta)^{1/2}} - \frac{3}{8} \frac{\alpha\beta}{(1+\beta)^{5/2}} + \alpha^2[\text{F1}] - \alpha^3[\text{F2}] \right] \\ \text{F1} &= \frac{5}{16} \frac{\beta}{(1+\beta)^{7/2}} - \frac{35}{64} \frac{\beta^2}{(1+\beta)^{9/2}} \\ \text{F2} &= \frac{35}{128} \frac{\beta}{(1+\beta)^{9/2}} - \frac{315}{256} \frac{\beta^2}{(1+\beta)^{11/2}} + \frac{1155}{1024} \frac{\beta^3}{(1+\beta)^{13/2}} \end{aligned}$$

where

$$\alpha = \left(\frac{s}{d}\right)^2 \quad \beta = \left(\frac{a}{d}\right)^2$$

This approximation becomes inaccurate when the source or detector diameters become too large compared with their spacing, but it has been shown<sup>6</sup> to give very accurate results over a wide range of dimensions.

Published values for  $\Omega$  can sometimes be found for more complicated geometric arrangements involving off-axis or volumetric sources, or detectors with more complex shapes. Some specific examples of data or descriptions of algorithms useful in solid angle computations are given in Refs. 7–20.

## VII. DEAD TIME

In nearly all detector systems, there will be a minimum amount of time that must separate two events in order that they be recorded as two separate pulses. In some cases the limiting time may be set by processes in the detector itself, and in other cases the limit may arise in the associated electronics. This minimum time separation is usually called the *dead time* of the counting system. Because of the random nature of radioactive decay, there is always some probability that a true event will be lost because it occurs too quickly following a preceding event. These “dead time losses” can become rather severe when high counting rates are encountered, and any accurate counting measurements made under these conditions must include some correction for these losses. In this section we discuss some simple models of dead time behavior of counting systems, together with two experimental methods of determining system dead time. Reference 21 is an excellent presentation of more detailed analyses of related topics that are beyond the present scope.

### A. Models for Dead Time Behavior

Two models of dead time behavior of counting systems have come into common usage: *paralyzable* and *nonparalyzable* response. These models represent idealized behavior, one or the other of which often adequately resembles the response of a real counting system. The fundamental assumptions of the models are illustrated in Fig. 4.7. At the center of the figure, a time scale is shown on which six randomly spaced events in the detector are

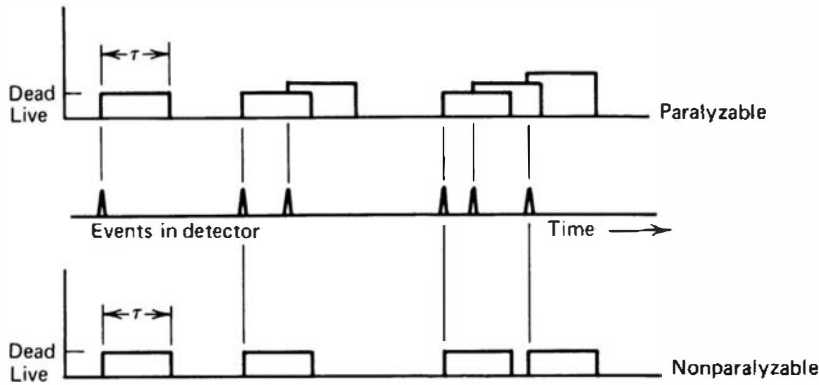


**Figure 4.7** Illustration of two assumed models of dead time behavior for radiation detectors.

indicated. At the bottom of the figure is the corresponding dead time behavior of a detector assumed to be nonparalyzable. A fixed time  $\tau$  is assumed to follow each true event that occurs during the “live period” of the detector. True events that occur during the dead period are lost and assumed to have no effect whatsoever on the behavior of the detector. In the example shown, the nonparalyzable detector would record four counts from the six true interactions. In contrast, the behavior of a paralyzable detector is shown along the top line of Fig. 4.7. The same dead time  $\tau$  is assumed to follow each true interaction that occurs during the live period of the detector. True events that occur during the dead period, however, although still not recorded as counts, are assumed to extend the dead time by another period  $\tau$  following the lost event. In the example shown, only three counts are recorded for the six true events.

The two models predict the same first-order losses and differ only when true event rates are high. They are in some sense two extremes of idealized system behavior, and real counting systems will often display a behavior that is intermediate between these extremes. The detailed behavior of a specific counting system may depend on the physical processes taking place in the detector itself or on delays introduced by the pulse processing and recording electronics.

In the discussion that follows, we examine the response of a detector system to a steady-state source of radiation, and we adopt the following definitions:

- $n$  = true interaction rate
- $m$  = recorded count rate
- $\tau$  = system dead time

We assume that the counting time is long so that both  $n$  and  $m$  may be regarded as average rates. In general, we would like to obtain an expression for the true interaction rate  $n$  as a function of the measured rate  $m$  and the system dead time  $\tau$ , so that appropriate corrections can be made to measured data to account for the dead time losses.

In the nonparalyzable case, the fraction of all time that the detector is dead is given simply by the product  $m\tau$ . Therefore, the rate at which true events are lost is simply  $nm\tau$ . But because  $n - m$  is another expression for the rate of losses,

$$n - m = nm\tau \tag{4.23}$$

Solving for  $n$ , we obtain

$$\boxed{n = \frac{m}{1 - m\tau}} \quad \text{Nonparalyzable model} \tag{4.24}$$

In the paralyzable case, dead periods are not always of fixed length, so we cannot apply the same argument. Instead, we note that rate  $m$  is identical to the rate of occurrences of time intervals between true events that exceed  $\tau$ . The distribution of intervals between random events

occurring at an average rate  $n$  was previously shown [Eq. (3.71)] to be

$$P_1(T) dT = ne^{-nT} dT \quad (4.25)$$

where  $P_1(T) dT$  is the probability of observing an interval whose length lies within  $dT$  about  $T$ .

The probability of intervals larger than  $\tau$  can be obtained by integrating this distribution between  $\tau$  and  $\infty$

$$P_2(\tau) = \int_{\tau}^{\infty} P_1(T) dT = e^{-n\tau} \quad (4.26)$$

The rate of occurrence of such intervals is then obtained by simply multiplying the above expression by the true rate  $n$

$$\boxed{m = ne^{-n\tau}} \quad \begin{array}{l} \text{Paralyzable} \\ \text{model} \end{array} \quad (4.27)$$

The paralyzable model leads to a more cumbersome result because we cannot solve explicitly for the true rate  $n$ . Instead, Eq. (4.27) must be solved iteratively if  $n$  is to be calculated from measurements of  $m$  and knowledge of  $\tau$ .

A plot of the observed rate  $m$  versus the true rate  $n$  is given in Fig. 4.8 for both models. When the rates are low the two models give virtually the same result, but the behavior at high rates is markedly different. A nonparalyzable system will approach an asymptotic value for the observed rate of  $1/\tau$ , which represents the situation in which the counter barely has time to finish one dead period before starting another. For paralyzable behavior, the observed rate is seen to go through a maximum. Very high true interaction rates result in a multiple extension of the dead period following an initial recorded count, and very few true events can be recorded. One must always be careful when using a counting system that may be paralyzable to ensure that ostensibly low observed rates actually correspond to low interaction rates rather than very high rates on the opposite side of the maximum. Mistakes in the interpretation of nuclear counting data from paralyzable systems have occurred in the past by overlooking the fact that there are always two possible true interaction rates corresponding to a given observed rate. As shown in Fig. 4.8, the observed rate  $m_1$  can correspond to either true rates  $n_1$  or  $n_2$ . The ambiguity can be resolved only by changing the true rate in a known direction while observing whether the observed rate increases or decreases.

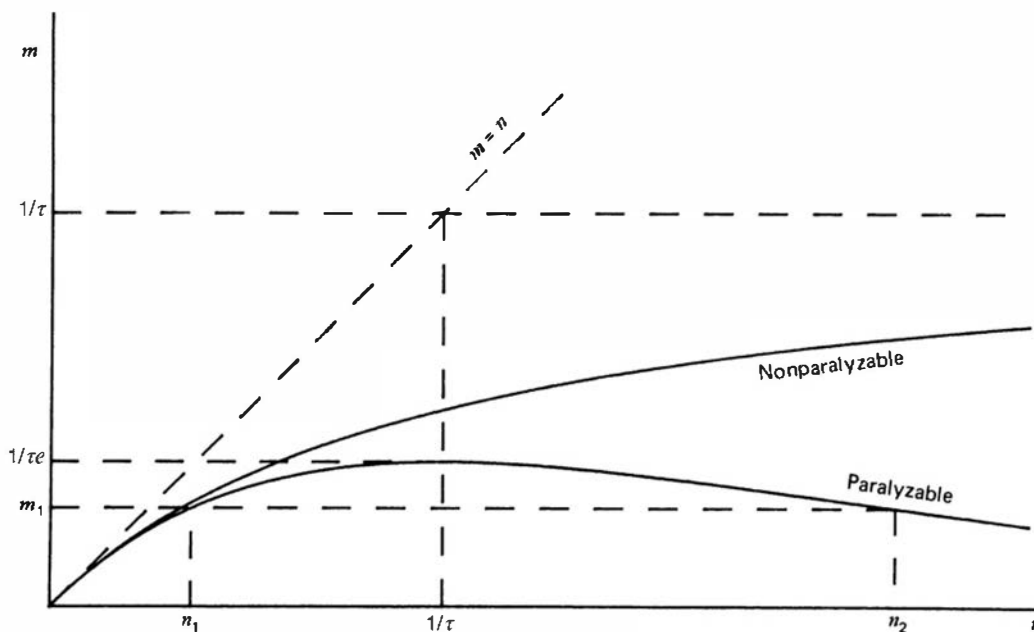


**Figure 4.8** Variation of the observed rate  $m$  as a function of the true rate  $n$  for two models of dead time losses.



For low rates ( $n \ll 1/\tau$ ) the following approximations can be written:

$$\text{Nonparalyzable} \quad m = \frac{n}{1 + n\tau} \cong n(1 - n\tau) \quad (4.28)$$

$$\text{Paralyzable} \quad m = ne^{-n\tau} \cong n(1 - n\tau) \quad (4.29)$$

Thus, the two models lead to identical results in the limit of small dead time losses.

If possible, one should avoid measurement conditions under which dead time losses are high because of the errors that inevitably occur in making corrections for the losses. The value of  $\tau$  may be uncertain or subject to variation, and the system behavior may not follow exactly either of the models described above. When losses are greater than 30 or 40%, the calculated true rate becomes very sensitive to small changes in the measured rate and the assumed system behavior. Instead, the user should seek to reduce the losses by changing the conditions of the measurement or by choosing a counting system with smaller dead time.

## B. Methods of Dead Time Measurement

In order to make dead time corrections using either model, prior knowledge of the dead time  $\tau$  is required. Sometimes this dead time can be associated with a known limiting property of the counting system (e.g., a fixed resolving time of an electronic circuit). More often, the dead time will not be known or may vary with operating conditions and must therefore be measured directly. Common measurement techniques are based on the fact that the observed rate varies nonlinearly with the true rate. Therefore, by assuming that one of the specific models is applicable, and by measuring the observed rate for at least two different true rates that differ by a known ratio, the dead time can be calculated.

The common example is the *two-source method*. The method is based on observing the counting rate from two sources individually and in combination. Because the counting losses are nonlinear, the observed rate due to the combined sources will be less than the sum of the rates due to the two sources counted individually, and the dead time can be calculated from the discrepancy.

To illustrate the method, let  $n_1$ ,  $n_2$ , and  $n_{12}$  be the true counting rates (sample plus background) with source 1, source 2, and the combined sources, respectively, in place. Let  $m_1$ ,  $m_2$ , and  $m_{12}$  represent the corresponding observed rates. Also, let  $n_b$  and  $m_b$  be the true and measured background rates with both sources removed. Then

$$\begin{aligned} n_{12} - n_b &= (n_1 - n_b) + (n_2 - n_b) \\ n_{12} + n_b &= n_1 + n_2 \end{aligned} \quad (4.30)$$

Now assuming the nonparalyzable model [Eq. (4.24)] and substituting, we obtain

$$\frac{m_{12}}{1 - m_{12}\tau} + \frac{m_b}{1 - m_b\tau} = \frac{m_1}{1 - m_1\tau} + \frac{m_2}{1 - m_2\tau} \quad (4.31)$$

Solving this equation explicitly for  $\tau$  gives the following result:

$$\tau = \frac{X(1 - \sqrt{1 - Z})}{Y} \quad (4.32)$$

where

$$\begin{aligned} X &\equiv m_1m_2 - m_b m_{12} \\ Y &\equiv m_1m_2(m_{12} + m_b) - m_b m_{12}(m_1 + m_2) \\ Z &\equiv \frac{Y(m_1 + m_2 - m_{12} - m_b)}{X^2} \end{aligned}$$

Because the method is essentially based on observing the difference between two nearly equal large numbers, careful measurements are required in order to get reliable values for the dead time. The measurement is usually carried out by counting source 1, placing source 2 nearby and measuring the combined rate, and then removing source 1 to measure the rate caused by source 2 alone. During this operation, care must be exercised not to move the source already in place, and consideration must be given to the possibility that the presence of a second source will scatter radiation into the detector that would not ordinarily be counted from the first source alone. In order to keep the scattering unchanged, a dummy second source without activity is normally put in place when the sources are counted individually. Best results are obtained by using sources active enough to result in a fractional dead time  $m_{12}\tau$  of at least 20%.

A second method can be carried out if a short-lived radioisotope source is available.<sup>†</sup> In this case the departure of the observed counting rate from the known exponential decay of the source can be used to calculate the dead time. The technique, known as the *decaying source method*, is based on the known behavior of the true rate  $n$ :

$$n = n_0 e^{-\lambda t} + n_b \quad (4.33)$$

where  $n_0$  is the true rate at the beginning of the measurement and  $\lambda$  is the decay constant of the particular isotope used for the measurement.

In the limit of negligible background, a simple graphical procedure can be applied to analyze the resulting data. Then Eq. (4.33) becomes

$$n \cong n_0 e^{-\lambda t} \quad (4.34)$$

By inserting Eq. (4.34) into Eq. (4.24) and carrying out some algebra, we get the following relation for the nonparalyzable model:

$$m e^{\lambda t} = -n_0 \tau m + n_0 \quad (4.35)$$

If we identify, as in Fig. 4.9a, the abscissa as  $m$  and the ordinate as the product  $m e^{\lambda t}$ , then Eq. (4.35) is that of a straight line. The experimental procedure consists of measuring the observed rate  $m$  as a function of time  $t$ , and thus defining points that should lie on this line starting from the right and moving left as the source decays. By fitting the best straight line to the data, the intercept will give  $n_0$ , the true rate at the beginning of the measurement, and the negative slope will give the product of  $n_0 \tau$ . The dead time  $\tau$  then follows directly from the ratio of the slope to the intercept.

For the paralyzable model, inserting Eq. (4.34) into Eq. (4.27) gives the following result:

$$\lambda t + \ln m = -n_0 \tau e^{-\lambda t} + \ln n_0 \quad (4.36)$$

Again by choosing the abscissa and ordinate as shown in Fig. 4.9b, the equation of a straight line results. In this case the intercept gives the value  $\ln n_0$ , whereas the slope again gives the negative of the product  $n_0 \tau$ . The dead time can simply be derived from these two values. The decaying source method offers the advantage of not only being able to measure the value of the dead time but also being able to test the validity of the assumed models. If a nonparalyzable model best describes the counting system, the data will most closely fit a straight line for the format shown in Fig. 4.9a. On the other hand, if a paralyzable model is more appropriate, the format shown in Fig. 4.9b will result in a more nearly linear plot of the data. In order to be effective, the measurements should be carried out for a time period at least equal to the half-life of the decaying radioisotope, and the initial loss fraction  $m\tau$  should be at least 20%.

<sup>†</sup>For laboratories with access to neutron irradiation facilities, a convenient isotope is  $^{116\text{m}}\text{In}$  (half-life of 54.3 min), which is readily produced by neutron absorption in an indium foil.

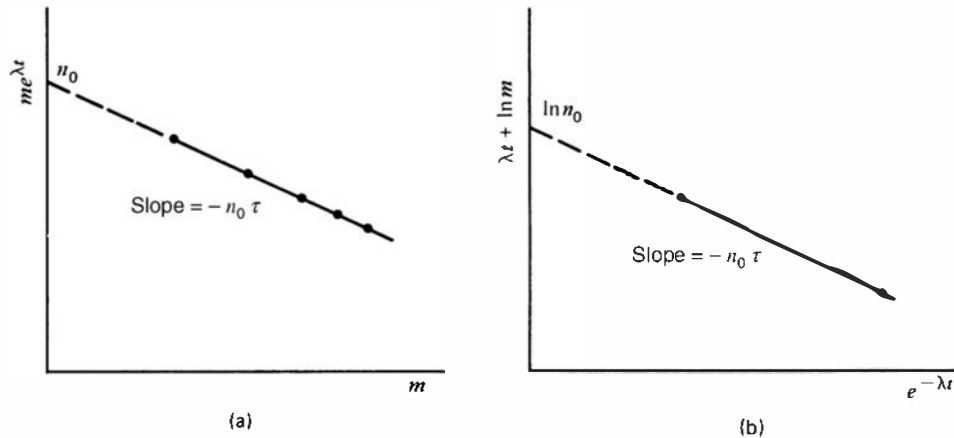


**Figure 4.9** Application of the decaying source method to determine dead time.

If the background is more than a few percent of the smallest measured rate, the graphical procedure can lead to significant errors. Although some improvement will result from subtracting the observed background rate from all the measured  $m$  values, this correction is not rigorous and an exact analysis can only be made by reverting back to Eq. (4.33). It then becomes necessary to use numerical computation techniques to derive values for  $n_0$  and  $\tau$  which, when inserted in an assumed model of the dead time behavior, result in a best fit to the measured data.

The methods described above are applicable to determine the dead time of simple counting systems in which all pulses above a threshold amplitude are recorded. For spectroscopic systems in which the pulse height spectrum is recorded from the detector, other methods are available to deal with counting losses that are based on the mixture of artificial pulses from a pulse generator into the signal processing chain. These pulser-based techniques are treated later in Chapter 17.

### C. Statistics of Dead Time Losses

When measuring radiation from steady-state sources, we normally assume that the true events occurring in the detector follow Poisson statistics in which the probability of an event occurring per unit time is a constant. The effect of system dead time is to remove selectively some of the events before they are recorded as counts. Specifically, events occurring after short time intervals following preceding events are preferentially discarded, and the interval distribution [Eq. (3.71)] is modified from its normal exponential shape. Dead time losses therefore distort the statistics of the recorded counts away from a true Poisson behavior. If the losses are small ( $n\tau$  less than 10 or 20%), however, this distortion has little practical effect on the validity of the statistical formulas for the prediction of statistical counting uncertainties developed in Chapter 3.

If the dead time losses are not small, the deviations from Poisson statistics become more significant. The discarding of events that occur after short time intervals causes the sequence of recorded counts to become somewhat more regular, and the variance expected in repeated measurements is reduced. Detailed analyses of the statistics of counts distorted by dead time are beyond the present scope, but can be found in Refs. 22–25.

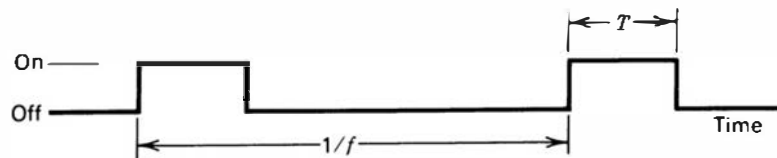
With either paralyzable or nonparalyzable behavior, there is some chance that more than one true event is lost per dead period. A recorded count therefore can correspond to the occurrence of any number of true events, from one to many. The relative probability that multiple true events are contained in a typical dead period will increase as the true event rate becomes higher. Because the true events still obey Poisson statistics, relatively simple analyses can be made to predict the probability that a typical recorded count results from the

combination of exactly  $x$  true events. These analyses are given later in this text, beginning on p. 658 in connection with the closely related topic of *pulse pile-up*.

### D. Dead Time Losses from Pulsed Sources

The analysis of counting losses due to detector dead time in the previous sections assumed that the detector was irradiated by a steady-state source of constant intensity. There are many applications in which the source of radiation is not continuous but instead consists of short pulses repeated at a constant frequency. For example, electron linear accelerators used to generate high-energy X-rays can be operated to produce pulses of a few microsecond width with a repetition frequency of several kilohertz. In such cases, the results given previously may not be applicable to correct properly for the effects of dead time losses. Substitute analytical methods must now be applied that make use of some of the statistical principles introduced in Chapter 3.

We confine our analysis to a radiation source that can be represented by the time-dependent intensity sketched below:



It is assumed that the radiation intensity is constant throughout the duration  $T$  of each pulse, and that the pulses occur at a constant frequency  $f$ . Depending on the relative value of the detector dead time  $\tau$ , several conditions may apply:

1. If  $\tau$  is much smaller than  $T$ , the fact that the source is pulsed has little effect, and the results given earlier in this section for steady-state sources may be applied with reasonable accuracy.
2. If  $\tau$  is less than  $T$  but not by a large factor, only a small number of counts may be registered by the detector during a single pulse. This is the most complicated circumstance and is beyond the scope of the present discussion. Detailed analysis of this case may be found in Refs. 26 and 27.
3. If  $\tau$  is larger than  $T$  but less than the "off" time between pulses (given by  $1/f - T$ ), the following analysis applies. Note that under these conditions, we can have a maximum of only one detector count per source pulse. Also, the detector will be fully recovered at the start of each pulse.

For the analysis that follows, it is no longer necessary that the radiation be constant over the pulse length  $T$ , but it is required that each radiation pulse be of the same intensity. We carry through the following definitions:

$$\begin{aligned} \tau &= \text{dead time of the detector system} \\ m &= \text{observed counting rate} \\ n &= \text{true counting rate (if } \tau \text{ were 0)} \\ T &= \text{source pulse length} \\ f &= \text{source pulse frequency} \end{aligned}$$

Since there can be at most a single count per pulse, the probability of an observed count per source pulse is given by  $m/f$ .

The average number of true events per source pulse is by definition equal to  $n/f$ . (Note that this average can be greater than 1.) We can apply the Poisson distribution [Eq. (3.24)] to predict

the probability that *at least one* true event occurs per source pulse:

$$\begin{aligned} P(> 0) &= 1 - P(0) \\ &= 1 - e^{-\bar{x}} \\ &= 1 - e^{-n/f} \end{aligned} \quad (4.37)$$

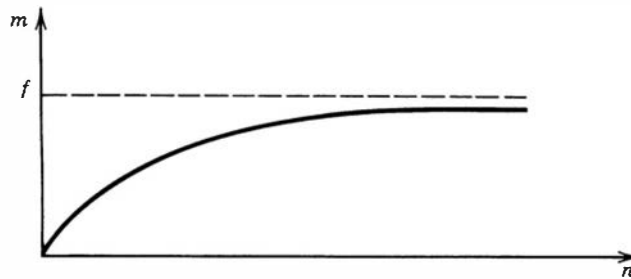
Since the detector is “live” at the start of each pulse, a count will be recorded if at least one true event occurs during the pulse. Only one such count can be recorded, so the above expression is also the probability of recording a count per source pulse. Equating the two expressions for this probability, we obtain

$$\frac{m}{f} = 1 - e^{-n/f}$$

or

$$m = f(1 - e^{-n/f}) \quad (4.38)$$

A plot of this behavior is shown below:



Under these conditions, the maximum observable counting rate is just the pulse repetition frequency, since no more than a single count can be recorded per pulse. Also, neither the specific length of the dead time nor the detailed dead time behavior of the system (whether it is paralyzable or nonparalyzable) has any influence on the losses.

Under normal circumstances, we are more interested in a correction formula to predict the true rate from the measured rate and the system dead time. Solving Eq. (4.38) for  $n$ , we derive

$$n = f \ln \left( \frac{f}{f - m} \right) \quad (4.39)$$

Recall that this correction is valid only under the conditions  $T < \tau < (1/f - T)$ .

In this case, the dead time losses are small under the condition  $m \ll f$ . Expanding the logarithmic term above for this limit, we find that a first-order correction is then given by

$$n \cong \frac{m}{1 - m/2f} \quad (4.40)$$

This result, because of its similarity to Eq. (4.24), can be viewed as predicting an *effective dead time* value of  $1/2f$  in this low-loss limit. Since this value is now one-half the source pulsing period, it can be many times larger than the actual physical dead time of the detector system.

## PROBLEMS

**4.1** Calculate the amplitude of the voltage pulse produced by collecting a charge equal to that carried by  $10^6$  electrons on a capacitance of 100 pF. ( $e = 1.602 \times 10^{-19}$  C)

**4.2** Compare the characteristics of pulse, MSV, and current mode operations as they are applied in radiation measurement systems. Include a table that lists the advantages and disadvantages of each.

**4.3** Derive Eq. (4.8).

**4.4** A detector with charge collection time of 150 ns is used with a preamplifier whose input circuit can be represented by the parallel combination of 300 pF and 10,000 ohms. Does this situation fall in the category of small or large collection circuit time constant?

**4.5** A scintillation counter operated at a given voltage produces a differential pulse height spectrum as sketched below:



(a) Draw the corresponding integral pulse height spectrum.

(b) Sketch the expected counting curve obtained by varying the voltage to the detector while counting above a fixed threshold.

**4.6** Sketch both the differential and integral pulse height spectra (using the same horizontal scale) for the following cases:

(a) Pulses with single amplitude of 1 V

(b) Pulses uniformly distributed in amplitude between 0 and 1 V

(c) Pulses distributed around an average amplitude of 1.5 V with a pulse height resolution of 8%

**4.7** A gamma-ray spectrometer records peaks corresponding to two different gamma-ray energies of 435 and 490 keV. What must be the energy resolution of the system (expressed as a percentage) in order just to distinguish these two peaks?

**4.8** In a detector with a Fano factor of 0.1 what should be the minimum number of charge carriers per pulse to achieve a statistical energy resolution limit of 0.5%?

**4.9** A pulse-processing system operated over a long period of time shows a typical drift that broadens single-amplitude pulses into a distribution with pulse height resolution of 2%. If this system is used with a detector with an intrinsic pulse height resolution of 4%, what will be the expected overall pulse height resolution?

**4.10** Find the solid angle subtended by the circular end surface of a cylindrical detector (diameter of 10 cm) for a point source located 20 cm from the surface along the cylindrical axis.

**4.11** The diameter of the moon as seen from earth subtends an angle of about  $0.5^\circ$ . Find the probability that a laser beam aimed in a random direction from the earth's surface will strike the moon.

**4.12** The detector of Problem 4.10 has an intrinsic peak efficiency at 1 MeV of 12%. The point source emits a 1 MeV gamma ray in 80% of its decays and has an activity of 20 kBq. Neglecting attenuation between the source and detector, calculate the number of counts that will appear under the 1 MeV full-energy peak in the pulse height spectrum from the detector over a 100-s count.

**4.13** A source of  $^{116m}\text{In}$  (half-life = 54.3 min) is counted using a G-M tube. Successive 1-min observations gave 131,340 counts at 12:00 noon and 93,384 counts at 12:40. Neglecting background and using a reasonable model for dead time losses, calculate the true interaction rate in the G-M tube at 12:00.

**4.14** Counters A and B are nonparalyzable with dead time of 30 and 100  $\mu\text{s}$ , respectively. At what true event rate will dead time losses in counter B be twice as great as those for counter A?

**4.15** A counter with negligible background gives exactly 10,000 counts in a 1-s period when a standard source is in place. An identical source is placed beside the first, and the counter now records 19,000 counts in 1 s. What is the counter dead time?

**4.16** A paralyzable detector system has a dead time of 1.5  $\mu\text{s}$ . If a counting rate of  $10^5$  per second is recorded, find the two possible values for the true interaction rate.

**4.17** As a source is brought progressively closer to a paralyzable detector, the measured counting rate rises to a maximum and then decreases. If a maximum counting rate of 50,000 per second is reached, find the dead time of the detector.

## REFERENCES

1. L. Purgel and N. Valcov, *Nucl. Instrum. Meth.* **B95**, 7 (1995).
2. J. M. Harrer and J. G. Beckerley, *Nuclear Power Reactor Instrumentation Systems Handbook*, Vol. 1, Chap. 5, TID-25952-PI (1973).
3. N. R. Campbell and V. J. Francis, *IEEE* **93**, Part III (1946).
4. D. V. Jordan et al., *Nucl. Instrum. Meth.* **A585**, 146 (2008).
5. L. Ruby, *Nucl. Instrum. Meth.* **A337**, 531 (1994).

## 130 Chapter 4 General Properties of Radiation Detectors

6. H. R. V. Carrillo, *Nucl. Instrum. Meth.* **A371**, 535 (1996). See also erratum published by the author as *Nucl. Instr. and Meth.* **A538**, 814 (2005).
7. H. Gotoh and H. Yagi, *Nucl. Instrum. Meth.* **96**, 485 (1971).
8. P. Oblozinsky and I. Ribansky, *Nucl. Instrum. Meth.* **94**, 187 (1971).
9. K. Verghese, R. P. Gardner, and R. M. Felder, *Nucl. Instrum. Meth.* **101**, 391 (1972).
10. M. Belluscio, R. De Leo, A. Pantaleo, and A. Vox, *Nucl. Instrum. Meth.* **114**, 145 (1974).
11. M. V. Green, R. L. Aamodt, and G. S. Johnston, *Nucl. Instrum. Meth.* **117**, 409 (1974).
12. R. Carchon et al., *Nucl. Instrum. Meth.* **128**, 195 (1975).
13. L. Wielopolski, *Nucl. Instrum. Meth.* **143**, 577 (1977).
14. J. Cook, *Nucl. Instrum. Meth.* **178**, 561 (1980).
15. L. Wielopolski, *Nucl. Instrum. Meth.* **226**, 436 (1984).
16. R. A. Rizk, A. M. Hathout, and A.-R. Z. Hussein, *Nucl. Instrum. Meth.* **A245**, 162 (1986).
17. S. Pommé et al., *Nucl. Instrum. Meth.* **A505**, 286 (2003).
18. J. T. Conway, *Nucl. Instrum. Meth.* **A562**, 146 (2006).
19. S. J. Cipolla, *Nucl. Instrum. Meth.* **A579**, 268 (2007).
20. S. Pommé and J. Paepen, *Nucl. Instrum. Meth.* **A579**, 272 (2007).
21. "Particle Counting in Radioactivity Measurements," ICRU Report 52, ICRU, Bethesda (1994).
22. J. W. Müller, *Nucl. Instrum. Meth.* **112**, 47 (1973).
23. J. W. Müller, *Nucl. Instrum. Meth.* **117**, 401 (1974).
24. J. Libert, *Nucl. Instrum. Meth.* **151**, 555 (1978).
25. G. Faraci and A. R. Pennisi, *Nucl. Instrum. Meth.* **212**, 307 (1983).
26. A. M. Cormack, *Nucl. Instrum. Meth.* **15**, 268 (1962).
27. C. H. Westcott, *Proc. R. Soc. London Ser.* **A194**, 508 (1948).

**GAS-FILLED DETECTORS**

**5.1 INTRODUCTION**

Gas-filled detectors operate by utilizing the ionization produced by radiation as it passes through a gas. Typically, such a counter consists of two electrodes to which a certain electrical potential is applied. The space between the electrodes is filled with a gas (Fig. 5.1). Ionizing radiation, passing through the space between the electrodes, dissipates part or all of its energy by generating electron-ion pairs. Both electrons and ions are charge carriers that move under the influence of the electrical field. Their motion induces a current on the electrodes, which may be measured (Fig. 5.1a). Or, through appropriate electronics, the charge produced by the radiation may be transformed into a pulse, in which case particles are counted individually (Fig. 5.1b). The first type of counter (Fig. 5.1a) is called *current* or *integrating chamber*; the second type (Fig. 5.1b) is called *pulse chamber*. To get an idea of what charges and currents one might expect to measure, consider this representative example.

For most gases, the average energy required to produce an electron-ion pair is about 30 eV. This number takes into account all collisions, including those that lead to excitation. If a 3-MeV alpha and beta particle deposits all its energy in the counter, it will produce, on the average,

$$\frac{3 \times 10^6}{30} = 10^5 \text{ electron-ion pairs}$$



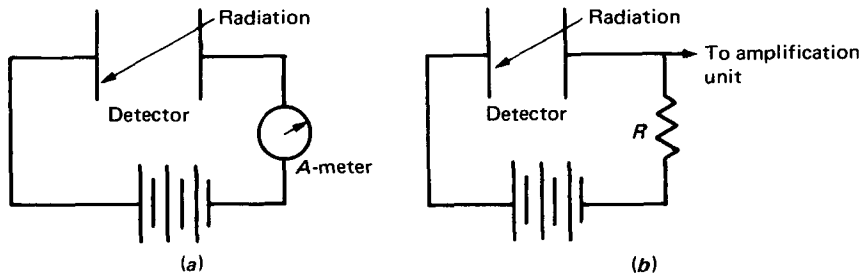


**Figure 5.1** A typical gas-filled detector: (a) the direct current produced in the circuit is measured; (b) individual pulses are detected.

A typical gas counter<sup>†</sup> has a capacitance of about 50 pF, and the charge will be collected in a time of the order of 1  $\mu$ s. If all the charge created by the 3-MeV particle is collected, the voltage and current expected are of the order of

$$V = \frac{Q}{C} \approx \frac{10^5 \times 1.6 \times 10^{-19} \text{ C/el}}{50 \times 10^{-12} \text{ F}} \approx 0.5 \times 10^{-3} \text{ V} \approx 0.5 \text{ mV}$$

$$i = \frac{Q}{t} \approx \frac{10^5 \times 1.6 \times 10^{-19}}{10^{-6}} \text{ A} \sim 1.6 \times 10^{-8} \text{ A}$$

In an ionized gas without an electric field, electrons and positive ions will move at random with an average kinetic energy equal to  $\frac{3}{2}kT$ , where  $k$  = Boltzmann's constant and  $T$  = temperature of the gas (Kelvin). When an electric field is present, both electrons and positive ions acquire a net velocity component along the lines of the electric field. Electrons move toward the positive electrode, positive ions toward the negative one. The force on either charge carrier is the same and equal to  $F = Ee$ , where  $E$  = electric field intensity, but the acceleration is quite different. The acceleration  $a$  is equal to  $F/M$ , where  $M$  is the mass of the ion or electron. Therefore, the acceleration of an electron will be thousands of times larger than the acceleration of an ion. The time it takes the electrons to reach the positive electrode of a typical counter is about 1  $\mu$ s. The corresponding time for the positive ions is about 1 ms, a thousand times longer.

The discussion up to this point has been limited to the effects of the ionization produced directly by the incident particle. This is called *primary* ionization. There are types of gas counters in which the electric field is so strong that the electrons of the primary ionization acquire enough kinetic energy between collisions to produce new electron-ion pairs. These new charges constitute the *secondary* ionization. Primary and secondary ionization are generated within such a short period of time that they contribute to one and the same pulse.

<sup>†</sup>Although the correct term is gas-filled detector or counter, the short term *gas counter* is frequently used.

## 5.2 RELATIONSHIP BETWEEN HIGH VOLTAGE AND CHARGE COLLECTED

Assume that the following experiment is performed (Fig. 5.2). A radioactive source of constant intensity is placed at a fixed distance from a gas counter. The high voltage (HV) applied to the counter may be varied with the help of a potentiometer. An appropriate meter measures the charge collected per unit time. If the HV applied to the counter is steadily increased, the charge collected per unit time changes as shown in Fig. 5.3. The curve of Fig. 5.3 is divided into five regions, which are explained as follows.

**Region I.** When the voltage is very low, the electric field in the counter is not strong, electrons and ions move with relatively slow speeds, and their recombination rate is considerable. As  $V$  increases, the field becomes stronger, the carriers move faster, and their recombination rate decreases up to the point where it becomes zero. Then, all the charge created by the ionizing radiation is being collected ( $V = V_1$ ). Region I is called the *recombination* region.

**Region II.** In region II, the charge collected stays constant despite a change in the voltage because the recombination rate is zero and no new charge is produced. This is called the *ionization* region.

**Region III.** In this region, the collected charge starts increasing because the electrons produce secondary ionization that results in charge multiplication. The electric field is so strong, in a certain fraction of the counter volume, that electrons from the primary ionization acquire enough energy between collisions to produce additional ionization. The *gas multiplication factor*—i.e., the ratio of the total ionization produced divided by the primary ionization—is, for a given voltage, independent of the primary ionization. Thus the output of the counter is proportional to the primary ionization. The pulse height at the output is proportional to the energy dissipated inside the counter; therefore particle

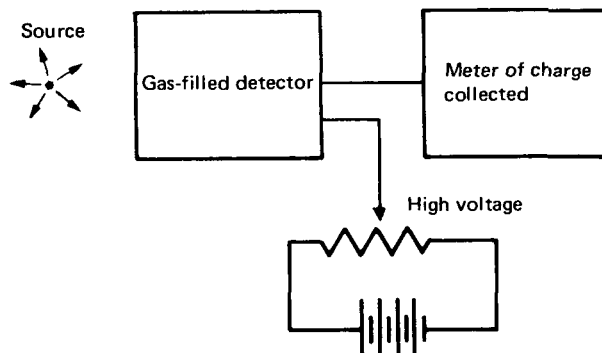


**Figure 5.2** Experimental setup for the study of the relationship between high voltage applied and charge collected.

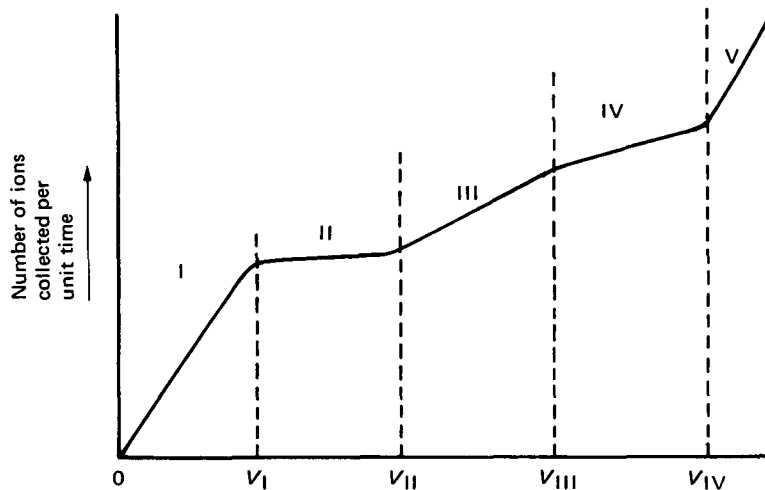


**Figure 5.3** The relationship between voltage applied to the counter and charge collected.

identification and energy measurement are possible. This region is, appropriately enough, called the *proportional* region.

**Region IV.** In this region, the electric field inside the counter is so strong that a single electron-ion pair generated in the chamber is enough to initiate an avalanche of electron-ion pairs. This avalanche will produce a strong signal with shape and height independent of the primary ionization and the type of particle, a signal that depends only on the electronics of the counter. Region IV is called the *Geiger-Müller (GM)* region.

**Region V.** If the applied voltage is raised beyond the value  $V_{IV}$ , a single ionizing event initiates a continuous discharge in the gas, and the device is not a particle detector anymore. No gas counter should operate with voltage  $V > V_{IV}$ .

If the graph discussed above is obtained using an  $\alpha$ ,  $\beta$ , or  $\gamma$  source, the results will be as shown in Fig. 5.4.

### 5.3 DIFFERENT TYPES OF GAS-FILLED DETECTORS

Gas counters take their name from the voltage region in which they operate. No counter operates in region I of Fig. 5.3, because a slight change in voltage will change the signal.

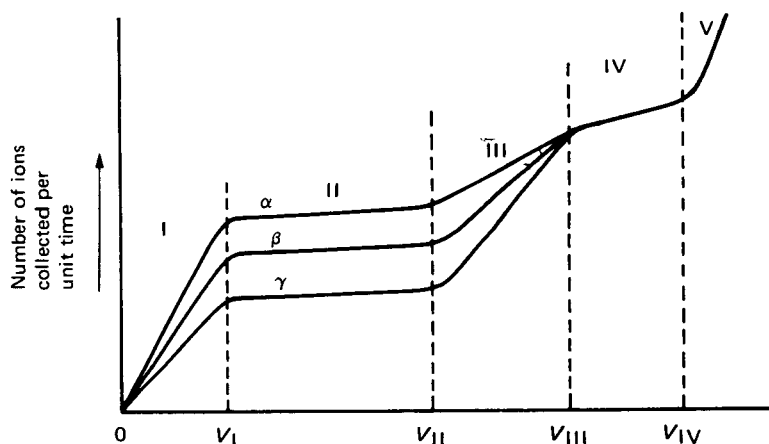


**Figure 5.4** The relationship between charge collected and applied voltage for three different types of particles. In region IV, the curve increases slightly but is the same for all particles.

*Ionization chambers* operate in region II. No charge multiplication takes place. The output signal is proportional to the particle energy dissipated in the detector; therefore measurement of particle energy is possible. Since the signal from an ionization chamber is not large, only strongly ionizing particles such as alphas, protons, fission fragments, and other heavy ions are detected by such counters. The voltage applied is less than 1000 V.

*Proportional counters* operate in region III. Charge multiplication takes place, but the output signal is still proportional to the energy deposited in the counter. Measurement of particle energy is possible. Proportional counters may be used for the detection of any charged particle.

Identification of the type of particle is possible with both ionization and proportional counters. An alpha particle and an electron having the same energy and entering either of the counters, will give a different signal. The alpha particle signal will be bigger than the electron signal. The voltage applied to proportional counters ranges between 800 and 2000 V.

*GM counters* operate in region IV. GM counters are very useful because their operation is simple and they provide a very strong signal, so strong that a preamplifier is not necessary. They can be used with any kind of ionizing radiation (with different levels of efficiency). The disadvantage of GM counters is that their signal is independent of the particle type and its energy. *Therefore, a GM counter provides information only about the number of particles.* Another minor disadvantage is their relatively long dead time (200 to 300  $\mu\text{s}$ ). (For more details about dead time, see Sec. 5.6.2.) The voltage applied to GM counters ranges from 500 to 2000 V.

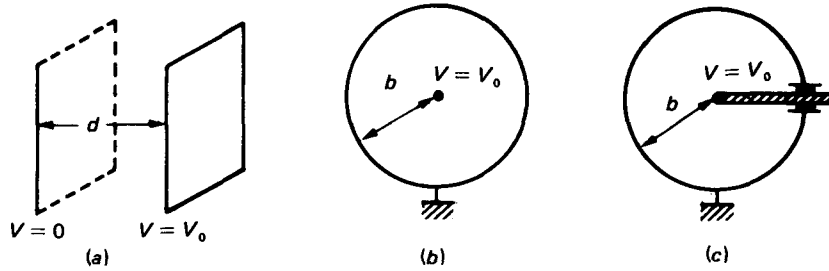


**Figure 5.5** The different geometries of gas-filled detectors: (a) parallel plate; (b) cylindrical; (c) spherical.

Gas counters may be constructed in any of three basic geometries: parallel plate, cylindrical, or spherical (Fig. 5.5). In a parallel-plate chamber, the electric field (neglecting edge effects) is uniform, with strength equal to

$$E = \frac{V_0}{d} \quad (5.1)$$

In the cylindrical chamber, the voltage is applied to a very thin wire, a few mills of an inch in diameter, stretched axially at the center of the cylinder. The cylinder wall is usually grounded. The electric field is, in this case,

$$E(r) = \frac{V_0}{\ln(b/a)} \frac{1}{r} \quad (5.2)$$

where  $a$  = radius of the central wire

$b$  = radius of the counter

$r$  = distance from the center of the counter

It is obvious from Eq. 5.2 that very strong electric fields can be maintained inside a cylindrical counter close to the central wire. Charge multiplication is achieved more easily in a cylindrical than in a plate-type gas counter. For this reason, proportional and GM counters are manufactured with cylindrical geometry.

In a spherical counter, the voltage is applied to a small sphere located at the center of the counter. The wall of the counter is usually grounded. The electric field is

$$E(r) = V_0 \frac{ab}{b-a} \frac{1}{r^2} \quad (5.3)$$

where  $a$ ,  $b$ , and  $r$  have the same meaning as in cylindrical geometry. Strong fields may be produced in a spherical counter, but this type of geometry is not popular because of construction difficulties.

A counter filled with a gas at a certain pressure may operate in any of the regions I–IV discussed earlier, depending on a combination of the following

parameters:

1. Size of the counter
2. Size of wire (in cylindrical counters)
3. Gas type
4. Gas pressure
5. Level of high voltage

Normally, gas counters are manufactured to operate in one region only. The user buys an ionization counter, a proportional counter, or a GM counter. The manufacturer has selected the combination of variables 1–4 listed above that results in the desired type of gas counter. The last variable, the high voltage applied, is not a fixed number, but a range of values. The range is specified by the manufacturer, but the user decides on the best possible value of HV.

The rest of this chapter discusses the special characteristics of the three types of gas counters.

## 5.4 IONIZATION CHAMBERS

### 5.4.1 Pulse Formation in an Ionization Chamber

The formation and shape of the signal in an ionization chamber will be analyzed for a parallel-plate counter as shown in Fig. 5.1*b*. The analysis is similar for a cylindrical or a spherical chamber.

Consider the ionization chamber shown in Fig. 5.6. The two parallel plates make a capacitor with capacitance  $C$ , and with the resistor  $R$  an  $RC$  circuit is formed. A constant voltage  $V_0$  is applied on the plates. The time-dependent

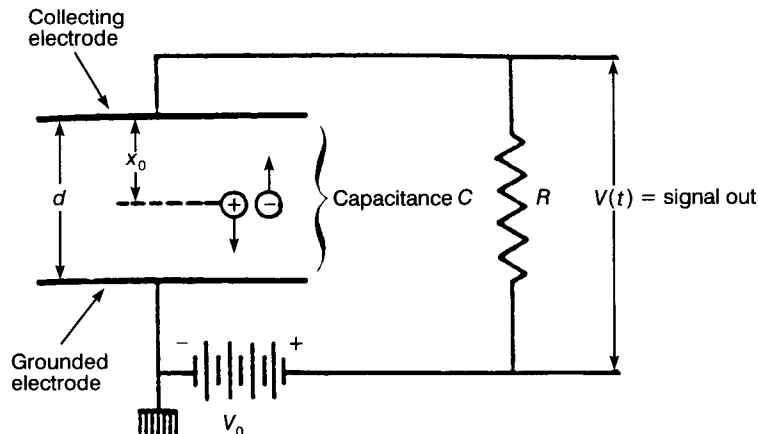


**Figure 5.6** The electronic circuit of a parallel-plate ionization chamber.

voltage  $V(t)$  across the resistor  $R$  represents the signal. The objective of this section is to obtain the function  $V(t)$ .

Assume that one electron-ion pair has been formed at a distance  $x_0$  from the collecting plate (collector). The electron and the ion start moving in the electric field, and they acquire kinetic energy at the expense of the electrostatic energy stored in the capacitance of the chamber. If the charge moves a distance  $dx$ , conservation of energy requires that

(Work on charges) = (change in electrostatic energy)

$$eE(dx^+ + dx^-) = d\left(\frac{Q^2}{2C}\right) = \frac{Q}{C} dQ \approx V_0(dQ^- + dQ^+) \quad (5.4)$$

where  $E$  = electric field intensity

$Q$  = charge on chamber plates

$dQ^+$ ,  $dQ^-$  = changes in positive, negative charge, respectively

It is assumed that the change in the charge ( $dQ$ ) is so small that the voltage  $V_0$  stays essentially constant. The voltage  $V(t)$  across the resistor  $R$  is the result of this change in the charge and is given by

$$V(t) = \frac{1}{C} \int_0^t dQ(t) = \frac{1}{C} \int_0^t (dQ^+ + dQ^-) \quad (5.5)$$

Substituting in Eq. 5.5 the value of  $dQ$  from Eq. 5.4, one obtains

$$V(t) = \frac{1}{C} \int_0^t \frac{e}{V_0} E(dx^+ - dx^-) \quad (5.6)$$

Let

$w^+$  = drift velocity of positive ions

$w^-$  = drift velocity of electrons

In general, the drift velocity is a function of the *reduced field strength*  $E/p$ , where  $p$  is the gas pressure in the chamber.

The derivation up to this point is independent of the chamber geometry. To proceed further requires substitution of the value of the electric field from either Eq. 5.1, 5.2, or 5.3. For a plate-type ionization chamber the field is constant (Eq. 5.1), independent of  $x$ , and so is the drift velocity. Therefore, Eq. 5.6 becomes

$$V(t) = \frac{e}{Cd} \int_0^t (w^+ + w^-) dt = -\frac{e}{Cd} (w^-t + w^+t) \quad (5.7)$$

The drift velocity of the electron is a few thousand times more than the velocity of the ion,<sup>†</sup> which means the electron will reach the collector plate before the

<sup>†</sup>Typical values of drift velocities are  $w^+ \approx 10$  m/s,  $w^- = 10^4 - 10^5$  m/s.

ion has hardly moved. Let

$T^{(+)}$  = time it takes for an ion to reach the cathode

$T^{(-)}$  = time it takes for an electron to reach the collector (anode)

Typical values of these times are

$$T^{(+)} \approx \text{ms} \quad T^{(-)} \approx \mu\text{s}$$

Equation 5.7 shows that for  $t < T^{(-)}$ , the voltage  $V(t)$  changes linearly with time (Fig. 5.7):

$$V(t) = -\frac{e}{Cd}(w^- + w^+)t \quad 0 < t \leq T^{(-)} \quad (5.8)$$

For  $T > T^{(-)}$ , the signal is

$$V(t) = -\frac{e}{Cd}(x_0 + w^+t) \quad t > T^{(-)} \quad (5.9)$$

Finally, after  $t = T^{(+)}$ , the ion reaches the grounded cathode and the signal reaches its maximum (negative) value, which is

$$V(T^+) = -\frac{e}{Cd}x_0 \quad t > T^{(+)} \quad (5.10)$$

If  $N$  electron-ion pairs are produced, the final voltage will be

$$V(T^+) = -\frac{Ne}{Cd}x_0 \quad t = T^{(+)} \quad (5.11)$$

For  $t > T^{(+)}$ , the pulse decays with decay constant  $RC$  (see Sec. 10.3).

The pulse profile of Fig. 5.7 was derived under the assumption that all ion pairs were produced at  $x = x_0$ . Actually, the ionization is produced along the track traveled by the incident particle. The final pulse will be the result of the superposition of many pulses with different  $T^{(-)}$  values. Because of this effect, the sharp change in slope at  $t = T^{(-)}$  will disappear and the pulse will be smoother.

The pulse of Fig. 5.7 is not suitable for counting individual particles because it does not decay quickly enough. A pulse-type counter should produce a signal that decays faster than the average time between the arrival of two successive particles. For example, if the counting rate is 1000 counts/min, a particle arrives at the counter, on the average, every 1/1000 min (60 ms).

In Fig. 5.7, the pulse could be stopped at time  $t = T^{(+)}$  by electronic means. Such a technique would produce pulses with height proportional to the total charge generated in the detector, but with a duration of a few hundreds of microseconds, which is unacceptably long. The method used in practice is to “chop off” the pulse at time  $t = T^{(-)}$ , which amounts to stopping the pulse after only the electrons are collected. The signal is then fed into an  $RC$  circuit that, as described in Chap. 10, changes the pulse as shown in Fig. 5.8.



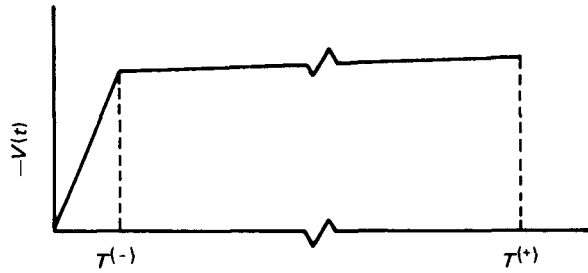


Figure 5.7 The voltage pulse generated by an ionization chamber.

Let  $V_i(t)$  be the signal at the output of the detector that is used as an input to an  $RC$  circuit. From Eq. 5.8,

$$V_i(t) = -\frac{e}{Cd}(w^- + w^+)t = kt \quad (5.8a)$$

Using this signal as an input, the output voltage across the resistor  $R_0$  is (see Secs. 10.3 and 10.4), for  $0 \leq t \leq T^{(-)}$  (Fig. 5.7),

$$V_0(t) = kC_0R_0(1 - e^{-t/C_0R_0}) \quad (5.12)$$

For  $t > T^{(-)}$ ,  $V_i(t)$  is essentially constant, and

$$V_0(t) = kC_0R_0(1 - e^{-T^{(-)}/C_0R_0})e^{-t/R_0C_0} \quad (5.13)$$

The signal  $V_0(t)$  is shown in Fig. 5.8b. Usually, the  $RC$  circuit is the first stage of the preamplifier, which accepts the signal of the ionization chamber.

The disadvantage of the signal in Fig. 5.8b is that its maximum value depends on the position where the ionization was produced. Indeed, from Eq. 5.12, one obtains for  $t = T^{(-)}$  (noting that  $k = -e(w^- + w^+)/Cd \approx -ew^-/Cd$ ,

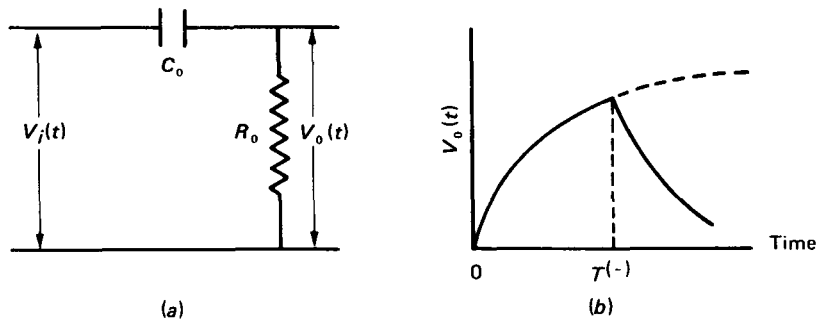


Figure 5.8 (a) The signal  $V_i(t)$  is fed into the  $RC$  circuit. (b) The output of the  $RC$  circuit decays quickly with a decay constant  $R_0C_0$ .

since  $w^- \gg w^+$ ,  $T^{(-)} \ll C_0 R_0$ , and  $T^{(-)} = x_0/w^-$

$$V(T^{(-)}) = -(ew^-/Cd)C_0 R_0(1 - e^{-T^{(-)}/C_0 R_0}) \approx -(ex_0/Cd) \quad (5.14)$$

Thus the peak value of the pulse in Fig. 5.8*b* depends on  $x_0$ . This disadvantage can be corrected in several ways. One is by placing a grid between the two plates and keeping it at an intermediate voltage  $V_g$  ( $0 < V_g < V_0$ ). For more details about the “gridded” ionization chamber, the reader should consult the references at the end of this chapter.

The analysis of the pulse formation in a cylindrical or a spherical counter follows the same approach. The results are slightly different because the electric field is not constant (see Eqs. 5.2 and 5.3), but the general shape of the signal is that shown in Fig. 5.7. (See Franzen & Cochran and Kowalski for detailed calculations of the pulse shapes for the three geometries of gas-filled chambers.)

#### 5.4.2 Current Ionization Chambers

An ionization chamber of the *current* type measures the average ionization produced by many incoming particles. This is achieved by measuring directly the electrical current generated in the chamber, using either a sensitive galvanometer for currents of  $10^{-8}$  A or higher (Fig. 5.9), or an electrometer (sometimes with an amplifier) for currents less than  $10^{-8}$  A. In the case of the electrometer, as shown in Fig. 5.10, the current is determined by measuring the voltage drop across the known resistance  $R$ . The voltage drop may be measured by the electrometer directly or after some amplification.

For current ionization chambers, it is very important to know the relationship between applied voltage and output current (for a constant radiation source). This relationship, which is shown in Fig. 5.11, consists of regions I and II of the graph of Fig. 5.3. The proper operating voltage of the ionization chamber is that for which all the ionization produced by the incident radiation is measured. If this is the case, a slight increase of the applied voltage will result in negligible change of the measured current. The voltage is then called the saturation voltage ( $V_s$ ), and the corresponding current is called saturation current. The value of the saturation current depends on the intensity and type of the radiation source (Fig. 5.11). It also depends, for the same radiation source, on the size and geometry of the chamber as well as on the type and pressure of the gas used. If one considers different gases, other things being equal, the highest current will be produced by the gas with the lowest average energy needed for the production of one electron-ion pair. Typical energies for common gases are given in Table 5.1.

During measurements of the ionization current with an electrometer, one would like to know the response of the measuring instrument if the signal from the ionization chamber changes. Assume that the current of the chamber changes suddenly from a value of  $i_1$  to  $i_2$ . The response of the electrometer is obtained by considering the equivalent electronic circuit of Fig. 5.10, shown in

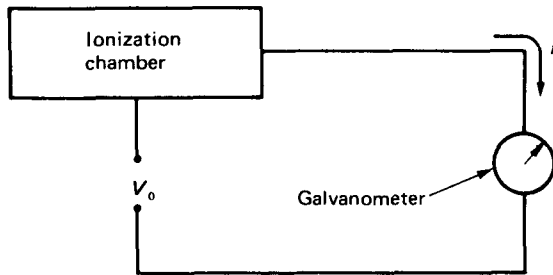


**Figure 5.9** Measurement of the current produced by an ionization chamber by using a galvanometer.

Fig. 5.12. The capacitor  $C$  represents the combined capacitance of the chamber and everything else. The resistor  $R$  represents a corresponding total resistance for the circuit. The signal to be measured is the voltage  $V(t)$ , where for  $t \leq 0$ ,

$$V_1 = i_1 R = i_1 R \quad (5.15)$$

At the  $t = 0$ , the current changes instantaneously from  $i_1$  to  $i_2$ , and the voltage will eventually become

$$V_2 = i_2 R \quad (5.16)$$

During the transition period, Kirchhoff's first law gives

$$i_2 = i_C + i_R = \frac{dQ(t)}{dt} + \frac{V(t)}{R} = C \frac{dV(t)}{dt} + \frac{V(t)}{R}$$

or

$$\frac{dV(t)}{dt} + \frac{1}{RC} V(t) = i_2 / C \quad (5.17)$$

The solution of this differential equation, with the initial condition given by Eq. 5.15, is

$$V(t) = i_2 R + R(i_1 - i_2)e^{-t/RC} \quad (5.18)$$

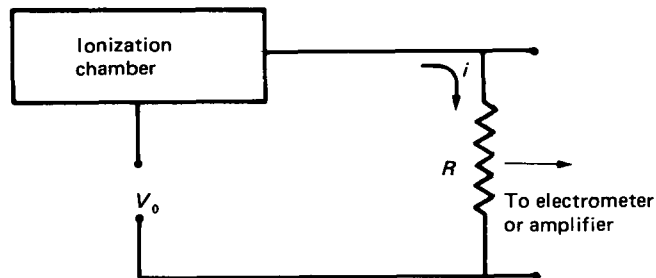


**Figure 5.10** Measurements of the current produced by an ionization chamber by using an electrometer.

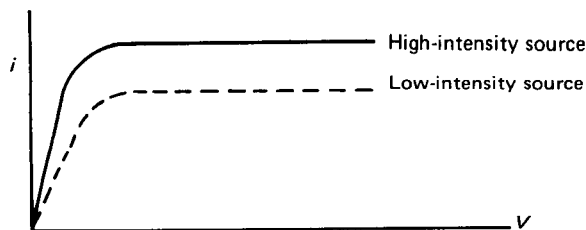


**Figure 5.11** The ionization chamber current as a function of applied voltage.

The function given by Eq. 5.18 is shown in Fig. 5.13. The response of the electrometer is exponential with a rate of change determined by the time constant  $RC$ . For fast response, the time constant should be as short as practically possible.

## 5.5 PROPORTIONAL COUNTERS

### 5.5.1 Gas Multiplication in Proportional Counters

When the electric field strength inside a gas counter exceeds a certain value, the electrons that move in such a field acquire, between collisions, sufficient energy to produce new ions. Thus, more electrons will be liberated, which in turn will produce more ions. The net effect of this process is multiplication of the primary ionization. The phenomenon is called *gas multiplication*.<sup>†</sup> To achieve the high field intensity needed for gas multiplication without excessive applied voltage, chambers operating in this mode are usually cylindrical with a very thin wire stretched axially at the center of the counter (Fig. 5.14). The wall of the counter is normally grounded and a positive voltage is applied to the central wire. In

<sup>†</sup>Also called gas gain or gas amplification.

**Table 5.1** Average Energy Needed for Production of One Electron-Ion Pair<sup>†</sup>

Gas	Energy per pair (eV)
H	36.3
He	42.3
A	26.4
Air	34
CO <sub>2</sub>	32.9
C <sub>2</sub> H <sub>6</sub> (ethane)	24.8
CH <sub>4</sub>	27.3

<sup>†</sup>From Franzen and Cochran.

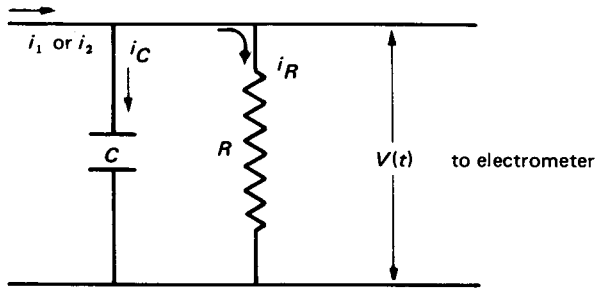


Figure 5.12 The equivalent electronic circuit of Fig. 5.10.

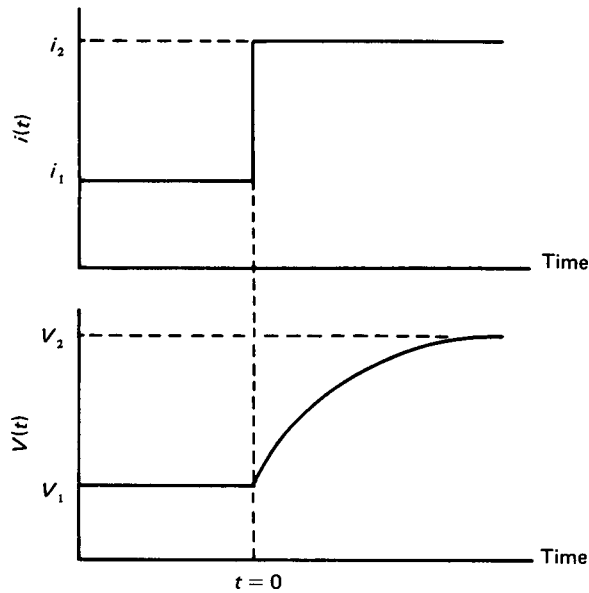


Figure 5.13 Response of an electrometer to a step change of the ionization current.

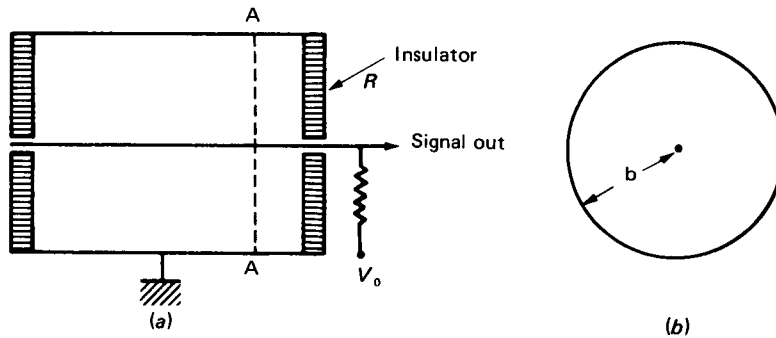


Figure 5.14 (a) A cylindrical gas-filled detector. (b) Cross section of the detector at AA.

such a geometry, the electrostatic field inside the chamber is radial and its intensity is

$$E(r) = \frac{V_0}{\ln(b/a)} \frac{1}{r} \quad (5.2)$$

The field intensity increases rapidly as the wire is approached. Since the radius  $a$  of the wire is a few mills of an inch and thousands of times smaller than the radius  $b$  of the counter, an extremely strong electric field is produced in a fraction of the chamber's volume. This volume is so small that the probability that the incident radiation will produce an electron ion pair in it is negligible.

In addition to the secondary electrons produced by collisions, electrons are also produced by two other processes:

1. Photoelectric interactions
2. Bombardment of the cathode surface by positive ions

The photoelectric interactions are caused by photons that are produced in the counter as a result of the ionization and excitation of the atoms and molecules of the gas. If the chamber is filled with a monatomic gas, these photons produce photoelectrons only when they strike the cathode (wall of cylinder) because they do not have enough energy to ionize the atoms of the gas. If the counter is filled with a gas mixture, however, photons emitted by molecules of one gas may ionize molecules of another.

Electrons are also emitted when the positive ions, which are produced in the chamber, reach the end of their journey and strike the cathode. The significance of this effect depends on the type of material covering the surface of the cathode and, more important, on the type of the gas filling the chamber.

The production of electrons by these processes results in the generation of successive avalanches of ionization because all the electrons, no matter how they are produced, migrate in the direction of the intense electric field and initiate additional ionization. The gas multiplication factor  $M$ , which is equal to the *total* number of free electrons produced in the counter when *one* pair is produced by the incident radiation, is calculated as follows. Let

$N$  = total number of electrons set free per primary electron-ion pair

$\delta$  = average number of photoelectrons produced per ion pair generated  
in the counter ( $\delta \ll 1$ )

The initial avalanche of  $N$  electrons will produce  $\delta N$  photoelectrons. Each photoelectron produces a new avalanche of  $N$  new electrons; therefore the second avalanche consists of  $\delta N^2$  electrons. The third avalanche will have  $\delta N^3$  electrons, and so on. The total number of electrons per initial ion pair produced is then

$$M = N + \delta N^2 + \delta N^3 + \dots$$

The magnitude of  $\delta N$  depends on the applied voltage. If  $\delta N < 1$ , the gas multiplication factor is

$$M = \frac{N}{1 - \delta N} \quad (5.19)$$

It should be noted that

1. If  $\delta N \ll 1$ , the photoelectric effect is negligible and  $M = N =$  initial gas multiplication (first avalanche).
2. If  $\delta N < 1$ ,  $M$  can become much larger than  $N$ .
3. If  $\delta N \geq 1$ ,  $M \rightarrow \infty$ , which means that a self-supporting discharge occurs in the counter.

The gas multiplication factor  $M$  is a function of the ratio  $V_0/\ln(b/a)$  and the product  $Pa$ , where  $P$  is the pressure of the gas in the counter (Rossi & Staub). Experimental results of  $M$  values for two gases are shown in Figs. 5.15 and 5.16. Diethorn<sup>1</sup> has obtained the equation

$$\ln M = \frac{V \ln 2}{\overline{\Delta V} \ln(b/a)} \ln \frac{V}{\overline{K} Pa \ln(b/a)} \quad (5.20)$$

where  $\overline{\Delta V}$  and  $\overline{K}$  are constants of the gas. Equation 5.20 has been tested and found to be valid.<sup>2-4</sup> As Figs. 5.15 and 5.16 show,  $M$  increases almost exponentially with applied voltage.

One method by which the strong dependence of  $M$  on applied voltage is reduced is by adding a small amount of a polyatomic organic gas in the gas of the counter. One popular mixture is 10 percent  $\text{CH}_4$  and 90 percent argon. The organic gases, called "quenching" gases, stabilize the operation of the counter by reducing the effect of the secondary processes. They achieve this because

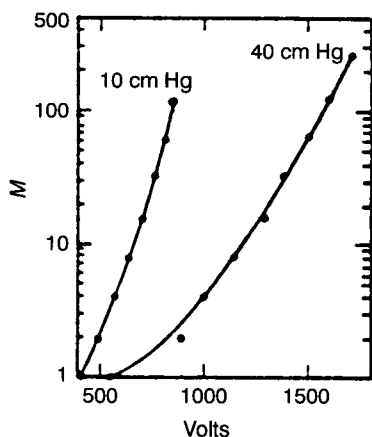


Figure 5.15 Gas multiplication  $M$  versus voltage. Gas is 93.6 percent pure argon ( $a = 0.005$  in,  $b = 0.435$  in, at two different pressures) (from Rossi and Staub).

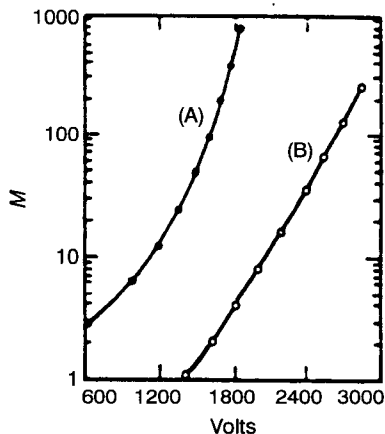


Figure 5.16 Gas multiplication  $M$  versus voltage. Gas is  $\text{BF}_3$ . (A)  $a = 0.005$  in,  $b = 0.75$  in,  $P = 10$  cmHg. (B)  $a = 0.005$  in,  $b = 0.78$  in,  $P = 80.4$  cmHg (from Rossi and Staub).

organic polyatomic molecules

1. dissociate rather than produce electrons when they hit the cathode
2. dissociate when they absorb a photon
3. have lower ionization potential than the molecules of the main gas; as a result, they are ionized in collisions with ions of the main gas and thus prevent the ions from reaching the cathode

The total charge produced in a proportional counter is

$$Q = MNe = M \frac{\Delta E}{W} e \quad (5.21)$$

where  $\Delta E$  = energy of the incident particle dissipated in the counter

$w$  = average energy required for production of one electron-ion pair

Equation 5.21 indicates that  $Q$  (output) is proportional to the energy deposited in the counter ( $\Delta E$ ). This is the reason why such counters are called proportional. The proportionality holds, however, only if the gas multiplication factor  $M$  is constant, independent of the primary ionization. The question then arises, under what conditions is this true?

A proportional counter is strictly proportional as long as the space charge due to the positive ions does not modify too much the electric field around the wire. The magnitude of the space charge is a function of the primary ionization and the gas multiplication. If the primary ionization is very small, the value of  $M$  may be  $10^5$  to  $10^6$  before the space charge affects the proportionality. On the other hand, if the primary ionization is too strong, the critical value of  $M$  is smaller. It has been reported<sup>5</sup> that there is a critical maximum value of the charge produced by the multiplication process beyond which proportionality does not hold. That number, obviously, depends on the counter (size, types of gas, etc.).



The events that produce the avalanches of electrons in a proportional counter are statistical in nature. The final multiplication factor  $M$  will not be constant but will show statistical fluctuations. The probability that the multiplication will have the value  $M$  is, according to Snyder,<sup>6</sup> equal to

$$P(M) = \frac{1}{\bar{M}} \exp\left(-\frac{M}{\bar{M}}\right) \quad (5.22)$$

where  $\bar{M}$  = mean multiplication factor. The variance of  $M$  is, from Eq. 5.22,

$$\sigma_M^2 = \bar{M}^2 \quad (5.23)$$

### 5.5.2 The Pulse Shape of a Proportional Counter

The shape of the pulse of a proportional counter is understood as one follows the events that lead to the formation of the pulse. A cylindrical counter will be considered, such as that shown in Fig. 5.14.

Assume that the incident particle generated  $N$  electron-ion pairs at a certain point inside the counter. The electrons start moving toward the wire (anode). As soon as they reach the region of the strong field close to the wire, they produce secondary ionization. Since all the secondary ionization is produced in the small volume surrounding the wire, the amplitude of the output pulse is independent of the position of the primary ionization. The electrons of the secondary ionization are collected quickly by the wire, before the ions have moved appreciably. The ion contribution to the pulse is negligible because the ions cross only a very small fraction of the potential difference on their way to the anode. The pulse developed in the central wire is almost entirely due to the motion of the ions. As the ions move toward the cathode, the voltage pulse on the wire begins to rise: quickly at first, when the ions are crossing the region of the intense electric field, and slower later, when the ions move into the region of low-intensity field. The voltage pulse as a function of time is given by (Kowalski)

$$V(t) = \frac{Q}{2C \ln(b/a)} \ln\left(1 + \frac{b^2}{a^2} \frac{t}{t_{\text{ion}}}\right) \quad (5.24)$$

where  $Q$  is given by Eq. 5.21

$C$  = capacitance of the counter

$t_{\text{ion}}$  = time it takes the ions to reach the cathode

The equation for  $t_{\text{ion}}$  is (Kowalski)

$$t_{\text{ion}} = \frac{P \ln(b/a)}{2V_0 \mu_{\text{ion}}} (b^2 - r^2) \quad (5.25)$$

where  $P$  = gas pressure

$\mu_{\text{ion}}$  = ion mobility in the field of the counter<sup>†</sup>

$r$  = point where the ion was produced

<sup>†</sup>The ion mobility is the proportionality constant between the drift velocity and the reduced field; thus  $w^+ = \mu^+ (E/P)$ .

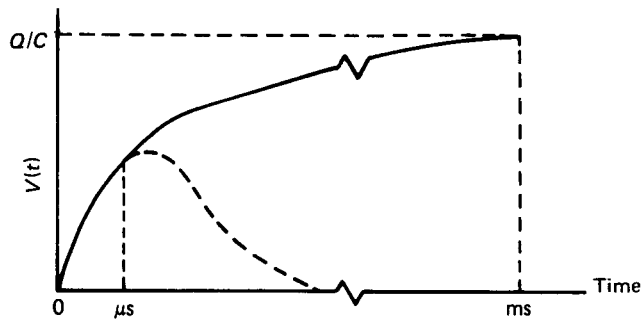


Figure 5.17 The voltage pulse of a proportional counter.

The pulse  $V(t)$  is shown by the solid line of Fig. 5.17. The pulse rises quickly and reaches half of its maximum in time of the order of microseconds. Then it bends and rises at a much slower rate, until about a millisecond later it reaches its final value,  $Q/C$ .

The pulse of Fig. 5.17 was derived under the assumption that all the ions were produced at the same point. In reality, the ions are produced along the track of the incident particle. This modifies the shape of the pulse during its initial rise but it leaves it virtually unaffected during the later period.

The pulse of Fig. 5.17 is unacceptably long, even for a modest counting rate. As in the case of the ionization chamber, the pulse is “chopped off” at some convenient time with the help of a differentiating circuit (Chap. 10). The result will be a pulse shown by the dashed line in Fig. 5.17.

### 5.5.3 The Change of Counting Rate with High Voltage— The High-Voltage Plateau

When a detector is used for the study of a phenomenon involving counting of particles, the investigator would like to be certain that changes in the counting rate are due to changes in the phenomenon under study and not due to changes of the environment such as atmospheric pressure, temperature, humidity, or voltage. For most radiation measurements, all these factors may be neglected except voltage changes.

Consider a gas-filled counter. For its operation, it is necessary to apply HV, usually positive, which may range from +300 to +3000 V, depending on the counter. For the specific counter used in an experiment, the observer would like to know by what fraction the counting rate will change if the HV changes by a certain amount. It is highly desirable to have a system for which the change in the counting rate is negligible, when the HV changes for a reason beyond the control of the investigator (e.g., change in the 110 V provided by the outlet on the wall, which may, in turn, cause a fluctuation in the output of the HV power supply). For this reason, the response of a counting system to such variations

ought to be known. This information is provided by the HV plateau of the counter. The determination of the HV plateau will be discussed below for a proportional counter. However, the experiment and the results are equally applicable for a GM counter.

The HV plateau is obtained by performing the experiment sketched in Fig. 5.18. A radioactive source, emitting a certain type of particles, is placed at a fixed distance from the counter. The signal from the detector is amplified with the help of a preamplifier and an amplifier. It is then fed through a discriminator, and pulses above the discriminator level are counted by the scaler. The counting rate of the scaler is recorded as a function of the HV, the only variable changed. The result of the experiment is shown in Fig. 5.19 (lower curve). Also shown in Fig. 5.19 (upper curve) is a part of the graph of Fig. 5.3 from regions II (ionization) and III (proportional) with the ordinate now shown as pulse height, which is, of course, proportional to the number of ions collected per unit time. The dashed line represents the discriminator level. The shape of the HV plateau is explained as follows.

For very low voltage ( $V < V_A$ ) the counting rate is zero. The source is there, ionization is produced in the counter, pulses are fed into the amplifier and the discriminator, but the scaler does not receive any signal because all the pulses are below the discriminator level. Hence, the counting rate is zero. As the HV increase beyond  $V_A$ , more ionization is produced in the counter, some pulse heights generated in it are above the discriminator level and the counting rate starts increasing. The counting rate keeps increasing with HV, since more and more pulses are produced with a height above the discriminator level. This continues up to the point when  $V \approx V_B$ . For  $V > V_B$ , the ionization is still increasing, the pulse height is also increasing, but all the pulses are now above the discriminator level. Since all the pulses are counted, each *pulse being recorded as one regardless of its height*, the counting rate does not change. This continues up to  $V \approx V_C$ . Beyond that point, the counting rate will start increasing again because the HV is so high that spurious and double pulses may be generated. The counter should not be operated beyond  $V = V_C$ .

The region of the graph between  $V_B$  and  $V_C$  is called the *HV plateau*. It represents the operational range of the counter. Although the manufacturer of the detector provides this information to the investigator, it is standard (and safe) practice to determine the plateau of a newly purchased counter before it is used in an actual measurement for the first time.

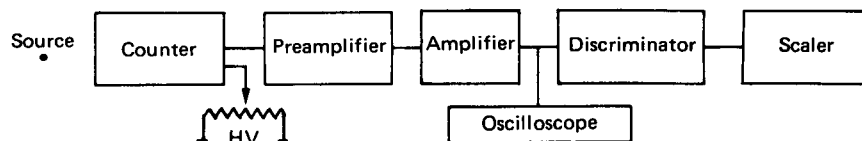


Figure 5.18 Experimental arrangement for the determination of the HV plateau.

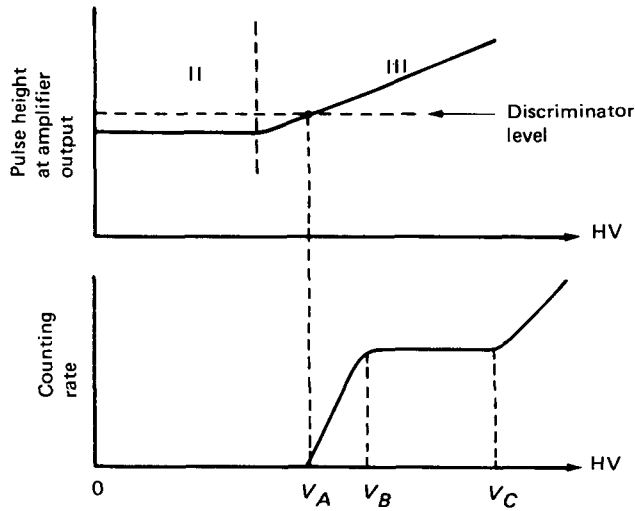


Figure 5.19 The HV plateau (lower curve).

The plateau of Fig. 5.19 is shown as completely flat. For most counters, the plateau has a positive slope that may be due to spurious counts or to increasing efficiency of the counter, or to both of these effects. Investigation of proportional counters<sup>7</sup> showed that the positive slope is the result of an increase in detector efficiency. For GM counters, on the other hand, the slope of the plateau is due to the production of more spurious counts.

The performance of a counter is expressed in terms of the slope of the plateau given in the form

$$\text{Plateau slope} = \frac{\Delta r/r}{\Delta V} \quad (5.26)$$

where  $\Delta r/r$  is the relative change of the counting rate  $r$  for the corresponding change in voltage  $\Delta V$ . Frequently, Eq. 5.26 is expressed in percent change of the counting rate per 100 V change of the high voltage, i.e.,

$$\text{Plateau slope} = \frac{100(\Delta r/r)}{\Delta V} (100) = 10^4 \frac{\Delta r/r}{\Delta V} \quad (5.27)$$

**Example 5.1** What is the change of counting rate per 100 V of the plateau for a counter having the plateau shown in Fig. 5.20?

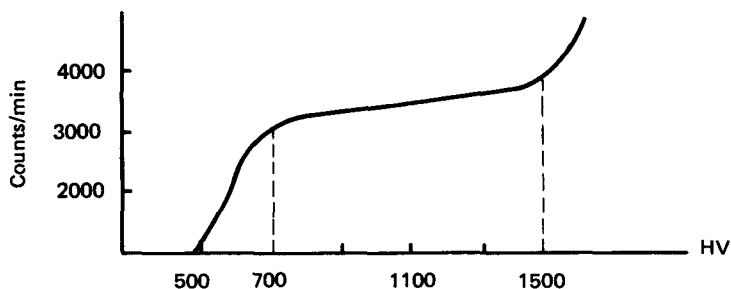


Figure 5.20 The HV plateau used in Example 5.1.

**Answer** The plateau extends from about 700 to 1500 V. The slope over that region is (using Eq. 5.27),

$$\frac{10^4(r_2 - r_1)/r_1}{V_2 - V_1} = \frac{10^4(3800 - 3000)/3000}{1500 - 700} = 3.3\% \text{ per } 100 \text{ V}$$

The location of the plateau of a proportional counter depends on the type of particles being detected. If a source emits two types of particles with significantly different primary ionization, two separate plateaus will be obtained, with the plateau corresponding to the more ionizing particles appearing first. Figure 5.21 shows such a plateau for a proportional counter detecting alpha and beta particles. The existence of two plateaus is a consequence of the fact that in the proportional region, differentiation of the ionization produced by different types of particles is still possible (see region III in Fig. 5.4). In the GM region this distinction is lost, and for this reason GM counters have only one HV plateau regardless of the type of incident radiation (region IV of Fig. 5.4).

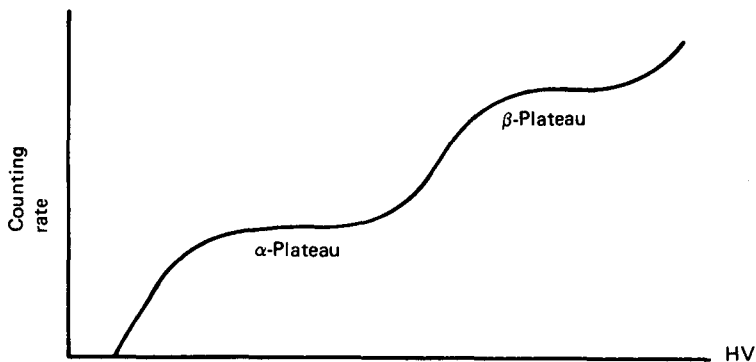


Figure 5.21 Alpha and beta plateaus of a proportional counter.

## 5.6 GEIGER-MÜLLER COUNTERS

### 5.6.1 Operation of a GM Counter and Quenching of the Discharge

A GM counter is a gas counter that operates in region IV of Fig. 5.3. Its construction and operation are in many ways similar to those of a proportional counter. The GM counter is usually cylindrical in shape, like most of the proportional counters. The electric field close to the central wire is so strong that  $N\delta \approx 1$  (see Sec. 5.5.1) and the gas multiplication factor  $M$  is extremely high. In a GM counter, a single primary electron-ion pair triggers a great number of successive avalanches. Therefore, the output signal is independent of the primary ionization.

The operation of the GM counter is much more complicated than that of the proportional counter. When the electrons are accelerated in the strong field surrounding the wire, they produce, in addition to a new avalanche of electrons, considerable excitation of the atoms and molecules of the gas. These excited atoms and molecules produce photons when they deexcite. The photons, in turn, produce photoelectrons in other parts of the counter. Thus the avalanche, which was originally located close to the wire, spreads quickly in most of the counter volume. During all this time, the electrons are continuously collected by the anode wire, while the much slower moving positive ions are still in the counter and form a positive sheath around the anode. When the electrons have been collected, this positive sheath, acting as an electrostatic screen, reduces the field to such an extent that the discharge should stop. However, this is not the case because the positive ions eject electrons when they finally strike the cathode, and since by that time the field has been restored to its original high value, a new avalanche starts and the process just described is repeated. Clearly, some means are needed by which the discharge is permanently stopped or “quenched.” Without quenching, a GM tube would undergo repetitive discharging. There are two general methods of quenching the discharge.

In *external quenching*, the operating voltage of the counter is decreased, after the start of the discharge until the ions reach the cathode, to a value for which the gas multiplication factor is negligible. The decrease is achieved by a properly chosen  $RC$  circuit as shown in Fig. 5.22. The resistance  $R$  is so high that the voltage drop across it due to the current generated by the discharge ( $i_d$ ) reduces the voltage of the counter below the threshold needed for the discharge to start (the net voltage is  $V_0 - i_d R$ ). The time constant  $RC$ , where  $C$  represents the capacitance between anode and ground, is much longer than the time needed for the collection of the ions. As a result, the counter is inoperative for an unacceptably long period of time. Or, in other words, its dead time is too long.

The *self-quenching* method is accomplished by adding to the main gas of the counter a small amount of a polyatomic organic gas or a halogen gas.

The organic gas molecules, when ionized, lose their energy by dissociation rather than by photoelectric processes. Thus, the number of photoelectrons,

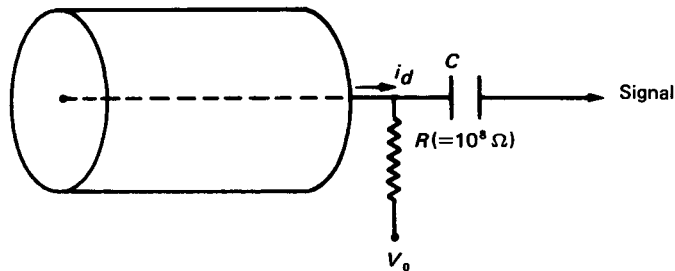


**Figure 5.22** The circuit used for external quenching of a GM counter.

which would spread and continue the avalanche, is greatly reduced. In addition, when the organic ions strike the surface of the cathode, they dissociate instead of causing the ejection of new electrons. Therefore, new avalanches do not start.

GM counters using an organic gas as a quenching agent have a finite lifetime because of the dissociation of the organic molecules. Usually, the GM counters last for  $10^8$  to  $10^9$  counts. The lifetime of a GM detector increases considerably if a halogen gas is used as the quenching agent. The halogen molecules also dissociate during the quenching process, but there is a certain degree of regeneration of the molecules, which greatly extends the useful lifetime of the counter.

### 5.6.2 The Pulse Shape and the Dead Time of a GM Counter

The signal of a GM counter is formed in essentially the same way as the signal of a proportional counter and is given by the same equation, Eq. 5.24. For GM counters the signal is the result of the sum of the contributions from all the positive ion avalanches produced throughout the volume of the counter. The final pulse is similar in shape to that shown in Fig. 5.17, except that the pulse rises much slower. The shape and height of GM counter pulses are not very important because the pulse is only used to signal the presence of the particle and nothing else. However, how one pulse affects the formation of the next one is important.

As discussed in Sec. 5.6.1, during the formation of a pulse, the electric field in the counter is greatly reduced because of the presence of the positive ions around the anode. If a particle arrives during that period, no pulse will be formed because the counter is insensitive. The insensitivity lasts for a certain time, called the dead time of the counter. Then, the detector slowly recovers, with the pulse height growing exponentially during the *recovery* period. This is illustrated in Fig. 5.23, which shows the change of the voltage and pulse for a typical GM counter. Typical values of dead time are from 100 to 300  $\mu\text{s}$ . If the dead time is 100  $\mu\text{s}$  and the counting rate is 500 counts/s, there is going to be a

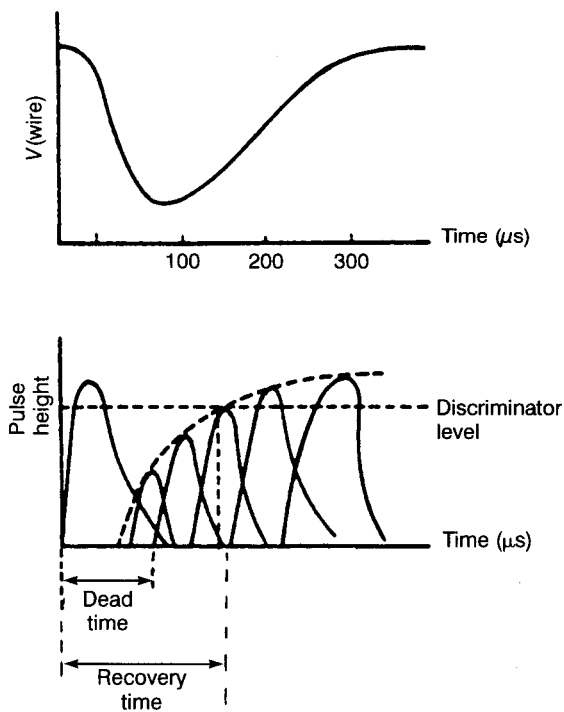


**Figure 5.23** Dead time and recovery time for a GM counter.

5 percent loss of counts due to dead time. Correction for dead time is described in Sec. 2.21.

## 5.7 GAS-FLOW COUNTERS

The gas counters described so far are all sealed. That is, the counter is a closed volume filled with a gas at a certain pressure. The radiation source is placed outside the detector; therefore, the particles have to penetrate the wall of the counter to be counted. In doing so, some particles may be absorbed by the wall and some may be backscattered; in the case of charged particles, they will all lose a certain fraction of their energy. To minimize these effects, most commercial gas counters have a thin window through which the radiation enters the counter. The window may still be too thick for some alpha and low-energy beta particles. For this reason, counters have been developed with the capability of having the source placed inside the chamber.

Gas counters of this type are called *gas-flow counters*. Their name comes from the fact that the gas flows continuously through the counter during operation. This is necessary because the detector cannot be sealed if the source is placed inside the chamber.



Gas-flow counters come in different geometries. Probably the most common one is that of the hemispherical detector as shown in Fig. 5.24. The high voltage is applied to a wire attached to the top of the hemisphere. The gas flows slowly through the counter, the flow rate being controlled by a regulator. At the exit, the gas goes through a liquid (e.g., some oil) and forms bubbles as it comes out. The formation of the bubbles indicates that the gas is flowing, and the rate of bubble formation gives an idea of the gas-flow rate.

Counting with gas-flow counters involves the following steps:

1. The chamber is opened and the sample is placed in its designated location inside the chamber.
2. The chamber is closed.
3. Gas from the gas tank is allowed to flow rapidly through the volume of the counter and purge it (for a few minutes).
4. After the counter is purged, the gas-flow rate is considerably reduced, to a couple of bubbles per second, and counting begins.

There are two advantages in placing the sample inside the detector:

1. The particles do not have to penetrate the window of the counter, where they might be absorbed, scattered out of the detector, or lose energy.
2. Close to 50 percent of the particles emitted by the source have a chance to be recorded in a hemispherical counter, or close to 100 percent in a spherical counter. If the source is placed outside the detector, there are always less than 50 percent of the particles entering the detector.

A hemispherical counter is also called a  $2\pi$  counter, while a spherical counter with the source located at its center is called a  $4\pi$  counter. Figure 5.24 shows a  $2\pi$  counter.

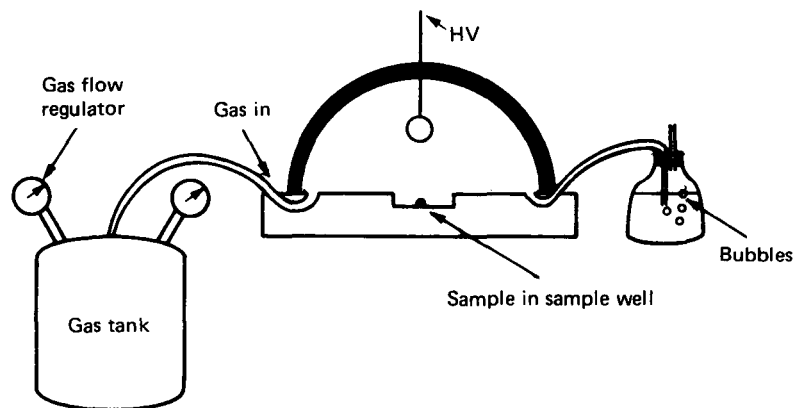


Figure 5.24 A hemispherical ( $2\pi$ ) gas-flow counter.

Gas-flow counters may operate as proportional or GM counters. In fact, there are commercial models that may operate in one or the other region depending on the voltage applied and the gas used. In a proportional gas-flow counter, the gas is usually methane or a mixture of argon and methane. In the GM region, the gas is a mixture of argon and isobutane.

In some gas-flow counter models, there is provision for placing a very thin window between the sample and the sensitive volume of the counter to reduce the effects of slight contamination of the sample well or of static charges that interfere with the measurement. In the counter of Fig. 5.24, the thin window will be placed on top of the sample well. A different arrangement is shown in Fig. 5.25.

Gas-flow counters are used as low-background alpha-beta detection systems. Requirements for low-background measurements arise in cases where the level of activity from the sample is very low, compared to background. Examples of such cases are samples that monitor contamination of water supplies or of air or ground.

There are commercially available systems that have a background counting rate of less than 1 count/min for betas and a considerably lower rate for alphas. Such a low background is achieved by shielding the counter properly (surrounding it with lead) and using electronic means to reject most of the background radiation. A system offered by one of the manufacturers uses two detectors. The first is the gas-flow counter and the second is a cosmic-ray detector (Fig. 5.26). The two detectors are operated in *anticoincidence* (see Sec. 10.8), which means that events due to particles going through both detectors (e.g., cosmic rays or other radiation from the environment) will not be counted. Only pulses produced by the activity of the sample in the gas-flow counter will be recorded.

Discrimination between alphas and betas can be achieved in many ways. The two methods most frequently used with gas-flow counters are based on range and energy differences. Before these methods are discussed, the reader

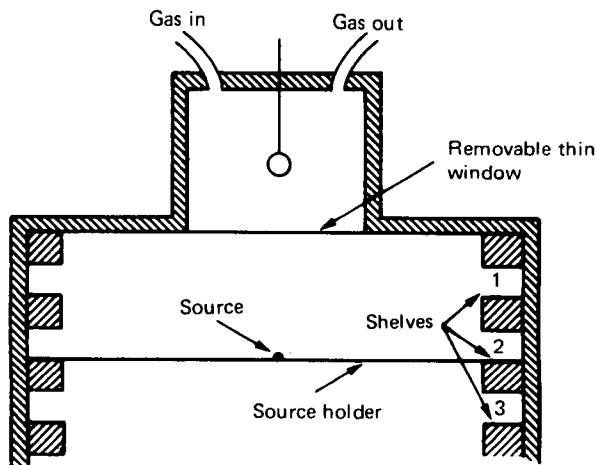


**Figure 5.25** A gas-flow counter with removable thin window and movable source holder.

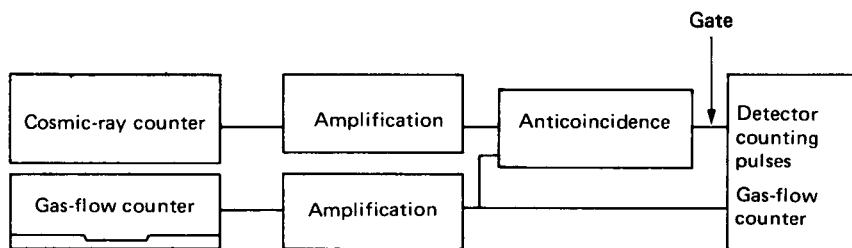


**Figure 5.26** A low-background alpha-beta counting system utilizing two counters and anticoincidence. The anticoincidence output gates the scaler to count only pulses from the gas-flow counter.

should recall that the maximum energy of most beta emitters is less than 2 MeV while the energy of alphas from most alpha emitters is 5–6 MeV.

Because the range of alphas is much shorter than that of betas, a sample can be analyzed for alpha and beta activity by counting it twice: once with a thin foil covering it to stop the alphas, and a second time without the foil to record alphas and betas.

Energy discrimination is based on the difference in pulse height produced by the two types of particles: the alphas, being more energetic, produce higher pulses; thus a simple discriminator at an appropriate level can reject the beta pulses.

### 5.7.1 The Long-Range Alpha Detector (LRAD)

A variation of the gas-flow counter has been developed<sup>8,9</sup> for the detection of alpha contamination. Common alpha particle detectors are limited by the short range of alphas in air. For example, the range of a 6-MeV alpha in air at normal temperature and pressure is about 46 mm. To circumvent this limitation, the LRAD does not measure the alphas directly. Instead, as shown schematically in Fig. 5.27, the ions created by the alphas in air are transported, with the help of airflow, and directed into an ion chamber. There, the current created by the ions is measured by an electrometer. Since the number of ions produced is proportional to the strength of the alpha source, the signal of the electrometer is also proportional to the alpha source strength.

In principle, a similar detector could be developed for any particle that produces ions. However, particles like electrons, gammas, and neutrons generate a much smaller number of ions than alpha particles do, traveling over the same distance. For this reason, an LRAD-type detector would have a smaller sensitivity for these other particles than for alphas. Of course, an LRAD-type detector would operate satisfactorily for the detection of protons, deuterons, and other heavy ions.

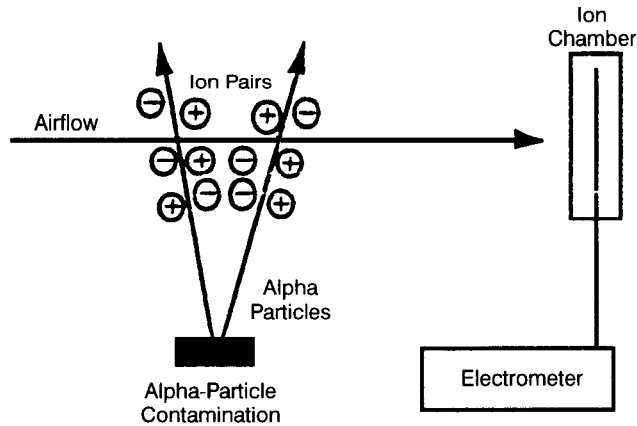


**Figure 5.27** The LRAD detects ions generated by alphas in air with the help of an ion chamber and an electrometer.

### 5.7.2 Internal Gas Counting

An alternative to the gas-flow counter is *internal gas counting*, which is used with low-energy  $\beta$ -emitters. In internal gas counting, a gaseous form of the radioisotope is introduced into the counter (usually a proportional counter) along with the counting gas. As with gas-flow counters, by having the source inside the counter, losses in the window are avoided and an increase in efficiency is achieved by utilizing a  $4\pi$  geometry.

Internal gas counting requires that corrections be made for wall and end effects and for the decrease in electric field intensity at the ends.<sup>10-12</sup> One way to reduce the end effect is to use a spherical proportional counter,<sup>13</sup> in which the anode wire is stretched along a diameter and the cathode is, of course, spherical. The electric field inside the sphere is

$$E = \frac{V}{\ln(b/a)} \frac{1}{r} \quad (5.2)$$

At a certain distance  $r$  from the anode, the electric field becomes stronger at the ends of the anode because  $b$ , the radius of the cathode, gets smaller. However, the supports of the wire tend to reduce the field. By properly adjusting the supports, one may make the field uniform. In cylindrical counters, corrections for end effects are applied by a length-compensation method.<sup>10</sup>

Internal gas counting is used for the production of standards. Using this technique, the National Bureau of Standards produced standards of  $^3\text{H}$ ,  $^{14}\text{C}$ ,  $^{37}\text{A}$ ,  $^{85}\text{K}$ ,  $^{131m}\text{Xe}$ , and  $^{133}\text{Xe}$ .

## 5.8 RATE METERS

A rate meter is a device that measures the average rate of incoming pulses. Rate meters are used for continuous monitoring of an event, where the average counting rate versus time rather than the instantaneous counting rate is needed.

The basic operation of a rate meter is to feed a known charge per pulse into a capacitor that is shunted by a resistor (Fig. 5.28). Let

$r$  = counting rate (pulses/s)

$q$  = charge per pulse

$V$  = voltage across capacitor

$R$  = resistance

$Q$  = capacitor charge

The net rate of change of  $Q$  with respect to time is given by

$$\frac{dQ}{dt} = (\text{charge fed by pulses/s}) - (\text{charge flowing through resistor})$$

or

$$\frac{dQ}{dt} = rq - \frac{Q}{RC} \quad (5.28)$$

The solution of this differential equation with the initial condition  $Q(0) = 0$  is

$$Q(t) = rqRC(1 - e^{-t/RC}) \quad (5.29)$$

or, if one writes the result in terms of the output voltage,

$$V(t) = \frac{Q(t)}{C} = rqR(1 - e^{-t/RC}) \quad (5.30)$$

For time  $t \gg RC$ , equilibrium is reached and the value of the voltage is

$$V_{\infty} = rqR \quad (5.31)$$

The signal of a rate meter is the voltage  $V_{\infty}$  given by Eq. 5.31. Notice that  $V_{\infty}$  is independent of the capacitance  $C$  and proportional to the counting rate  $r$ . The voltage  $V_{\infty}$  is measured with an appropriate voltmeter.

If a pulse-type detector is used, the counts accumulated in the scaler have a statistical uncertainty that is calculated as shown in Chap. 2. If a rate meter is used, what is the uncertainty of the measurement? To obtain the uncertainty, one starts with Eq. 5.29, which gives the charge of the capacitor  $C$ . It is important to note that the charge changes exponentially with time. Thus, the contribution of the charge from a pulse arriving at  $t = 0$  is not instantaneous but continues for a period of time.

Consider an observation point  $t_0$  (Fig. 5.29). The standard deviation  $\sigma_Q$  of the charge collected at  $t = t_0$  is the result of contributions from pulses having

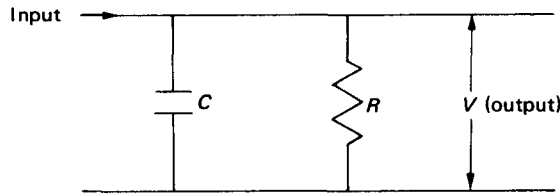


Figure 5.28 The circuit of a rate meter.

arrived earlier. If the counting rate is  $r$ , the number of pulses in a time interval  $\Delta t$  is, on the average,  $r \Delta t$ . The statistical uncertainty of this number is  $\pm \sqrt{r \Delta t}$ , or the uncertainty of the charge is  $\pm q\sqrt{r \Delta t}$ . One can show that a single pulse arriving at time  $t$  contributes to the signal at time  $t = t_0$ , an amount of charge equal to  $q \exp[-(t_0 - t)/RC]$ . Therefore, the variance of the charge at time  $t = t_0$  is

$$\sigma_Q^2 = \int_0^{t_0} (q\sqrt{r} dt e^{-(t_0-t)/RC})^2 \quad (5.32)$$

Integration of Eq. 5.32 gives the result

$$\sigma_Q^2 = 0.5q^2 r RC (1 - e^{-2t_0/RC}) \quad (5.33)$$

For  $t_0 \gg RC$ , Eq. 5.33 takes the form

$$\sigma_Q = q \sqrt{\frac{r(RC)}{2}} \quad (5.34)$$

At equilibrium,  $Q = r q RC$  (from Eq. 5.29); therefore,

$$\sigma_r = \frac{\sigma_Q}{qRC} = \sqrt{\frac{r}{2RC}} \quad (5.35)$$

and

$$\frac{\sigma_r}{r} = \sqrt{\frac{1}{2RCr}} \quad (5.36)$$

The quantity  $RC$  is the time constant of the circuit shown in Fig. 5.28. Equation 5.36 states that any instantaneous reading on a rate meter has a relative standard error equal to that of a total number of counts obtained by counting for a time equal to  $2RC$  (assuming the background is negligible).

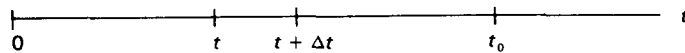


Figure 5.29 Pulses arriving during  $\Delta t$ , and at  $t$ , contribute to  $\sigma_Q$  at  $t = t_0$ .

## 5.9 GENERAL COMMENTS ABOUT CONSTRUCTION OF GAS-FILLED DETECTORS

This section summarizes the important characteristics of gas counters.

**Geometry.** Parallel-plate counters are almost exclusively ionization chambers. The intense fields needed for gas multiplication can be produced only in cylindrical or spherical geometry.

In the cylindrical geometry, which is the most frequently used, the strong electric field exists close to the central wire. The wire is usually made of tungsten or platinum. It has a diameter of 25–100  $\mu\text{m}$  (few mills of an inch); it must be uniform in radius, without any bends or kinks, and be placed concentrically with the outer cylinder. Of particular importance is the smoothness of the central wire. Any kinks or tiny specks of material attached to its surface amount to pointed tips where very high electric fields are generated. Such a high field is a source of spurious discharges that interfere with counting.

**Gases and pressures used.** For ionization chambers, almost any gas or pressure may be used. Even atmospheric air has been used.

For proportional or GM counters, the noble gases—argon in particular—are normally used. A small percentage of additional gases is also used for quenching purposes. In proportional counters, methane is frequently added to the main gas. The so-called P-10 mixture, consisting of 90 percent argon and 10 percent methane, is extensively used. Another mixture is 4 percent isobutane and 96 percent helium. Several gas pressures have been used. As Figs. 5.15 and 5.16 show, the gas multiplication depends on the pressure. Usually the pressure is less than 1 atm. Of course, gas-flow counters operate at ambient pressure.

As discussed in Sec. 5.6.1, the quenching gas in a GM counter is either an organic polyatomic molecule such as ethyl alcohol, or a halogen such as bromine or chlorine. A typical mixture is 0.1 percent chlorine in neon. The gas pressure in a GM counter is, in most cases, less than 1 atm. The pressure affects the operating voltage.

**Counter window.** When the source is placed outside the counter, it is very important for the radiation to enter the counter after traversing as thin a wall material as possible. Any material in the path of radiation may scatter, absorb, or cause energy loss. This is particularly critical in the measurement of alphas and low-energy betas, which have a very short range. It is not important for neutron and gamma counters.

All counters have walls as thin as possible (or practical), but in addition, many commercial designs have an area on the surface of the counter designated as the “window,” consisting of a very thin material. In cylindrical counters, the window is usually the front end of the cylinder (the other end houses electrical connectors). There are some cylindrical counters with windows located on the cylindrical surface.

Materials and thicknesses of windows are

1. Glass, down to  $0.30\text{--}0.40 \text{ kg/m}^2$  ( $100 \mu\text{m}$ )
2. Aluminum,  $0.25\text{--}0.30 \text{ kg/m}^2$  ( $100 \mu\text{m}$ )
3. Steel,  $0.60\text{--}0.80 \text{ kg/m}^2$  ( $80 \mu\text{m}$ )
4. Mica,  $0.01 \text{ kg/m}^2$  ( $3 \mu\text{m}$ )
5. Mylar (plain or aluminized),  $0.01 \text{ kg/m}^2$
6. Special ultrathin membranes or foils,  $\sim 10^{-3} \text{ kg/m}^2$

## PROBLEMS

- 5.1 Sketch the HV plateau of a counter, if all the pulses out of the amplifier have exactly the same height.
- 5.2 How would the sketch of Prob. 5.1 change if there are two groups of pulses out of the amplifier (two groups, two different pulse heights)?
- 5.3 Sketch counting rate versus discriminator threshold, assuming that the electronic noise consists of pulses in the range  $0 < V < 0.1 \text{ V}$  and all the pulses due to the source have height equal to  $1.5 \text{ V}$ .
- 5.4 In a cylindrical gas counter with a central wire radius equal to  $25 \mu\text{m}$  ( $0.001 \text{ in}$ ), outer radius  $25 \text{ mm}$  ( $\sim 1 \text{ in}$ ), and  $1000 \text{ V}$  applied between anode and cathode, what is the distance from the center of the counter at which an electron gains enough energy in  $1 \text{ mm}$  of travel to ionize helium gas? (Take  $23 \text{ eV}$  as the ionization potential of helium.)
- 5.5 A GM counter with a mica window is to be used for measurement of  $^{14}\text{C}$  activity. What should the thickness of the window be if it is required that at least 90 percent of the  $^{14}\text{C}$  betas enter the counter?
- 5.6 What is the minimum pressure required to stop 6-MeV alphas inside the argon atmosphere of a spherical gas counter with a 25-mm radius? Assume the alpha source is located at the center of the counter.
- 5.7 What is the ratio of the saturation ionization currents for a chamber filled with He versus one filled with  $\text{CH}_4$  (other things being equal)?
- 5.8 Show that the variance of  $M$  is equal to  $\bar{M}^2$  if the probability distribution is given by Eq. 5.22.
- 5.9 Calculate the maximum value of the positive ion time given by Eq. 5.25 for a cylindrical counter with a cathode radius equal to  $19 \text{ mm}$  ( $\sim 0.75 \text{ in}$ ) and a central anode wire with a radius of  $25 \mu\text{m}$  ( $\sim 0.001 \text{ in}$ ). The high voltage applied is  $1000 \text{ V}$ ; the pressure of the gas is  $13.3 \text{ kPa}$  ( $10 \text{ cmHg}$ ), and the mobility of the ions is  $13.34 \text{ Pa m}^2/(\text{V s})$ .
- 5.10 The observed counting rate of a counter is  $22,000 \text{ counts/min}$ . What is the error in the true counting rate if the dead time is  $300 \mu\text{s}$  and no dead-time correction is applied?

## BIBLIOGRAPHY

- Eichholz, G. G., and Poston, J. W., *Nuclear Radiation Detection*, Lewis Publishers, Chelsea, Michigan, 1985.
- Fenyves, E., and Haiman, O., *The Physical Principles of Nuclear Radiation Measurements*, Academic Press, New York, 1969.
- Franzen, W., and Cochran, L. W., "Pulse Ionization Chambers and Proportional Counters," in A. H. Snell (ed.), *Nuclear Instruments and Their Uses*, Wiley, New York, 1962.



Gillespie, A. B., *Signal, Noise and Resolution in Nuclear Counter Amplifiers*, McGraw-Hill, New York, 1953.

Knoll, G. F., *Radiation Detection and Measurement*, 2nd ed., Wiley, New York, 1989.

Kowalski, E., *Nuclear Electronics*, Springer-Verlag, New York-Heidelberg-Berlin, 1970.

Price W. J., *Nuclear Radiation Detection*, McGraw-Hill, New York, 1964.

Rossi, B. B., and Staub, H. H., *Ionization Chambers and Counters*, McGraw-Hill, New York, 1949.

Tait, W. H., *Radiation Detection*, Butterworth, London, 1980.

## REFERENCES

1. Diethorn, W., NYO-0628, 1956.
2. Kiser, R. W., *Appl. Sci. Res.* **8B**:183 (1960).
3. Williams, W., and Sara, R. I., *Int. J. Appl. Rad. Isotopes* **13**:229 (1962).
4. Bennett, E. F., and Yule, T. J., ANL-7763, 1971.
5. Hanna, G. C., Kirkwood, H. W., and Pontecorvo, B., *Phys. Rev.*, **75**:985 (1949).
6. Snyder, H. S., *Phys. Rev.* **72**:181 (1947).
7. Champion, P. J., *Nucl. Instrum. Meth.* **112**:75 (1973).
8. MacArthur, D. W., Allander, K. S., Bounds, J. A., Butterfield, K. B., and McAtee, J. L., *Health Phys.* **63**:324 (1992).
9. MacArthur, D. W., Allander, K. S., Bounds, J. A., and McAtee, J. L., *Nucl. Technol.* **102**:270 (1993).
10. Mann, W. B., Seliger, H. H., Marlow, W. F., and Medlock, R. W., *Rev. Sci. Instrum.* **31**:690 (1960).
11. Garfunkel, S. B., Mann, W. B., Schima, F. J., and Unterweger, M. P., *Nucl. Instrum. Meth.* **112**:59 (1973).
12. Bambynek, W., *Nucl. Instrum. Meth.* **112**:103 (1973).
13. Benjamin, P. W., Kemsholl, C. D., and Redfearn, J., *Nucl. Instrum. Meth.* **59**:77 (1968).

**SCINTILLATION DETECTORS**

**6.1 INTRODUCTION**

Scintillators are materials—solids, liquids, gases—that produce sparks or scintillations of light when ionizing radiation passes through them. The first solid material to be used as a particle detector was a scintillator. It was used by Rutherford, in 1910, in his alpha-scattering experiments. In Rutherford's experimental setup, alpha particles hit a zinc sulfide screen and produced scintillations, which were counted with or without the help of a microscope—a very inefficient process, inaccurate and time consuming. The method was abandoned for about 30 years and was remembered again when advanced electronics made possible amplification of the light produced in the scintillator.

The amount of light produced in the scintillator is very small. It must be amplified before it can be recorded as a pulse or in any other way. The amplification or multiplication of the scintillator's light is achieved with a device known as the *photomultiplier tube* (or *phototube*). Its name denotes its function: it accepts a small amount of light, amplifies it many times, and delivers a strong pulse at its output. Amplifications of the order of  $10^6$  are common for many commercial photomultiplier tubes. Apart from the phototube, a detection system that uses a scintillator is no different from any other (Fig. 6.1).

The operation of a scintillation counter may be divided into two broad steps:

1. Absorption of incident radiation energy by the scintillator and production of photons in the visible part of the electromagnetic spectrum

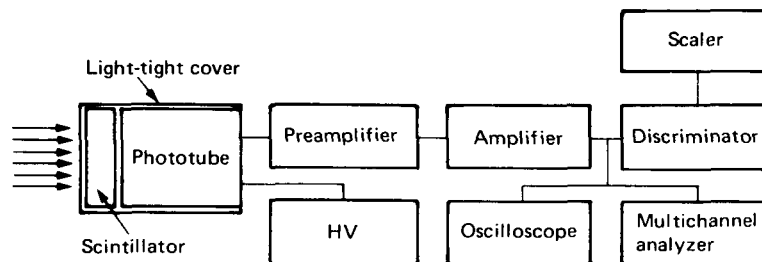


**Figure 6.1** A detection system using a scintillator.

2. Amplification of the light by the photomultiplier tube and production of the output pulse

The sections that follow analyze these two steps in detail. The different types of scintillators are divided, for the present discussion, into three groups:

1. Inorganic scintillators
2. Organic scintillators
3. Gaseous scintillators

## 6.2 INORGANIC (CRYSTAL) SCINTILLATORS

Most of the inorganic scintillators are crystals of the alkali metals, in particular alkali iodides, that contain a small concentration of an impurity. Examples are NaI(Tl), CsI(Tl), CaI(Na), LiI(Eu), and CaF<sub>2</sub>(Eu). The element in parentheses is the impurity or activator. Although the activator has a relatively small concentration—e.g., thallium in NaI(Tl) is 10<sup>-3</sup> on a per mole basis—it is the agent that is responsible for the luminescence of the crystal.

### 6.2.1 The Mechanism of the Scintillation Process

The luminescence of inorganic scintillators can be understood in terms of the allowed and forbidden energy bands of a crystal. The electronic energy states of an atom are discrete energy levels, which in an energy-level diagram are represented as discrete lines. In a crystal, the allowed energy states widen into bands (Fig. 6.2). In the ground state of the crystal, the uppermost allowed band that contains electrons is completely filled. This is called the *valence band*. The next allowed band is empty (in the ground state) and is called the *conduction band*. An electron may obtain enough energy from incident radiation to move from the valence to the conduction band. Once there, the electron is free to move anywhere in the lattice. The removed electron leaves behind a hole in the valence band, which can also move. Sometimes, the energy given to the electron

is not sufficient to raise it to the conduction band. Instead, the electron remains electrostatically bound to the hole in the valence band. The electron-hole pair thus formed is called an *exciton*. In terms of energy states, the exciton corresponds to elevation of the electron to a state higher than the valence but lower than the conduction band. Thus, the exciton states form a thin band, with the upper level coinciding with the lower level of the conduction band (Fig. 6.2). The width of the exciton band is of the order of 1 eV, whereas the gap between valence and conduction bands is of the order of 8 eV.

In addition to the exciton band, energy states may be created between valence and conduction bands because of crystal imperfections or impurities. Particularly important are the states created by the activator atoms such as thallium. The activator atom may exist in the ground state or in one of its excited states. Elevation to an excited state may be the result of a photon absorption, or of the capture of an exciton, or of the successive capture of an electron and a hole. The transition of the impurity atom from the excited to the ground state, if allowed, results in the emission of a photon in times of the order of  $10^{-8}$  s. If this photon has a wavelength in the visible part of the electromagnetic spectrum, it contributes to a scintillation. Thus, production of a scintillation is the result of the occurrence of these events:

1. Ionizing radiation passes through the crystal.
2. Electrons are raised to the conduction band.
3. Holes are created in the valence band.

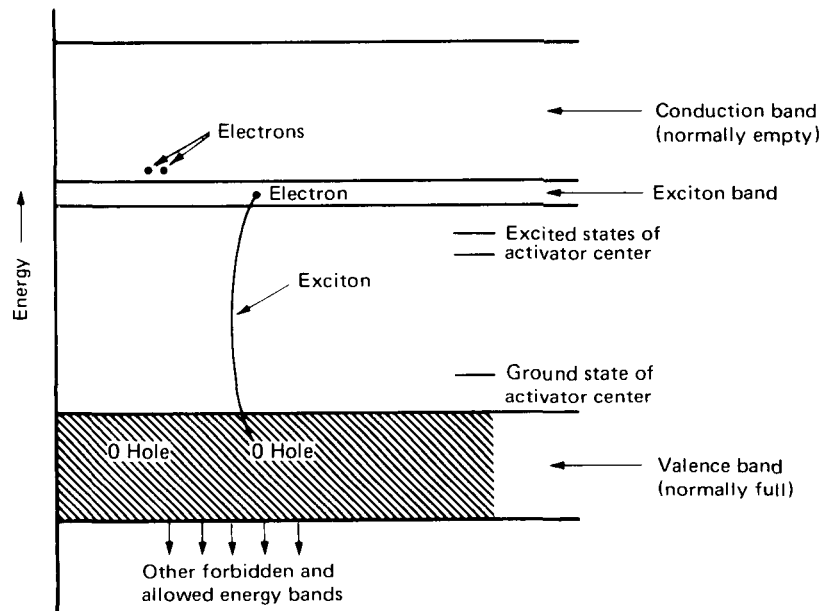
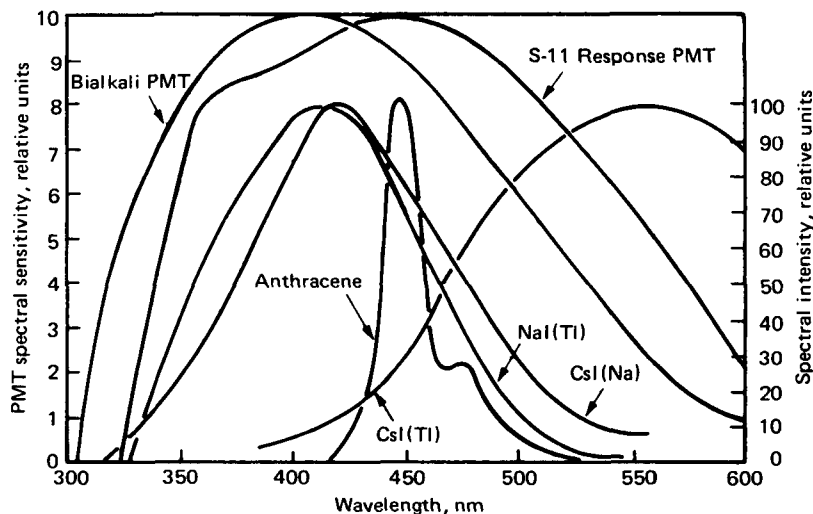


Figure 6.2 Allowed and forbidden energy bands of a crystal



**Figure 6.3** Emission spectra of NaI(Tl), CsI(Tl), CsI(Na), and anthracene, compared to the spectral response of two photocathode materials. PMT, photomultiplier tube (from Harshaw Research Laboratory Report, Harshaw Chemical Company, 1978).

4. Excitons are formed.
5. Activation centers are raised to the excited states by absorbing electrons, holes, and excitons.
6. Deexcitation is followed by the emission of a photon.

The light emitted by a scintillator is primarily the result of transitions of the activator atoms, and not of the crystal. Since most of the incident energy goes to the lattice of the crystal—eventually becoming heat—the appearance of luminescence produced by the activator atoms means that energy is transferred from the host crystal to the impurity. For NaI(Tl) scintillators, about 12 percent of the incident energy appears as thallium luminescence.<sup>1</sup>

The magnitude of light output and the wavelength of the emitted light are two of the most important properties of any scintillator. The light output affects the number of photoelectrons generated at the input of the photomultiplier tube (see Sec. 6.5), which in turn affects the pulse height produced at the output of the counting system. Information about the wavelength is necessary in order to match the scintillator with the proper photomultiplier tube. Emission spectra of NaI(Tl), CsI(Na), and CsI(Tl) are shown in Fig. 6.3. Also shown in Fig. 6.3 are the responses of two phototube cathode materials. Table 6.1 gives the most important properties of some inorganic scintillators.

The light output of the scintillators depends on temperature. Figure 6.4 shows the temperature response of NaI(Tl), Cs(Tl), and CsI(Na).

**Table 6.1 Properties of Certain Inorganic Scintillators**

Material	Wavelength of maximum emission (nm)	Scintillation efficiency (relative, %)	Decay time ( $\mu$ s)	Density ( $10^3$ kg/m <sup>3</sup> )
NaI(Tl)	410	100	0.23	3.67
CaF <sub>2</sub> (Eu)	435	50	0.94	3.18
CsI(Na)	420	80	0.63	4.51
CsI(Tl)	565	45	1.00	4.51
Bi <sub>4</sub> Ge <sub>3</sub> O <sub>12</sub>	480	8	0.30	7.13
CdWO <sub>4</sub>	530	20	0.90	7.90
<sup>6</sup> LiI(Eu)	470	30	0.94	3.49

### 6.2.2 Time Dependence of Photon Emission

Since the photons are emitted as a result of decays of excited states, the time of their emission depends on the decay constants of the different states involved. Experiments show that the emission of light follows an exponential decay law of the form

$$N(t) = N_0 e^{-t/T} \quad (6.1)$$

where  $N(t)$  = number of photons emitted at time  $t$

$T$  = decay time of the scintillator (see Table 6.1)

Most of the excited states in a scintillator have essentially the same lifetime  $T$ . There are, however, some states with longer lifetimes contributing a slow component in the decay of the scintillator known as *afterglow*. It is present to some extent in all inorganic scintillators and may be important in certain measurements where the integrated output of the phototube is used. Two scintillators with negligible afterglow are CaF<sub>2</sub>(Eu) and Bi<sub>4</sub>Ge<sub>3</sub>O<sub>12</sub> (bismuth orthogermanate).

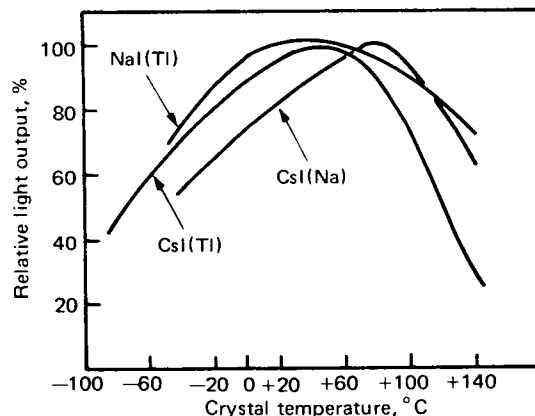


**Figure 6.4** Temperature dependence of light output of NaI(Tl), CsI(Tl), and CsI(Na) (from Harshaw Research Laboratory Report).

In a counting system using a scintillator, the light produced by the crystal is amplified by a photomultiplier tube and is transformed into an electric current having the exponential behavior given by Eq. 6.1. This current is fed into an  $RC$  circuit as shown in Fig. 6.5, and a voltage pulse is produced of the form

$$V(t) = V_{\infty}(e^{-t/RC} - e^{-t/T}) \quad (6.2)$$

In practice, the value of  $RC$  is selected to be of the order of a few hundreds of microseconds. Thus, for short times—i.e.,  $t \ll RC$ , which is the time span of interest—Eq. 6.2 takes the form

$$V(t) = V_{\infty}(1 - e^{-t/T}) \quad (6.2a)$$

Notice that the rate at which the pulse rises (risetime) is determined by the decay time  $T$ . In certain measurements, e.g., coincidence-anticoincidence measurements (Chap. 10), the timing characteristics of the pulse are extremely important.

### 6.2.3 Important Properties of Certain Inorganic Scintillators

**NaI(Tl).** NaI(Tl) is the most commonly used scintillator for gamma rays. It has been produced in single crystals of up to 0.75 m ( $\sim 30$  in) in diameter and of considerable thickness (0.25 m  $\approx 10$  in). Its relatively high density ( $3.67 \times 10^3$  kg/m<sup>3</sup>) and high atomic number combined with the large volume make it a

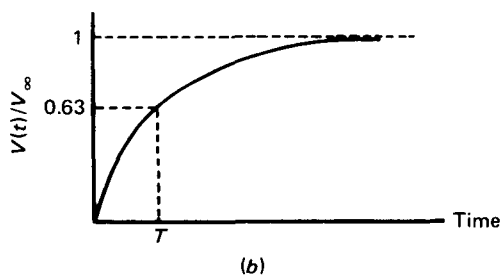
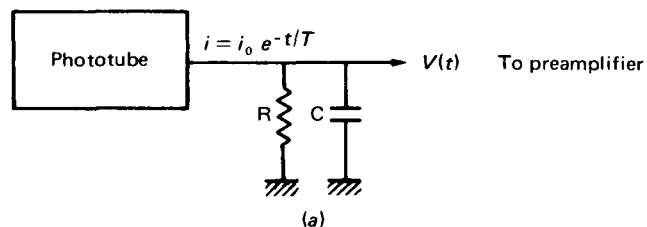


**Figure 6.5** (a) A voltage pulse results from the exponential current. (b) The shape of the pulse for  $RC \gg T$ .

$\gamma$ -ray detector with very high efficiency. Although semiconductor detectors (Chap. 7 and 12) have better energy resolution, they cannot replace the NaI(Tl) in experiments where large detector volumes are needed.

The emission spectrum of NaI(Tl) peaks at 410 nm, and the light-conversion efficiency is the highest of all the inorganic scintillators (Table 6.1). As a material, NaI(Tl) has many undesirable properties. It is brittle and sensitive to temperature gradients and thermal shocks. It is also so hygroscopic that it should be kept encapsulated at all times. NaI always contains a small amount of potassium, which creates a certain background because of the radioactive  $^{40}\text{K}$ .

**CsI(Tl).** CsI(Tl) has a higher density ( $4.51 \times 10^3 \text{ kg/m}^3$ ) and higher atomic number than NaI; therefore its efficiency for gamma detection is higher. The light-conversion efficiency of CsI(Tl) is about 45 percent of that for NaI(Tl) at room temperature. At liquid nitrogen temperatures (77K), pure CsI has a light output equal to that of NaI(Tl) at room temperature and a decay constant equal to  $10^{-8} \text{ s}$ .<sup>2</sup> The emission spectrum of CsI(Tl) extends from 420 to about 600 nm.

CsI is not hygroscopic. Being softer and more plastic than NaI, it can withstand severe shocks, acceleration, and vibration, as well as large temperature gradients and sudden temperature changes. These properties make it suitable for space experiments. Finally, CsI does not contain potassium.

**CsI(Na).** The density and atomic number of CsI(Na) are the same as those of CsI(Tl). The light-conversion efficiency is about 85 percent of that for NaI(Tl). Its emission spectrum extends from 320 to 540 nm (see Fig. 6.3). CsI(Na) is slightly hygroscopic.

**CaF<sub>2</sub>(Eu).** CaF<sub>2</sub>(Eu) consists of low-atomic-number materials, and for this reason makes an efficient detector for  $\beta$  particles<sup>3</sup> and X-rays<sup>4</sup> with low gamma sensitivity. It is similar to Pyrex and can be shaped to any geometry by grinding and polishing. Its insolubility and inertness make it suitable for measurements involving liquid radioisotopes. The light-conversion efficiency of CaF<sub>2</sub>(Eu) is about 50 percent of that for NaI(Tl). The emission spectrum extends from about 405 to 490 nm.

**LiI(Eu).** LiI(Eu) is an efficient thermal-neutron detector through the reaction  ${}^6_3\text{Li}(n, \alpha){}^3_1\text{H}$ . The alpha particle and the triton, both charged particles, produce the scintillations. LiI has a density of  $4.06 \times 10^3 \text{ kg/m}^3$ , decay time of about 1.1  $\mu\text{s}$ , and emission spectrum peaking at 470 nm. Its conversion efficiency is about one-third of that for NaI. It is very hygroscopic and is subject to radiation damage as a result of exposure to neutrons.

**Other inorganic scintillators.** Many other scintillators have been developed for special applications. Examples are  $\text{Bi}_4\text{Ge}_3\text{O}_{12}$ ,  $\text{CdWO}_4$ , and more recently<sup>5</sup>  $\text{MF}_2:\text{UF}_4:\text{CeF}_3$ , where M stands for one of the following: Ca, Sr, Ba. This last



scintillator, containing 2 percent  $\text{UF}_4$  and using Ce as the fluorescing agent, has been used for detection of fission fragments.

### 6.3 ORGANIC SCINTILLATORS

The materials that are efficient *organic scintillators* belong to the class of aromatic compounds. They consist of planar molecules made up of benzenoid rings. Two examples are toluene and anthracene, having the structures shown in Fig. 6.6.

Organic scintillators are formed by combining appropriate compounds. They are classified as unitary, binary, ternary, and so on, depending on the number of compounds in the mixture. The substance with the highest concentration is called the *solvent*. The others are called *solutes*. A binary scintillator consists of a solvent and a solute, while a ternary scintillator is made of a solvent, a primary solute, and a secondary solute. Table 6.2 lists the most common compounds used.

#### 6.3.1 The Mechanism of the Scintillation Process

The production of light in organic scintillators is the result of molecular transitions. Consider the energy-level diagram of Fig. 6.7, which shows how the potential energy of a molecule changes with interatomic distance. The ground state of the molecule is at point  $A_0$ , which coincides with the minimum of the potential energy. Ionizing radiation passing through the scintillator may give energy to the molecule and raise it to an excited state, i.e., the transition  $A_0 \rightarrow A_1$  may occur. The position  $A_1$  is not the point of minimum energy. The molecule will release energy through lattice vibrations (that energy is eventually dissipated as heat) and move to point  $B_1$ . The point  $B_1$  is still an excited state and, in some cases, the molecule will undergo the transition  $B_1 \rightarrow B_0$  accompanied by the emission of the photon with energy equal to  $E_{B_1} - E_{B_0}$ . This transition, if allowed, takes place at times of the order of  $10^{-8}$  s. It should be noted that the energy of the emitted photon ( $E_{B_1} - E_{B_0}$ ) is less than the energy that caused the excitation ( $E_{A_1} - E_{A_0}$ ). This difference is very important because otherwise the emission spectrum of the scintillator would completely coincide with its absorption spectrum and no scintillations would be produced. A more detailed description of the scintillation process is given in the references (see Birks and Ref. 6).

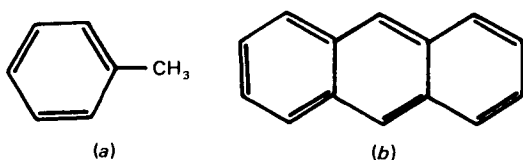


Figure 6.6 Molecular structure of (a) toluene and (b) anthracene.

**Table 6.2 Organic Scintillator Compounds<sup>†</sup>**

Compound	Formula	Application <sup>‡</sup>
Benzene	$C_6H_6$	S
Toluene	$C_6H_5CH_3$	S
<i>p</i> -Xylene	$C_6H_4(CH_3)_2$	S
1,2,4-Trimethylbenzene (pseudocumene)	$C_6H_3(CH_3)_3$	S
Hexamethylbenzene	$C_6(CH_3)_6$	S
Styrene monomer	$C_6H_5C_2H_3$	S
Vinyltoluene monomer	$C_6H_4CH_3C_2H_3$	S
Naphthalene	$C_{10}H_8$	S', C
Anthracene	$C_{14}H_{10}$	C
Biphenyl	$C_{12}H_{10}$	S'
<i>p</i> -Terphenyl	$C_{18}H_{14}$	C, PS
<i>p</i> -Quaterphenyl	$C_{24}H_{18}$	C
<i>trans</i> -Stilbene	$C_{14}H_{12}$	C
Diphenylacetylene	$C_{14}H_{10}$	C
1,1',4,4'-Tetraphenylbutadiene	$C_{28}H_{22}$	SS
Diphenylstilbene	$C_{26}H_{20}$	SS
PPO (2,5-diphenyloxazole)	$C_{15}H_{11}NO$	PS
$\alpha$ -NPO [2-(1-Naphthyl)-5-phenyloxazole]	$C_{19}H_{13}NO$	PS
PBD [2-Phenyl,5-(4-biphenyl)-1,3,4-oxadiazole]	$C_{20}H_{14}N_2O$	PS
BBO [2,5-Di(4-biphenyl)-oxazole]	$C_{27}H_{19}NO$	SS
POPOP {1,4-Bis[2-(5-phenyloxazolyl)]-benzene}	$C_{24}H_{16}N_2O_2$	SS
TOPOT {1,4-Di[2-(5- <i>p</i> -tolylloxazolyl)]-benzene}	$C_{26}H_{20}N_2O_2$	SS
DiMePOPOP {1,4-Di[2-(4-methyl-5-phenyloxazolyl)]-benzene}	$C_{26}H_{20}N_2O_2$	SS

<sup>†</sup>From <sup>6</sup>.

<sup>‡</sup>S—primary solvent; S'—secondary solvent; PS—primary solute; SS—secondary solute; C—crystal scintillator.

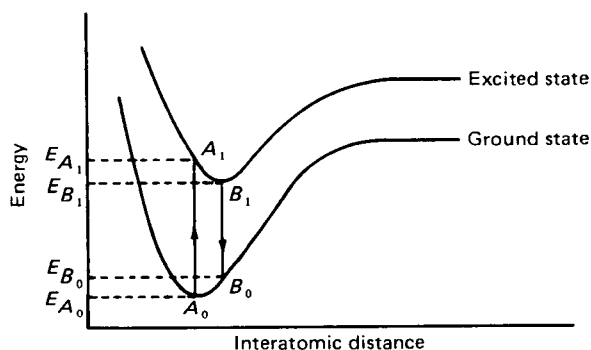


**Figure 6.7** A typical (simplified) energy diagram of a molecule.

One of the important differences between inorganic and organic scintillators is in the response time, which is less than 10 ns for the latter (response time of inorganic scintillators is  $\sim 1 \mu\text{s}$ ; see Table 6.1) and makes them suitable for fast timing measurements (see Chap. 10). Table 6.3 lists important properties of some organic scintillators.

### 6.3.2 Organic Crystal Scintillators

No activator is needed to enhance the luminescence of organic crystals. In fact, any impurities are undesirable because their presence reduces the light output, and for this reason, the material used to make the crystal is purified. Two of the most common organic crystal scintillators are anthracene and *trans*-stilbene.

Anthracene has a density of  $1.25 \times 10^3 \text{ kg/m}^3$  and the highest light conversion efficiency of all organic scintillators (see Table 6.3)—which is still only about one-third of the light conversion efficiency of NaI(Tl). Its decay time ( $\sim 30 \text{ ns}$ ) is much shorter than that of inorganic crystals. Anthracene can be obtained in different shapes and sizes.

*trans*-Stilbene has a density of  $1.15 \times 10^3 \text{ kg/m}^3$  and a short decay time (4–8 ns). Its conversion efficiency is about half of that for anthracene. It can be obtained as a clear, colorless, single crystal with a size up to several millimeters. Stilbene crystals are sensitive to thermal and mechanical shock.

### 6.3.3 Organic Liquid Scintillators

The organic liquid scintillators consist of a mixture of a solvent with one or more solutes. Compounds that have been used successfully as solvents include xylene, toluene, and hexamethylbenzene (see Table 6.2). Satisfactory solutes include *p*-terphenyl, PBD, and POPOP.

In a binary scintillator, the incident radiation deposits almost all of its energy in the solvent but the luminescence is due almost entirely to the solute. Thus, as in the case of inorganic scintillators, an efficient energy transfer is

**Table 6.3 Properties of Certain Organic Scintillators**

Material	Wavelength of maximum emission (nm)	Relative scintillation efficiency (%)	Decay time (ns)	Density ( $10^3 \text{ kg/m}^3$ )
Anthracene	445	100	$\sim 30$	1.25
<i>trans</i> -Stilbene	385	$\sim 60$	4–8	1.16
NE 102	350–450	$\sim 65$	2	1.06
NE 110	350–450	60	3	1.06
NE 213 (liquid)	350–450	$\sim 60$	2	0.867
PILOT B	350–450	68	2	1.06
PILOT Y	350–450	64	$\sim 3$	1.06

taking place from the bulk of the phosphor to the material with the small concentration (activator in inorganic scintillators, solute in organic ones). If a second solute is added, it acts as a *wavelength shifter*, i.e., it increases the wavelength of the light emitted by the first solute, so that the emitted radiation is better matched with the characteristics of the cathode of the photomultiplier tube.

Liquid scintillators are very useful for measurements where a detector with large volume is needed to increase efficiency. Examples are counting of low-activity  $\beta$ -emitters ( $^3\text{H}$  and  $^{14}\text{C}$  in particular), detection of cosmic rays, and measurement of the energy spectrum of neutrons in the MeV range (see Chap. 14) using the scintillator NE 213. The liquid scintillators are well suited for such measurements because they can be obtained and used in large quantities (kiloliters) and can form a detector of desirable size and shape by utilizing a proper container.

In certain cases, the radioisotope to be counted is dissolved in the scintillator, thus providing  $4\pi$  geometry and, therefore, high detection efficiency. In others, an extra element or compound is added to the scintillator to enhance its detection efficiency without causing significant deterioration of the luminescence. Boron, cadmium, or gadolinium,<sup>7-9</sup> used as additives, cause an increase in neutron detection efficiency. On the other hand, fluorine-loaded scintillators consist of compounds in which fluorine has replaced hydrogen, thus producing a phosphor with a low neutron sensitivity.

#### 6.3.4 Plastic Scintillators

The plastic scintillators may be considered as solid solutions of organic scintillators. They have properties similar to those of liquid organic scintillators (Table 6.3), but they have the added advantage, compared to liquids, that they do not need a container. Plastic scintillators can be machined into almost any desirable shape and size, ranging from thin fibers to thin sheets. They are inert to water, air, and many chemicals, and for this reason they can be used in direct contact with the radioactive sample.

Plastic scintillators are also mixtures of a solvent and one or more solutes. The most frequently used solvents are polystyrene and polyvinyltoluene. Satisfactory solutes include *p*-terphenyl and POPOP. The exact compositions of some plastic scintillators are given in Ref. 10.

Plastic scintillators have a density of about  $10^3 \text{ kg/m}^3$ . Their light output is lower than that of anthracene (Table 6.3). Their decay time is short, and the wavelength corresponding to the maximum intensity of their emission spectrum is between 350 and 450 nm. Trade names of commonly used plastic scintillators are Pilot B, Pilot Y, NE 102, and NE 110. The characteristics of these phosphors are discussed in Refs. 11-13. Plastic scintillators loaded with tin and lead have been tried as X-ray detectors in the 5-100 keV range.<sup>14,15</sup> Thin plastic scintillator films (as thin as  $20 \times 10^{-5} \text{ kg/m}^2 = 20 \text{ } \mu\text{g/cm}^2$ ) have proven to be useful detectors in time-of-flight measurements<sup>16-18</sup> (see Chap. 13).

## 6.4 GASEOUS SCINTILLATORS

Gaseous scintillators are mixtures of noble gases.<sup>19,20</sup> The scintillations are produced as a result of atomic transitions. Since the light emitted by noble gases belongs to the ultraviolet region, other gases, such as nitrogen, are added to the main gas to act as wavelength shifters. Thin layers of fluorescent materials used for coating the inner walls of the gas container achieve the same effect.

Gaseous scintillators exhibit the following features:

1. Very short decay time
2. Light output per MeV deposited in the gas depending very little on the charge and mass of the particle being detected
3. Very low efficiency for gamma detection

These properties make the gaseous scintillators suitable for the energy measurement of heavy charged particles (alphas, fission fragments, other heavy ions).

## 6.5 THE RELATIONSHIP BETWEEN PULSE HEIGHT AND ENERGY AND TYPE OF INCIDENT PARTICLE

To measure the energy of the incident particle with a scintillator, the relationship between the pulse height and the energy deposited in the scintillator must be known. Because the pulse height is proportional to the output of the photomultiplier, which output is in turn proportional to the light produced by the scintillator, it is necessary to know the light-conversion efficiency of the scintillator as a function of type and energy of incident radiation. The rest of this section presents experimental results for several cases of interest.

### 6.5.1 The Response of Inorganic Scintillators

**Photons.** The response of NaI(Tl) to gammas is linear, except for energies below 400 keV, where a slight nonlinearity is present. Experimental results are shown in Fig. 6.8.<sup>21</sup> More details about the NaI(Tl) response to gammas are given in Chap. 12.

**Charged particles.** For protons and deuterons, the response of the scintillator is proportional to the particle energy, at least for  $E > 1$  MeV. For alpha particles, the proportionality begins at about 15 MeV (Fig. 6.9).<sup>22</sup> Theoretical aspects of the response have been studied extensively.<sup>23-26</sup> Today, inorganic scintillators are seldom used for detection of charged particles.

**Neutrons.** Because neutrons are detected indirectly through charged particles produced as a result of nuclear reactions, to find the response to neutrons, one

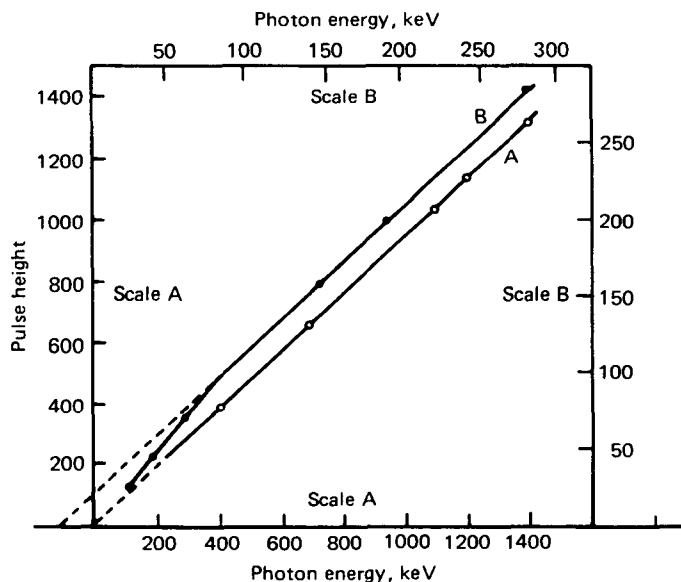


**Figure 6.8** Pulse height versus energy for a NaI(Tl) crystal. The region below 300 keV has been expanded in curve B to show the nonlinearity (from Ref. 21).

looks at the response to alphas and protons. LiI(Eu), which is the crystal used for neutron detection, has essentially the same response as NaI(Tl) (Fig. 6.9).

### 6.5.2 The Response of Organic Scintillators

**Charged particles.** Experiments have shown that organic crystal scintillators (e.g., anthracene) exhibit a direction-dependent response to alphas<sup>27</sup> and protons.<sup>28</sup> An adequate explanation of the direction-dependent characteristics of the response does not exist at present. The user should be aware of the phenomenon to avoid errors.

The response of plastic and liquid scintillators to electrons, protons, and alphas is shown in Figs. 6.10, 6.11, and 6.12.<sup>29-31</sup> Notice that the response is not linear, especially for heavier ions. The response has been studied theoretically by many investigators (Birks and Refs. 32-35).

**Photons and neutrons.** Organic scintillators are not normally used for detection of gammas because of their low efficiency. The liquid scintillators NE 213<sup>†</sup> is being used for  $\gamma$  detection in mixed neutron-gamma fields<sup>36</sup> because of its

<sup>†</sup> NE 213 consists of xylene, activators, and POPOP as the wavelength shifter. Naphthalene is added to enhance the slow components of light emission. The composition of NE 213 is given as CH<sub>1.21</sub> and its density as  $0.867 \times 10^3$  kg/cm<sup>3</sup>.

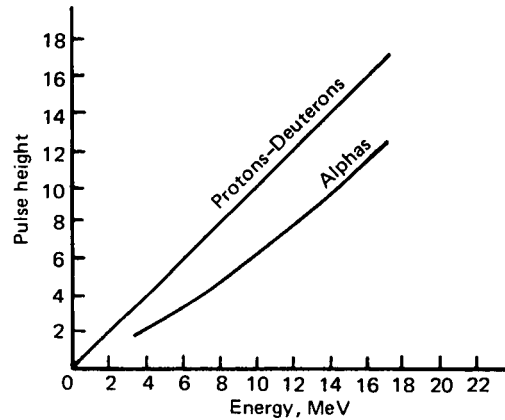


**Figure 6.9** Pulse height versus energy for a NaI(Tl) crystal resulting from charged particles (from Ref. 22).

ability to discriminate against neutrons. Neutrons are detected by NE 213 through the proton-recoil method. More details about the use of the NE 213 scintillator and its response function are given in Chaps. 12 and 14.

## 6.6 THE PHOTOMULTIPLIER TUBE

### 6.6.1 General Description

The photomultiplier tube or phototube is an integral part of a scintillation counter. Without the amplification produced by the photomultiplier, a scintilla-

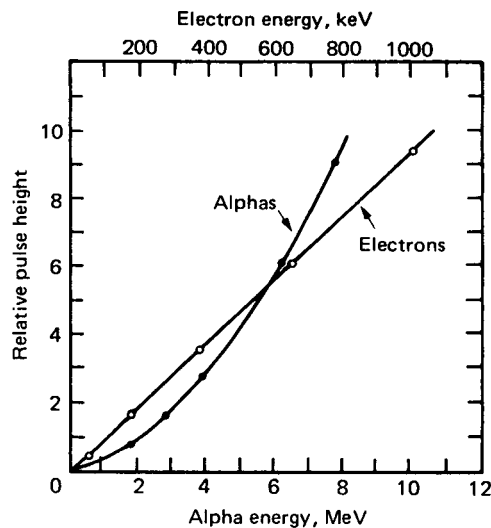


**Figure 6.10** Pulse height versus energy for a liquid scintillator resulting from alphas and electrons (from Ref. 29).

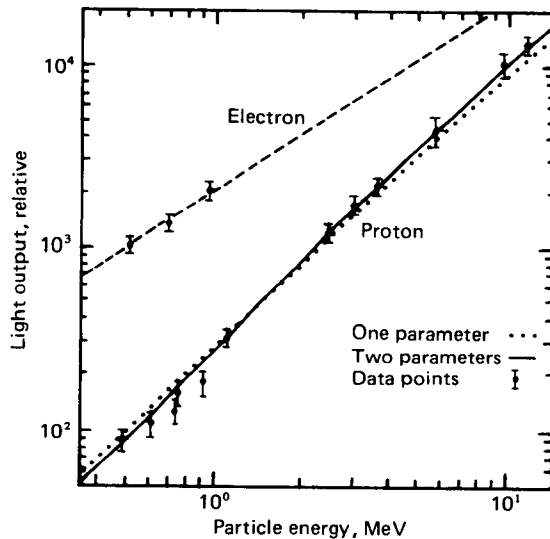


**Figure 6.11** Plastic scintillator (NE 102) response to electrons and protons (from Ref. 30).

tor is useless as a radiation detector. The photomultiplier is essentially a fast amplifier, which in times of  $10^{-9}$  s amplifies an incident pulse of visible light by a factor of  $10^6$  or more.

A photomultiplier consists of an evacuated glass tube with a photocathode at its entrance and several dynodes in the interior (Fig. 6.13). The anode, located at the end of a series of dynodes serves as the collector of electrons. The photons produced in the scintillator enter the phototube and hit the photocathode, which is made of a material that emits electrons when light strikes it. The electrons emitted by the photocathode are guided, with the help of an electric field, toward the first dynode, which is coated with a substance that emits secondary electrons, if electrons impinge upon it. The secondary electrons from the first dynode move toward the second, from there toward the third, and so on. Typical commercial phototubes may have up to 15 dynodes. The production of secondary electrons by the successive dynodes results in a final amplification of the number of electrons as shown in the next section.

The electric field between dynodes is established by applying a successively increasing positive high voltage to each dynode. The voltage difference between two successive dynodes is of the order of 80–120 V (see Sec. 6.6.2).

The photocathode material used in most commercial phototubes is a compound of cesium and antimony (Cs-Sb). The material used to coat the dynodes is either Cs-Sb or silver-magnesium (Ag-Mg). The secondary emission rate of the dynodes depends not only on the type of surface but also on the voltage applied.

A very important parameter of every photomultiplier tube is the spectral sensitivity of its photocathode. For best results, the spectrum of the scintillator should match the sensitivity of the photocathode. The Cs-Sb surface has a maximum sensitivity at 440 nm, which agrees well with the spectral response of



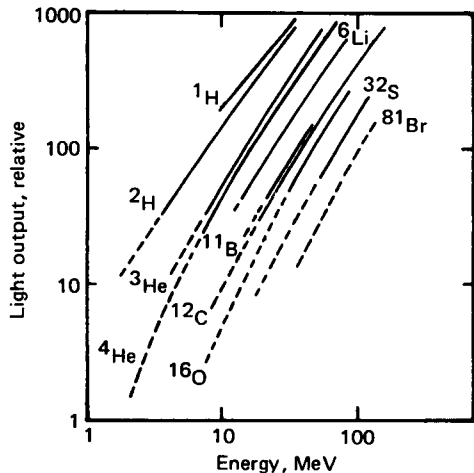


Figure 6.12 Plastic scintillator (NE 102) response to heavy ions (from Ref. 31).

most scintillators (Tables 6.1 and 6.3). Such a response, called S-11, is shown in Fig. 6.3. Other responses of commercial phototubes are known as S-13, S-20, etc.

Another important parameter of a phototube is the magnitude of its *dark current*. The dark current consists mainly of electrons emitted by the cathode after thermal energy is absorbed. This process is called *thermionic emission*, and a 50-mm-diameter photocathode may release in the dark as many as  $10^5$  electrons/s at room temperature. Cooling of the cathode reduces this source of noise by a factor of about 2 per 10–15°C reduction in temperature. Thermionic emission may also take place from the dynodes and the glass wall of the tube, but this contribution is small. Electrons may be released from the photocathode as a result of its bombardment by positive ions coming from ionization of the residual gas in the tube. Finally, light emitted as a result of ion recombination may release electrons upon hitting the cathode or the dynodes. Obviously, the magnitude of the dark current is important in cases where the radiation source

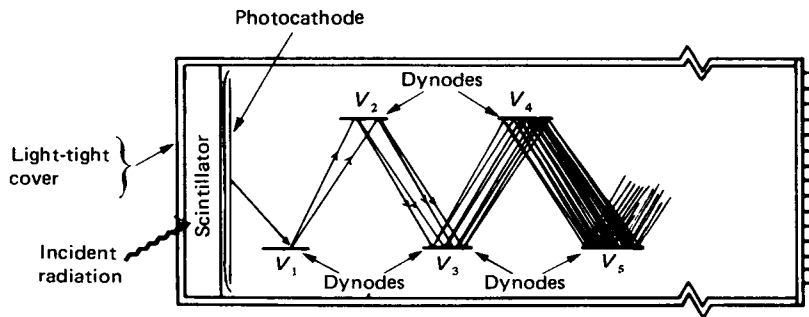


Figure 6.13 Schematic diagram of the interior of a photomultiplier tube.

is very weak. Both the dark current and the spectral response should be considered when a phototube is to be purchased.

Recall that the electrons are guided from one dynode to the next by an electric field. If a magnetic field is present, it may deflect the electrons in such a way that not all of them hit the next dynode, and the amplification is reduced. Even the earth's weak magnetic field may sometimes cause this undesirable effect. The influence of the magnetic field may be minimized by surrounding the photomultiplier tube with a cylindrical sheet of metal, called  $\mu$ -metal. The  $\mu$ -metal is commercially available in various shapes and sizes.

Commercial photomultiplier tubes are made with the variety of geometrical arrangements of photocathode and dynodes. In general, the photocathode is deposited as a semitransparent layer on the inner surface of the end window of the phototube (Fig. 6.14). The external surface of the window is, in most phototubes, flat for easier optical coupling with the scintillator (see Sec. 6.7). Two different geometries for the dynodes are shown in Fig. 6.14.

### 6.6.2 Electron Multiplication in a Photomultiplier

The electron multiplication  $M$  in a photomultiplier can be written as

$$M = (\theta_1 \epsilon_1)(\theta_2 \epsilon_2) \cdots (\theta_n \epsilon_n) \quad (6.3)$$

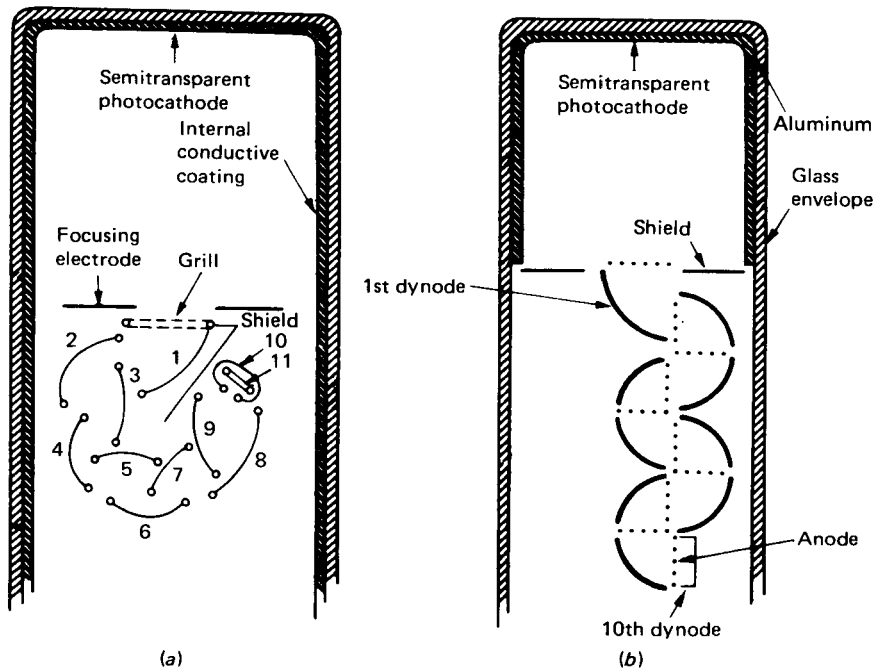


**Figure 6.14** Two dynode arrangements in commercial phototubes: (a) Model 6342 RCA, 1–10 are dynodes, 11 is anode; (b) Model 6292 DuMont.

where

$n$  = number of dynodes

$$\epsilon_i = \frac{\text{number of electrons collected by } i\text{th dynode}}{\text{number of electrons emitted by } (i - 1)\text{th dynode}}$$

$$\theta_i = \frac{\text{number of electrons emitted by } i\text{th dynode}}{\text{number of electrons impinging upon } i\text{th dynode}}$$

If  $\theta_i$  and  $\epsilon_i$  are constant for all dynodes, then

$$M = (\theta\epsilon)^n \quad (6.4)$$

The quantity  $\epsilon$  depends on the geometry. The quantity  $\theta$  depends on the voltage between two successive dynodes and on the material of which the dynode is made. The dependence of  $\theta$  on voltage is of the form

$$\theta = kV^a \quad (6.5)$$

where  $V = V_i - V_{i-1}$  = potential difference between two successive dynodes, assumed the same for all dynode pairs

$k, a$  = constants (the value of  $a$  is about 0.7)

Using Eq. 6.5, the multiplication  $M$  becomes

$$M = \epsilon^n (kV^a)^n = CV^{an} \quad (6.6)$$

where  $C = (\epsilon k)^n$  = constant, independent of the voltage.

Equation 6.6 indicates that the value of  $M$  increases with the voltage  $V$  and the number of stages  $n$ . The number of dynodes is limited, because as  $n$  increases, the charge density between two dynodes distorts the electric field and hinders the emission of electrons from the previous dynode with the lower voltage. In commercial photomultipliers, the number of dynodes is 10 or more. If one takes  $n = 10$  and  $\epsilon\theta = 4$ , typical value, the value of  $M$  becomes equal to  $10^6$ .

To apply the electric field to the dynodes, a power supply provides a voltage adequate for all the dynodes. A voltage divider, usually an integral part of the preamplifier, distributes the voltage to the individual dynodes. When reference is made to *phototube voltage*, one means the total voltage applied. For example, if 1100 V are applied to a phototube with 10 dynodes, the voltage between any two dynodes is 100 V.

## 6.7 ASSEMBLY OF A SCINTILLATION COUNTER AND THE ROLE OF LIGHT PIPES

A scintillation counter consists of the scintillator and the photomultiplier tube. It is extremely important that these two components be coupled in such a way that a maximum amount of light enters the phototube and strikes the photocathode. This section presents a brief discussion of the problems encountered during the assembly of a scintillation counter, with some of the methods used to solve them.

A solid scintillator is coupled to the photomultiplier through the end window of the tube (Fig. 6.15). During the transfer from the scintillator to the photocathode, light may be lost by leaving through the sides and front face of the scintillator, or by being reflected back to the scintillator when it hits the window of the phototube.

To avoid loss of light through the sides and front face, the scintillator is painted with a material that reflects toward the crystal the light that would otherwise escape. Examples of reflecting materials commercially available are alpha alumina and  $\text{Al}_2\text{O}_3$ .

To avoid reflection of light from the end window of the phototube, a transparent viscous fluid (such as Dow-Corning 200 Silicone fluid) is placed between the scintillator and the phototube (Fig. 6.15). The optical fluid minimizes reflection because it reduces the change of the index of refraction during the passage of light from the scintillator to the phototube. A sharp change in the index of refraction results in a small critical angle of reflection, which in turn increases total reflection.

In certain experiments, the scintillator has to be a certain distance away from the photocathode. Such is the case if the phototube should be protected from the radiation impinging upon the scintillator or from a magnetic field. Then a *light pipe* is interposed between the scintillator and the phototube. The light pipe is made of a material transparent to the light of the scintillator. Lucite, quartz, plexiglas, and glass have been used in many applications to form light pipes of different lengths and shapes. Light pipes of several feet—sometimes with bends—have been used with success. The optical coupling of the light pipe at both ends is accomplished by the same methods used to couple the scintillator directly to the phototube.

One of the major reasons for using scintillators is their availability in large sizes. In fact, commercially available scintillators are larger than the biggest commercial photomultipliers. In cases where the scintillator is too large, multiple phototubes are coupled to the same crystal. Figure 6.16 shows a  $\text{NaI}(\text{Tl})$  crystal coupled to six photomultipliers.

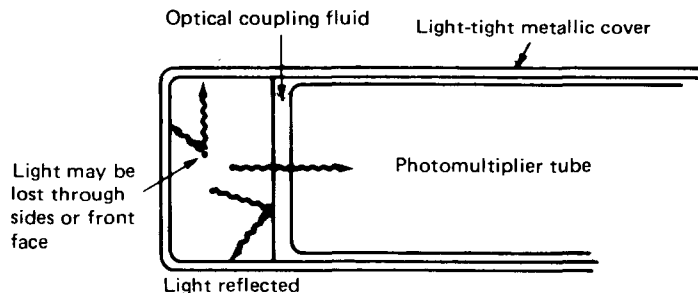


**Figure 6.15** Assembly of a scintillation counter.



**Figure 6.16** A special 30-in (0.762-m) diameter scintillator crystal coupled to six photomultiplier tubes (from Harshaw Chemical Company).

When a liquid scintillator is used, the phototube is optically coupled to the scintillator through a window of the vessel containing the liquid scintillator. The efficiency of such a counting system increases by using a large volume of liquid and more than one photomultiplier tube (Fig. 6.17).

### **6.8 DEAD TIME OF SCINTILLATION COUNTERS**

The *dead time* or *resolving time* is the minimum time that can elapse after the arrival of two successive particles and still result in two separate pulses (see Sec.

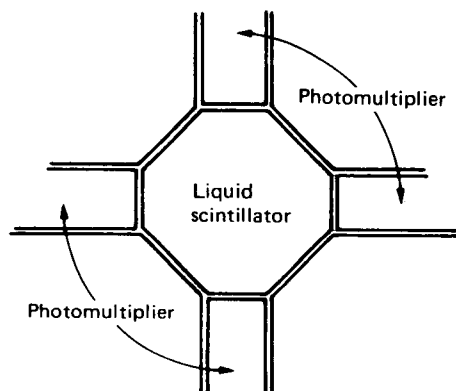


**Figure 6.17** A counting system using a liquid scintillator and four photomultiplier tubes.

2.21). For a scintillation counter this time is equal to the sum of three time intervals:

1. Time it takes to produce the scintillation, essentially equal to the decay time of the scintillator (see Eq. 6.1 and Tables 6.1 and 6.3).
2. Time it takes for electron multiplication in the phototube, of the order of 20–40 ns.
3. Time it takes to amplify the signal and record it by a scaler. The resolving time of commercial scalers is of the order of 1  $\mu$ s. The time taken for amplification and discrimination is negligible.

By adding the three above components, the resulting dead time of a scintillation counter is of the order of 1–5  $\mu$ s. This is much shorter than the dead time of gas-filled counters, which is of the order of tens to hundreds of microseconds.

Scintillators are detectors with fast response. As seen in Tables 6.1 and 6.3, the risetime of the pulse is very short for all of them. Short risetime is important in measurements that depend on the time of arrival of the particle (see Chap. 10).

## 6.9 SOURCES OF BACKGROUND IN A SCINTILLATION COUNTER

One of the major sources of background in a scintillation counter is the dark current of the phototube (see Sec. 6.6.1). Other background sources are naturally occurring radioisotopes, cosmic rays, and phosphorescing substances.

The holder of a liquid scintillator may contain small amounts of naturally occurring isotopes. In particular,  $^{40}\text{K}$  is always present (isotopic abundance of  $^{40}\text{K}$  is 0.01 percent). Another isotope,  $^{14}\text{C}$ , is a constituent of contemporary organic materials. Solvents, however, may be obtained from petroleum, consisting of hydrocarbons without  $^{14}\text{C}$ .

The term *phosphorescence* refers to delayed emission of light as a result of deexcitation of atoms or molecules. Phosphorescent half-lives may extend to hours. This source of background may originate in phosphorescent substances contained in the glass of the phototube, the walls of the sample holder, or the sample itself.

*Cosmic rays*, which are highly energetic charged particles, produce background in all types of detectors, and scintillators are no exception. The effect of cosmic-ray background, as well as that of the other sources mentioned earlier, will be reduced if two counters are used in coincidence or anticoincidence.

## 6.10 THE PHOSWICH DETECTOR

The phoswich detector is used for the detection of low-level radiation in the presence of considerable background. It consists of two different scintillators coupled together and mounted on a single photomultiplier tube.<sup>1</sup> By utilizing the difference in the decay constants of the two phosphors, differentiation between events taking place in the two detectors is possible. The combination of crystals used depends on the types of particles present in the radiation field under investigation.<sup>37, 38</sup>

The basic structure of a phoswich detector is shown in Fig. 6.18. A thin scintillator (scintillator A) is coupled to a larger crystal (scintillator B), which in turn is coupled to the cathode of a single phototube. Two examples of scintillators used are these:

1. NaI(Tl) is the thin scintillator (A) and CsI(Tl) is the thick one (B). Pulses originating in the two crystals are differentiated based on the difference between the  $0.25\text{-}\mu\text{s}$  decay constant of the NaI(Tl) and the  $1\text{-}\mu\text{s}$  decay constant of the CsI(Tl). Slow pulses come from particles losing energy in the CsI(Tl) or in both crystals simultaneously. In a mixed low-energy-high-energy photon field, the relatively fast pulses of the NaI(Tl) will come from the soft

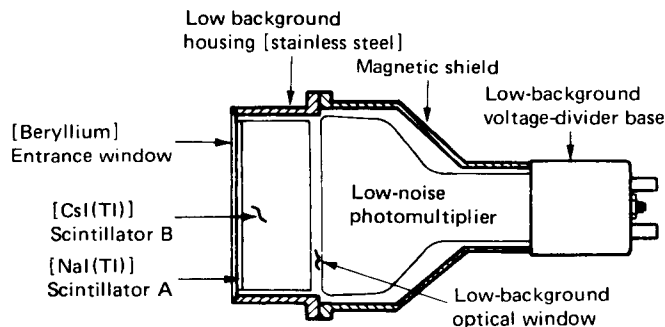


**Figure 6.18** A Phoswich detector (from Harshaw Chemical Company).

component of the radiation. [Soft photons will not reach the CsI(Tl).] Phoswich detectors of this type have been used in X-ray and  $\gamma$ -ray astronomy, in detection of plutonium in the environment, and in other cases of mixed-radiation fields.

2.  $\text{CaF}_2(\text{Eu})$  is the thin scintillator (A) and  $\text{NaI}(\text{Tl})$  is the thick one (B). This combination is used for measurements of low-energy beta particles in the presence of a gamma background. The thin (0.1 mm)  $\text{CaF}_2(\text{Eu})$  crystal detects the betas, but is essentially transparent to gammas because of its relatively low atomic number and thickness. A quartz window is usually placed between the two scintillators to stop the betas that did not deposit all their energy in the  $\text{CaF}_2(\text{Eu})$ . The fast pulses of the  $\text{NaI}(\text{Tl})$ , which are due to gammas, are time-discriminated against the slower pulses from the  $\text{CaF}_2(\text{Eu})$  ( $T = 0.94 \mu\text{s}$ ). Thus, the background due to gammas is reduced.

## PROBLEMS

- 6.1 If the dead time of a detection system using a scintillator is  $1 \mu\text{s}$ , what is the gross counting rate that will result in a loss of 2 percent of the counts?
- 6.2 A typical dead time for a scintillation detector is  $5 \mu\text{s}$ . For a gas counter, the corresponding number is  $200 \mu\text{s}$ . If a sample counted with a gas counter results in 8 percent loss of gross counts due to dead time, what is the corresponding loss in a scintillation counter that records the same gross counting rate?
- 6.3 A parallel beam of 1.5-MeV gammas strikes a 25-mm-thick  $\text{NaI}$  crystal. What fraction of these gammas will have at least one interaction in the crystal ( $\mu = 0.0047 \text{ m}^2/\text{kg}$ )?
- 6.4 What is the range of 2-MeV electrons in a plastic scintillator? Assume that the composition of the scintillator is  $\text{C}_{10}\text{H}_{11}$  ( $\rho = 1.02 \times 10^3 \text{ kg/m}^3$ ).
- 6.5 Consider two electrons, one with kinetic energy 1 MeV, the other with 10 MeV. Which electron will lose more energy going through a 1-mm-thick plastic scintillator? Consider both ionization and radiation loss. Composition of the scintillator is given in Prob. 6.4. For radiation loss, use

$$Z_{\text{eff}} = \frac{N_H Z_H^2 + N_C Z_C^2}{N_H Z_H + N_C Z_C}$$

- 6.6 A phoswich detector consists of a 1-mm-thick  $\text{NaI}(\text{Tl})$  scintillator coupled to a 25-mm-thick  $\text{CsI}(\text{Tl})$  scintillator. A 0.1-mm-thick beryllium window protects the  $\text{NaI}(\text{Tl})$  crystal. If the detector is exposed to a thin parallel beam of 150-keV X-rays and 1.5-MeV  $\gamma$  rays, what are the fractions of interactions of each type of photon in each scintillator?

## BIBLIOGRAPHY

- Birks, J. B., *The Theory and Practice of Scintillation Counting*, McMillan Co., New York, 1964.
- Eichholz, G. G., and Poston, J. W., *Nuclear Radiation Detection*, Lewis Publishers, Chelsea, Michigan 1985.
- Fenyves, E., and Haiman, O., *The Physical Principles of Nuclear Radiation Measurements*, Academic Press, New York, 1969.
- Knoll, G. F., *Radiation Detection and Measurement*, 2nd ed., Wiley, New York, 1989.



- Price, W. J., *Nuclear Radiation Detection*, McGraw-Hill, New York, 1964.  
 Ross, H., Noakes, J. E., and Spaulding, J. D., *Liquid Scintillation Counting and Organic Scintillators*,  
 Lewis Publishers, Chelsea, Michigan, 1991.  
 Snell, A. H. (ed.), *Nuclear Instruments and Their Uses*, Wiley, New York, 1962.  
 Tait, W. H., *Radiation Detection*, Butterworth, London, 1980.

## REFERENCES

1. Heath, R. L., Hofstadter, R., and Hughes, E. B., *Nucl. Instrum. Meth.* **162**:431 (1979). (Review article listing 127 references.)
2. Aliaga-Kelly, D., and Nicoll, D. R., *Nucl. Instrum. Meth.* **43**:110 (1966).
3. Colmenares, C., Shapiro, E. G., Barry, P. E., and Prevo, C. T., *Nucl. Instrum. Meth.* **114**:277 (1974).
4. Campbell, M., Ledingham, K. W. D., Baillie, A. D., and Lynch, J. G., *Nucl. Instrum. Meth.* **137**:235 (1976).
5. Catalano, E., and Czirr, J. B., *Nucl. Instrum. Meth.* **143**:61 (1977).
6. Brooks, F. D., *Nucl. Instrum. Meth.* **162**:477 (1979). (Review article listing 274 references.)
7. Bollinger, L. M., and Thomas, G. E., *Rev. Sci. Instrum.* **28**:489 (1957).
8. Hellstrom, J., and Beshai, S., *Nucl. Instrum. Meth.* **101**:267 (1972).
9. Bergere, R., Beil, H., and Veyssiere, A., *Nucl. Phys.* **A121**:463 (1968).
10. Swank, R. K., *Annu. Rev. Nucl. Sci.* **4**:111 (1954).
11. Walker, J. K., *Nucl. Instrum. Meth.* **68**:131 (1969).
12. Moszynski, M., and Bengtson, B., *Nucl. Instrum. Meth.* **142**:417 (1977).
13. Moszynski, M., and Bengtson, B., *Nucl. Instrum. Meth.* **158**:1 (1979).
14. Eriksson, L. A., Tsai, C. M., Cho, Z. H., and Hurlbut, C. R., *Nucl. Instrum. Meth.* **122**:373 (1974).
15. Becker, J., Eriksson, L., Monberg, L. C., and Cho, Z. H., *Nucl. Instrum. Meth.* **123**:199 (1975).
16. Muga, M. L., Burnsed, D. J., Steeger, W. E., and Taylor, H. E., *Nucl. Instrum. Meth.* **83**:135 (1970).
17. Muga, M. L., *Nucl. Instrum. Meth.* **95**:349 (1971).
18. Batra, R. K., and Shotter, A. C., *Nucl. Instrum. Meth.* **124**:101 (1975).
19. Policarpo, A. J. P. L., Conde, C. A. N., and Alves, M. A. F., *Nucl. Instrum. Meth.* **58**:151 (1968).
20. Morgan, G. L., and Walter, R. L., *Nucl. Instrum. Meth.* **58**:277 (1968).
21. Engelkemeir, B., *Rev. Sci. Instrum.* **27**:989 (1956).
22. Eby, F. S., and Jentschke, W. K., *Phys. Rev.* **96**:911 (1954).
23. Murray, R. B., and Meyer, A., *Phys. Rev.* **122**:815 (1961).
24. Meyer, A., and Murray, R. B., *Phys. Rev.* **128**:98 (1962).
25. Prescott, J. R., and Narayan, G. H., *Nucl. Instrum. Meth.* **75**:51 (1969).
26. Hill, R., and Collinson, A. J. L., *Nucl. Instrum. Meth.* **44**:245 (1966).
27. Brand, W., Dobrin, R., Jack, H., Aubert, R. L., and Roth, S., *Con. J. Phys.* **46**:537 (1968).
28. Brooks, F. D., and Jones, D. T. L., *Nucl. Instrum. Meth.*, **121**:69 (1974).
29. Flynn, K. F., Glendenin, C. E., Steinberg, E. P., and Wright, P. M., *Nucl. Instrum. Meth.* **27**:13 (1964).
30. Craun, R. L., and Smith, D. L., *Nucl. Instrum. Meth.* **80**:239 (1970).
31. Becchetti, F. D., Thorn, C. E., and Levine, M. S., *Nucl. Instrum. Meth.* **138**:93 (1976).
32. Chou, C. N., *Phys. Rev.* **87**:376, 904 (1952).
33. Wright, G. T., *Phys. Rev.* **91**:1282 (1953).
34. Voltz, R., Lopes da Silva, J., Laustriat, G., and Coche, A., *J. Chem. Phys.* **45**:3306 (1966).
35. Voltz, R., du Pont, H., and Laustriat, G., *J. Physique* **29**:297 (1968).
36. Ingersoll, D. T., and Wehring, B. W., *Nucl. Instrum. Meth.* **147**:551 (1977).
37. Pastor, C., Benrachi, F., Chambon, B., Cheynis, B., Drain, D., Dauchy, A., Giorni, A., and Morand, C., *Nucl. Instrum. Meth.* **227**:87 (1984).
38. Pouliot, J., Chan, Y., Dacal, A., Harmon, A., Knop, R., Ortiz, M. E., Plagnol, E., and Stokstad, R. G., *Nucl. Instrum. Meth.* **270**:69 (1988).

**SEMICONDUCTOR DETECTORS**

**7.1 INTRODUCTION**

*Semiconductor detectors* are solid-state devices that operate essentially like ionization chambers. The charge carriers in semiconductors are not electrons and ions, as in the gas counters, but electrons and “holes.”<sup>1,2</sup> At present, the most successful semiconductor detectors are made of silicon and germanium. Other materials have been tried, however, with some success, e.g., CdTe and HgI<sub>2</sub>.

The most important advantage of the semiconductor detectors, compared to other types of radiation counters, is their superior *energy resolution*: the ability to resolve the energy of particles out of a polyenergetic energy spectrum (energy resolution and its importance are discussed in Chaps. 9, 12–14). Other advantages are

1. Linear response (pulse height versus particle energy) over a wide energy range
2. Higher efficiency for a given size, because of the high density of a solid relative to that of a gas
3. Possibility for special geometric configurations
4. Fast pulse risetime (relative to gas counters)
5. Ability to operate in vacuum
6. Insensitivity to magnetic fields

The characteristics of a semiconductor detector depend not only on the type of material used—e.g., Si or Ge—but also on the way the semiconductor is

shaped and treated. The type, size, shape, and treatment of the crystal play a role in the operation and performance of a semiconductor detector.

This chapter first discusses the fundamentals of energy states in crystals, a subject necessary for understanding the creation and movement of electrons and holes in a solid. The properties of semiconductors are discussed next, with special emphasis given to the properties of silicon and germanium. The principle of construction and operation is accompanied by a description of the different types of detectors available in the market. Future prospects in this field are also discussed.

## 7.2 ELECTRICAL CLASSIFICATION OF SOLIDS

Solids are divided according to their electrical conductivity into three groups: conductors, insulators, and semiconductors. If a piece of solid material is placed in an electric field, whether or not current will flow depends on the type of material. If current flows, the material is a *conductor*. If current is zero at low temperatures but larger than zero at higher temperatures, the material is a *semiconductor*. If current is zero at all temperatures, the material is an *insulator*.

*Conductivity* and *electric current* mean motion of electrons, and according to the results of this simple experiment,

1. In conductors, electrons can move freely at any voltage different than zero.
2. In insulators, electrons cannot move under any voltage (except, of course, when the voltage is so high that an electrical discharge occurs).
3. In semiconductors, electrons cannot move at low temperatures (close to absolute zero) under any voltage. As the temperature of a semiconductor increases, however, electrons can move and electric current will flow at moderate voltages.

These properties can be explained by examining the electronic structure of crystals.

### 7.2.1 Electronic States in Solids—The Fermi Distribution Function

In a free atom the electrons are allowed to exist only in certain discrete energy states (Fig. 7.1a). In solids, the energy states widen into energy bands. Electrons can exist only in bands 1, 3, and 5, but not in bands 2 and 4 (Fig. 7.1b). An electron can move from band 1 to band 3 if

1. The electron acquires the energy  $E_g$  necessary to cross the forbidden gap
2. There is an empty state in band 3, which the jumping electron can occupy<sup>†</sup>

<sup>†</sup>This constraint is due to the Pauli principle, which forbids two or more electrons to be in the same state.

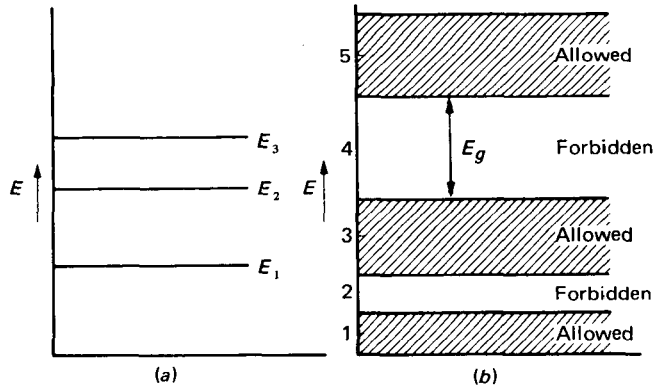


**Figure 7.1** (a) The atomic energy levels are discrete lines. (b) In a solid, the allowed energy states become energy bands.

The energy distribution of electronic states is described in terms of the following quantities:

$N(E)dE$  = number of electrons per unit volume with energy between  $E$  and  $E + dE$

$S(E)dE$  = number of allowed electronic energy states, per unit volume, in the energy interval between  $E$  and  $E + dE$

$P(E)$  = probability that a state of energy  $E$  is occupied  
= *Fermi distribution function*

Then

$$N(E) dE = P(E)[S(E) dE] \quad (7.1)$$

The form of  $P(E)$  is given by

$$P(E) = \frac{1}{1 + e^{(E-E_f)/kT}} \quad (7.2)$$

where  $E_f$  = Fermi energy

$k$  = Boltzmann constant

$T$  = temperature, Kelvin

The *Fermi energy*  $E_f$  is a constant that does not depend on temperature but it does depend on the purity of the solid. The function  $P(E)$  is a universal function applying to all solids and having these properties (Fig. 7.2):

1. At  $T = 0$ ,

$$P(E) = 1 \quad E < E_f$$

$$P(E) = 0 \quad E > E_f$$

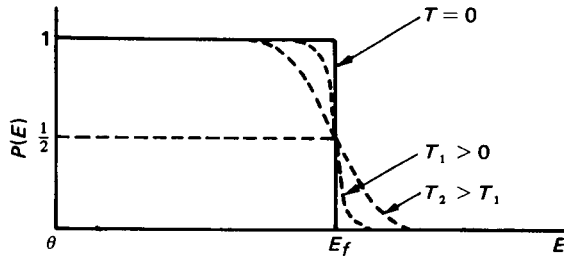


Figure 7.2 The Fermi distribution function.

2. At any  $T$ ,

$$P(E_f) = \frac{1}{2}$$

3. For  $T > 0$ , the function  $P(E)$  extends beyond  $E_f$ . If  $E - E_f \gg kT$ ,  $P(E)$  takes the form

$$P(E) = \frac{1}{1 + e^{(E-E_f)/kT}} \sim \frac{1}{e^{(E-E_f)/kT}} = \exp\left(-\frac{E - E_f}{kT}\right) \quad (7.3)$$

which resembles the classical Boltzmann distribution.

Notice that at  $T = 0$  (Fig. 7.2), all the states are occupied for  $E < E_f$  but all the states are empty for  $E > E_f$ .

### 7.2.2 Insulators

In insulators, the highest allowed band, called the *valence band*, is completely occupied (Fig. 7.3). The next allowed band, called the *conduction band*, is completely empty. As Fig. 7.3 shows, the gap is so wide that the number of occupied states in the conduction band is always zero. No electric field or temperature rise can provide enough energy for electrons to cross the gap and reach the conduction band. Thus, insulators *are* insulators because it is impossible for electrons to be found in the conduction band, where under the influence of an electric field, they would move and generate an electric current.

### 7.2.3 Conductors

In conductors, the conduction band is partially occupied (Fig. 7.4). An electron close to the top of the filled part of this band (point A, Fig. 7.4) will be able to move to the empty part (part B) under the influence of any electric field other than zero. Thus, because of the lack of a forbidden gap, there is no threshold of electric field intensity below which electrons cannot move. Motion of the charge carriers and, consequently, conductivity are always possible for any voltage applied, no matter how small.

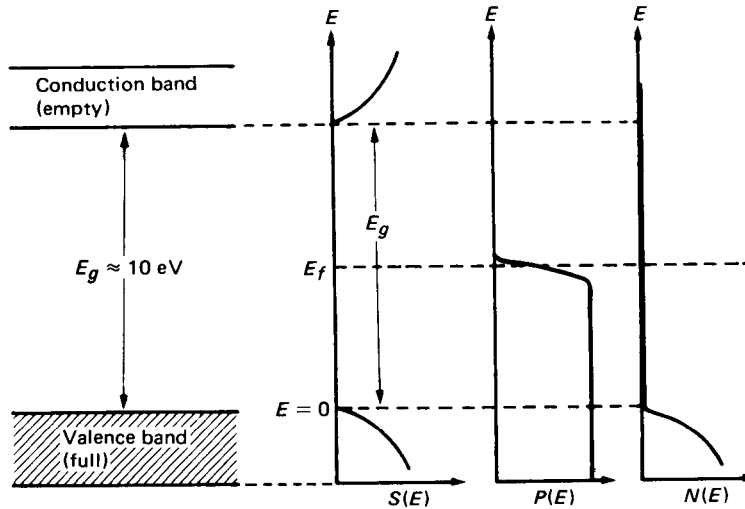


**Figure 7.3** All the energy states in the conduction band of an insulator are empty. Since there are no charge carriers, the conductivity is zero.

### 7.3 SEMICONDUCTORS

In semiconductors, the valence band is full and the conduction band is empty, but the energy gap between these two bands is very small. At very low temperatures, close to  $T = 0$ , the conductivity of the semiconductors is zero and the energy-band picture looks like that of an insulator (Fig. 7.3). As temperature increases, however, the “tail” of the Fermi distribution brings some electrons into the conduction band and conductivity increases (Fig. 7.5). That is, as temperature increases, some electrons obtain enough energy to cross over to the

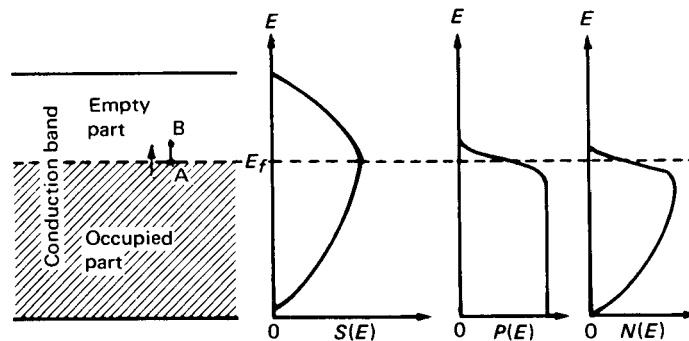


**Figure 7.4** In conductors, the conduction band is partially occupied. If an electric field is applied, the electrons move and conductivity is not zero.

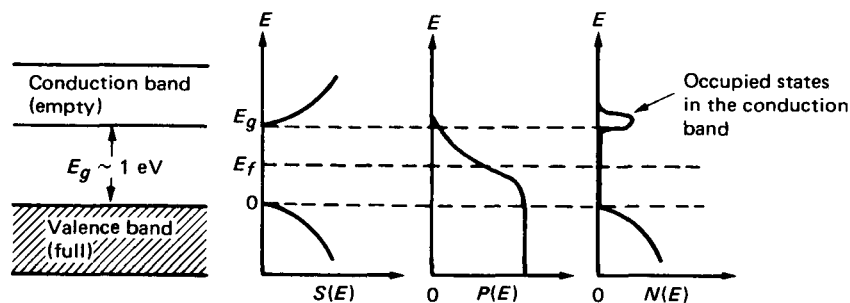


**Figure 7.5** In semiconductors, the energy gap is relatively narrow. As temperature increases, some electrons have enough energy to be able to move to the conduction band and conductivity appears.

conduction band. Once there, they will move under the influence of an electric field for the same reason that electrons of conductors move.

When an electron moves to the conduction band, an empty state is left in the valence band. This is called a *hole*. A hole is the absence of an electron. When the electron moves in one direction, the hole moves in the opposite direction (Fig. 7.6). Holes are treated as particles with positive charges:  $-(-e) = +e$ . They contribute to the conductivity in the same way electrons do (see Sec. 7.3.2). In a pure and electrically neutral semiconductor, the number of electrons is always equal to the number of holes.

Heat—i.e., temperature increase—is not the only way energy may be given to an electron. Absorption of radiation or collision with an energetic charged particle may produce the same effect. The interaction of ionizing radiation with a semiconductor is a complex process and there is no agreement upon a common model explaining it. One simplified model is the following.

An energetic incident charged particle collides with electrons of the semiconductor and lifts them, not only from the valence to the conduction band but also from deeper lying occupied bands to the conduction band, as shown in Fig. 7.7a. Electrons appear in normally empty bands and holes appear in normally fully occupied bands. However, this configuration does not last long. In times of the order of  $10^{-12}$  s, the interaction between electrons and holes makes the electrons concentrate at the bottom of the lowest lying unoccupied (conduction) band. The holes, on the other hand, concentrate near the top of the highest full (valence) band. During this deexcitation process, many more electrons and holes are generated. Because of this multistep process, the average energy necessary for the creation of one electron-hole pair is much larger than the energy gap  $E_g$ . For example, for silicon at room temperature,  $E_g = 1.106$  eV, and the average energy for the production of one electron-hole pair is 3.66 eV.

In the absence of an electric field, the final step of the deexcitation process is the recombination of electrons and holes and the return of the crystal to its neutral state.

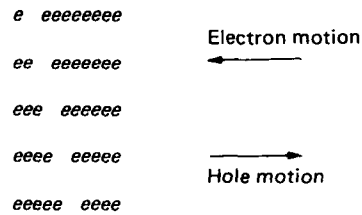


**Figure 7.6** Electrons and holes move in opposite directions. A hole behaves like a positively charged carrier.

### 7.3.1 The Change of the Energy Gap with Temperature

The value of the energy gap  $E_g$  (Fig. 7.5) is not constant, but it changes with temperature as shown in Fig. 7.8. For silicon and germanium,  $E_g$  initially increases linearly as temperature decreases; but at very low temperatures,  $E_g$  reaches a constant value.

The average energy needed to create an electron-hole pair follows a similar change with temperature (Fig. 7.9).

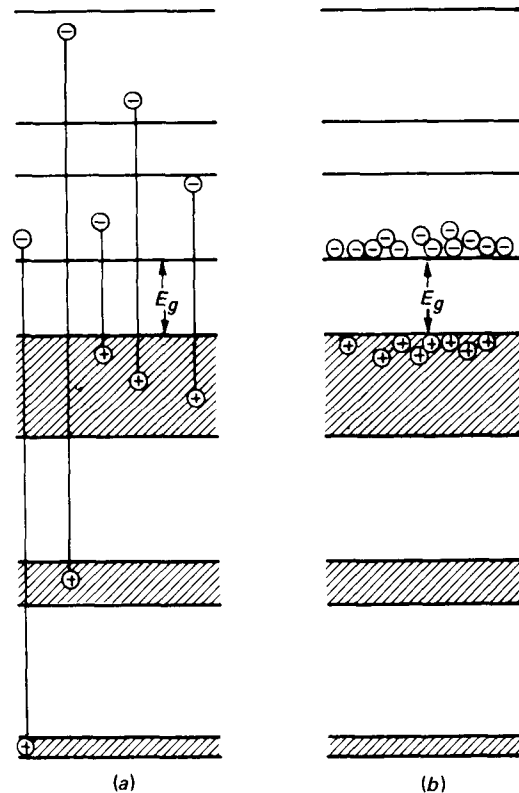


**Figure 7.7** (a) Collisions with an energetic charged particle raise electrons to the conduction bands. (b) After times of the order of  $10^{-12}$  s, electrons and holes tend to deexcite to the upper part of the valence band and lower part of the conduction band, respectively.



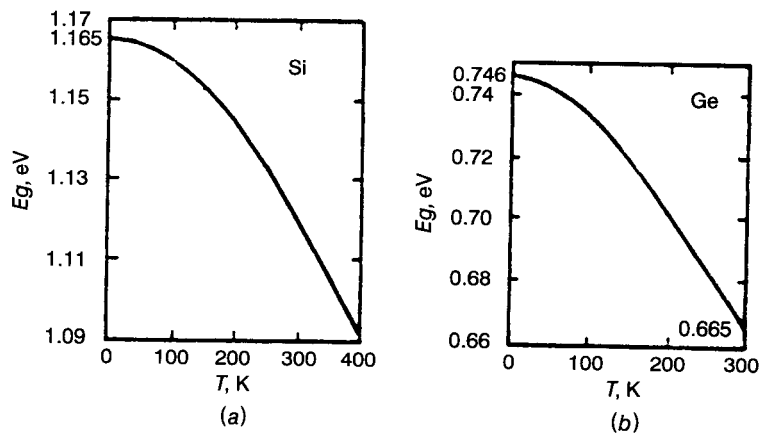


Figure 7.8 The variation of  $E_g$  with temperature: (a) for silicon; (b) for germanium (from Chap. 1.1.1 of Bertolini & Coche).

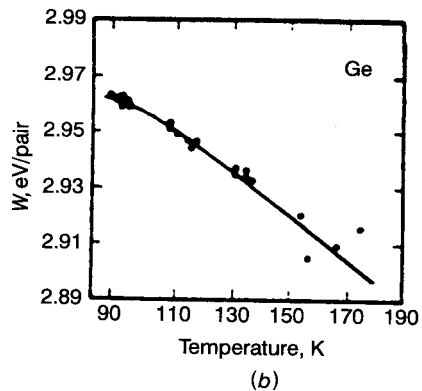
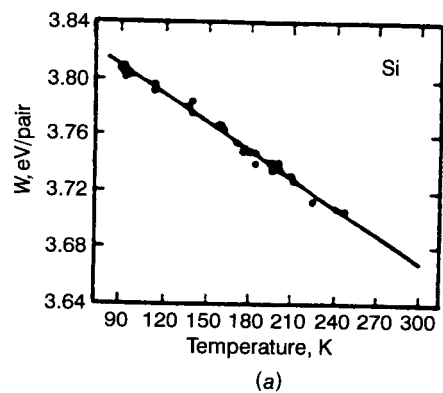


Figure 7.9 Energy needed to produce an electron-hole pair in (a) silicon and (b) germanium, as a function of temperature (from Ref. 3).

### 7.3.2 Conductivity of Semiconductors

Conductivity  $\sigma$  is the inverse of resistivity and is defined by

$$j = \sigma E \quad (7.4)$$

where  $j$  = current density (A/m<sup>2</sup>)

$\sigma$  = conductivity [A/(V m)]

$E$  = electric field (V/m)

Another expression for the current density is

$$j = eNv \quad (7.5)$$

where  $N$  = number of charge carriers/m<sup>3</sup>

$v$  = speed of carriers

Using Eqs. 7.4 and 7.5, one obtains the following equation:

$$\sigma = eN \frac{v}{E} \quad (7.6)$$

The ratio  $v/E$  is given a new name, *mobility of the carrier*:

$$\mu = (v/E) \quad (7.7)$$

All the types of charge carriers present in a medium contribute to the conductivity. In the case of semiconductors, both electrons and holes should be taken into account when conductivity is calculated, and the expression for the conductivity becomes (using Eqs. 7.6 and 7.7).

$$\sigma = e(N_e \mu_e + N_p \mu_p) \quad (7.8)$$

where  $N_e$  and  $N_p$  are charge carrier concentrations and  $\mu_e$  and  $\mu_p$  are mobilities of electrons and holes, respectively. According to Eq. 7.8, the conductivity changes if the mobility of the carriers or their concentration or both change.

The mobilities of electrons and holes are independent of the electric field over a wide range of carrier velocities, but they change with temperature. If the temperature decreases, the mobility of both carriers increases. The mobility of electrons and holes in pure germanium as a function of temperature is shown in Fig. 7.10.<sup>4</sup> The mobility changes at  $\mu \sim T^{-\alpha}$  with  $\alpha \approx 1.5$ , for  $T < 80$  K. For  $T > 80$  K, the value of  $\alpha$  is somewhat larger. It is worth noting that for  $T < 80$  K,  $\mu_n \approx \mu_p$ .

In a pure semiconductor,  $N_e = N_p$  and each one of these quantities is given by the equation

$$N_e = N_p = AT^{1.5} \exp\left(-\frac{E_g}{2kT}\right) \quad (7.9)$$

where  $A$  is a constant independent of  $T$ .

The motion of the carriers in a semiconductor is also affected by the presence of impurities and defects of the crystal. A small amount of impurities is always present, although impurities are usually introduced deliberately to make

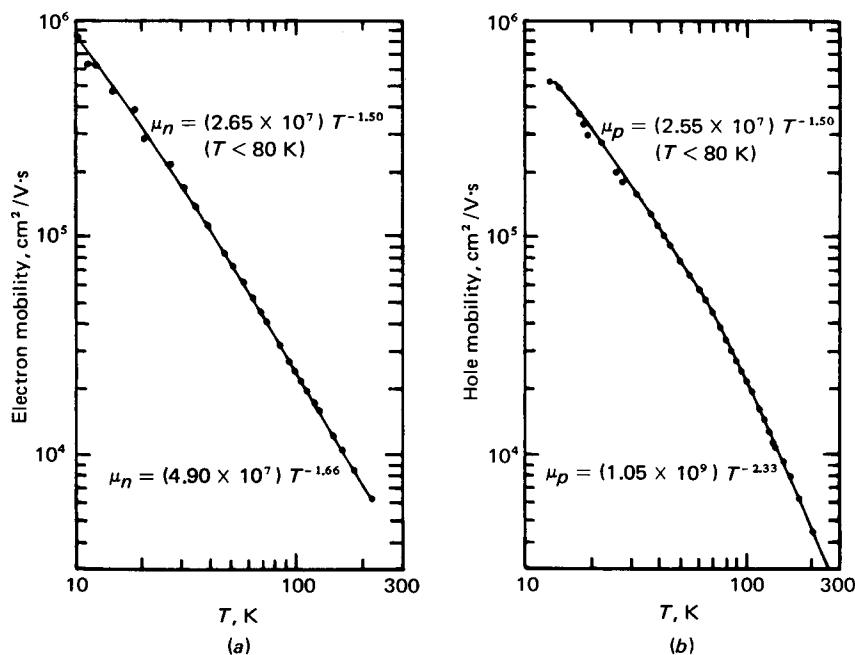


**Figure 7.10** (a) Electron mobility versus temperature for *n*-type germanium. (b) Hole mobility versus temperature for *p*-type germanium (from Ref. 4).

the properties of the crystal more appropriate for radiation detection (see Sec. 7.3.3). Crystal defects are present too. Even if one starts with a perfect crystal, defects are produced by the incident particles (this is called *radiation damage*). In the language of energy bands, impurities and defects represent new energy states that may trap the carriers. Trapping is, of course, undesirable because it means loss of part of the charge generated by the incident particle.

For semiconductors, the probability that an electron will move from the valence to the conduction level is proportional to the factor (Eq. 7.3)

$$\exp\left(-\frac{E_g}{2kT}\right) \quad (7.10)$$

( $E_f$  is located in the middle of the gap; thus  $E - E_f = E_g/2$ .) Because of the exponential form of Eq. 7.10, there are always some electrons in the conduction band. These electrons produce a leakage current. Obviously, a successful detector should have as low a leakage current as possible to be able to detect the ionization produced by the incident radiation. The leakage current decreases with temperature, and for two different materials it will be smaller for the material with the larger energy gap.

### 7.3.3 Extrinsic and Intrinsic Semiconductors—The Role of Impurities

The properties of a pure semiconductor change if impurities are introduced. With impurities present, new states are created and the semiconductor obtains extra electrons or extra holes, which increase the conductivity of the material.

Actually, pure semiconductors are not available. All materials contain some impurities and for this reason they are called *impure* or *extrinsic*, in contrast to a pure semiconductor, which is called *intrinsic*. In most cases, controlled amounts of impurities are introduced purposely by a process called *doping*, which increases the conductivity of the material by orders of magnitude.

Doping works in the following way. Consider silicon (Si), which has four valence electrons. In a pure Si crystal, every valence electron makes a covalent bond with a neighboring atom (Fig. 7.11a). Assume now that one of the atoms is replaced by an atom of arsenic (As), which has five valence electrons (Fig. 7.11b). Four of the valence electrons form covalent bonds with four neighboring Si atoms, but the fifth electron does not belong to any chemical bond. It is bound very weakly and only a small amount of energy is necessary to free it, i.e., to move it to the conduction band. In terms of the energy-band model, this fifth electron belongs to an energy state located very close to the conduction band. Such states are called *donor* states (Fig. 7.12), and impurity atoms that create them are called *donor* atoms. The semiconductor with donor atoms has a large number of electrons and a small number of holes. Its conductivity will be due mainly to electrons, and it is called an *n-type* semiconductor (n is for negative).

If a gallium atom is the impurity, three valence electrons are available; thus only three Si bonds will be matched (Fig. 7.13). Electrons from other Si atoms can attach themselves to the gallium atom, leaving behind a hole. The gallium atom will behave like a negative ion after it accepts the extra electron. In terms of the energy-band theory, the presence of the gallium atom creates new states very close to the valence band (Fig. 7.14). These are called *acceptor* states. The impurity is called an *acceptor* atom. For every electron that moves to the acceptor states, a hole is left behind. The acceptor impurity atoms create holes. The charge carriers are essentially positive, and the semiconductor is called *p-type*.

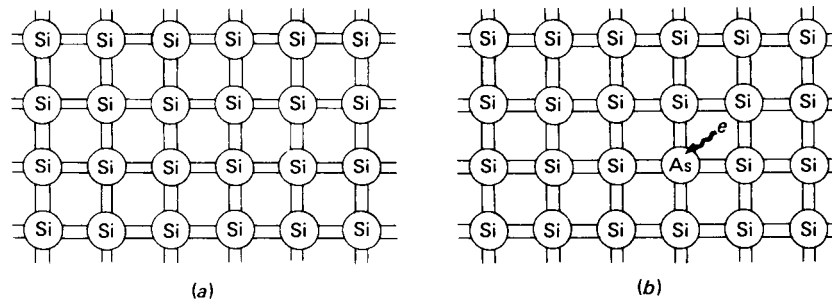


**Figure 7.11** (a) Pure (intrinsic) silicon. (b) Silicon doped with arsenic. The fifth electron of the arsenic atom is not tightly bound, and little energy is needed to move it to the conduction band.

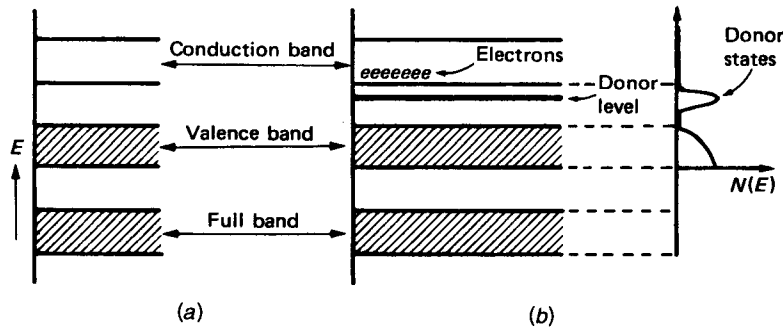


**Figure 7.12** (a) Intrinsic and (b) n-type semiconductor. New electron states (donor states) are created close to the conduction band.

Interstitial atoms can act as donors or acceptors. Lithium, as an interstitial in either silicon or germanium, creates donor states very close to the conduction band. Copper and nickel introduce donor states midway between the valence and conduction bands. Gold may act as either an acceptor or donor, depending on its position on the lattice.

For every atom of n-type or p-type impurity, an electron or hole is located at the donor or acceptor state, respectively. The material is still neutral, but when conductivity appears,

Electrons are the major carriers for n-type semiconductors.  
Holes are the major carriers for p-type semiconductors.

Since the addition of impurities creates new states that facilitate the movement of the carriers, it should be expected that the conductivity of a semiconductor increases with impurity concentration. Figures 7.15 and 7.16 show how the resistivity of germanium and silicon changes with impurity concentration.

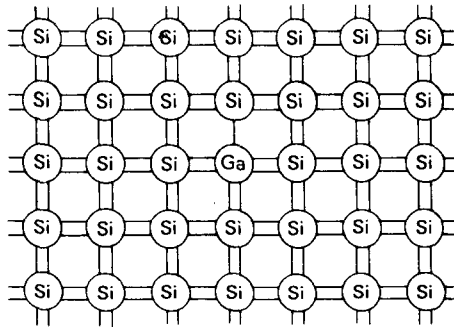
The energy gap  $E_g$  depends on temperature, as shown in Fig. 7.8, and on the number of impurities and defects of the crystal. With increasing temperatures, if  $E_g$  is small as in germanium, the electrical conduction is dominated by electron-hole pairs created by thermal excitation and not by the presence of the impurity atoms. Therefore, at high enough temperatures, any semiconductor can be considered as intrinsic.

Table 7.1 presents the most important physical and electrical properties of silicon and germanium, the two most widely used semiconductors.

## 7.4 THE p-n JUNCTION

### 7.4.1 The Formation of a p-n Junction

As stated in the introduction to this chapter, semiconductor detectors operate like ionization counters. In ionization counters (see Chap. 5), the charges



**Figure 7.13** Silicon doped with gallium. One of the covalent bonds is not matched.

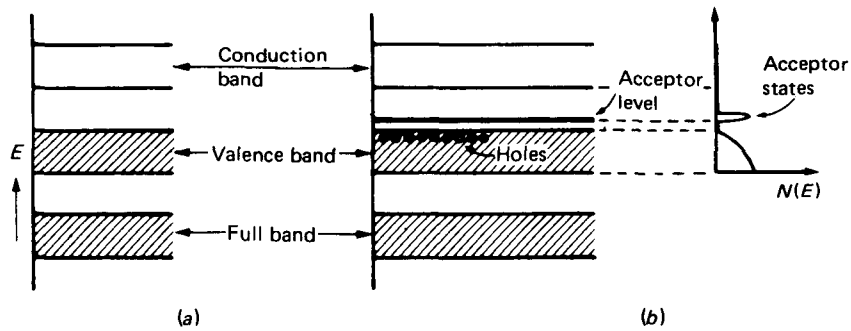


**Figure 7.14** (a) Intrinsic and (b) p-type semiconductor. New hole states (acceptor states) are created close to the top of the valence band.

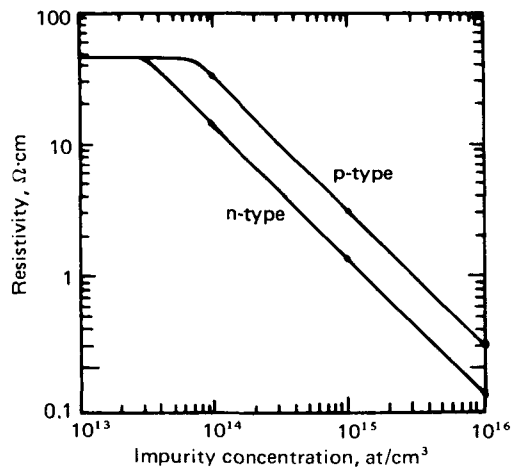


**Figure 7.15** Resistivity as a function of impurity concentration in germanium (from Chap. 1.1.3 of Bertolini & Coche).

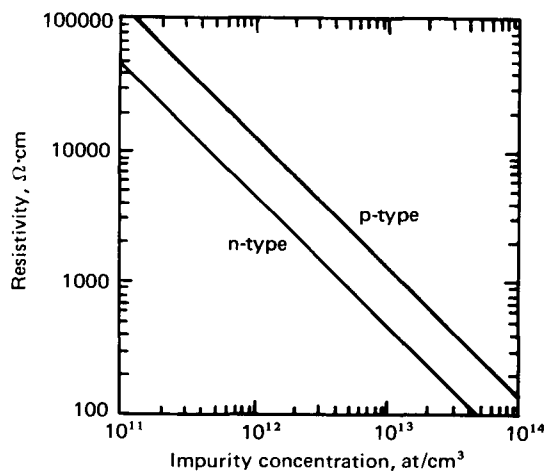


**Figure 7.16** Resistivity as a function of impurity concentration in silicon (from Chap. 1.1.3 of Bertolini & Coche).

produced by the incident radiation are collected with the help of an electric field from an external voltage. In semiconductor detectors, the electric field is established by a process more complicated than in gas counters, a process that depends on the properties of n- and p-type semiconductors. The phenomena involved will be better understood with a brief discussion of the so-called p-n junction.

An n-type semiconductor has an excess of electron carriers. A p-type has excess holes. If a p-type and an n-type semiconductor join together, electrons and holes move for two reasons:

1. Both electrons and holes will move from areas of high concentration to areas of low concentration. This is simply diffusion, the same as neutron diffusion or diffusion of gas molecules.
2. Under the influence of an electric field, both electrons and holes will move, but in opposite directions because their charge is negative and positive, respectively.

Consider two semiconductors, one p-type, the other n-type, in contact, without an external electric field (Fig. 7.17). The n-type semiconductor has a high electron concentration; the p-type has a high hole concentration. Electrons will diffuse from the n- to the p-type; holes will diffuse in the opposite direction. This diffusion will produce an equilibrium of electron and hole concentrations, but it will upset the original charge equilibrium. Originally, both p- and n-type semiconductors were electrically neutral, but as a result of the diffusion, the n-type region will be positively charged, while the p-type region will be negatively charged. After equilibrium is established, a potential difference exists between the two regions. This combination of p- and n-type semiconductor with a potential difference between the two types constitutes a p-n junction.

The potential  $V_0$  (Fig. 7.17a) depends on electron-hole concentrations and is of the order of 0.5 V. If an external voltage  $V_b$  is applied with the positive pole

**Table 7.1 Properties of Si and Ge (from Fenvres and Haiman and Ref. 2)**

Property	Si	Ge
Atomic number	14	32
Atomic weight	28.1	72.6
Density (300 K)	$2.33 \times 10^3 \text{ kg/m}^3$	$5.33 \times 10^3 \text{ kg/m}^3$
Energy gap ( $E_g$ ), 300 K	1.106 eV	0.67 eV
Energy gap ( $E_g$ ), 0 K	1.165 eV	0.75 eV
Average energy per electron-hole pair, 77 K	3.7 eV	2.96 eV
Average energy per electron-hole pair, 300 K	3.65 eV	—
Diffusion voltage ( $V_0$ )	0.7 V	0.4 V
Atomic concentration	$5 \times 10^{28} \text{ m}^{-3}$	$4.5 \times 10^{28} \text{ m}^{-3}$
Intrinsic carrier concentration (300 K)	$1.5 \times 10^{16} \text{ m}^{-3}$	$2.4 \times 10^{19} \text{ m}^{-3}$
Intrinsic resistivity (300 K)	$2.3 \times 10^3 \Omega \cdot \text{m}$	$0.47 \Omega \cdot \text{m}$
Intrinsic resistivity (77 K)	$\infty$	$5 \times 10^2 \Omega \cdot \text{m}$
Electron mobility (300 K)	$0.1350 \text{ m}^2/\text{V}\cdot\text{s}$	$0.3900 \text{ m}^2/\text{V}\cdot\text{s}$
Hole mobility (300 K)	$0.0480 \text{ m}^2/\text{V}\cdot\text{s}$	$0.1900 \text{ m}^2/\text{V}\cdot\text{s}$
Electron mobility (77 K)	$4.0\text{--}7.0 \text{ m}^2/\text{V}\cdot\text{s}$	$3.5\text{--}5.5 \text{ m}^2/\text{V}\cdot\text{s}$
Hole mobility (77 K)	$2.0\text{--}3.5 \text{ m}^2/\text{V}\cdot\text{s}$	$4.0\text{--}7.0 \text{ m}^2/\text{V}\cdot\text{s}$
Dielectric constant	12	16

connected to the n side, the total potential across the junction becomes  $V_0 + V_b$ . This is called *reverse bias*. Such external voltage tends to make the motion of both electrons and holes more difficult. In the region of the changing potential, there is an electric field  $E = -\partial V/\partial x$ . The length  $X_0$  of the region where the potential and the electric field exist increases with reverse bias. Calculation

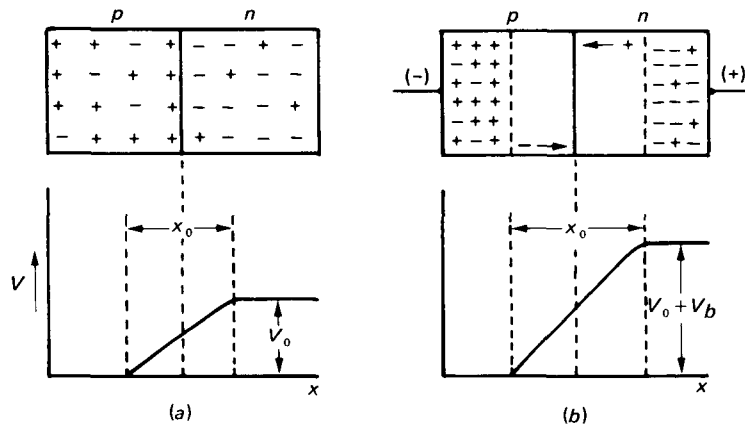


**Figure 7.17** (a) A p-n junction without external voltage. (b) If a reverse voltage is applied externally, the potential across the junction increases, and so does the depth  $x_0$  along which an electric field exists.



shows that

$$X_0 \approx \sqrt{\mu_p \rho (V_0 + V_b)} \quad \text{for p-type semiconductor} \quad (7.11a)$$

and

$$X_0 \approx \sqrt{\mu_n \rho (V_0 + V_b)} \quad \text{for n-type semiconductor} \quad (7.11b)$$

where  $\rho(\Omega \cdot \text{m})$  is the resistivity of the crystal. Application of a negative potential on the n side will have the opposite effect. The total potential difference will be  $V_0 - V_b$ . This is called *forward bias*. For a successful detector, reverse bias is applied. Since, usually,  $V_b \gg V_0$ ,  $X_0 \sim \sqrt{V_b}$ .

In practice, a p-n junction is not made by bringing two pieces of semiconductor into contact. Instead, one starts with a semiconductor of one type (say, n-type) and then transforms one end of it into the other type (p-type).

#### 7.4.2 The p-n Junction Operating as a Detector

The operation of a semiconductor detector is based, essentially, on the properties of the p-n junction with reverse bias (Fig. 7.18). Radiation incident upon the junction produces electron-hole pairs as it passes through it. For example, if a 5-MeV alpha particle impinges upon the detector and deposits all its energy there, it will create about

$$\frac{5 \times 10^6 \text{ eV}}{3 \text{ eV/pair}} \sim 1.7 \times 10^6 \text{ electron-hole pairs}$$

Electrons and holes are swept away under the influence of the electric field and, with proper electronics, the charge collected produces a pulse that can be recorded.

The performance of a semiconductor detector depends on the region of the p-n junction where the electric field exists (region of width  $X_0$ , Fig. 7.18). Electrons and holes produced in that region find themselves in an environment similar to what electrons and ions see in a plate ionization chamber (see Sec. 5.4). There are some differences, however, between these two types of detectors.

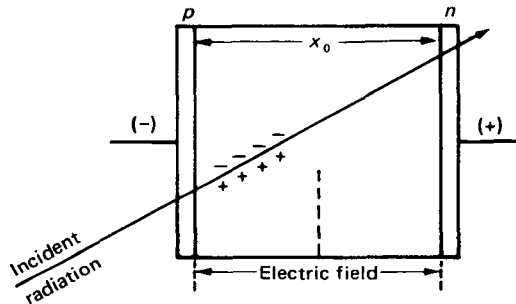


Figure 7.18 A p-n junction with reverse bias operating as a detector.

In a gas counter, the electron mobility is thousands of times bigger than that of the ions. In semiconductors, the electron mobility is only about two to three times bigger than that of the holes. The time it takes to collect all the charge produced in a gas counter is of the order of milliseconds. In semiconductors, the sensitive region of the counter is only a few millimeters, and the speed of electrons and holes is such that the charge carriers can traverse the sensitive region and be collected in times of the order of  $10^{-7}$  s.

It is always the objective in either an ionization or a semiconductor detector to collect all the charges produced by the incident particle. This is achieved by establishing an electric field in the detector such that there is zero recombination of electrons and ions (or holes) before they are collected. In a semiconductor detector, even if recombination is zero, some charge carriers may be lost in "trapping" centers of the crystal, such as lattice imperfections, vacancies and dislocations. The incident radiation creates crystal defects that cause deterioration of the detector performance and, thus, reduce its lifetime (see Sec. 7.6).

The capacitance of p-n junction is important because it affects the energy resolution of the detector. For a detector such as that shown in Fig. 7.18, the capacitance  $C$  is given by

$$C = \epsilon \frac{A}{4\pi X_0} \quad (7.12)$$

where  $\epsilon$  = dielectric constant of the material

$A$  = surface area of the detector

$X_0$  = depletion depth (detector thickness)

Combining Eqs. 7.11 and 7.12,

$$C \sim \frac{1}{\sqrt{V_b}}$$

To summarize, a material that will be used for the construction of a detector should have certain properties, the most important of which are the following:

1. *High resistivity.* This is essential, since otherwise current will flow under the influence of the electric field, and the charge produced by the particles will result in a pulse that may be masked by the steadily flowing current.
2. *High carrier mobility.* Electrons and holes should be able to move quickly and be collected before they have a chance to recombine or be trapped. High mobility is in conflict with property (1) because in high-resistivity materials, carrier mobility is low. Semiconductor materials doped with impurities have proven to have the proper resistivity-carrier mobility combination.
3. *Capability of supporting strong electric fields.* This property is related to property (1). Its importance stems from the fact that the stronger the field, the better and faster the charge collection becomes. Also, as the electric field increases, so does the depth of the sensitive region (Eq. 7.11a) for certain detectors.

4. *Perfect crystal lattice.* Apart from externally injected impurities, the semiconductor detector material should consist of a perfect crystal lattice without any defects, missing atoms, or interstitial atoms. Any such defect may act as a “trap” for the moving charges.

## 7.5 THE DIFFERENT TYPES OF SEMICONDUCTOR DETECTORS

The several types of semiconductor detectors that exist today differ from one another because of the material used for their construction or the method by which that material is treated. The rest of this section describes briefly the method of construction and the characteristics of the most successful detectors—made of silicon or germanium—and two promising ones made of CdTe and HgI<sub>2</sub>.

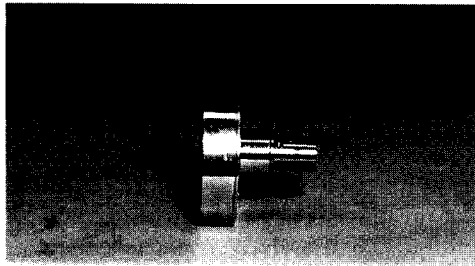
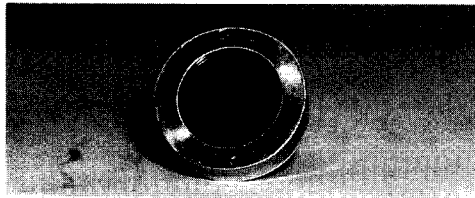
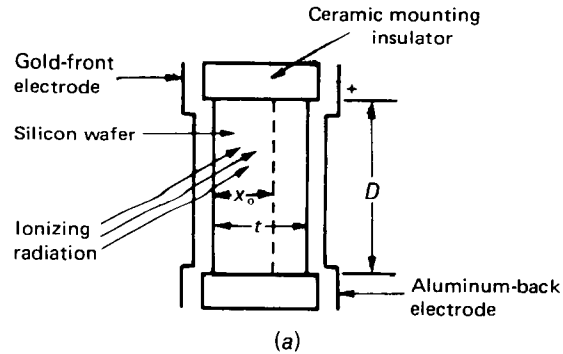
### 7.5.1 Surface-Barrier Detectors

Silicon of high purity, usually n-type, is cut, ground, polished, and etched until a thin wafer with a high-grade surface is obtained. The silicon is then left exposed to air or to another oxidizing agent for several days. As a result of surface oxidization, surface energy states are produced that induce a high density of holes and form, essentially, a p-type layer on the surface (Fig. 7.19). A very thin layer of gold evaporated on the surface serves as the electrical contact that will lead the signal to the preamplifier. In Fig. 7.19,  $X_0$  is the depth of the sensitive region,  $t$  is the total silicon thickness, and  $D$  is the diameter of the detector. The size of the detector is the length (or depth)  $X_0$ .

### 7.5.2 Diffused-Junction Detectors

Silicon of high purity, normally p-type, is the basic material for this detector type. As with surface-barrier detectors, the silicon piece has the shape of a thin wafer. A thin layer of n-type silicon is formed on the front face of the wafer by applying a phosphorus compound to the surface and then heating the assembly to temperatures as high as 800–1000° C for less than an hour. The phosphorus diffuses into the silicon and “dopes” it with donors (Fig. 7.20). The n-type silicon in front and the p-type behind it form the p-n junction.

Both surface-barrier and diffused-junction detectors are used for the detection of charged particles. To be able to measure the energy of the incident radiation, the size  $X_0$  of the detector should be at least equal to the range of the incident particle in silicon. The value of  $X_0$  depends on the resistivity of the material (which in turn, depends on impurity concentration) and on the applied voltage, as shown by Eq. 7.11. Blankenship and Borkowski have designed a nomogram relating all these quantities.<sup>5</sup> Figure 7.21 shows a simplified version of the nomogram, and Ex. 7.1 explains its use.



(b)

**Figure 7.19** A typical surface barrier detector: (a) a schematic representation; (b) photograph of a commercial detector (reproduced from *Instruments for Research and Applied Science* by permission of EG & G ORTEC, Oak Ridge, Tennessee).

**EXAMPLE 7.1** What is the bias needed for a surface-barrier detector made of p-type silicon with resistivity  $1.5 \text{ k}\Omega \text{ cm}$ , used for the detection of 10-MeV alpha particles?

**ANSWER** The bias is found by following these steps:

1. Find the range of a 10-MeV alpha particle in silicon. From Sec. 4.6, one obtains  $R = 65 \text{ }\mu\text{m}$  (point A in Fig. 7.21).
2. Define point B on the resistivity scale for p-type silicon.
3. Draw the straight line defined by points A and B.
4. The required bias (point C) is the intersection of the line AB with the bias scale ( $V_b \approx 35 \text{ V}$ ).

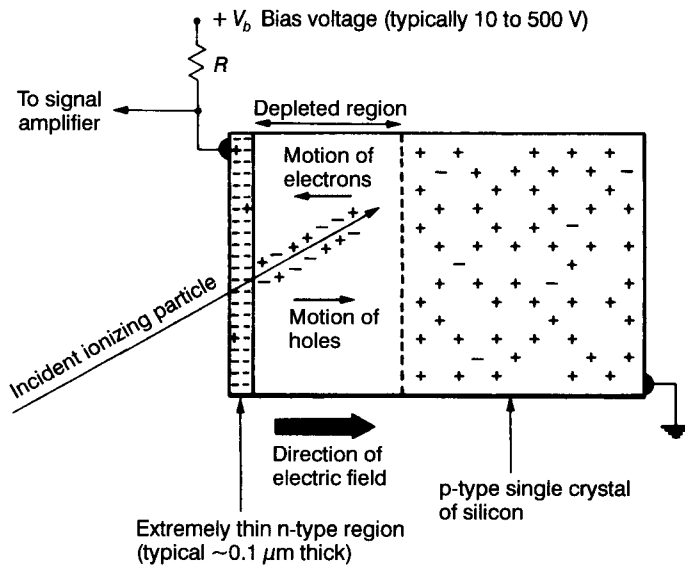


Figure 7.20 A diffused-junction detector.

The nomogram of Fig. 7.21 also gives the capacitance of the detector. Of course, the capacitance can also be calculated using Eq. 7.11.

### 7.5.3 Silicon Lithium-Drifted [Si(Li)] Detectors

For both surface-barrier and diffused-junction detectors, the sensitive region—i.e., the actual size of the detector—has an upper limit of about 2000 μm. This limitation affects the maximum energy of a charged particle that can be measured. For electrons in Si, the range of 2000 μm corresponds to an energy of about 1.2 MeV; for protons the corresponding number is about 18 MeV; for alphas, it is about 72 MeV. The length of the sensitive region can be increased if lithium ions are left to diffuse from the surface of the detector toward the other side. This process has been used successfully with silicon and germanium and has produced the so-called Si(Li) (pronounced silly) and Ge(Li) (pronounced jelly) semiconductor detectors. Lithium-drifted detectors have been produced with depth up to 5 mm in the case of Si(Li) detectors and up to 12 mm in the case of Ge(Li) detectors.

The lithium drifting process, developed by Pell,<sup>6,7</sup> consists of two major steps: (1) formation of an n-p junction by lithium diffusion, and (2) increase of the depletion depth by ion drifting.

The n-p junction is formed by letting lithium diffuse into a p-type silicon. The diffusion can be accomplished by several methods.<sup>8-11</sup> Probably the simplest method consists of painting a lithium-in-oil suspension onto the surface

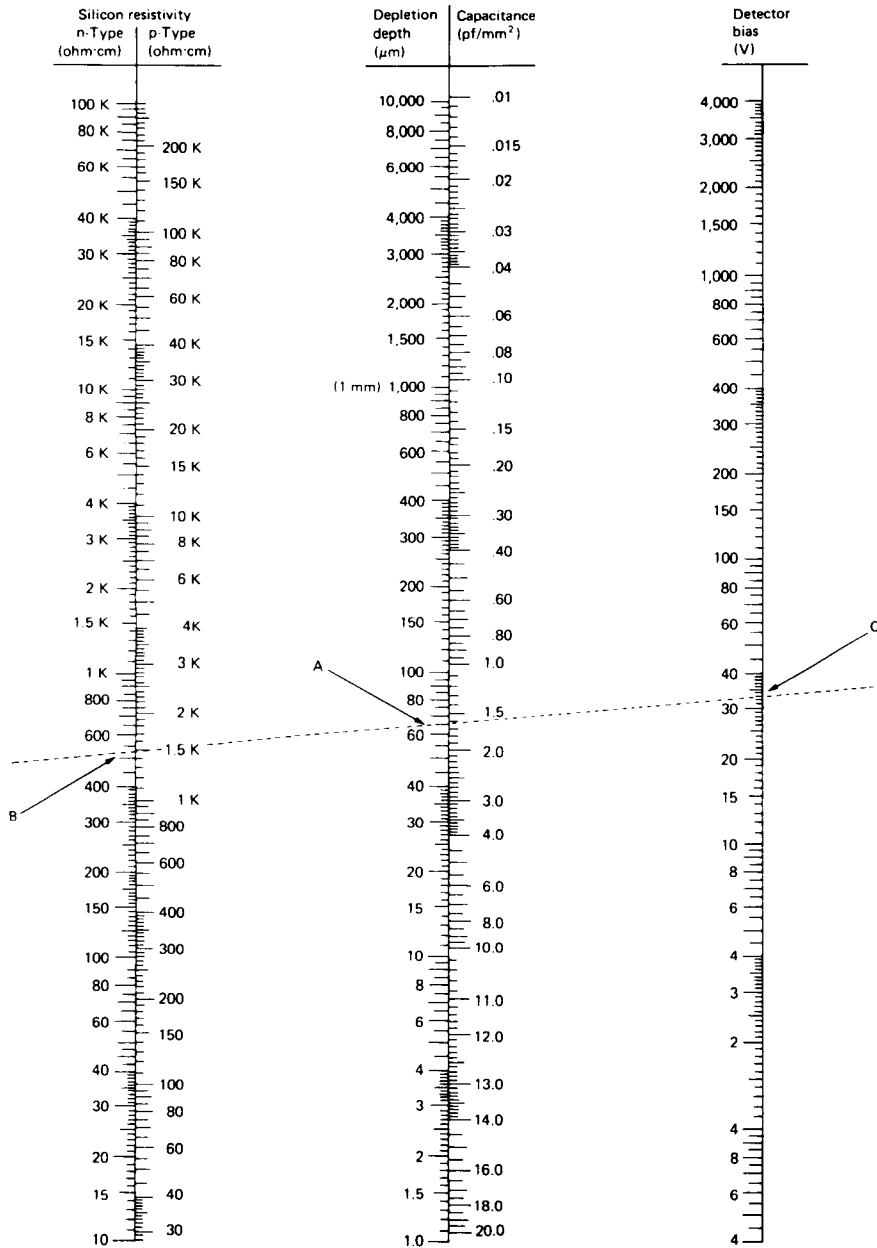
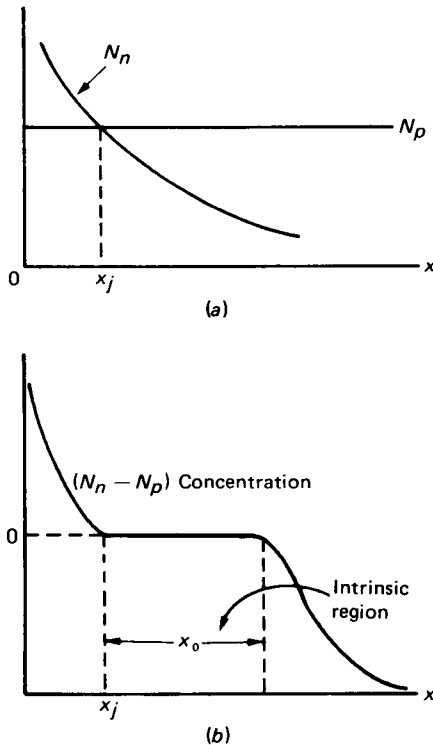


Figure 7.21 The Blankenship and Borkowski<sup>5</sup> nomogram that relates resistivity, detector thickness, and detector bias. The detector capacitance as a function of detector thickness is also given.



**Figure 7.22** (a) During the diffusion of lithium, the donor concentration changes with depth as shown. (b) During drifting (at elevated temperature and under reverse bias), and almost intrinsic region is formed with thickness  $x_0$ .

from which drifting is to begin. Other methods are lithium deposition under vacuum, or electrodeposition. After the lithium is applied on the surface, the silicon wafer is heated at 250–400° C for 3–10 min in an inert atmosphere, such as argon or helium.

Lithium is an n-type impurity (donor atom) with high mobility in silicon (and germanium; see next section). When the diffusion begins, the acceptor concentration ( $N_p$ ) is constant throughout the silicon crystal (Fig. 7.22a), while the donor concentration ( $N_n$ ) is high on the surface and zero everywhere else. As the diffusion proceeds, the donor concentration changes with depth, as shown in Fig. 7.22a. At the depth  $x_j$  where

$$N_n(x_j) = N_p$$

and n-p junction has been formed (Fig. 7.22b).

After the diffusion is completed, the crystal is left to cool, the excess lithium is removed, and ohmic contacts are put on the n and p sides of the junction. The contact on the p side is usually formed by evaporating aluminum or gold doped with boron. The contact on the n side can be formed by using pure gold or antimony-doped gold.

Drifting is accomplished by heating the junction to 120–150° C while applying a reverse bias that may range from 25 V up to about 1000 V. In general, the higher the temperature and the voltage are, the faster the drifting proceeds. Depending on the special method used, the semiconductor may be under vacuum or in air or be placed in a liquid bath (e.g., silicon oil or fluorocarbon). The electric field established by the reverse bias tends to move the n-type atoms (lithium) toward the p side of the junction. As a result, the concentration of lithium atoms becomes lower for  $x < x_j$  (Fig. 7.22a) and higher for  $x > x_j$ . For  $x < x_j$ ,  $N_n$  cannot become less than  $N_p$  because then a local electric field would appear pushing the lithium atoms toward the n side. Similarly, for  $x > x_j$ ,  $N_n$  cannot increase very much because the local electric field works against such a concentration. Thus, a region is created that looks like an intrinsic semiconductor because  $N_n \approx N_p$ . For long drifting times, the thickness of the intrinsic region  $X_0(t)$  as a function of time is given by

$$X_0(t) = \sqrt{2V\mu_{\text{Li}}t} \quad (7.13)$$

where  $V$  = applied voltage

$\mu_{\text{Li}}$  = mobility of Li ions in silicon at the drifting temperature

The mobility of lithium, which increases with temperature,<sup>12</sup> has a value of about  $5 \times 10^{-14}$  m<sup>2</sup>/V s at  $T = 150^\circ$  C. Drifting is a long process. Depending on the desired thickness, drifting may take days and sometimes weeks.

**EXAMPLE 7.2** How long will it take to obtain an intrinsic region of 1.5 mm in a silicon wafer drifted at 150° C under a reverse bias of 500 V?

**ANSWER** Using Eq. 7.13 with  $\mu_{\text{Li}} = 5 \times 10^{-14}$  m<sup>2</sup>/V s, one obtains

$$t = \frac{X_0^2(t)}{2V\mu_{\text{Li}}} = \frac{(1.5 \times 10^{-3})^2 \text{ m}^2}{2(500 \text{ V})[5 \times 10^{-14} \text{ m}^2/(\text{V s})]} = 4.5 \times 10^4 \text{ s} = 12.5 \text{ h}$$

After drifting is completed, the Si(Li) detector is mounted on a cryostat, since the best results are obtained if the detector is operated at a very low temperature. Usually, this temperature is 77K, the temperature of liquid nitrogen. Si(Li) detectors may be stored at room temperature for a short period of time without catastrophic results, but for longer periods it is advisable to keep the detector cooled at all times. The low temperature is necessary to keep the lithium drifting at a “frozen” stage. At room temperature, the mobility of lithium is such that its continuous diffusion and precipitation<sup>12</sup> will ruin the detector.

Si(Li) detectors are used for detection of charged particles and especially X-rays. Their characteristics with respect to energy measurements are described in Chaps. 12 and 13.



### 7.5.4 Germanium Lithium-Drifted [Ge(Li)] Detectors

Ge(Li) detectors are not made anymore; they have been replaced by pure germanium crystals. Historically, Ge(Li) detectors dominated the gamma detection field for about 15 years (until about 1985). Since there may still be some Ge(Li)'s operating, a brief discussion is presented in this section.

Ge(Li) detectors are made from horizontally grown or pulled single crystals of germanium. As the crystal is grown, it is doped with acceptor impurities such as indium, gallium, or boron, and becomes a p-type semiconductor. Germanium crystals may be cut to length and shaped by a variety of means, including the use of diamond wheels or band saws. In these mechanical operations, great care must be taken not to fracture the brittle material.

Lithium drifting in germanium follows the same approach as in silicon. The deposition and diffusion of lithium are accomplished by one of the methods discussed in the previous section. The ohmic contacts are made by electrolytic deposition of gold,<sup>13</sup> by using gallium-indium<sup>14</sup> or mercury-indium,<sup>15</sup> or by ion implantation.<sup>16</sup> The drifting process itself takes place at a lower temperature ( $< 60^\circ\text{C}$ ) than for silicon, with the germanium diode in air<sup>17</sup> or immersed in a liquid maintained at its boiling point.<sup>18</sup>

After the drifting process has been completed, the detector is mounted on a cryostat and is always kept at a low temperature (liquid nitrogen temperature  $\sim 77\text{ K}$ ). Keeping the Ge(Li) detector at a low temperature is much more critical than for a Si(Li) detector. The mobility of the lithium atoms in germanium is so high at room temperature that the detector will be ruined if brought to room temperature even for a short period of time. If this happens, the detector may be redrifted, but at a considerable cost.

### 7.5.5 Germanium (Ge) Detectors

The production of high-purity germanium (HPGe) with an impurity concentration of  $10^{16}$  atoms/cm<sup>3</sup> or less has made possible the construction of detectors without lithium drifting.<sup>19-21</sup> These detectors are now designated as Ge, not HPGe, and are simply formed by applying a voltage across a piece of germanium. The sensitive depth of the detector depends on the impurity concentration and the voltage applied, as shown in Fig. 7.23.

The major advantage of Ge versus Ge(Li) detectors is that the former can be stored at room temperature and cooled to liquid nitrogen temperature (77 K) *only* when in use. Cooling the detector, when in use, is necessary because germanium has a relatively narrow energy gap, and at room or higher temperatures a leakage current due to thermally generated charge carriers induces such noise that the energy resolution of the device is destroyed.

Germanium detectors are fabricated in many different geometries, thus offering devices that can be tailored to the specific needs of the measurement. Two examples, the coaxial and the well-type detector, are shown in Fig. 7.24.

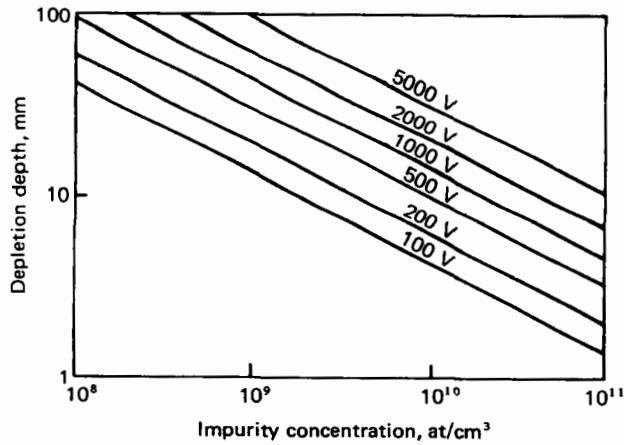


**Figure 7.23** Depletion depth as a function of impurity concentration and applied voltage for planar diodes of high-purity germanium (from Ref. 21).

More details about these detectors are presented in Chap. 12 in connection with  $\gamma$ -ray spectroscopy.

### 7.5.6 CdTe and HgI<sub>2</sub> Detectors

The major disadvantage of lithium-drifted detectors is the requirement for continuous cooling. In the case of Ge detectors, the requirement for cooling

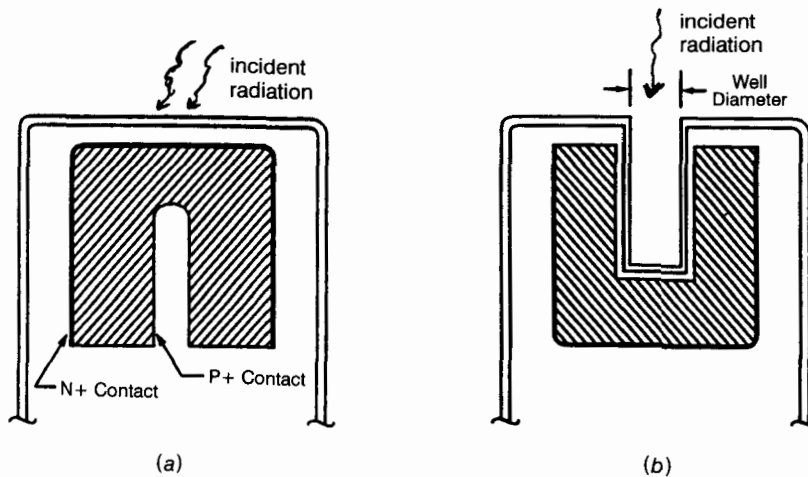


**Figure 7.24** Two examples of geometries used for Ge Detectors; (a) coaxial; (b) well type (from Canberra Nuclear, *Edition Nine Instruments Catalog*).

during operation is also a disadvantage. Cooling requires a cryostat, which makes the counter bulky and thus impossible to use in cases where only a small space is available; another disadvantage is the cost of continuously buying liquid nitrogen. There is a great incentive, therefore, to develop semiconductor detectors that can be stored and operated at room temperature. Two materials that have been studied and show great promise for the construction of such detectors are CdTe and HgI<sub>2</sub>.<sup>22-35</sup> A comprehensive review of the state-of-the-art (until 1978) for both materials can be found in Ref. 36.

Successful detectors using CdTe or HgI<sub>2</sub> have been constructed with thickness up to 0.7 mm and area 100 mm<sup>2</sup> (as of 1978).<sup>31</sup> These detectors are small in size, compared to Si(Li) or Ge(Li) detectors, but the required detector volume depends on the application. For CdTe and HgI<sub>2</sub>, the favored applications are those that require a small detector volume: monitoring in space,<sup>37</sup> measurement of activity in nuclear power plants,<sup>38</sup> medical portable scanning,<sup>39</sup> or medical imaging devices.<sup>40</sup> Although the detector volume is small, efficiency is considerable because of the high atomic number of the elements involved (Table 7.2). The energy needed for the production of an electron-hole pair is larger for CdTe and HgI<sub>2</sub> than it is for Si and Ge; as a result, the energy resolution of the former is inferior to that of the latter (see also Chap. 12). But CdTe and HgI<sub>2</sub> detectors are used in measurements where their energy resolution is adequate while, at the same time, their small volume and, in particular, their room-temperature operation offers a distinct advantage over Si(Li) and Ge(Li) detectors.

## 7.6 RADIATION DAMAGE TO SEMICONDUCTOR DETECTORS

The fabrication and operation of a semiconductor detector are based on the premise that one starts with a perfect crystal containing a known amount of impurities. Even if this is true at the beginning, a semiconductor detector will suffer damage after being exposed to radiation. The principal type of radiation damage is caused by the collision of an incident particle with an atom. As a result of the collision, the atom may be displaced into an interstitial position, thus creating an interstitial-vacancy pair known as the *Frenkel defect*. A recoiling

**Table 7.2 Properties of Si, Ge, CdTe, and HgI<sub>2</sub>**

Material	Atomic number	Energy gap (eV)	Energy needed to form the pair (eV)
Si	14	1.106 (300 K)	3.65 (300 K)
Ge	32	0.67 (77 K)	2.96 (77 K)
CdTe	48 and 52	1.47 (300 K)	4.43 (300 K)
HgI <sub>2</sub>	80 and 53	2.13 (300 K)	4.22 (300 K)

**Table 7.3 Particle Fluence That Causes Significant Radiation Damage**

	Heavy ions (particles/m <sup>2</sup> )	Alphas ( $\alpha$ /m <sup>2</sup> )	Fast neutrons (n/m <sup>2</sup> )
Junction detectors	10 <sup>12</sup>	10 <sup>14</sup>	
Si(Li)		10 <sup>12</sup>	10 <sup>14</sup>
Ge(Li) or Ge			10 <sup>13</sup> –10 <sup>14</sup>

atom may have enough energy to displace other atoms; therefore an incident particle may produce many Frenkel defects.

Crystal defects affect the performance of the detector because they may act as trapping centers for electrons and holes or they may create new donor or acceptor states. New trapping centers and new energy states change the charge collection efficiency, the leakage current, the pulse risetime, the energy resolution, and other properties of the detector. The changes are gradual, but the final result is shortening of the detector lifetime.

Electrons and photons cause negligible radiation damage compared to charged particles and neutrons. Heavier and more energetic charged particles cause more damage than lighter and less energetic particles.<sup>2,21</sup> Also, the damage is not the same for all detector types. Table 7.3 gives the fluences that cause considerable radiation damage for different detectors and bombarding particles.

Ge detectors are not affected by gammas, but they are damaged by the neutrons in a mixed n- $\gamma$  field.

## PROBLEMS

7.1 What is the probability that an electron energy state in Ge will be occupied at temperature  $T = 300$  K if the energy state is greater than the Fermi energy by 2 eV?

7.2 Repeat Prob. 7.1 for  $T = 77$  K.

7.3 The energy gap for diamond is 7 eV. What temperature will provide thermal energy ( $kT$ ) equal to that amount?

7.4 What should be the maximum thickness of the gold layer covering the front face of a surface barrier detector used for the measurement of 10-MeV alphas, if the energy loss of the alphas traversing the layer should be less than 0.1 percent of the kinetic energy?

7.5 Repeat Prob. 7.4 for 6-MeV electrons.

7.6 The thickness of the gold layer covering the front face of a semiconductor detector may be measured by detecting particles entering the detector at two different angles. Calculate that thickness if alphas that enter in a direction perpendicular to the front face register as having energy 4.98 MeV, but those that enter at a 45° angle register as having energy 4.92 MeV.

7.7 What is the average distance traveled in Si by a 50-KeV gamma before it has an interaction? What is the corresponding distance in Ge?

7.8 Lithium has been drifted in germanium at 50° C under a reverse bias of 500 V for 2 weeks. What is your estimate of the drifting depth? [ $\mu_{\text{Li}} = 1.5 \times 10^{-13}$  m<sup>2</sup>/(V s)]

7.9 A parallel beam of 0.5-MeV gammas is normally incident upon 2-mm-thick-crystals of Si, Ge, CdTe, and HgI<sub>2</sub>. What fraction of photons will interact at least once in each crystal?

## BIBLIOGRAPHY

- Bertolini, G., and Coche, A., *Semiconductor Detectors*, North-Holland Publishing Co., Amsterdam, 1968.
- Brown, W. L., Higinbotham, W. A., Miller, G. L., and Chace, R. L. (eds.), "Semiconductor Nuclear Particle Detectors and Circuits," proceedings of a conference conducted by the Committee of Nuclear Science of the National Academy of Sciences, NAS Publication 1593, Washington, D.C. (1969).
- Dearnaley, G., and Northrop, D. C., *Semiconductor Counters for Nuclear Radiations*, E & F.N. Spon. Ltd., London, 1964.
- Eichholz, G. G., and Poston, J. W., *Nuclear Radiation Detection*, Lewis Publishers, Chelsea, Michigan, 1985.
- Fenyves, E., and Haiman, O., *The Physical Principles of Nuclear Radiation Measurements*, Academic Press, New York, 1969.
- Knoll, G. F., *Radiation Detection and Measurement*, 2nd ed., Wiley, New York, 1989.
- Price, W. J., *Nuclear Radiation Detection*, McGraw-Hill, New York, 1964.
- Tait, W. H., *Radiation Detection*, Butterworth, London, 1980.

## REFERENCES

1. McKenzie, J. M., *Nucl. Instrum. Meth.* **162**:49 (1979).
2. Ewan, G. T., *Nucl. Instrum. Meth.* **162**:75 (1979).
3. Pehl, R. H., Goulding, F. S., Landis, D. A., and Lenzlinger, M., *Nucl. Instrum. Meth.* **59**:45 (1968).
4. Delaet, L. H., Schoenmaekers, W. K., and Guislain, H. J., *Nucl. Instrum. Meth.* **101**:11 (1972).
5. Friedland, S. S., Mayer, J. W., and Wiggins, J. S., *IRE Trans. Nucl. Sci.* **NS-7**(2-3):181 (1960).
6. Pell, E. M., *J. Appl. Phys.* **31**:291 (1960).
7. Mayer, J. W., *J. Appl. Phys.* **33**:2894 (1962).
8. Elliott, J. H., *Nucl. Instrum. Meth.* **12**:60 (1961).
9. Baily, N. A., and Mayer, J. W., *Radiology* **76**:116 (1961).
10. Siffert, P., and Coche, A., *Compt. Rend.* **256**:3277 (1963).
11. Dearnaley, G., and Lewis, J. C., *Nucl. Instrum. Meth.* **25**:237 (1964).
12. Siffert, P., and Coche, A., "Behavior of Lithium in Silicon and Germanium," in G. Bertolini and A. Coche (eds.), *Semiconductor Detectors*, North-Holland Publishing Co., Amsterdam, 1968.
13. Janarek, F. J., Helenberg, H. W., and Mann, H. M., *Rev. Sci. Instrum.* **36**:1501 (1965).
14. Mooney, J. B., *Nucl. Instrum. Meth.* **50**:242 (1967).
15. Hansen, W. L., and Jarrett, B. V., *Nucl. Instrum. Meth.* **31**:301 (1964).
16. Meyer, O., and Haushahn, G., *Nucl. Instrum. Meth.* **56**:177 (1967).
17. Ewan, G. T., and Tavendale, A. J., *Can. J. Phys.* **42**:3386 (1964).
18. Cappellani, E., Fumagulli, W., and Restelli, G., *Nucl. Instrum. Meth.* **37**:352 (1965).
19. Hall, R. N., and Soltys, T. J., *IEEE Trans. Nucl. Sci.* **NS-18**:160 (1971).
20. Hansen, W. L., *Nucl. Instrum. Meth.* **94**:377 (1971).
21. Pehl, R. H., *Physics Today* **30**:11, 50, 53 (1977).
22. Siffert, I., Gonidec, J. P., and Cornet, A., *Nucl. Instrum. Meth.* **115**:13 (1974).
23. Eichinger, P., Halder, N., and Kemmer J., *Nucl. Instrum. Meth.* **117**:305 (1974).
24. Jones, L. T., and Woollam, P. B., *Nucl. Instrum. Meth.* **124**:591 (1975).
25. Iwanczyk, J., and Dabrowski, A. J., *Nucl. Instrum. Meth.* **134**:505 (1976).

26. Siffert, P., *Nucl. Instrum. Meth.* **150**:1 (1978).
27. Dabrowski, A. J., Iwanczyk, J., and Szymczyk, W. M., *Nucl. Instrum. Meth.* **150**:25 (1978).
28. Schieber, M., Beinglass, I., Dishon, G., Holzer, A., and Yaron, G., *Nucl. Instrum. Meth.* **150**:71 (1978).
29. Shalev, S., *Nucl. Instrum. Meth.* **150**:79 (1978).
30. Caine, S., Holzer, A., Beinglass, I., Dishon, G., Lowenthal, E., and Schieber, M., *Nucl. Instrum. Meth.* **150**:83 (1978).
31. Whited, R. C., and Schieber, M. M., *Nucl. Instrum. Meth.* **162**:113 (1979).
32. Ristinen, R. A., Peterson, R. J., Hamill, J. J., and Becchetti, F. D., *Nucl. Instrum. Meth.* **188**:445 (1981).
33. Markakis, J. M., *Nucl. Instrum. Meth.* **263**:499 (1988).
34. Courat, B., Fourrier, J. P., Silga, M., and Omaly, J., *Nucl. Instrum. Meth.* **269**:213 (1988).
35. McKee, B. T. A., Goetz, T., Hazlett, T., and Forkert, L., *Nucl. Instrum. Meth.* **272**:825 (1988).
36. "International Workshop on Mercuric Iodide and Cadmium Telluride Nuclear Detectors," *Nucl. Instrum. Meth.* **150**:1–112 (1978).
37. Lyons, R. B., *Rev. Phys. Appl.* **12**:385 (1977).
38. Jones, L. T., *Rev. Phys. Appl.* **12**:379 (1977).
39. Vogel, J., Ullman, J., and Entine, G., *Rev. Phys. Appl.* **12**:375 (1977).
40. Canali, C., Gutti, E., Kozlov, S. F., Manfredi, P. F., Manfredotti, C., Nava, F., and Quirini, A., *Nucl. Instrum. Meth.* **160**:73 (1979).

## References

- 1- Joseph Magill and Jean Galy " Radioactivity · Radionuclides · Radiation" Springer is a part of Springer Science+Business Media springeronline.com© Springer-Verlag Berlin Heidelberg and European Communities Printed in Germany. 2005
- 2- GREGORY R. CHOPPIN JAN-OLOV LILJENZIN JAN RYDBERG Radiochemistry and Nuclear Chemistry 2002 by Butterworth-Heinemann
- 3- G. Knoll Radiation measurements 2010
- 4- Nicholas Tsoulfanidis MEASUREMENT AND DETECTION OF RADIATION Second Edition University of Missouri-Rolla 1995